1-1-2012

Bone microstructure, turnover and peri-articular osteopathies.

Jane C. Holland
Royal College of Surgeons in Ireland, jholland@rcsi.ie

Bone microstructure, turnover and peri-articular osteopathies

RCSI

A thesis submitted to the Royal College of Surgeons in Ireland

for the Degree of Doctor in Philosophy

Jane Catherine Holland

MA MSc MD MRCSI

Supervised by Prof TC Lee

Department of Anatomy

Royal College of Surgeons in Ireland

External Examiners

Prof Richard Aspden

Dr Glenn Dickson

Internal Examiner

Dr Kevin McGuigan

Contents

Illustrations

Illustrations (cont.)

Illustrations (cont.)

Tables

Graphs

Graphs (cont.)

Acknowledgements

This work was performed in the Department of Anatomy, in the Royal College of Surgeons in Ireland. To facilitate this animal experiment, an animal license, number B100/2443, was granted by the Department of Health under the Cruelty to Animals Act, 1876 and also approved by the ethics committee in the School of Veterinary Science in UCD. I gratefully acknowledge funding from the Higher Education Authority in Ireland under the PRTLI Cycle III and from the Research Committee of RCSI.

I was extremely fortunate to have guidance from a number of colleagues who were absolutely indispensable to my training in the techniques needed for this thesis, and in teaching me about bones; Oran Kennedy, Orlaith Brennan and John O'Brien within RCSI, and Nicholas Mahony and Peter O'Reilly in Trinity College Dublin. Their good-natured support continued throughout the length of this research, always willing to trouble-shoot and offer advice. It would be a much poorer body of work without their assistance and insight. Oran and Orlaith were also responsible for shepherding the flock of sheep within this study for approximately $2^1/_2$ years, under the supervision of Dr Susan Rackard, Lecturer in Small Animal Surgery UCD; absolutely none of this research would have been possible without their care and attention for the animals involved. I would also like to especially thank Fergal O'Brien, who was instrumental in initiating and overseeing this animal model here in RCSI, and whose laboratory facilities, equipment and office were always open to me.

Other colleagues also cheerfully assisted me over the years; our technicians Vincent McDonagh and Peter Kellaghan, who were always happy to give help when needed, and my academic colleagues Alice McGarvey, Garry Duffy, Jackie Daly, Alec Elliott, Tom Farrell, Henry Osbourne, Ronan Conroy & Richard Arnett. I'm also very grateful to other researchers within RCSI, John Gleeson, Peter Mauer, Ciara Murphy and Claire Tierney, who also gave helping hands along the way. I would particularly like to thank our secretary and administrator, Mary Brennan, who has been a wonderful aide since she has joined the department, and her predecessor, Amanda Campbell.

Absolutely none of this work would have happened without my supervisor, Professor Clive Lee, who I would like to sincerely thank for his continued encouragement, support, and above all else his patience, over the course of this research. The book has taken quite some time, but is now finally finished!

Declarations

I declare that this thesis, which I submit to RCSI for examination in consideration of the award of a Ph.D., is my own personal effort. Where any of the content presented is the result of input or data from a related collaborative research programme this is duly acknowledged in the text such that it is possible to ascertain how much of the work is my own. I have not already obtained a degree in RCSI or elsewhere on the basis of this work. Furthermore, I took reasonable care to ensure that the work is original, and, to the best of my knowledge, does not breach copyright law, and has not been taken from other sources except where such work has been cited and acknowledged within the text.

Signed 

Student Number 6120091

Date 2/11/12

Summary / abstract

Sheep are a practical model for postmenopausal pathologies and have been used for investigation of a number of conditions to date, including the bone diseases osteoporosis and osteoarthritis (Newton, 2004; Parker *et al*, 2003; Thorndike *et al*, 1998). With regard to many of the structural parameters, the ovine stifle joint may be considered to be a 1:3 scale model of the human knee joint (Osterhoff *et al*, 2010). 23 sheep were examined in this study; 10 of the sheep underwent ovariectomy (OVX), while the remainder (n=13) were kept as controls (CON). Five fluorochrome dyes were administered intravenously at 12 week intervals via the jugular vein to both groups, to label sites of bone turnover. These animals were then sacrificed at 12 months post-operatively.

My data showed significant alterations within the subchondral trabecular architecture at one-year post-ovariectomy, with reduced bone volume fraction, thinning of individual trabeculae and an increase in trabecular separation; these findings are consistent with those elsewhere in the ovine skeleton (Cornish *et al.*, 2006; Jiang *et al*, 2005; Mitton *et al.*, 1998; Mittra *et al.*, 2005; Nafei *et al.*, 2000; Newton *et al.*, 2004; Schorlemmer *et al.*, 2003). In addition, I confirmed that bone turnover was significantly higher in both trabecular bone and the subchondral bone plate at one-year post-ovariectomy. Remodelling of trabecular bone was due to both classically described hemi-osteonal and intra-trabecular osteonal remodelling, while osteons within the subchondral plate have relatively late mineralisation of lamellae.

The presence of osteopenia and elevated subchondral bone turnover within the medial tibial plateau provides a possible mechanism for subchondral microfractures in the aetiology of spontaneous osteonecrosis of the knee (SPONK). Further utilisation of the ovariectomised ewe would be useful for further study in this field.

I was unable to detect any measurable difference in osteoarthritis between the two study groups. While previous studies have suggested a link between trabecular thinning and osteoarthritis, I was unable to confirm this. Osteoarthritis was associated with a thinning of the subchondral plate, specifically the subchondral cortical bone. I found no correlation between bone turnover rates of either the subchondral trabecular bone or bone plate with osteoarthritis. I conclude that while ovariectomy may not increase the risk of osteoarthritis *per se*, it will cause osteopenia; if osteoarthritis then occurs, the synergy between these two disease processes will mean that the osteoarthritis in the ovariectomised group will be more severe.

Abbreviations

2D	2-dimensional
3D	3-dimensional
A-R-F sequence	Activation – resorption - formation sequence
BMD	Bone mineral density
BMU	Basic multicellular unit
BV	Bone volume
BV / TV	Bone volume fraction
Ca	Calcium
CT	Computed tomography
μCT	Micro-computed tomography
DEXA	Dual Energy X-ray Absorptiometry
DPX	Distyrene / Plasticizer / Xylene mountant
EPS	Epifluorescence microscopy
GAG	Glycosaminoglycan
h	Planck's constant
HA	Hydroxyapatite
hv	Photon energy
IV	Intravenous
MMA	Methyl Methacrylate
OA	Osteoarthritis
OARSI	Osteoarthritis Research Society International
OP	Osteoporosis
OVX	Ovariectomised
PG	Proteoglycan
PMMA	Polymerised Methyl Methacrylate
SCP	Subchondral Bone Plate
SOP	Standard Operating Procedure
SPONK	Spontaneous osteonecrosis of the knee
Tb	Trabecular
TbN	Trabecular Number
TbSp	Trabecular separation
TbTh	Trabecular thickness
TGF-β	Transforming growth factor -β
THR	Total hip replacement

Abbreviations(cont.)

TKR	Total knee replacement
TV	Total volume
UV	Ultraviolet
v	Frequency of light
WHO	World Health Organization
ZCC	Zone of calcified cartilage

Publications, Presentations and Prizes

Papers:

Subchondral trabecular structural changes in the proximal tibia in an ovine model of increased bone turnover.

JC Holland, O Brennan, OD Kennedy, S Rackard, FJ O'Brien, TC Lee

PMID: 21477184 - J Anat 2011: 218; 619–624

Subchondral osteopenia and accelerated bone remodelling post-ovariectomy – a possible mechanism for subchondral microfractures in the aetiology of spontaneous osteonecrosis of the knee?

JC Holland, O Brennan, OD Kennedy, S Rackard, FJ O'Brien, TC Lee

In press: Journal of Anatomy

Abstracts:

1. Subchondral structural changes in the proximal tibia in an Ovariectomised Ovine Model

   JC Holland, OD Kennedy, O Brennan, NJ Mahony, S Rackard, FJ O'Brien, TC Lee

   Bone, Volume 44, Supplement 2, June 2009, Pages S282-S283

2. The relationship between Osteoarthritis and Osteoporosis in an Ovariectomised Ovine model

   JC Holland, O Brennan, O Kennedy, S Rackard, FJ O'Brien, TC Lee

   Proceedings of the 14th Annual Conference of the Section of Bioengineering of the Royal Academy of Medicine in Ireland 2008; p16

The work in this thesis has been presented at the following international and national conferences:

1. Subchondral structural changes in the proximal tibia in an Ovariectomised Ovine Model

   JC Holland, OD Kennedy, O Brennan, NJ Mahony, S Rackard, FJ O'Brien, TC Lee

   European Calcified Tissue Society, Vienna, Austria, May 2009

2. The relationship between Osteoarthritis and Osteoporosis in an Ovariectomised Ovine model

   JC Holland, O Brennan, O Kennedy, S Rackard, FJ O'Brien, TC Lee

   RCSI Research Day, Dublin, 26/3/08

3. The relationship between Osteoarthritis and Osteoporosis in an Ovariectomised Ovine model

   J C Holland, O Brennan, O Kennedy, S Rackard, FJ O'Brien, TC Lee

   Bioengineering in Ireland[14], Ballincar, Sligo, 25/1/08

CHAPTER 1: INTRODUCTION AND LITERATURE REVIEW

1.1 INTRODUCTION

The skeleton is not a static structure, but is instead in a constant state of flux, adapting its form in response to alterations in dynamic load (Wolff, 1970) and also repairing or replacing bone damaged at an microstructural level (Burr, 2002). It is composed of connective tissue, the two predominant types being bone and cartilage. There are over 200 bones within the human skeleton and so, in order for these bones to form a cohesive skeletal system, they must connect or *articulate* with each other; they do this at interfaces called *joints* (Standring *et al*, 2005).

A number of conditions affect the human skeleton, particularly in older age and (in women) post-menopausally. The three I will discuss within this thesis are osteoporosis, spontaneous osteonecrosis of the knee (SPONK) and osteoarthritis. Osteoporosis is described as a metabolic bone disease, characterised by a loss or thinning of bone (Rubin *et al*, 2004). It results in considerable morbidity as it results in an increased fracture risk; the one most classically described is a fracture of the hip (Johnell *et al*, 2004). SPONK is a localized lesion that occurs at the knee joint; the aetiology is uncertain, but the main hypotheses at present are that it is initiated by vascular insufficiency or trauma (Akamatsu *et al*, 2012; Narváez *et al*, 2003; Yamamoto & Bullough, 2000). Osteoarthritis is perhaps the most puzzling at present. Originally considered a disease of articular cartilage alone, some researchers then turned their focus to the underlying subchondral bone (Burr, 2004; Radin & Rose, 1986). While many now accept that it is a disease of the joint, cartilage and bone combined, the query is now being raised as to whether it is perhaps a more generalised metabolic disorder (Aspden, 2008).

Before investigating these more clinical aspects however, I will first describe the tissues and structures involved in some greater detail; cartilage, bone and the synovial joint.

1.2 HYALINE CARTILAGE

1.2.1 Cartilage matrix

Cartilage is defined as being a connective tissue – it incorporates cells which lie within an extracellular matrix. This matrix consists of a ground substance, within which other components, such as collagen fibres and glycoproteins, are embedded. The ground substance is a firm gel, rich in carbohydrates and minerals. Typically, the cartilage matrix is extremely well hydrated, with 70 to 80% of the "wet weight" of cartilage accounted for by water (Allen, 1998) (Table 1.1). The matrix composition and cellular morphology vary according to the cartilage site and function and differences can be extremely marked between superficial and deep layers of articular cartilage; this will be examined in more detail when discussing the synovial joint.

	Wet weight	**Dry weight**	
Water	65 – 80 %$^{\Phi}$		Inorganic salts (Na^+, Ca^+, K^+, Cl^-) dissolved in the water
Collagen	10 – 30 %$^{\Phi}$	Up to 60 %$^{\dagger\lambda}$	Mainly type II collagen (80 – 90%)$^{*\dagger\Phi}$ Types VI, IX, X, XI, XII, and XIV are present in small amounts$^{*\Phi}$
Non-collagenous matrix proteins			
Proteoglycans	5 – 10 %$^{\Phi}$	Up to 25 %	Predominantly aggrecan (80 – 90%)†
Others		15 – 20 %†	i.e. glycoproteins
Cells	2 %$^{\Phi}$	< 10 %	
*Allen, 1998; †Kelly *et al*, 2004; $^{\Phi}$Kuettner *et al*, 1991; $^{\lambda}$Standring *et al*, 2005; www.med.tu.ac.th/6000/Bone_web/ lecture_2005_musculoskeleton.pdf			

Table 1.1 Components of hyaline cartilage

Collagen comprises up to 60% of the "dry weight" of the cartilage matrix. Of this, up to 90% is type II collagen, which is encoded for on the long arm of chromosome 12 (Genetics Home Reference, 2006). It consists of three $\alpha 1$ chains which are produced intracellularly, within the rough endoplasmic reticulum, in a procollagen form (Kuettner *et al*, 1991). These are assembled together in a triple helix formation and transported to the Golgi apparatus; this helix is then secreted (as tropocollagen) by the fabricating cell into the extracellular space (Standring *et al*, 2005). After cleavage of propeptide components and subsequent conversion to a collagen molecule, fibrillogenesis occurs, whereby numerous molecules associate together to form a microfibril (Standring *et al*, 2005). These may be of varying thickness; superficial fibres may be thinner than those within the deeper layers (Kuettner *et al*, 1991). The arrangement of the molecules within this microfibril, and the gaps between the adjacent molecules, give rise to the classical "banding" appearance seen in electron microscopy (Figure 1.1) (Mathews & van Holde, 1990).

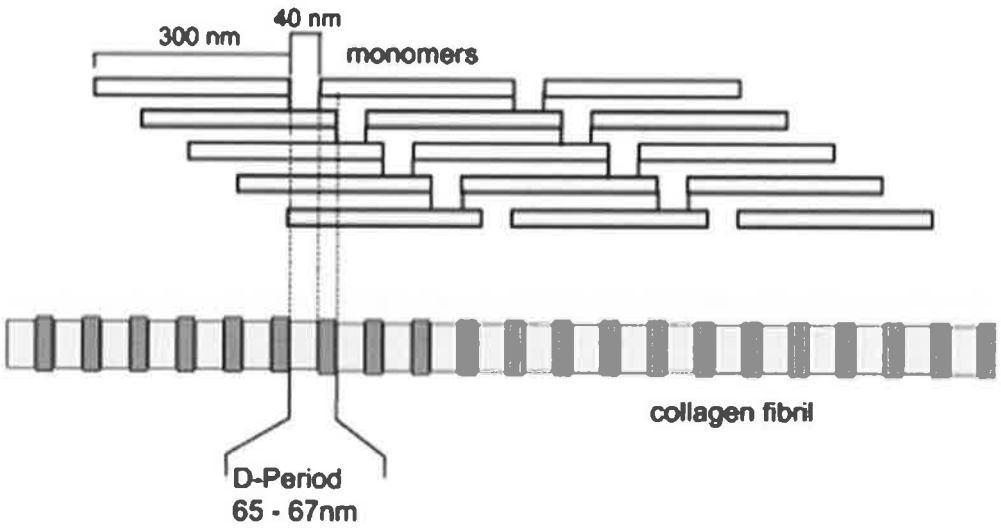

Arrangement of collagen molecules into a microfibril. This "quarter-staggered" arrangement of parallel molecules gives rise to the classic "banding" appearance seen with electron microscopy (Gelse et al, 2003)

Figure 1.1 Collagen microfibril formation and microscopic "banding"

These collagen fibrils interweave and form cross-linkages to form a three-dimensional framework (Kuettner *et al*, 1991; Mathews & van Holde, 1990). The exact number and orientation of these collagen fibres vary according to age, site or position within the cartilage itself (Standring *et al*, 2005).

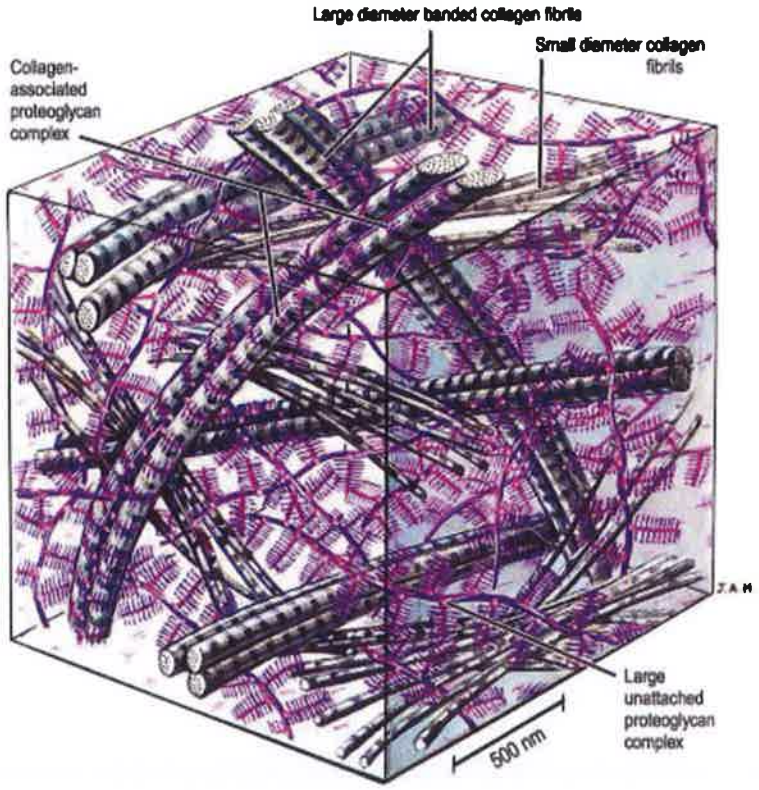

Figure 1.2 Cartilage matrix (Standring *et al*, 2005)

In addition to the type II collagen described above, there are small amounts of other forms present within articular cartilage, many of which are non-fibrillar (Figure 1.2). One of these is type IX collagen which has a number of highly unusual features with regard to its structure; its α2 (IX) chain has one or more glycosaminoglycan chains (chondroitin sulphate or dermatan sulphate) covalently bound to it, making type IX collagen, by definition, a proteoglycan (Kuettner *et al*, 1991). With regard to function, type IX collagen molecules are covalently linked to at least one fibril of type II collagen. They typically make up approximately 5-20% of the total collagen in articular cartilage (McCormack *et al*, 1987); if they are not present, the resultant collagen framework can become disorganized, with subsequent alteration of biomechanical properties (Kuettner *et al*, 1991).

Type X collagen has a much simpler structure; it consists of three identical α1 (X) chains (long arm of chromosome 6; Genetics Home Reference, 2006). It is a short chain collagen, made by hypertrophic chondrocytes during endochondral ossification or at the tidemark of the zone of calcified cartilage (Kuettner *et al*, 1991). Type XI collagen is formed by three individual chains; α1 (XI), α2 (XI) and α3 (XI), with the α3 (XI) chain probably being identical to the α1 chain of type II collagen (Genetics Home Reference, 2006). It is thought to be responsible for the thickness and spacing of the type II collagen fibrils, playing an important role as regards the structure of the collagen framework within cartilage (Kuettner *et al*, 1991). Type VI collagen, which accounts for 1 to 2 % of the collagen present within articular cartilage, is a non-fibrillar collagen (Kuettner *et al*, 1991). It incorporates three different chains within its helical structure; α1 (VI), α2 (VI) and α3 (VI) (Genetics Home Reference, 2006). It has the ability to bind intercellular matrix proteins, such as the proteoglycans biglycan and decorin (Poole *et al*, 2001).

Within the three dimensional framework formed by the collagen molecules above, lie other constituents. Proteoglycans are found in large quantities; they are important with regard to water retention and resistance to compressive forces within the cartilage (Poole *et al*, 2001). They are characterized by the presence of a central, protein core, to which are attached numerous side-chains of glycosaminoglycans (GAGs – previously called mucopolysaccharides) (Mathews & van Holde, 1990). The structure of both the protein core and the side-chains may vary, giving rise to different subclasses of proteoglycan (Figure 1.3) (Roughley *et al*, 1994).

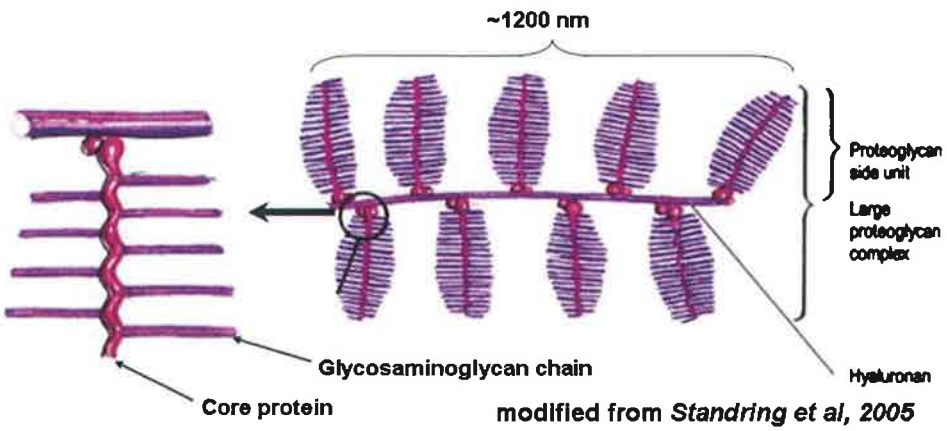

Figure 1.3 Proteoglycan structure

The most predominant proteoglycan found in articular hyaline cartilage is aggrecan (so named because it bonds with Hyaluronan; Culav *et al*, 1999). Its core protein is highly glycosylated, with approximately 100 chondroitin sulphate and 20 – 50 keratan sulphate chains attached (Culav *et al*, 1999; Kuettner *et al*, 1991). These aggrecan molecules are highly negatively charged and can absorb as much as 50 times their weight in water (Allan, 1998). This negative charge allows repulsion between aggrecan molecules, counteracting compressive forces; the osmotic pressure of their extreme hydration also assists in resisting deformation (Kuettner *et al*, 1991). A small number of other proteoglycans are present in cartilage; decorin, which coats the collagen fibrils, and biglycan, which is predominantly found in the pericellular matrix (Bock *et al*, 2001).

Some non-collagenous proteins may also be present within the cartilage matrix. The first of these is fibromodulin; this can in fact be present in a proteoglycan form as it may be glycosylated with keratan sulphate chains (Kuettner *et al*, 1991). It is found bound to collagen, and may play a role in the formation of the collagen framework by controlling fibril formation (Culav *et al*, 1999). Chondrocalcin is identical with the C-propeptide of type II pro-collagen; it has a high affinity for hydroxyapatite, suggesting a role in calcification (Kuettner *et al*, 1991). Anchorin CII, also referred to as Cartilage Annexin V, appears to act as a collagen "receptor" on the surface of chondrocytes; a number of functions have been ascribed to it, including binding of collagen and calcium channel formation (Mollenhauer *et al*, 1999).

1.2.2 Cartilage cells

The chondrocytes are responsible for secretion and maintenance of the cartilaginous matrix. Chondrocytes are derived from mesenchymal stem cells, with many authors referring to the initial immature cell as a *chondroblast* (Standring *et al*, 2005). These cells may initially be linked, but cell-cell connections are eventually disrupted as they become separated by the secretion of extracellular matrix (Standring *et al*, 2005). Once these cells are surrounded by matrix and lying within their lacunae, they are then referred to as mature chondrocytes (Figure 1.4). While lacunae within the superficial layer of cartilage typically contain a single chondrocyte, those within the deeper layers may house more than one.

Chondrocytes also display heterogeneity with regard to morphology and function, i.e. variations in shape and cell metabolism (Kuettner *et al*, 1991). Young chondrocytes may be slightly flattened, with rounded nuclei and may have more than one nucleolus; mature chondrocytes expand in size and become increasingly spherical (Standring *et al*, 2005). Their internal structure also reflects their function; young, active cells have a basophilic cytoplasm, due to an extensive rough endoplasmic reticulum, with associated Golgi apparatus and protein transport systems (Standring *et al*, 2005). As the cell becomes less active with age, the cytoplasm will then appear more vacuolated, due to the presence of large lipid droplets (Standring *et al*, 2005).

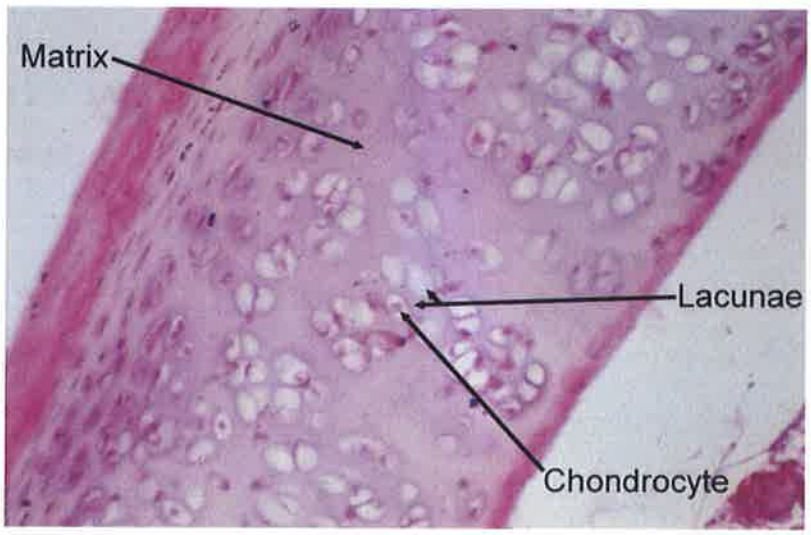

Figure 1.4 Human hyaline cartilage (Haematoxylin & Eosin stain)

1.3 BONE

1.3.1 Bone matrix

Bone is also a connective tissue, but its high mineral content gives it a greater stiffness and rigidity than cartilage. It may therefore be described as having an organic matrix, composed of collagen and other protein molecules, and an inorganic matrix, consisting of mineral salts. As with cartilage, this matrix is well hydrated, although not to the same extreme; 10 to 20% of the "wet weight" of bone is due to its water content (Standring *et al*, 2005). The composition of the matrix may vary with species, location and metabolic state – Table 1.2 outlines typical values for mature, human bone.

	Wet weight	**Dry weight**	
Water	10 – 20%		Inorganic salts (Na^+, Ca^+, K^+, Cl^-) dissolved in the water
Organic matrix			
Collagen		Approx 25%	Typically type I, with trace amounts of type III and type V
Non-collagenous matrix proteins		5 %	Predominantly proteoglycans and glycoproteins
Inorganic matrix, mineral salts		Approx 60%	Chiefly calcium and phosphate hydroxides, hydroxyapatite
Cells		10 %	
Standring *et al*, 2005			

Table 1.2 Constituents of bone

(i) Organic matrix

The organic matrix of bone is extremely tough and is essential for bone strength; without it bone would be a brittle material, easily damaged by application of shear or tensile forces. The predominant component is type I collagen, although small amounts of type V are present, which are generally found interacting with the type I collagen fibrils (Bilezikian *et al*, 2002; Standring *et al*, 2005). Type I collagen is composed of three polypeptide chains, typically two α1 (I) chains and one α2 (I) chain (encoded on the long arms of chromosomes 17 and 7 respectively), but may occasionally consist of three α1 (I) chains alone (Bilezikian *et al*, 2002; Genetics Home Reference, 2006). These chains are initially individually coiled in a left-handed helix, and then assembled together in a right-handed helix formation. As with collagen II (Section 1.1.1), the helix is secreted into the extracellular space after this folding has occurred. Non-helical extensions are removed and the collagen molecules are combined to form collagen microfibrils (Bilezikian *et al*, 2002).

Multiple microfibrils subsequently combine together to form collagen fibrils. These lie within the ground substance of the bone, in parallel or irregular arrays (in lamellar or woven bone respectively – see Section 1.2.3) (Standring *et al*, 2005). Secretion and deposition of collagen in this manner is the initiating step in bone formation, and is mainly produced by osteoblasts; it is referred to as osteoid in this form, prior to its eventual mineralisation (Standring *et al*, 2005). With regard to the deposition of mineral salts, it is reported that up to two-thirds of the mineral content of bone is found *within* the collagen fibrils, rather than surrounding them (Standring *et al*, 2005). The gaps between the collagen molecules, as they combine to form microfibrils (Figures 1.1 and 1.5, Section 1.1.1), are thought to be where initial crystallization of these minerals from their soluble forms occurs, with deposition ensuing thereafter (Bilezikian *et al*, 2002).

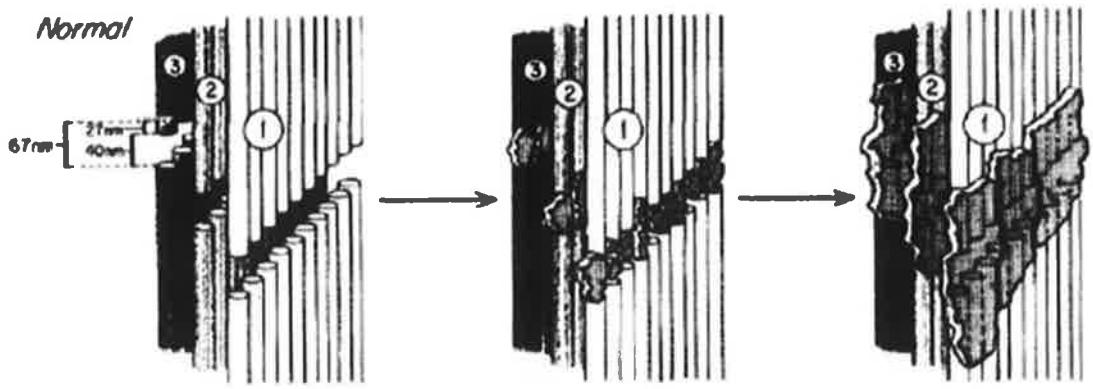

Landis W.J., Bone, 16(5):533–544, 1995

Figure 1.5 Deposition of mineral salts within collagen microfibrils

In addition to type I collagen, small amounts of other collagens are present within bone. The small amounts of type V collagen present are thought to play a part in fibrillogenesis of the type I tropocollagen molecules, regulating fibril diameter and orientation (Standring *et al.* 2005). It can be formed either by three α1 (V) chains or two α1 (V) chains and one α2 (V) chain, encoded for on the long arms of chromosomes 9 and 2 respectively (Genetics Home Reference, 2010). Over 50% of classical Ehlers-Danlos syndrome cases are caused by mutations in the gene for the α1 (V) chain; abnormalities in the α2 (V) chain will cause a less common form (Genetics Home Reference, 2010). Type III collagen is also encoded for on the long arm of chromosome 2; an abnormality in this gene will also give rise to a form of Ehlers-Danlos syndrome (Genetics Home Reference, 2010).

While collagen is the predominant constituent of the organic matrix within bone, a number of other, non-collagenous, components also exist; the proteoglycans and glycoproteins. The most common proteoglycans found in bone are decorin and biglycan, which in bone typically have GAGs of chondroitin sulphate; it is hypothesized that they are prime facilitators of hydroxyapatite precipitation and crystallization (Bilezikian *et al*, 2002). These proteoglycans have also been found to bind to transforming growth factor (TGF)-β, and to inhibit bone-cell attachment *in vitro*, suggesting a functional role in cell-matrix interactions (Bilezikian *et al*, 2002).

Increasing numbers of glycoproteins have been identified within the organic matrix in recent years (Table 1.3). These are proteins which carry covalently attached oligosaccharide or polysaccharide chains (Mathews & van Holde, 1990). Within bone, they are mainly produced by osteoblasts, but at different stages of maturation, and so exhibit a wide variety of functions, from cell proliferation and adhesion to hydroxyapatite crystallization and matrix mineralisation. Clinically, many of these glycoproteins are easily quantified by standard hospital laboratory techniques, and are used as markers or indicators for specific cell function and disease states.

Name	**Produced by**	**Main functions**
Alkaline phosphatase	Various cells and isoenzymes	*Essential for normal matrix mineralisation. Reliable serum indicator of osteoblast function.
Osteonectin	Osteoblasts, platelets	*†Binds to collagen and hydroxyapatite. May mediate hydroxyapatite crystallization and deposition.
Osteocalcin	Osteoblasts	†Binds to hydroxyapatite and calcium. May regulate osteoclast activity. Used as a serum marker of new bone formation
Osteopontin (BSP-I)	Osteoblasts	*†Mediates cell attachments, including osteoclasts. Possible role in bone loss secondary to oestrogen-deficiency
Bone Sialoprotein (BSP-II)	Chondrocytes, osteoblasts and osteoclasts etc.	*High affinity for calcium. Initiates hydroxyapatite crystallization *in vitro*. Mediates cell attachments.
*Bilezikian *et al*, 2002; †Standring *et al*, 2005		

Table 1.3 Principal glycoproteins within the organic bone matrix

(ii) Inorganic matrix and mineral salts

It is the mineral content of the bone, or its inorganic matrix, which is responsible for its rigidity and resistance to compressive forces – without mineralisation, bone would be a flexible, malleable material. Initially, an unmineralised matrix containing collagen and other organic components is deposited by active osteoblasts; this is referred to as osteoid (Section 1.2.4) (Buckwalter *et al*, 1987). These osteoblasts will then regulate the subsequent mineralisation of this matrix. The speed (also called lag time) and method of mineral deposition will vary according to species, pathology and type of bone. Lamellar bone will reach 70 – 80% mineralisation within 3 weeks or so; here, initial nucleation of crystals appears to begin in the spaces between collagen molecules, as they combine themselves in the characteristic "quarter-staggered" arrangement to form microfibrils (Figures 1.1 & 1.5) (Standring *et al*, 2005). Mineralisation within woven bone progresses at a faster rate, and appears to be initiated away from the osteoblast surfaces, by the budding and releasing of matrix vesicles; initial crystallization occurs within these vesicles, which then rupture, providing a nidus for mineralisation of the intercellular matrix (Bilezikian *et al*, 2002).

The predominant mineral found within bone is hydroxyapatite, incorporating calcium, phosphate and hydroxyl ions - $Ca_{10}(PO_4)_6(OH)_2$ (Standring *et al*, 2005). This is extremely relevant with regard to homeostasis of these minerals within the body - 99% of the total body of content of calcium is found deposited in bone in this fashion, and 85% of total phosphate (Whitby *et al*, 1994). Other minerals are also present within bone, although many only in trace amounts; examples include magnesium, citrate, sodium, potassium, carbonate, chloride, aluminium, lead, copper, iron and zinc (Bilezikian *et al*, 2002; Whitby *et al*, 1994).

1.3.2 Bone cells

Four different cell types are associated with bone tissue. Those that are concerned with bone formation are closely related, all being derived from mesenchymal stem cells (as are chondrocytes); these are the osteoprogenitor cell, the osteoblast and the mature osteocyte (Aubin, 1998; Bilezikian *et al*, 2002; Ross *et al*, 1989; Standring *et al*, 2005). The osteoclast, responsible for bone resorption, is of a different origin; it is thought to share a common precursor with the monocyte-macrophage lineage (Bilezikian *et al*, 2002; Standring *et al*, 2005).

(i) Osteoprogenitor cell

Osteoprogenitor or bone lining cells populate the innermost lining of the periosteum, and also line the inner surfaces of the bone marrow cavity (endosteal lining cells) and the Haversian and Volkmann's canals (Section 1.2.3) (Standring *et al*, 2005). They are derived from mesenchymal stem cells, with limited capacity for self-renewal, and eventually undergo further differentiation in response to an appropriate signal (Rodan, 1992). In addition to developing into osteoblasts (and hence osteocytes), they have the ability to differentiate into adipose cells, chondroblasts, and fibroblasts (Aubin, 1998). Furthermore, it has been demonstrated that even after differentiation to a mature, osteocalcin-expressing osteoblast, these daughter cells still retain the potential to transdifferentiate to an adipocyte lineage (Aubin, 1998).

Microscopically, this cell may be difficult to visualize using transmitted light alone, typically being a small, lightly staining, spindle-shaped cell (Rubin *et al*, 2004). Their internal morphology varies according to site and activity (Aubin, 1998). When these cells are present on growing bones, they have a slightly basophilic cytoplasm, due to the presence of rough endoplasmic reticulum, free ribosomes and Golgi apparatus. When growth or remodelling of the underlying bone is not occurring, the cells only have a scant number of cytoplasmic organelles present (Rodan, 1992; Ross *et al*, 1989).

(ii) Osteoblast

Osteoblasts are derived from osteoprogenitor cells and have responsibility for the production and subsequent mineralisation of the surrounding bone matrix (Standring *et al*, 2005). With regard to morphology, they are generally cuboidal or polygonal (15 – 30 μm in diameter), with a single nucleus and basophilic cytoplasm (Standring *et al*, 2005). Further characteristics of these cells reflect their main functions; synthesis and secretion. The marked cytoplasmic basophilia is due to a prominent Golgi apparatus, with extensive rough endoplasmic reticulum and free ribosomes (Rubin *et al*, 2004; Standring *et al*, 2005). Electron microscopy reveals multiple, fine cytoplasmic processes that can extend from their plasma membranes to communicate with other cells via gap junctions; these may be other surface osteoblasts, or cells embedded within the matrix - the osteocytes (Ross *et al*, 1989; Rubin *et al*, 2004; Wood & Ellis, 1994).

With regard to matrix formation, the osteoblasts initially produce an eosinophilic, unmineralised matrix named osteoid at a rate of approximately 0.5 - 1μm per day. Mineral salts are then subsequently deposited and this mineralisation lag time may vary with species and pathology. However, because of this, active osteocytes are rarely seen lying *directly* on the bone surface, rather they are separated from it by a thin, eosinophilic seam of osteoid (Rubin *et al*, 2004). The osteoblast has a functional life span of approximately 5 – 6 months; this can vary and may range from between 3 and 18 months (Rodan, 1992; Ross *et al*, 1989; Wood & Ellis, 1994).

(iii) Osteocyte

The osteoblast will eventually become entirely surrounded by the matrix which it has secreted; this mineralizes, and the cell becomes trapped within a lacuna – it is now a mature osteocyte (Figure 1.6; Rubin *et al*, 2004). The osteocytes are the most numerous cell type within mature bone and are usually easily recognizable, being situated in an orderly fashion within the bone matrix (Figure 1.8; Standring *et al*, 2005). They are typically stellate, approximately 25 μm in diameter, and have a single nucleus (Bilezikian *et al*, 2002; Standring *et al*, 2005). In contrast to osteoblasts, they have few cytoplasmic organelles. While the osteoblasts are highly active in secretion and mineralisation of matrix, the mature osteocytes have a more limited capacity, being mainly concerned with homeostasis, and hence they have less need for extensive protein production and secretion mechanisms (Bilezikian *et al*, 2002). They do, however, share with osteoblasts the characteristic of multiple cytoplasmic processes, by which the embedded osteocytes may communicate with each other (Rubin *et al*, 2004). These processes run in fine channels within the bone matrix, named *canaliculi*, which may be as little as 0.25 μm in diameter (Standring *et al*, 2005). Some authors describe this network of interconnected osteocytes as the *osteocyte syncytium*, reflecting the functional coordination of these cells with regard to calcium homeostasis and bone maintenance (Bilezikian *et al*, 2002). There are estimated to be approximately 26,000 lacunae and 1 x 10^6 canaliculi per mm^3 of cortical bone (Martin & Burr, 1989).

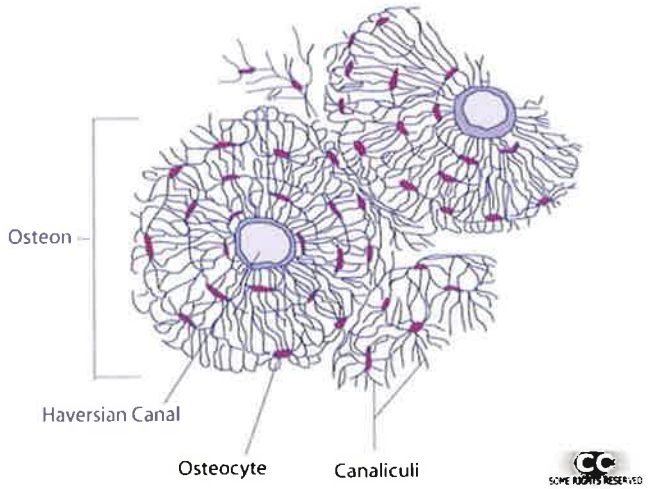

From: Gray's Anatomy of the Human Body, amended by Bduttabaruah

Figure 1.6 Osteocytes within compact bone

(iv) Osteoclast

As stated previously, osteoclasts derive from a different lineage than those cells concerned with bone formation and maintenance. They develop from stem cells within the bone marrow, specifically those of the monocyte-macrophage family (Athanasou, 1996; Bilezikian *et al*, 2002). Morphologically, they are the largest of the bone cells, being 40 – 100 μm in diameter. They possess a variable number of nuclei (typically 15 – 20) and contain many cytoplasmic lysosomes, rich in enzymes and acids (Athanasou, 1996). Perhaps their most striking feature, however, is the *ruffled border*, where the cell membrane is highly convoluted or folded (Athanasou, 1996; Bilezikian *et al*, 2002). This occurs along the side of the osteoclast that lies upon the adjacent bone and is concerned with resorption. At its edge, is the *sealing zone*; this adheres tightly to the bone, and so encloses a small space between the osteoclast and the bone into which carbonic acid enzymes, such as collagenase, are released and bone resorption occurs (Bilezikian *et al*, 2002). As this progresses, the osteoclast is then visualized lying within a depression on the bone surface; this is called a Howship's lacuna or resorption bay (Athanasou, 1996; Bilezikian *et al*, 2002).

Functionally, the osteoclast is magnificently designed for resorption of mature bone; additionally, it is effective with regard to resorption of calcified cartilage (Bilezikian *et al*, 2002; Rubin *et al*, 2004). It is limited, however, in that it cannot function if the matrix is not mineralized; bone lined by osteoid or unmineralised cartilage is safe from its depredation (Rubin *et al*, 2004). This can be problematic in diseases such as rickets; the failure of the growth plate to calcify normally protects it from osteoclastic resorption, with subsequent overgrowth and hypertrophy (Rubin *et al*, 2004).

1.3.3 Structure of bone

(i) Macroscopic structure

Bones typically appear white or pale yellow to the naked eye; on further examination, they can be seen to be composed of bone tissue of varying apparent density (ratio of bone mass to volume). Briefly, cortical bone appears to be solid, with a ratio of > 0.7; it composes up to 80% of the mature skeleton and will typically form the hard, outer surface of all bones, providing mechanical strength and protection (Carter & Beaupré, 2001). Cancellous bone has a ratio of < 0.7 and may also be referred to as spongy, or trabecular bone; the cut surface of cancellous bone has a honeycomb appearance, due to the interlacing of multiple, small trabeculae (Carter & Beaupré, 2001; Rubin *et al*, 2004).

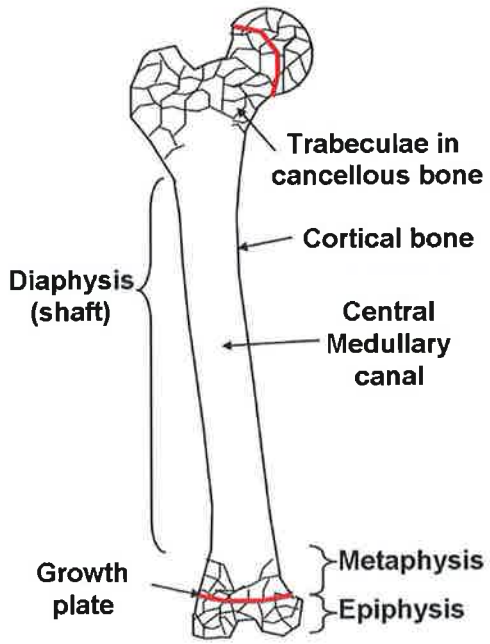

Figure 1.7 Structure of a long bone

Bones may initially be classified into different groups according to their shape (long, short, flat and irregular). With regard to long bones, a number of different anatomical parts may be identified (Figure 1.7). The shaft, or diaphysis, of a long bone is mainly composed of a cylinder of cortical bone with a small number of trabeculae on the inner surface, facing an internal medullary cavity (Rubin *et al*, 2004). At either end of the bone are the epiphyses, extending from the growth plates within the bone to the articulating surfaces at either extremity. Between the epiphysis and diaphysis lies a section of transitional bone, with cortical and cancellous components, named the metaphysis (Rubin *et al*, 2004).

As mentioned previously, an articular surface will usually be present at either end of a long bone; this is where it articulates with an adjoining bone to form a joint. The articular surface is covered with cartilage, typically hyaline, which overlies a plate of subchondral cortical bone, supported by underlying trabeculae (Burr, 2003). On the external surface of the remainder of the bone lies the periosteum; this is a covering of dense connective tissue, the inner layer of which will contain variable numbers of osteoblasts, the outer layer being fibrous (Standring *et al*, 2005). A comparable covering also lines the inner cavities and surfaces of the bone, namely the central medullary canal and the trabeculae within the cancellous components; this is termed the endosteum and may provide a total surface area of $7.5m^2$ in an adult (Standring *et al*, 2005).

Within the central medullary canal and the spaces between the trabeculae of the cancellous bone lies the bone marrow, of which there are three main forms; red marrow, which is haemopoetic, yellow marrow, mainly composed of adipose tissue, and white marrow, which may be quite fibrotic (Rubin *et al*, 2004). The vascular supply to a large bone has a number of components. The diaphysis will generally be supplied by nutrient arteries which pass through foramina in the cortical bone to enter the medullary cavity; here they will divide into numerous branches which form a sinusoidal network within the substance of the bone (Rubin *et al*, 2004; Standring *et al*, 2005). The metaphysis shares this blood supply, but also receives contributions from small arteries that arise in the overlying periosteum and enter the bone locally (Rubin *et al*, 2004; Standring *et al*, 2005). The epiphyses have a separate blood supply; their nutrient arteries entering distal to the growth plate (Standring *et al*, 2005).

(ii) Microscopic structure

With regard to description of the intermediate or microscopic structure of bone, there are a number of factors to be taken into consideration, which leads to variation between classification systems. First, the orientation of the collagen fibres may be *woven* or *lamellar*, referring to the orientation of the collagen fibres within the resultant matrix (Rubin *et al*, 2004). Additionally, bone may be referred to as *primary* if it is deposited where bone has not existed before (but requires some form of pre-existing structure i.e. cartilage) and *secondary* if it is produced as a result of resorption of existing bone and deposition of new bone in its place (Martin & Burr, 1989).

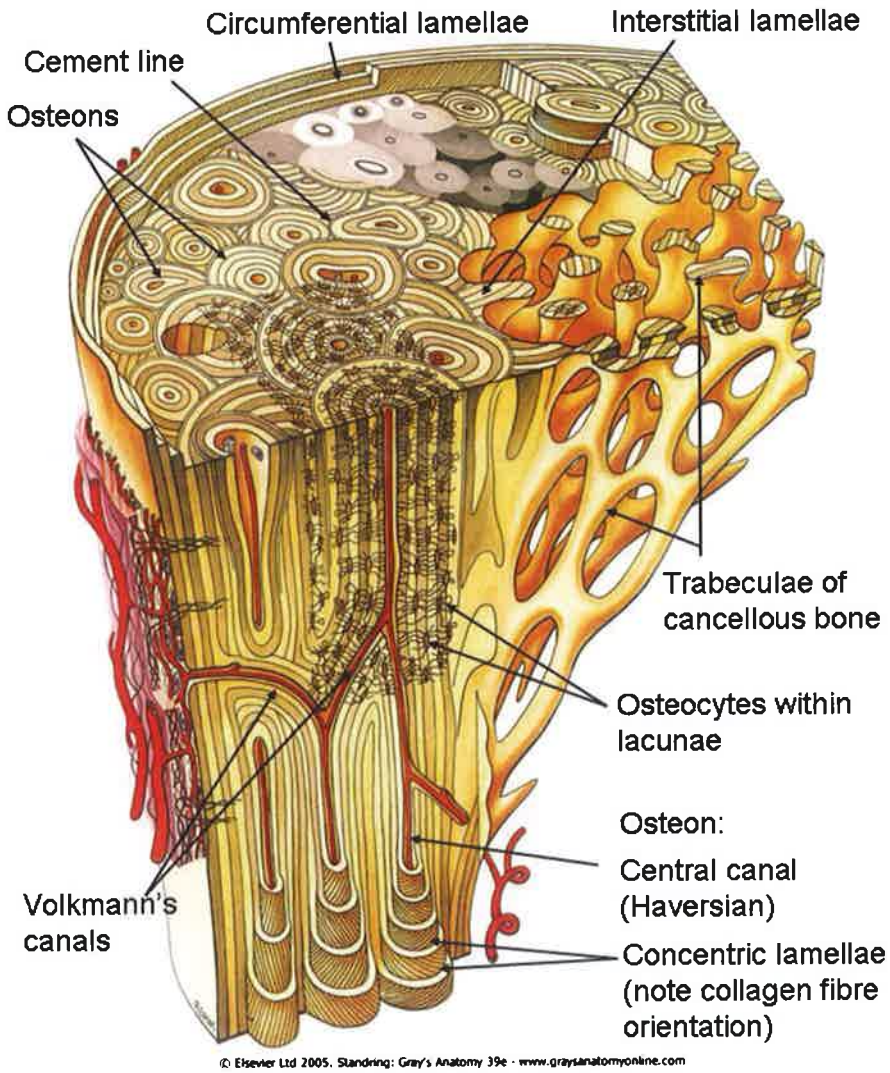

Figure 1.8 Microstructure of Bone (Standring *et al*, 2005)

Woven Bone

The primary microscopic feature of woven bone is the irregular arrangement of the collagen fibres within the bone matrix; other features include numerous osteocytes present within the matrix and variance in the number and morphology of these cells. Woven bone is deposited more quickly than other forms and is the only form of bone that may be formed by the body *de novo*, without need for a pre-existing substrate or scaffold on which to grow (Frost, 2004; Martin & Burr, 1989). It is typically seen in rapidly deposited fracture calluses or at tumour sites; while it is found naturally in foetal skeletons and those below 5 years of age, its presence in an adult skeleton is always abnormal (Martin & Burr, 1989; Rubin *et al*, 2004).

Lamellar Bone

Lamellar bone is formed at a slower rate than woven bone, and has a highly organized microstructure; it is the normal form found within the adult skeleton (Rubin *et al*, 2004). It is characterized by the regular, parallel arrangement of the collagen I fibrils and the uniform morphology and distribution of the osteocytes within its substance (Rubin *et al*, 2004). There are four subtypes of lamellar bone (Martin & Burr, 1989; Rubin *et al*, 2004):

- Circumferential
    - These lamellae are arranged as circular rings forming the outer (periosteal) and inner (endosteal) layers of the cortex of the bone, i.e. the entire circumference of the whole bone (Figures 1.8 & 1.9).

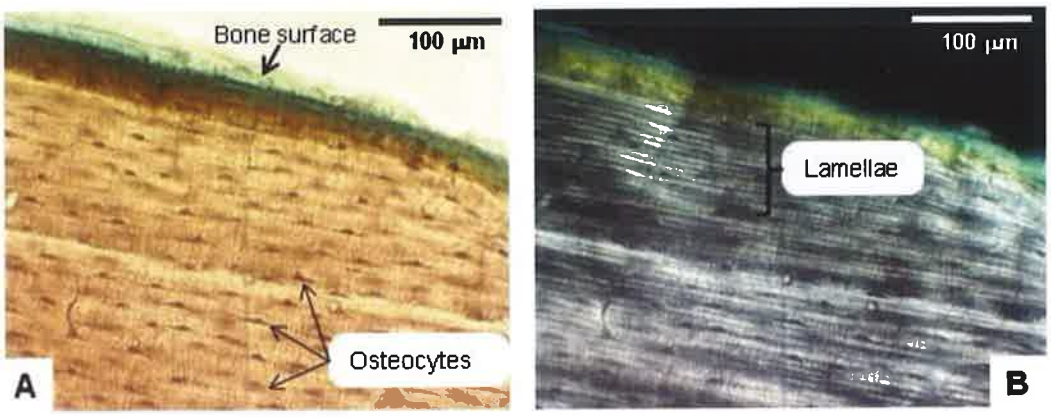

Circumferential lamellar bone viewed under (A) transmitted and (B) polarized light
Slide prepared by TC Lee; photography by JC Holland

Figure 1.9 Circumferential lamellar bone (Ovine)

- Concentric
    - Concentric lamellae are arranged in rings around a central vascular channel, forming an osteon, which may be primary or secondary.
    - The primary osteon, as the name suggests, is new bone, formed on a pre-existing substrate. The main distinguishing characteristic between primary and secondary osteons is that primary osteons lack a cement line (Figure 1.8).
    - The secondary osteon is formed as a result of bone remodelling (Section 1.2.4). The central channel is referred to as a *Haversian canal*; additional vascular channels run horizontally between the Haversian canals, these are referred to as *Volkmann's canals*.
- Interstitial
    - These are seen in circumferential or concentric lamellar bone that has been subsequently remodelled, leaving remnants of the original bone wedged between the newly-formed osteons (Figure 1.10).

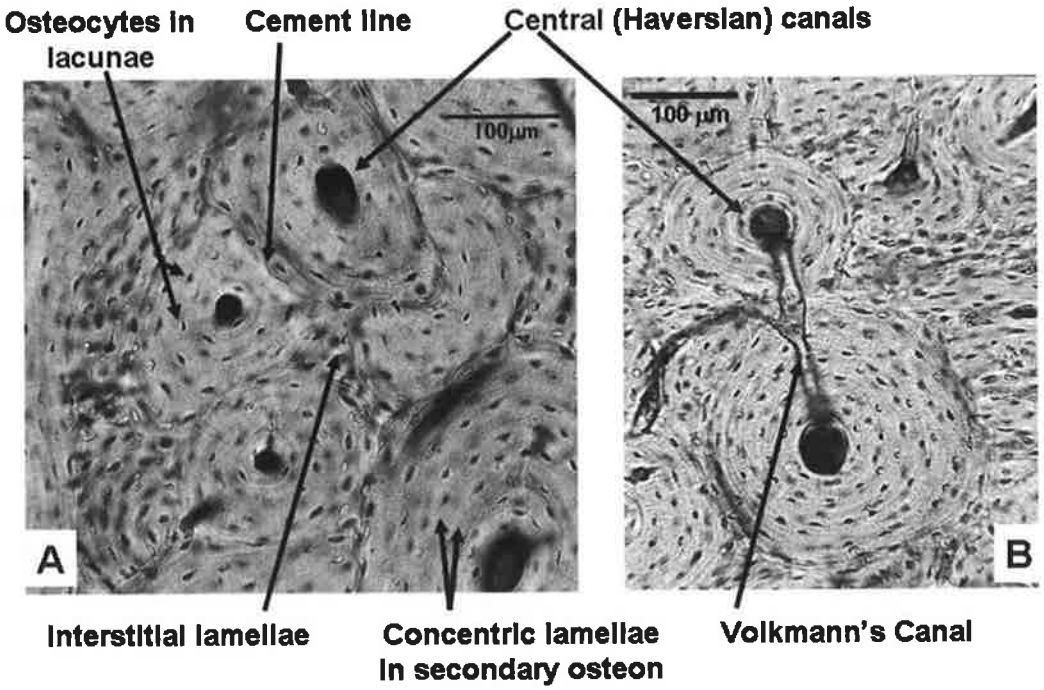

Figure 1.10 Concentric and interstitial lamellar bone (transverse section – ovine bone)

- Trabecular
    - Sheets of lamellar bone perforated by marrow spaces to form the trabeculae of cancellous bone (Figure 1.8).
    - Trabecular bone may be further described as "rod-like" or "plate-like"

Fibrolamellar Bone

While the woven and lamellar forms of bone as described above are those most frequently seen in nature, a third form may be found in large, rapidly growing animals. While much less common in humans, it has been observed in growing children, particularly when undergoing rapid growth spurts. This is referred to as fibrolamellar, or *plexiform* bone (Figure 1.11) (Martin & Burr, 1989).

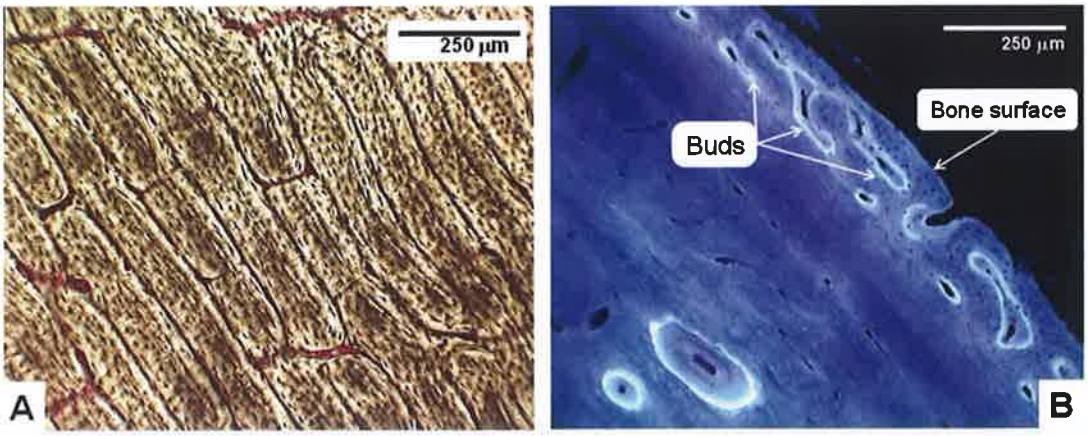

(A) Ovine plexiform bone viewed under light microscopy
(B) Formation of plexiform bone by periosteal budding, labelled by fluorochrome administration *in vivo*, viewed under UV epifluorescence

Slides prepared by TC Lee Photographs by Jane Holland

Figure 1.11 Fibrolamellar or plexiform bone (ovine)

Fibrolamellar bone may be thought of as a compromise; it is deposited rapidly, like woven bone, but allows for greater mechanical strength (although not quite as great as lamellar bone). Like other forms of primary bone, it must be formed on a pre-existing substrate. It forms from buds that initially grow perpendicularly from the surface of the existing bone, then horizontally. The buds then unite with each other, and a vascular space is enclosed, between the "bridge" formed by the buds and the surface of the pre-existing bone. This space is then gradually filled as bone is gradually deposited along its surfaces (Martin & Burr, 1989).

1.3.4 Bone formation, growth and maintenance

(i) Ossification

During embryogenesis, the skeleton develops from mesenchymal cells, typically of mesodermal origin; within the head and neck, some neural crest cells will also contribute to development of skull and facial bones by differentiation into mesenchymal cells (Sadler, 2004). While the majority of the skeletal bones develop by endochondral ossification from a hyaline cartilage model, a small number will form by a process known as intramembranous ossification (Standring *et al*, 2005).

Intramembranous ossification

Intramembranous ossification is classically described during formation of the flattened bones of the cranial vault, although a small number of additional skeletal bones are formed in this manner (i.e. mandible, clavicle) (Sadler, 2004). The mesenchymal cells involved in this process are derived from the *neural crest* and not from mesoderm-derived cells, as is the case in endochondral ossification (Sadler, 2004). These mesenchymal cells initially form layers or "membranes" that become highly vascular. Some of the cells within this layer undergo vasculogenesis, differentiating into blood cells to form capillaries which contribute to this vascularity; others develop into osteoprogenitor cells and begin the process of ossification (Standring *et al*, 2005).

The osteoprogenitor cells proliferate in proximity to the developing capillary network and differentiate to form osteoblasts. These osteoblasts then proceed to secrete osteoid and collagen fibres from the cell surfaces that face away from the blood vessels (Standring *et al*, 2005). Mineralisation of the matrix then progresses; the earliest crystals, which provide a nidus for further mineralisation, are produced by the budding and releasing of matrix vesicles from the osteoblasts, as described in Section 1.2.1 (Standring *et al*, 2005). As mineralisation of the osteoid progresses radially from this ossification centre, spicules of bone are formed within the mesenchymal membrane; osteoblasts may become trapped within this calcified matrix and thus differentiate into osteocytes (Gilbert, 6th edn). Finally, a condensation of mesenchymal cells at the periphery of the newly-formed bone will form the periosteum (Standring *et al*, 2005).

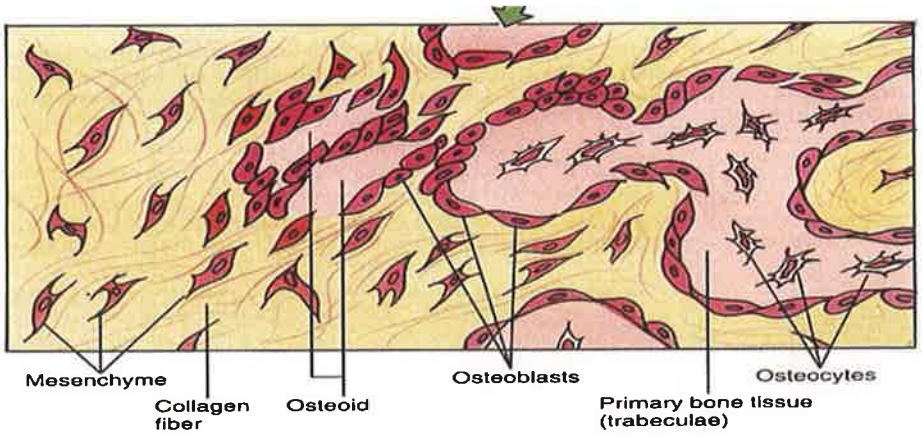

http://www.mc.vanderbilt.edu/histology/labmanual2002/labsection1/boneform&synovialjoints03.htm

Taken from: **Gartner and Hiatt, Color Textbook of Histology**, *p. 122, Figure 7-12*

Figure 1.12 Intramembranous ossification

Endochondral ossification

The majority of skeletal bones are formed by endochondral ossification. This involves initial formation of a cartilaginous *anlage*, or model, which will then develop and eventually be replaced by bone (Rubin *et al*, 2004). The majority of the mesenchymal cells involved with this development are derived from paraxial and lateral plate mesoderm within the developing embryo. Part of the paraxial mesoderm differentiates into *sclerotomes* by the 4th week of development, which will be the point of origin of most of the mesenchymal cells; the remainder are derived from the mesoderm of the body wall, which develops from the lateral plate mesoderm (Sadler, 2004).

The initial step in endochondral ossification is formation of the cartilaginous anlage (Figure 1.13). This begins by the differentiation of the mesenchymal cells into chondroblasts, which clump together to form compact nodules. Additional mesenchymal cells form a surrounding, vascular perichondrium. The chondroblasts within the nodule proliferate and lay down an extracellular collagenous matrix, thus initiating formation of the *anlage* by interstitial growth. Additional chondroblasts lining the perichondrium also contribute to cartilage formation on the periphery of the *anlage*; this process is termed appositional growth (Rubin *et al*, 2004).

The next stage in this process is the development of the primary ossification centre. Chondrocytes within the *anlage* stop dividing and begin to hypertrophy, so that the matrix lying between the cells becomes compressed into thin septae or struts; the components within the matrix are further altered by the chondrocytes so that it becomes mineralised by calcium carbonate (Gilbert, 6th edn). As the matrix mineralises, nutrients can no longer diffuse into the *anlage* to supply the chondrocytes; apoptosis of these cells occurs, with subsequent lacunae remaining (Rubin *et al*, 2004; Standring *et al*, 2005).

In conjunction with these alterations within the shaft, the perichondrium will also metamorphose. The cells lining the perichondrium undergo a form of intramembranous ossification in order to form a collar of bone surrounding the shaft of the anlage; the perichondrium is now renamed the periosteum (Standring *et al*, 2005). Small osteogenic buds are then formed from the periosteum, and penetrate through the bone collar to reach the lacunae within the shaft, bringing with them blood vessels, mesenchymal cells and osteoclasts (Standring *et al*, 2005). Osteoblasts then proceed to deposit osteoid, which mineralises to form bone, along the surfaces of the calcified cartilage struts; when these struts are fully encased by woven bone, they are termed primary trabeculae, or the *primary spongiosum* (Rubin *et al*, 2004; Standring *et al*, 2005).

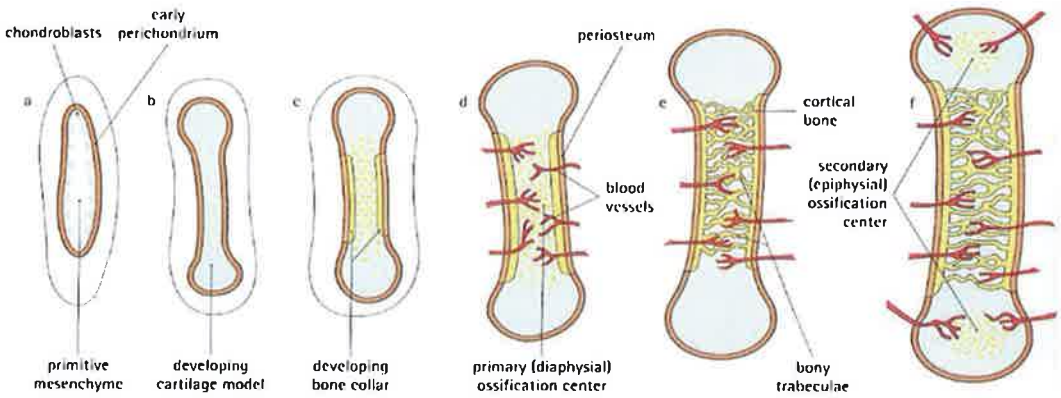

http://www.mc.vanderbilt.edu/histology/labmanual2002/labsection1/boneform&synovialjoints03.htm

***Taken from*: Stevens and Lowe, Human Histology**, *p. 246, Figure 13.24*

Figure 1.13 Endochondral ossification

Within the developing bone, ossification typically proceeds from the primary centre to extend both proximally and distally along the diaphysis; the primary trabeculae so formed will eventually undergo osteoclastic resorption and new bone deposition (remodelling) in order to form secondary trabeculae (Standring *et al*, 2005). In addition to the primary ossification centre within the diaphysis, secondary ossification centres will form within the epiphyseal cartilages at either end of the bone, usually postnatally (Figure 1.14) (Rubin *et al*, 2004; Standring *et al*, 2005). As the secondary centres enlarge, they do so in a pattern referred to as hemispherisation (Rubin *et al*, 2004). The ossification of the cartilaginous anlage progresses, until the ossification fronts meet; at this point a zone of cartilage is then trapped between the epiphysis and the diaphysis, and is referred to as the epiphyseal or growth plate (Rubin *et al*, 2004).

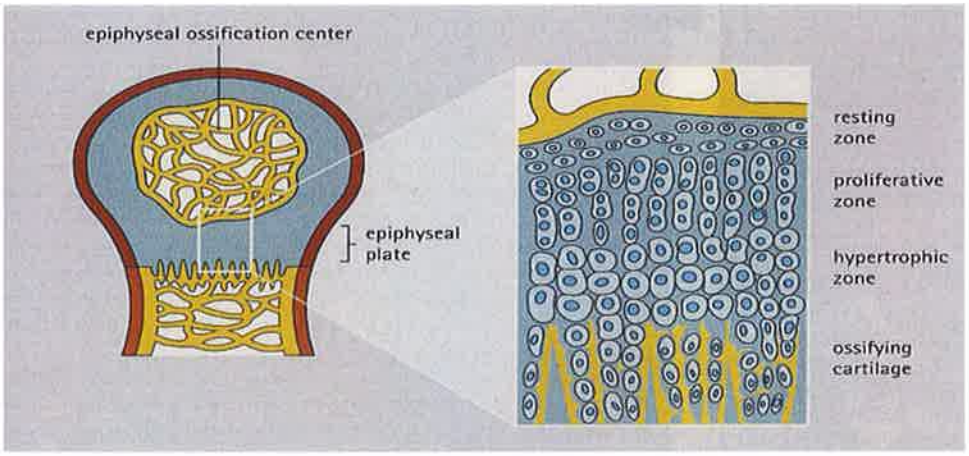

http://www.mc.vanderbilt.edu/histology/labmanual2002/labsection1/boneform&synovialjoints03.htm

Taken from: **Stevens and Lowe, Human Histology,** ***p. 247, Figure 13.25.***

Figure 1.14 Secondary ossification centre and epiphyseal plate

The epiphyseal plate can be more precisely described as a layer of modified cartilage; new cartilage continues to be formed here, which is then replaced by bone, and so the bone continues to enlarge in length during development (Rubin *et al*, 2004; Standring *et al*, 2005). The epiphyseal plate can be divided into layers, with chondrocytes at different stages of their life cycle being present in each layer (Rubin *et al*, 2004). This epiphyseal plate is eventually obliterated and replaced by bone. The age at which this process is complete is dependent on a number of factors, including gender, hormonal influences and the specific bone involved (Rubin *et al*, 2004; Standring *et al*, 2005).

(ii) Modelling

So, during development and growth, an increase in the length of the bone can be attributed to continuous endochondral ossification occurring at the epiphyseal plates, as described above. An increase in the *diameter* of the bone may occur as a result of intramembranous ossification by the periosteum of the diaphysis, with resorption occurring at the endosteum. This alteration or adaptation of the bone may be referred to as modelling; more precisely, modelling can be described as either bone formation or deposition occurring in the absence of prior resorption, or bone resorption without immediate bone formation or deposition occurring at the same surface (Martin & Burr, 1989). An example is seen in the diagram below (Figure 1.15), where the diameter of the diaphysis increases due to bone formation on the periosteal surface in parallel with bone resorption on the endosteal surface. Bone modelling may result in an increase or a decrease in bone volume; if resorption and formation occur simultaneously at separate surfaces of the bone, it is possible that the *overall* volume of the bone is unchanged (Martin *et al*, 1998).

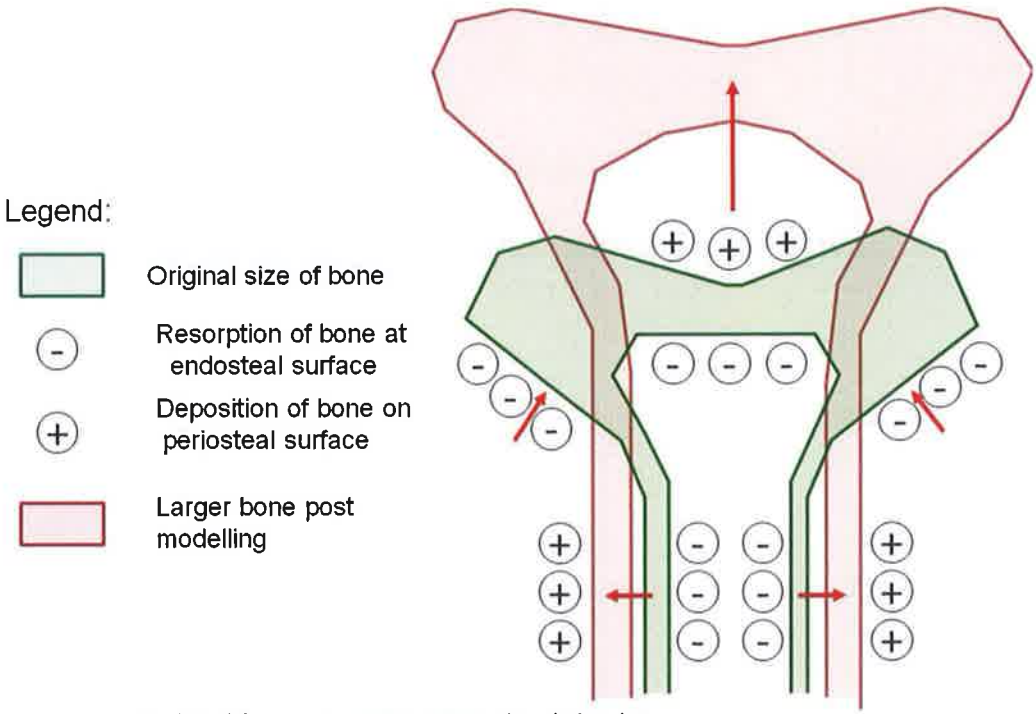

Modified from: **Jee WSS, 1983**, The skeletal tissues;
In **Weiss L (Ed.)** ***Histology, Cell and Tissue Biology***

Figure 1.15 Bone modelling

(iii) Remodelling

In contrast to bone modelling, remodelling involves the processes of bone resorption and formation occurring in succession. In this process, older bone is removed and replaced with new bone; the volume of bone is unchanged (or decreased), it is the microstructure of the bone which is altered. Remodelling consists of an activation phase (A), followed by bone resorption (R) and then eventual formation of new bone (F) – the A-R-F sequence (Martin & Burr, 1989). Remodelling of bone is thought to serve three main functions: it allows the body to mobilise minerals deposited within the skeleton; it allows for functional adaptation of the bone in response to mechanical stimuli (Section 1.3.1); and it accommodates repair of accumulated damage within the skeleton (Burr, 2002). This is performed by a group of cells acting in concert to form a functional unit – the basic multicellular unit (BMU), which consists of around 10 osteoclasts and a few hundred osteoblasts (Martin *et al*, 1998). While a BMU may have a life span of 2 – 8 months, those of the individual cells within it will be much shorter (Parfitt, 1994).

Described simply, the BMU functions by removing old mineralised bone at its "cutting edge", and then depositing new bone within the resulting void to form a secondary osteon with a central (Haversian) canal and blood vessel. The cutting edge progresses at a rate of 20 - 40μm/day; resorption of bone takes 3 weeks, with deposition of new bone complete after 3 months (Martin *et al*, 1998; Parfitt, 2002). A more detailed explanation of the remodelling sequence divides this process into 6 sequential phases. ***Origination*** of a new BMU will occur on the surface of a region of quiescent bone, where precursor cells for the BMU are recruited and subsequently differentiate into osteoclasts. The cutting edge of the BMU forms and advances at a rate of 20 – 40μm per day as ***resorption*** of bone by osteoclasts occurs; this will typically be 200 - 300μm in diameter. A ***reversal*** period then ensues, with cessation of osteoclastic activity and convergence of osteoblasts. ***Formation*** of new bone follows; osteoid is deposited in lamellae by the osteoblasts and begins to mineralise after 15 days (Figures 1.16 & 1.17). ***Mineralisation*** is initially rapid (60% complete after 24 hours) but then slows, with full mineralisation taking 6 months or so to accomplish. The final stage in this cycle is a return to ***quiescence*** (Bilezikian, 2004).

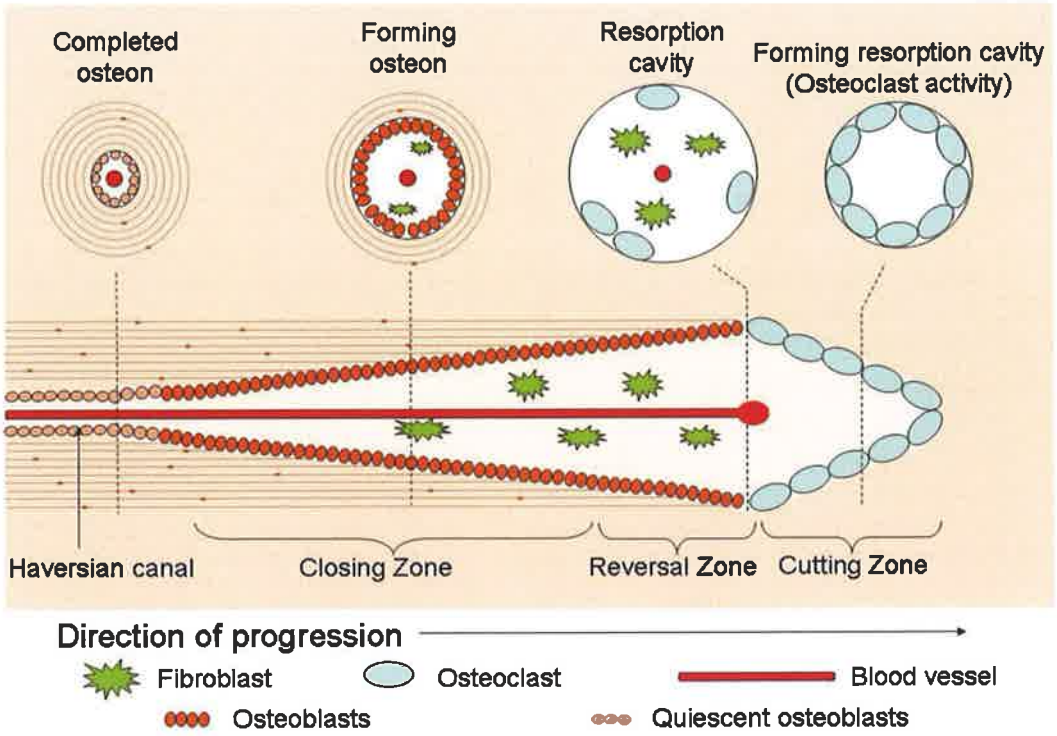

Figure 1.16 Bone remodelling – cortical BMU

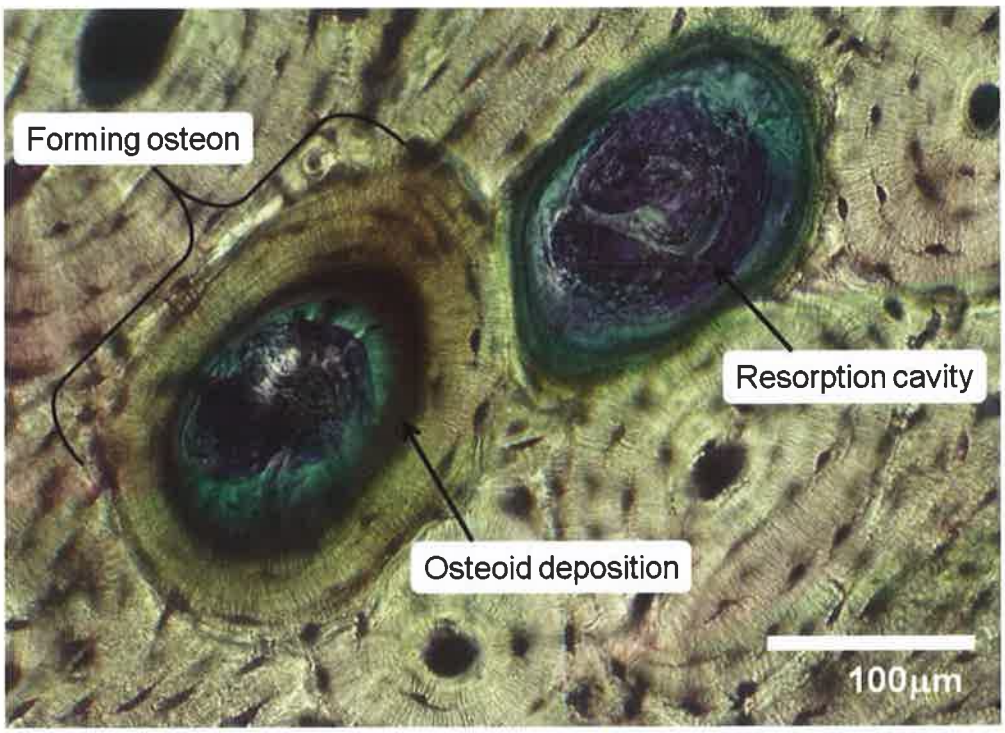

Secondary osteon formation by Basic Multicellular Units

Figure 1.17 Secondary osteon formation by BMUs

With regard to remodelling of cancellous bone, the mechanism is similar to that described above, but with modifications. So, in cancellous bone, the osteoclasts will initially cut a trench along the surface of a trabecula, rather than travelling through the substance of the bone to form a void – so called hemiosteonal remodelling (Parfitt, 1994). A reversal phase again occurs, followed by deposition of osteoid by osteoblasts to fill in this surface defect (Figure 1.18). Cancellous bone has a high rate of activation frequency – the rate of BMU formation and initiation – often attributed to its higher surface:volume ratio (Bilzekian, 2004). Some authors believe that up to 20% of cancellous bone may be undergoing remodelling at any given time under physiological conditions, whereas compact, or cortical, bone has a lower rate, with approximately 5% of the cortical skeleton being replaced each year by remodelling (Bilezikian, 2004). This assumption is not necessarily true; Parfitt (2002b) noted that '*it has often been asserted, without qualification, that cancellous bone has higher turnover than cortical bone.*' He then expands upon this statement, explaining that there are circumstances in which this is indeed true, but there are also circumstances in which it is not. However, this discussion will be revisited in Chapter 4.

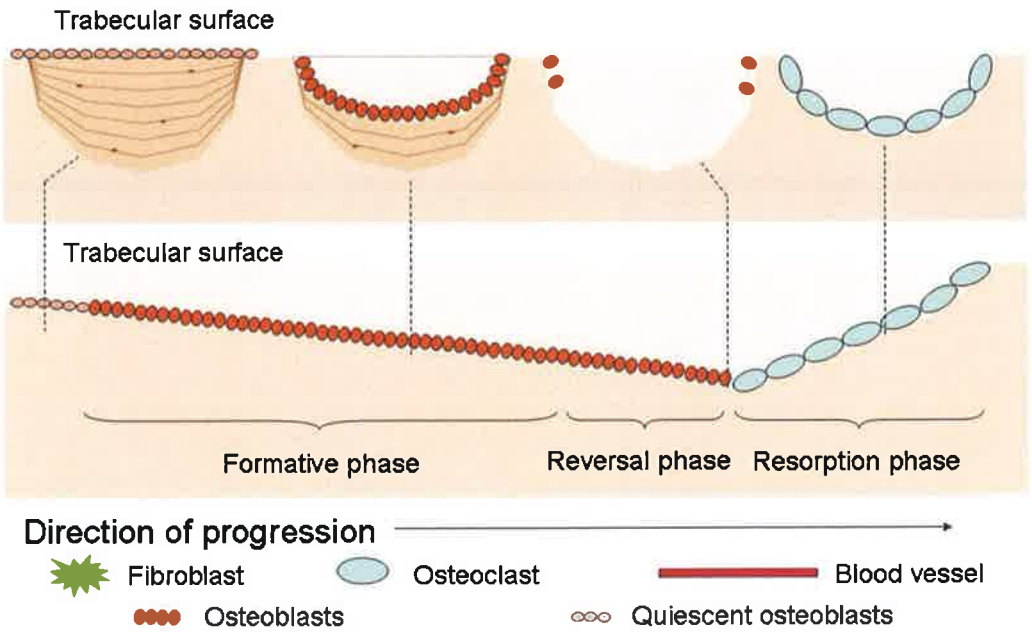

Figure 1.18 Bone remodelling – cancellous BMU

(iv) Labelling of modelling and remodelling

As detailed in the previous sections, modelling can be described as either bone formation occurring in the absence of prior resorption at a surface, or at a different surface, or bone resorption without immediate bone formation. In contrast to bone modelling, remodelling involves the processes of bone resorption and formation occurring in succession at the same site. It is often estimated that approximately 20% of the cancellous bone surface is being remodelled in the typical human skeleton at any given time (Bilezikian *et al*, 2004). Both processes, however, involve the deposition and subsequent mineralisation of osteoid by osteoblasts (Buckwalter *et al*, 1987; Standring *et al*, 2005). By use of dyes which bind to the newly-deposited calcium as it is laid down, it is possible to examine bone formation histologically.

The first documented observations along these lines are from the 18th Century. Mr John Belchier, a London surgeon, noticed marked pigmentation of pork bones served to him during a meal, while the soft tissues were untinged. Despite attempting a number of methods to remove the dye, "*I have macerated them in water for many weeks together; have boiled them often, and steeped them in spirits*", all proved ineffectual (Belchier, 1736a). After further experimentation, he found that the pigmentation was due to the consumption of Madder root (*Rubia tinctorum*) as part of the animals' feed (Belchier, 1736b). It was confirmed shortly thereafter that dye was only deposited in those parts of the bone that were actively mineralising at the time madder was fed to the animal in question (Hall, 1992). This discovery led to further madder dye experiments conducted by John Hunter, who studied growing chickens and clearly demonstrated that longitudinal bone growth occurred because of new bone generated at the physes at the ends of long bones (Sissons, 1983). The predominant dye found with the madder root is alizarin, and related compounds are still in use in bone histology today (Lee *et al*, 2003).

Following more modern experiments, tetracyclines were also observed to bind to bone in regions of new bone proliferation, in patterns virtually identical to those reported for alizarins (Milch *et al*, 1958). In view of the fact that tetracyclines bind to calcium ions in vivo and in vitro, it was postulated that the tetracyclines bind to calcium in regions of physiologically available bone (Milch *et al*, 1958). It is now confirmed that these, among other stains, are able to bind to calcifying sites within bone; the active iminodiacetic acid groups of the compounds do this by forming chelate complexes with apatite (Lee *et al*, 2003; Rahn *et al*, 1971 ; Rahn, 2003). Administration of a number of these dyes (Figure 1.19), termed polychrome sequential labelling, allows histological examination of the dynamic process of bone deposition.

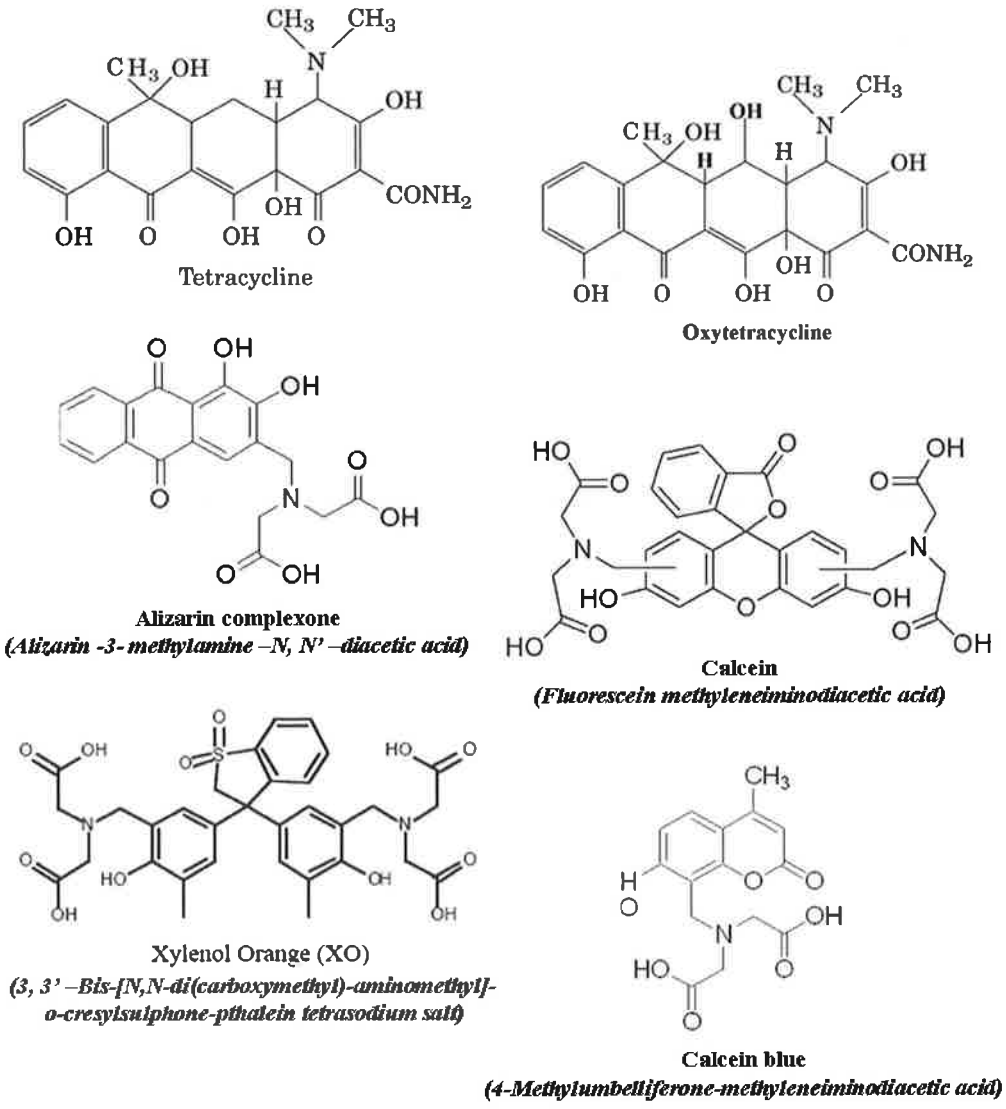

Figure 1.19 Chemical composition of chelating agents

The original madder root dye is detectable with the naked eye or normal light microscopy. However, many dyes currently used for this staining technique typically have fluorophores attached; the dye is then called a fluorochrome, which has a property called fluorescence (Figure 1.20). Fluorescence is the ability to absorb light at a particular wavelength and to then emit light of a longer wavelength after a brief interval, termed the fluorescence lifetime (Molecular Expressions Optical Microscopy Primer). The Irish scientist George Stokes was one of the first to describe the properties of fluorophores, eventually formulating Stoke's Law, which holds that the wavelength of emitted fluorescent light is always greater than the wavelength of the exciting light (Molecular Expressions Optical Microscopy Primer; Figure 1.20). The aforementioned polychrome sequential labelling is therefore made possible, as the different dyes within a specimen may be visualised under different wavelengths of light, allowing for discreet identification of each in turn within the same specimen, without overlap or confusion (Benske *et al*, 1988; Lee *et al*, 2003; Table 4.1).

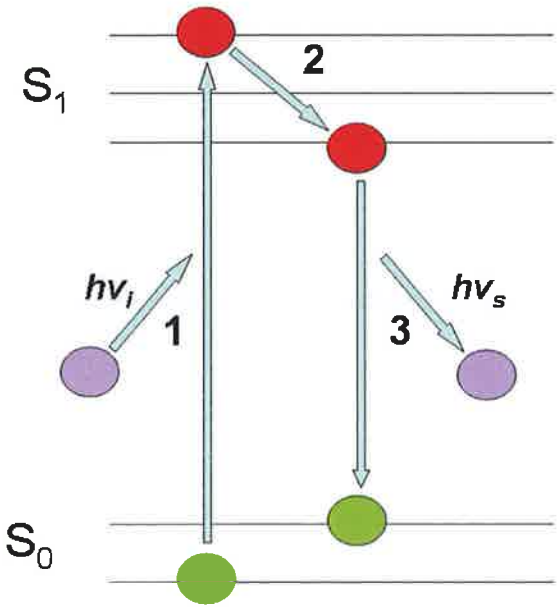

S_0 – ground state of fluorophore
S_1 – exited state of fluorophore
hv_i – photon energy level (excitation)
hv_s – photon energy level (emission)

The fluorophore exists in a resting or ground state (S_0) initially

1. Excitation
The fluorophore absorbs light energy, a photon, with an energy of hv_i. It is then excited to a higher vibrational level in the first excited state (S_1)

2. Relaxation
Rapid relaxation occurs within the next picosecond, and the fluorophore is now at a lower vibrational level in the first excited state

3. Fluorescence
The fluorophore returns to its ground state (S_0), emitting a photon, hv_s, such that $hv_s < hv_i$

Figure 1.20 Fluorophores and fluorescence

The method by which these fluorochromes are visualised in histological specimens is by use of epifluorescence microscopy. A specialised microscope is used which projects light of specific wavelengths upon the specimen, and then separates out the emitted fluorescence from this excitation light. These microscopes are typically configured that a shutter may be employed so that only the emission light reaches the eye, or other detector, allowing easier viewing of the fluorescing sections of the specimen (Figure 1.21 a). A number of different filters may be imposed along the path leading from the epifluorescence light source to alter the wavelength of light illuminating the specimen (Figure 1.21 b & c), allowing the observation of different fluorochromes in turn (Table 1.4; Figure 1.22).

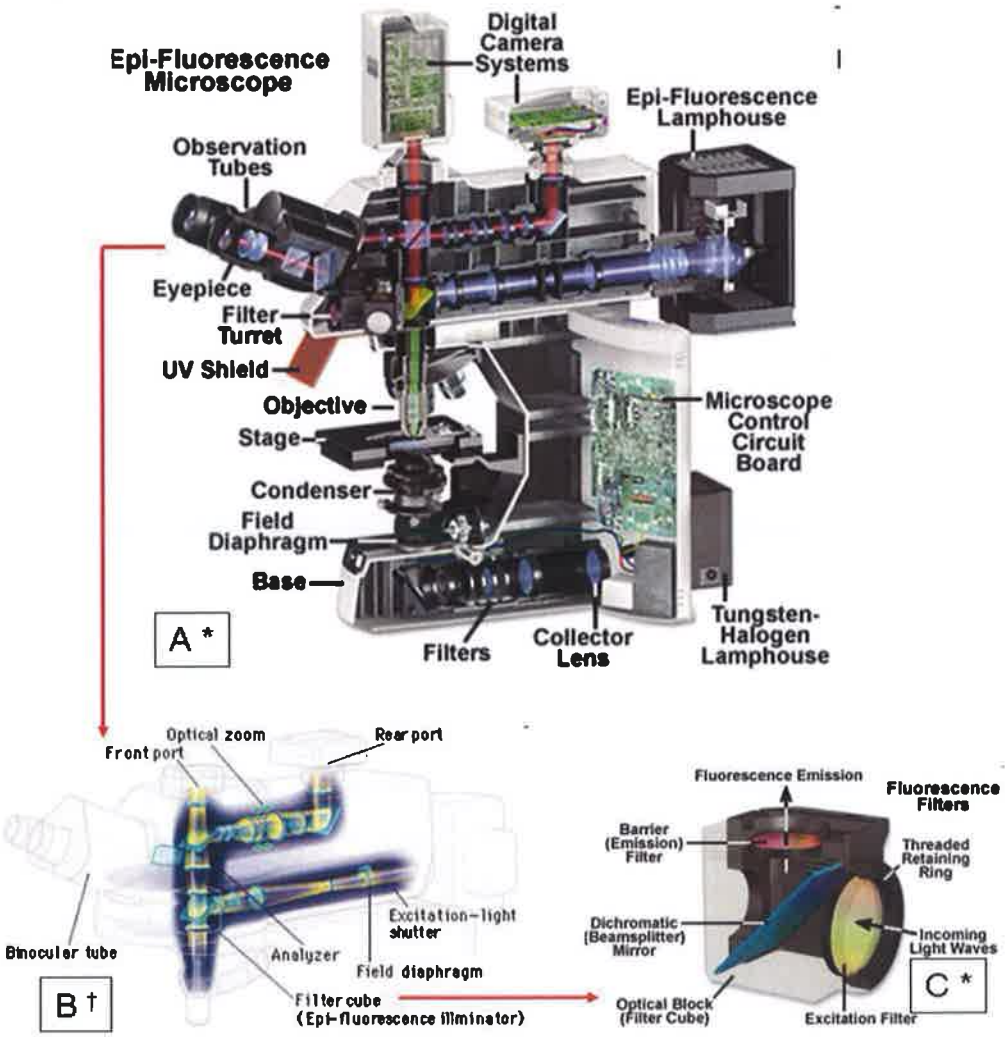

* http://www.microscopyu.com/articles/fluorescence/fluorescenceintro.html

† http://www.nikoninstruments.eu/Products/Microscope-Systems/Upright-Microscopes/Biological/Eclipse-90i/(key_features)

Figure 1.21 Epifluorescence microscope

Fluorochrome	Wavelength (nm)		Observed colour			
	Excitation	Emission	Transmitted light	Ultraviolet light ($\lambda = 365$)	Blue Epifluorescence ($\lambda = 470$)	Green Epifluorescence ($\lambda = 546$)
Oxytetracycline	390	520	Yellow	Yellow / Green	Yellow (Gold)	Faint red
Alizarin Complexone	580	625	Red	Dark Red	Bright orange / red	Dull Orange
Calcein	495	540	Green	Light Green	Light yellow/ green	Bright Orange
Xylenol Orange	377	615	Orange	Orange	Orange	Brightest Orange
Calcein Blue	375	435	Blue	Sky blue	Yellow (green)	Red

Table 1.4 Fluorochrome identification during epifluorescence microscopy

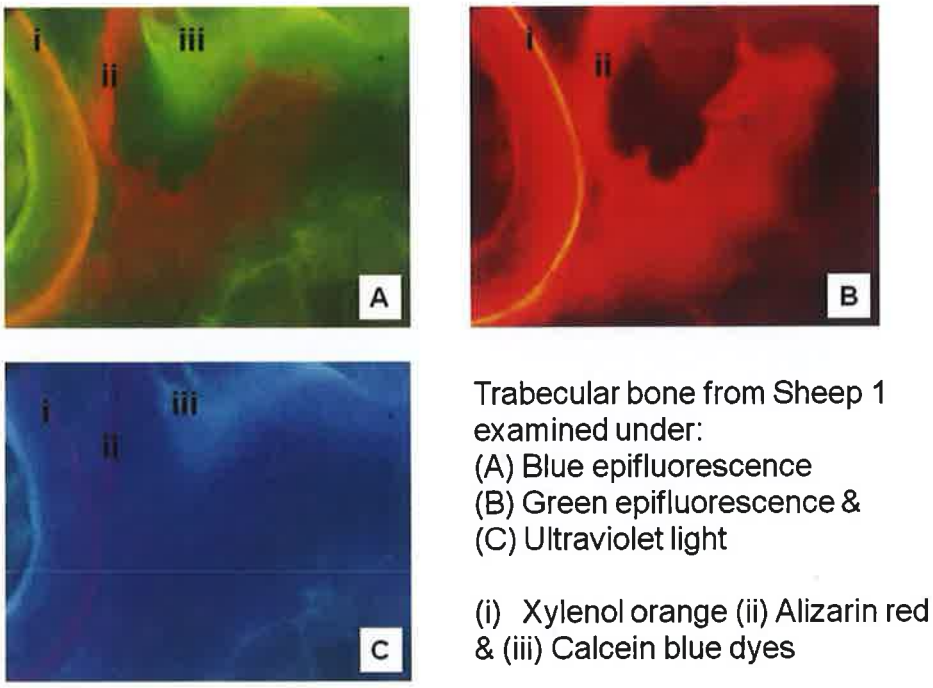

Figure 1.22 Trabecular bone with multiple fluorochromes

Of note, repeated microscopy and excitation of the fluorochromes within these specimens may lead to a phenomenon called photo-bleaching, whereby a fluorophore permanently loses the ability to fluoresce. This may be as a result of covalent bonds formed between molecules during transition between states of the fluorophore. The rate at which this phenomenon occurs varies. Some fluorophores bleach quickly after emitting only a few photons, while others are a great deal more robust and can undergo thousands or millions of transitions before any evidence of bleaching becomes apparent (MicroscopyU, accessed 6/10/2010). I did not experience this difficulty with any of the fluorochromes used within this study.

(v) Mechanical adaptation of bone

The skeleton is in a constant state of flux, with old bone resorption and new bone formation continually occurring. What, then, are the stimuli which influence this continual adaptation?

One of the main functions of the skeleton is to act as a scaffold, providing a rigid framework for muscular attachment, the leverage for locomotion, and support for internal viscera. As such, its efficacy can be increased by an ability to respond to alterations in dynamic load and thus adapt its form to improve function. This process is referred to as mechanical adaptation, and the law describing it is named for Julius Wolff, who noted the similarity between stress trajectories in a Culmann crane and the orientation of trabeculae within the proximal femur (Figure 1.23) (Bilezikian *et al*, 2004; Frost, 2004; Lee & Taylor, 1999; Martin & Burr, 1989).

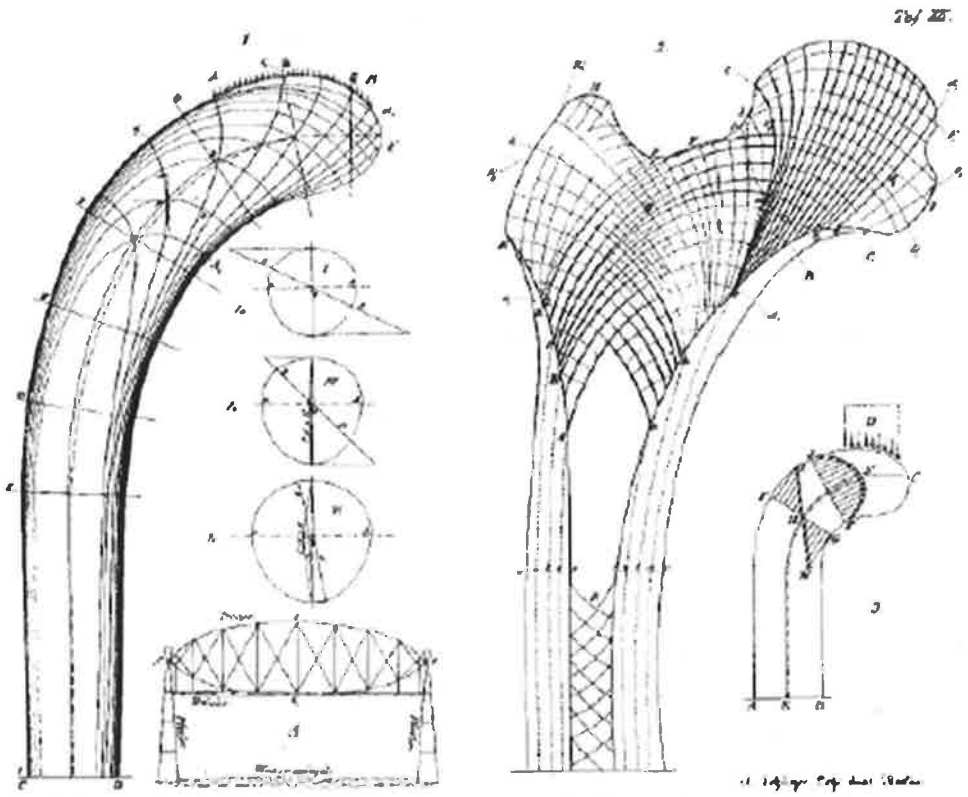

Stress trajectories in a Culmann's crane

Trabecular orientation within proximal femur

Taken from: Wolff J, 1870

Figure 1.23 Comparison of Culmann crane & femoral head

In order to appreciate this ability of bone to adapt in response to mechanical stimuli, a basic understanding of its mechanical properties is useful. The behaviour of a whole bone in reaction to an exterior stimulus is a sum of both the material properties of the bone tissue and the geometry of how that tissue is arranged within the bone, referred to as structural properties, i.e. trabecular orientation within cancellous bone (Bilezikian, 2004). When an external force is applied to an object, it will either be moved (accelerated) or will experience internal deformation as it absorbs the kinetic energy of the force (Bilezikian, 2004). Before exploring the processes involved in this latter scenario further, we need first to properly define two mechanical terms - stress and strain (Bilezikian, 2004; Martin RB *et al*, 1998).

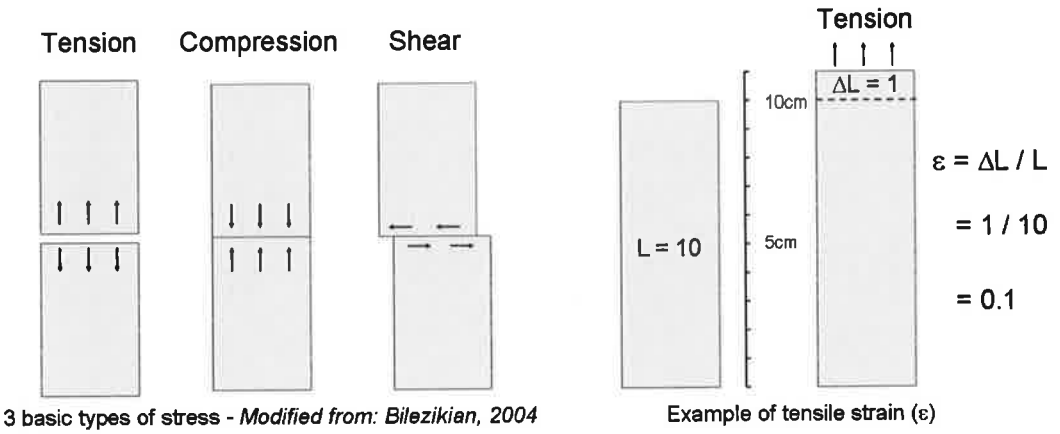

Figure 1.24 Stress and strain

Simply defined, stress (σ) is the load per unit area applied to an object, and so is measured in newtons per unit area (i.e. N/m^2). Stress may be defined as tensile, compressive or shear, depending on the direction of the applied load; in practice two or all of these forms of stress may occur in combination (Figure 1.24) (Bilezikian, 2004; Martin RB *et al*, 1998). Additionally, a material may react very differently according to the form of stress applied; a material which is strong in compression may fail quickly when shear stress or tension is applied. Strain (ε) is the resulting deformation that occurs within the object and is expressed as the percentage of change between the original and eventual dimensions of that object; it may also be expressed as a ratio of the elongation experienced by the object to its original length (Bilezikian, 2004). In Figure 1.24 above, an example of tensile strain is shown, with an object undergoing a 10% deformation, or a strain of 0.1.

So, stress applied to bone, even that which occurs during normal locomotion, will create internal strains. The structural and material properties of the bone, trabecular orientation, and density or stiffness of the bone will have an influence on the magnitude and distribution of these strains. Furthermore, many of these stresses applied to the skeleton can be described as cyclic, rather than static. The gait cycle is a prime example of a repeating pattern of stance and swing phases, where the bones are sequentially loaded and then not loaded. It seems certain that it is these strain cycles, rather than constant, static loads, that are the main factors giving rise to bone adaptation (Figure 1.25; Taylor *et al*, 2006). These cycles induce movement of fluid within the canaliculi and lacunae of the bone, subjecting the osteocytes to fluid shear stresses and prompting an adaptation response; application of a constant load will not alter the fluid dynamics within the bone to this degree and so will have little or no stimulatory effect on the osteocytes (Burr *et al*, 2002; Turner, 1998).

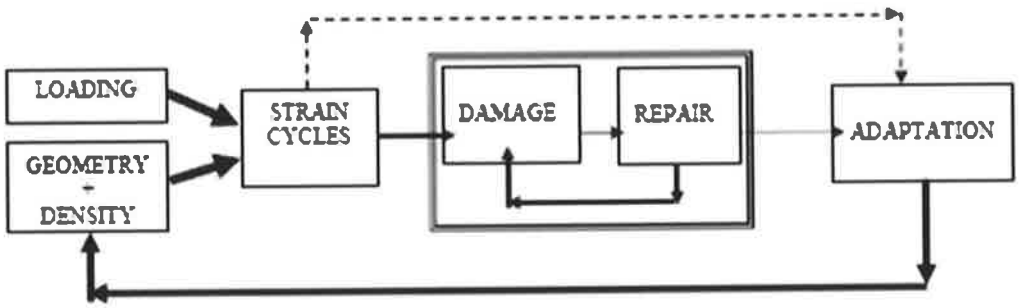

From: **Taylor D, Hazenberg J, Lee TC. The cellular transducer in bone: What is it? Technology and Health Care 2006; 14: 367–377**

Figure 1.25 Strain and adaptation

1.3.5 Bone microdamage

(i) Introduction

Adaptation is one clinically relevant response of a whole bone to the application of load. But what happens when the ability of the bone to adapt is exceeded, whether due to a single application of an exorbitant load or continual, over-exposure to what would otherwise be a bearable load if it were not repeated? Both the structural and material properties of the whole bone play roles in its ability to withstand stress; we can further investigate or quantify the material properties of any object by investigating the exact relationship between the stress applied and the strain observed experimentally – the stress-strain curve.

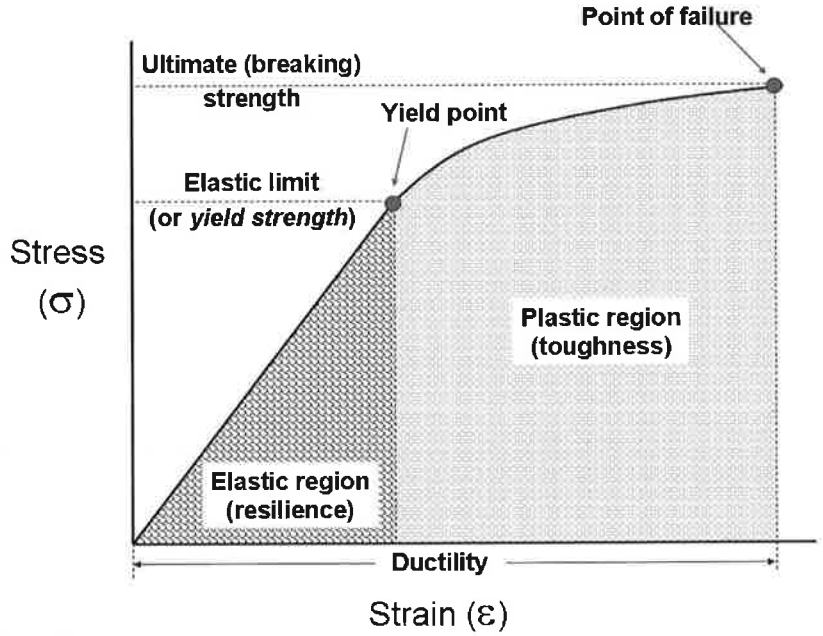

Figure 1.26 Stress vs. strain

Figure 1.26 shows a standard stress-strain curve (Bilezikian, 2004). The initial portion of the graph shows a linear relationship between the stress applied and the strain undergone by the material; this is the elastic region, and the material will revert back to its original size and conformation when the stress is removed. The slope of this line can be quantified and is referred to as *Young's modulus*, a measurement of the stiffness of a material. If more stress is applied, the material passes its *Yield point*. Beyond this, the slope is no longer linear and any further stress applied causes permanent deformation; this is referred to as the plastic region. More stress can then be applied until the material finally fails; the degree of strain present at the point of failure is the ductility of the material (Martin *et al*, 1998; Turner & Burr, 1993).

Young's modulus can vary considerably between materials, for example between a sheet of glass and a piece of rubber tubing. The former is said to be a ***brittle material***; the material may withstand a great deal of stress without deformation, but once its yield point has been passed, it is unable to withstand the application of much additional stress, and will rapidly reach its failure point (Bilezikian, 2004). The total strain exhibited (ductility) is typically low or even absent. In contrast, a ***rubbery material*** will usually reach its yield point with very little stress applied, and will then proceed to show a large degree of plastic deformation before final failure (Bilezikian, 2004). A ***ductile material*** falls between these two extremes, as shown in Figure 1.27.

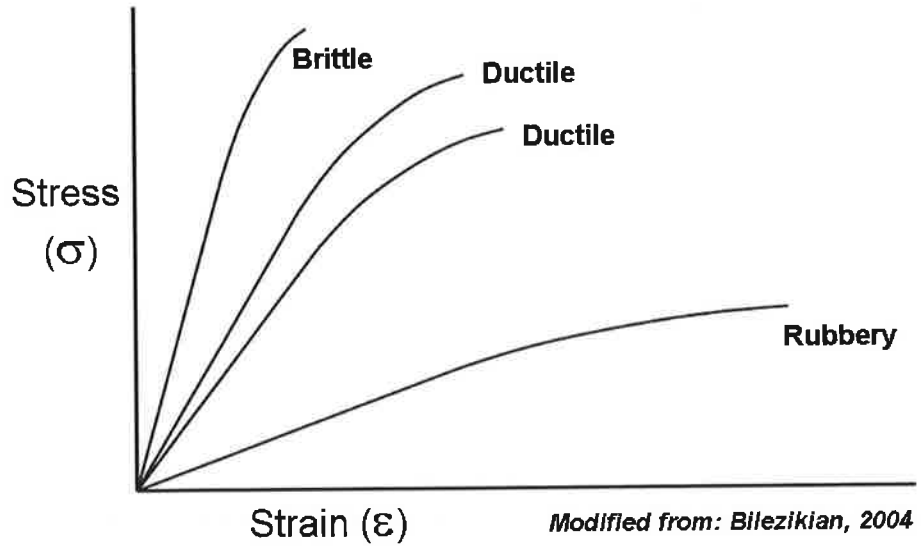

Figure 1.27 Stress – strain curves

When a material is homogeneous or isotropic, for example a metal ingot, it will always behave in the same manner regardless of the direction of the applied load. Bone, like many other biological materials, is an inhomogeneous composite material; therefore mechanical properties such as Young's modulus will vary depending on the load orientation – this is ***anisotropy***. Furthermore, other factors such as the degree of mineralisation within the bone will also affect its material properties, both between species and between individuals (Bilezikian, 2004; Martin & Burr, 1989).

(ii) Fatigue behaviour

It is apparent that a material, subjected to a stress exceeding its ultimate strength, will fracture. It is also possible, however, for a material or object to fail more gradually, when repeatedly exposed to stresses that fall below this threshold; these are colloquially termed stress fractures. The mechanisms of relevance in the development of these fractures are ***fatigue*** and ***creep*** behaviour.

Fatigue behaviour can be defined as "*the progressive loss of strength and stiffness that occurs prior to failure in materials subjected to repeated loads*" (Martin & Burr, 1989). Each loading cycle produces a small amount of microdamage; this damage then accumulates during repeated cycles, until failure finally occurs. The load applied during each cycle is the stress amplitude (S); in practice, this may fluctuate from cycle to cycle. It typically displays a roughly inverse relationship with the number of number of cycles to failure (N) - the greater the stress amplitude, the lower the number of cycles needed for failure of the material to occur (Figure 1.28) (Martin *et al*, 1998).

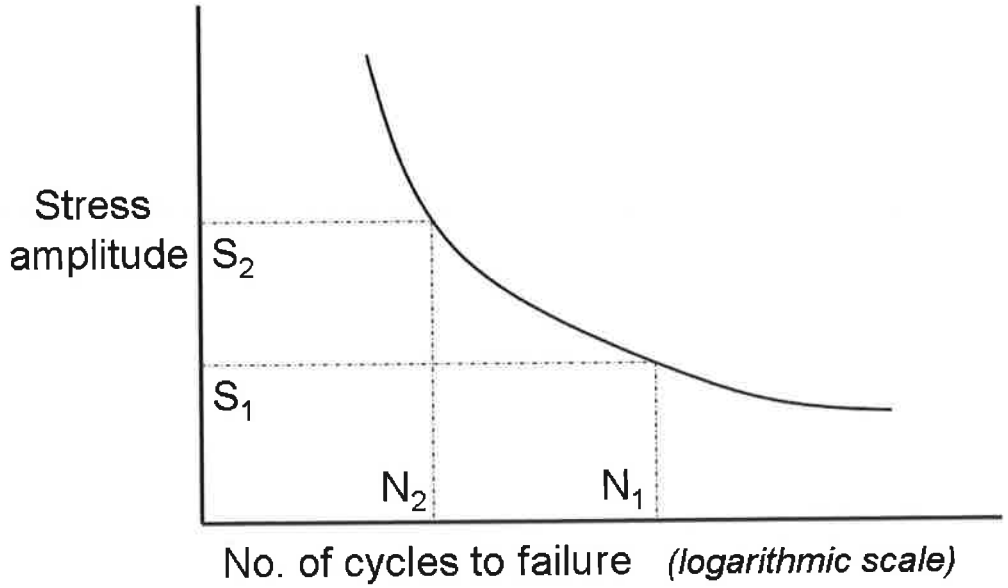

Figure 1.28 Fatigue – the S-N curve

Fatigue causes failure in a "brittle" manner – even in materials that would typically be ductile by nature. Rather than causing plastic deformation, the repeated loads cause microdamage in the form of microcracks, present at a microscopic level within the material (Martin *et al*, 1998; Turner & Burr, 1993).

The manner in which microcracks form and propagate within a fibre-reinforced composite material, such as bone, have a marked effect on its overall resistance to fatigue failure. The process has three distinct phases (Figure 1.29).

In phase I, initial application of a load causes initiation of microdamage within the material. There is an associated rapid, but initially limited, loss of stiffness within the material, measured as a reduction in Young's modulus). In the next phase, the damage accumulation and the loss of stiffness stabilise and enter a state of equilibrium. There are 2 main reasons for this state: firstly, the progress of the cracks in a linear fashion across the specimen is stopped by interfaces within the material (i.e. between lamellae); secondly, the large number of microcracks now present give rise to a large crack surface area, which can absorb a great deal of the energy within the material, and thus prevent formation of new microcracks. In phase III, the microcracks reach a critical length; the high energy levels within the crack now mean that further advancement of the crack actually *releases* energy, rather than requiring energy to propagate as before. Damage accumulation is now accelerated, with a corresponding sharp decline in Young's modulus and the point of failure is rapidly reached (Martin *et al*, 1998; Turner & Burr, 1993).

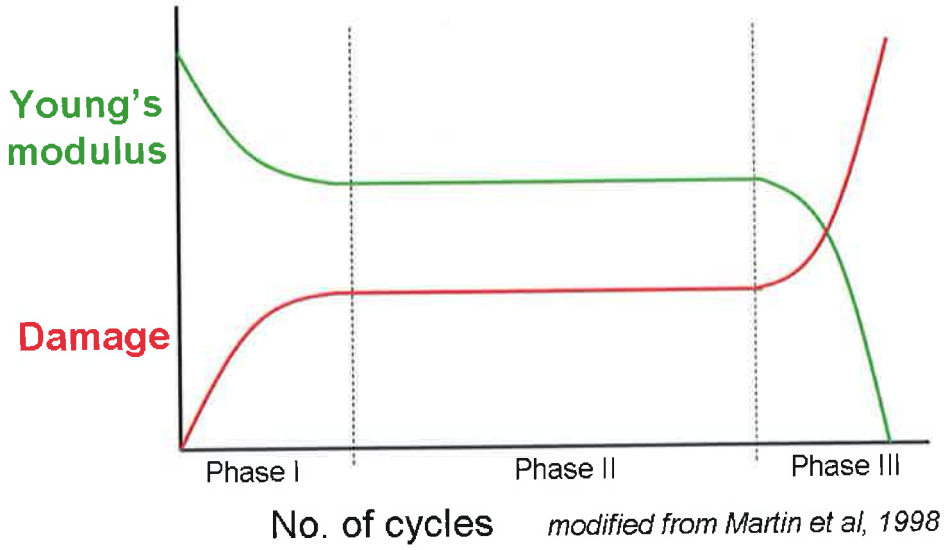

Figure 1.29 Fatigue in a composite material

(iii) Creep behaviour

If fatigue behaviour within a material can be defined as accumulated strain due to ***cyclic*** loading, creep behaviour may be explained as the reaction of a material exposed to a ***constant*** load over time. Bone has viscoelastic properties; it deforms under sustained stress and its material properties will also alter according to the rate at which a stress or load is applied. After application of the load there is an initial period of rapid elastic deformation, which then levels to a plateau. Following this, the material may either reach viscoelastic equilibrium, or a point of failure (Figure 1.30) (Bilezikian, 2004; Martin *et al*, 1998).

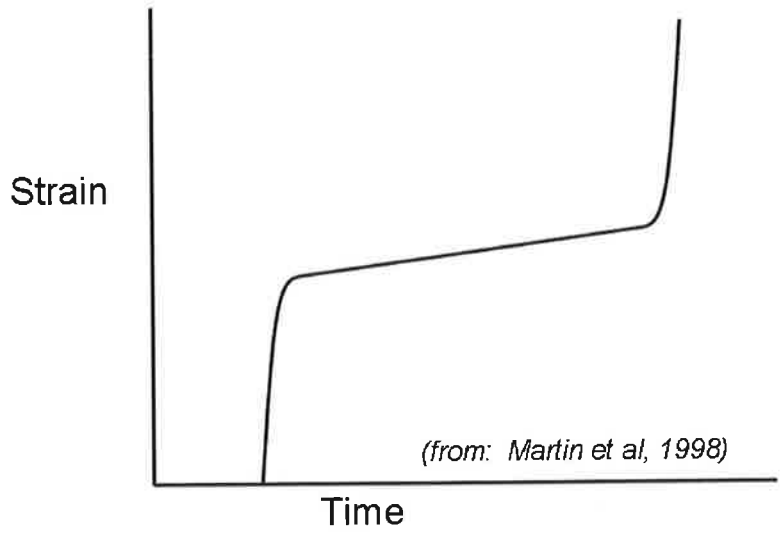

Figure 1.30 Creep behaviour

1.4 THE SYNOVIAL JOINT

1.4.1 Structure and sustenance

(i) Overview

The human body contains over 200 bones. In order for these bones to form a cohesive skeletal system, they must connect or *articulate* with each other; they do this at interfaces called *joints*. There are three main types of joints, classified by structure: fibrous, cartilaginous and synovial. It is synovial joints within which osteoarthritis develops, so I will discuss the structure of this joint type in further detail, omitting the other two.

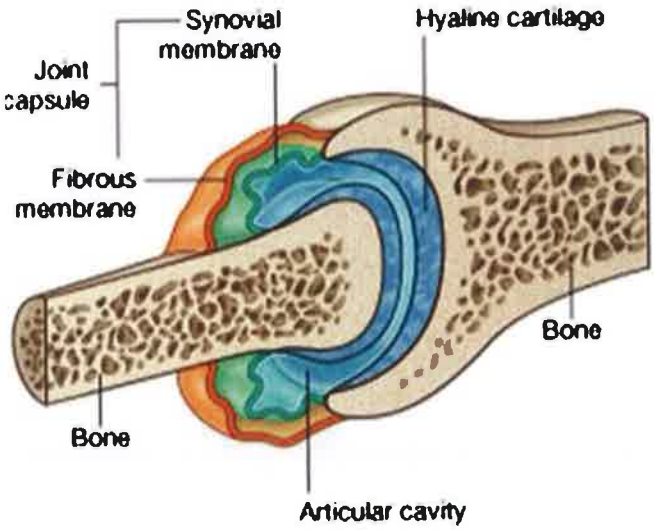

Figure 1.31 Synovial joint structure – macroscopic (Drake *et al*, 2005)

Synovial joints are designed to permit a large degree of movement between the bones involved. The articulating surfaces of the bones are covered with hyaline cartilage, with an articular cavity between them (Figure 1.31). A *joint capsule* will surround and define this articular cavity; this is a membrane which runs from one bone to the other, with its attachment typically at the *articular margins* (the interface between the hyaline cartilage and bone). The outer layer of this capsule is fibrous and is a major contributor to stabilization of the joint. The inner capsular layer is the thin synovial membrane, which produces synovial fluid; this is the lubricant which lies within the articular cavity, reducing friction and nourishing the cartilage (Standring *et al*, 2005).

The articular surfaces consist of an underlying platform of bone which is covered by articular hyaline cartilage. These two tissues may be further subdivided into different layers or zones, all of which have varying material and structural properties, which give the synovial joint its mechanical properties as a whole (Standring *et al*, 2005).

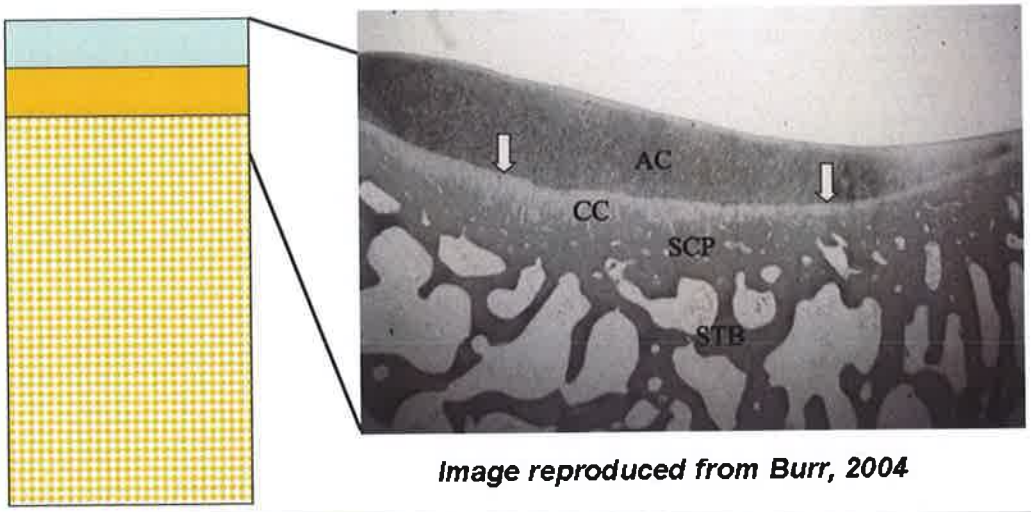

Image reproduced from Burr, 2004

Legend:	**Abbrev.**
Articular cartilage	AC
Calcified cartilage	CC
Subchondral cortical bone	SCC / SCP
Subchondral trabecular bone	SCT / STB

Figure 1.32 Synovial joint structure – microscopic (1)

As depicted in Figure 1.32 above, the most superficial layer is that of the articular cartilage, the deepest zone of which is calcified (zone of calcified cartilage – ZCC). A *tidemark* can be visualised at the interface between the calcified and non-calcified cartilaginous zones. Underlying this is a plate of cortical bone, which is supported from beneath by the subchondral trabecular bone (Burr, 2004). Of note, while the calcified cartilage and subchondral bone plate are easily differentiated in microscopy, this is not the case in MicroCT. For this reason, the two tissues are considered together as the *subchondral plate* for MicroCT analyses in this thesis.

(ii) Articular hyaline cartilage

Macroscopically, the layer of articular hyaline cartilage typically has a smooth, shiny, white-blue appearance to the naked eye; the thickness of this layer will vary from 1 - 7mm, following the shape and contours of the underlying bone. Unlike bone, cartilage has no blood or nerve supply; it receives its nutrients via diffusion from the synovial fluid within the joint, and disposes of the products of metabolism into the same medium.

Microscopically, areas of articular cartilage may be observed to differ from each other in appearance, depending on whether they are superficial or deep (Figure 1.33). This is due to the arrangement of collagen fibres within the matrix of the cartilage and morphology of the embedded chondrocytes; it is referred to as *zonation*, and four structural zones are described (Standring *et al*, 2005).

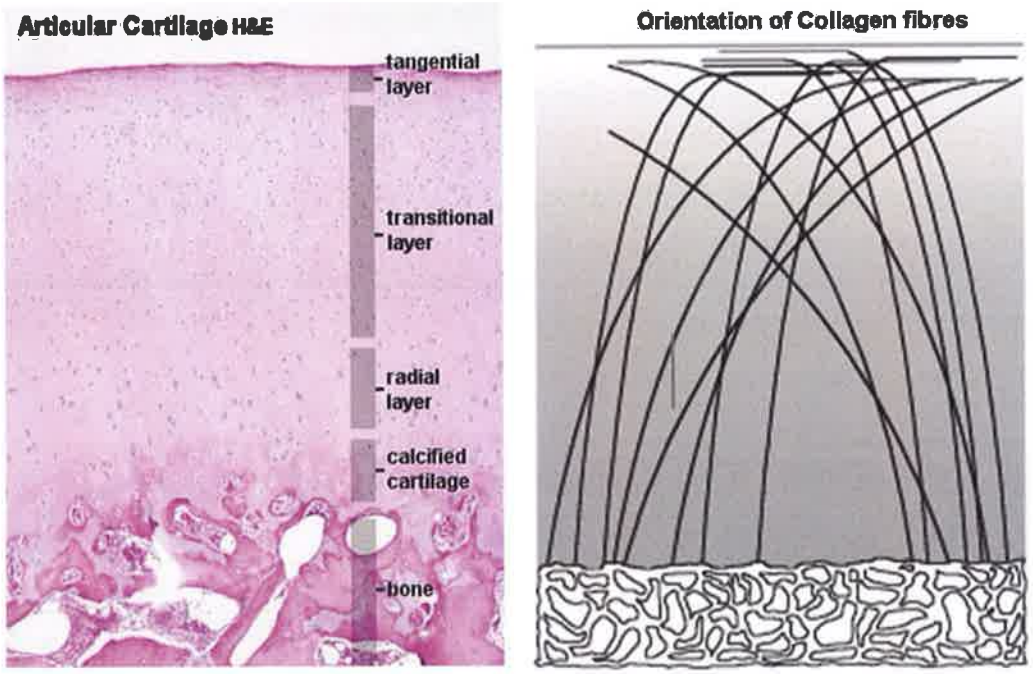

Figure 1.33 Orientation of collagen fibres within articular cartilage

Tangential zone

This is the most superficial layer of the articular cartilage; it has a high concentration of collagen fibres, which are found running parallel to the surface (Poole *et al*, 2001). The most superficial part of this contains no cells and is often referred to as the *lamina splendens*. Deep to this, oval or flattened chondrocytes may be seen, also running parallel to the articular surface. The orientation of the collagen fibres in this layer gives it its resilience to shear stresses (Poole *et al*, 2001), (Figure 1.34).

Transitional zone

As the name suggests, this layer is a transition from the tangential layer (resisting shear stresses) to the radial layer (resisting compressive forces). The chondrocytes are larger and more rounded here; they may be seen in isolation and in small groups (Poole *et al*, 2001). There is a very high concentration of proteoglycans within this layer, typically more so than in any of the other layers within the cartilage (Poole *et al*, 2001). The collagen fibres here run obliquely through the matrix.

Radial zone

This layer is designed to withstand compressive forces and evenly distribute the applied load to the underlying tissues. The collagen fibres are arranged radially (i.e. perpendicular to the articular surface) with large, round chondrocytes arranged in vertical columns among them.

Zone of calcified cartilage (ZCC)

This is the deepest layer of the articular cartilage, lying upon the subchondral bone plate. As the name suggests, the cartilage here is calcified. Both the osteochondral interface and the *tidemark* between the ZCC and the overlying radial zone of cartilage have ridges and indentations, to allow transformation of shear stresses between these layers into simpler compressive and tensile loads (Burr, 2004; Oegema *et al*, 1997). The ZCC is thought to function as a layer of intermediate stiffness between the subchondral bone and the overlying cartilage (Poole *et al*, 2001).

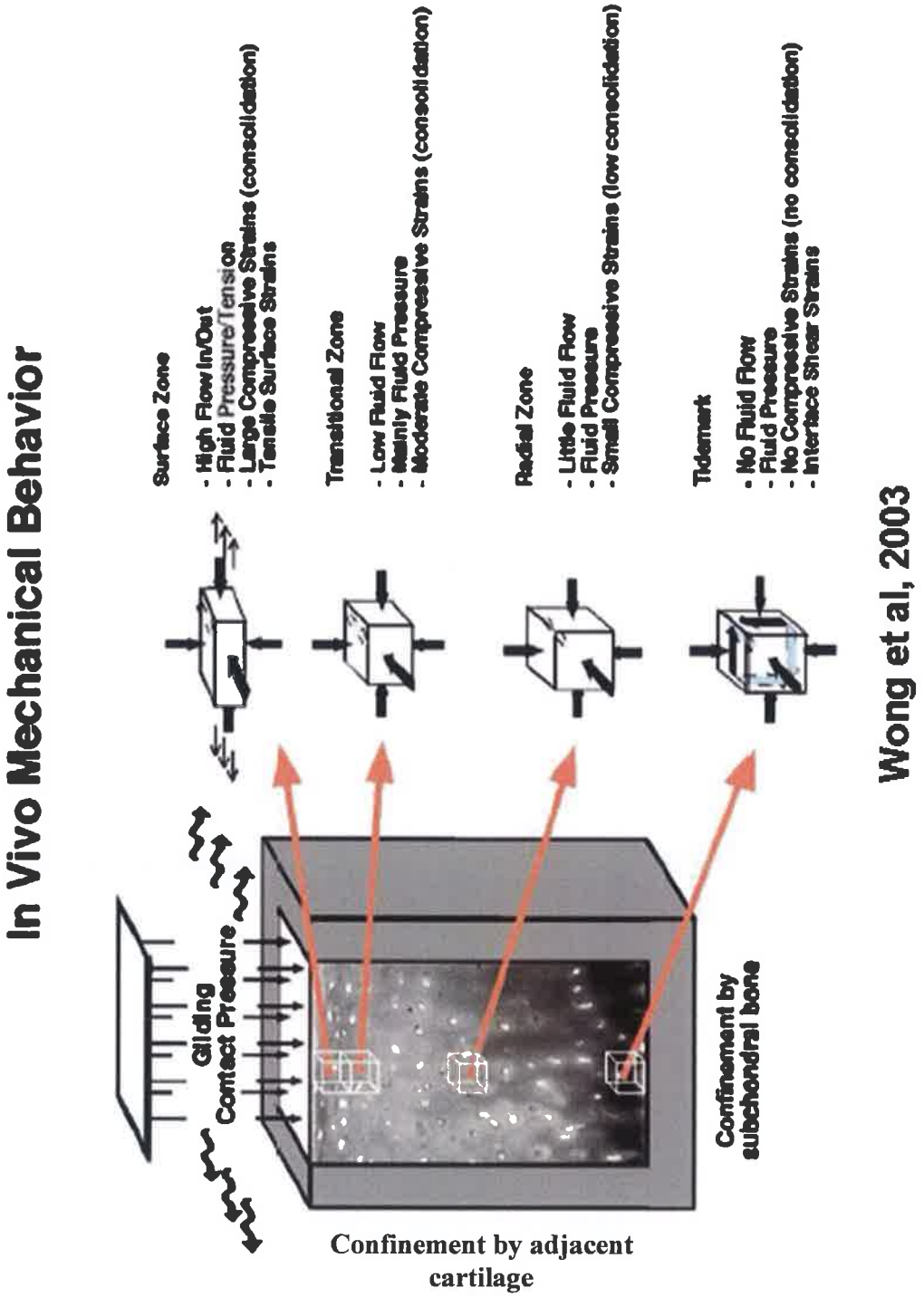

Figure 1.34 Biomechanical behaviour of articular cartilage

(iii) Subchondral cortical bone

Deep to the zone of calcified cartilage, and highly interdigitated with it, lies the subchondral bone plate (Figure 1.35). This is a layer of lamellar bone, which interdigitates with the overlying layer of calcified cartilage at the osteochondral interface. The thickness of this plate may vary slightly within the joint; where the joint surface is concave, such as the tibial plateau, it will typically be thicker within the central area (Duncan *et al*, 1987; Noble *et al*, 1985).

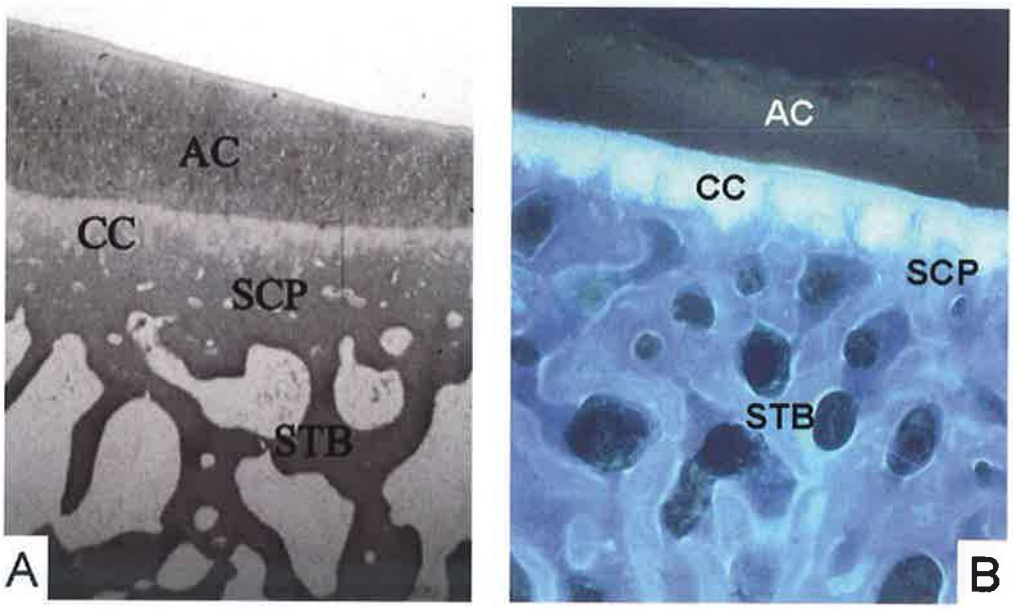

Burr, 2004

Epifluorescence microscopy, medial tibial plateau

Articular cartilage (AC), Calcified cartilage (CC), Subchondral cortical plate (SCP), Subchondral trabecular bone (STB)

Figure 1.35 Synovial joint structure – microscopic (2)

(iv) Subchondral trabecular bone

The subchondral plate is supported from below by the subchondral trabecular bone. These trabeculae are orientated in different directions, or *anisotropically*, in order to distribute the load transmitted from the overlying subchondral plate. While trabeculae are typically structured in a "rod-like" manner, "plate-like" trabecular bone is frequently observed in the subchondral region.

(v) Physiological sustenance

The skeleton is in a constant state of flux, adapting its form in response to alterations in dynamic load, thus improving function. The same is true of the tissues within the synovial joint. The first ongoing process in the subchondral region is that of endochondral ossification, whereby the zone of calcified cartilage is replaced by bone. The rate at which this process occurs alters throughout life; in humans the rate typically declines until the sixth decade, and then increases again with advancing age (Lane *et al*, 1980). The calcified cartilage is penetrated by blood vessels from below and is replaced by osteoblasts that lie in proximity to the aforementioned blood vessel (Figure 1.36 b) (Bullough *et al*, 1983).

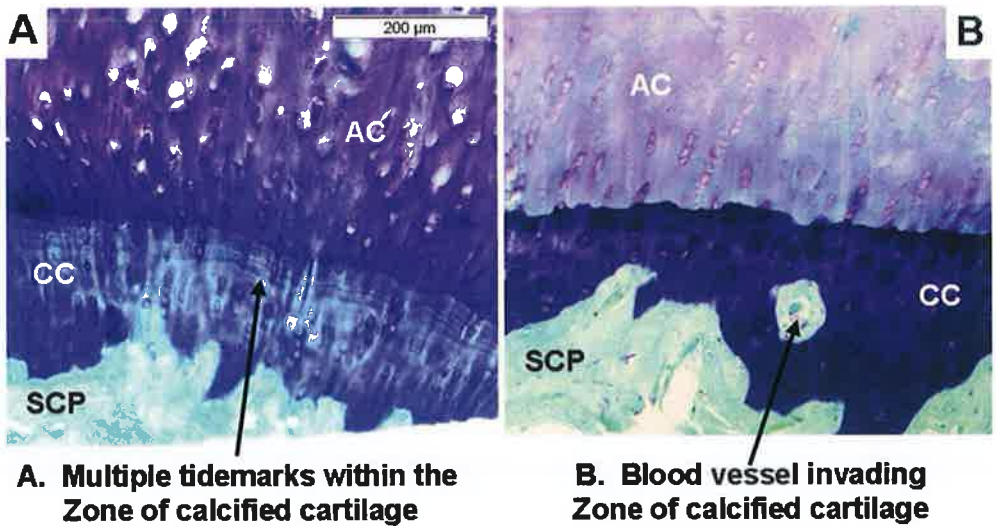

Articular cartilage (AC), Calcified cartilage (CC), Subchondral cortical plate (SCP) Images JCH, Ovine tibial plateau, Toluidine Blue with Fast Green counterstain

Figure 1.36 Calcification front and endochondral ossification

It might initially be supposed that this replacement of the calcified cartilage with bone will lead to a reduction in the height of the former zone, but this has been shown to not always be the case. Instead, the tidemark, or junction between the calcified and non-calcified articular cartilage will also advance (Figure 1.36 a); this typically occurs in equilibrium with the underlying endochondral ossification, so that the zone of calcified cartilage is unchanged in height (Bullough *et al*, 1983; Burr, 2003). This equilibrium will alter with age; the rate of endochondral ossification increases, but the same degree of acceleration fails to occur at the calcification front, leading to a thinner calcified cartilage layer (Lane *et al*, 1980).

1.4.2 The Knee Joint

(i) Structure

The human knee joint is the largest and most complex joint within the human body. It may be described as being formed by three joints within a single joint cavity; patellofemoral and the medial and lateral tibiofemoral joints. The articulating surfaces that form these joints are the medial and lateral femoral condyles, the two articular surfaces on the tibial plateau and the posterior surface of the patella. All of the articulating surfaces are lined with articular hyaline cartilage and the peripheries of the facets on the tibial plateau are overlain by fibrocartilaginous menisci (Figure 1.37).

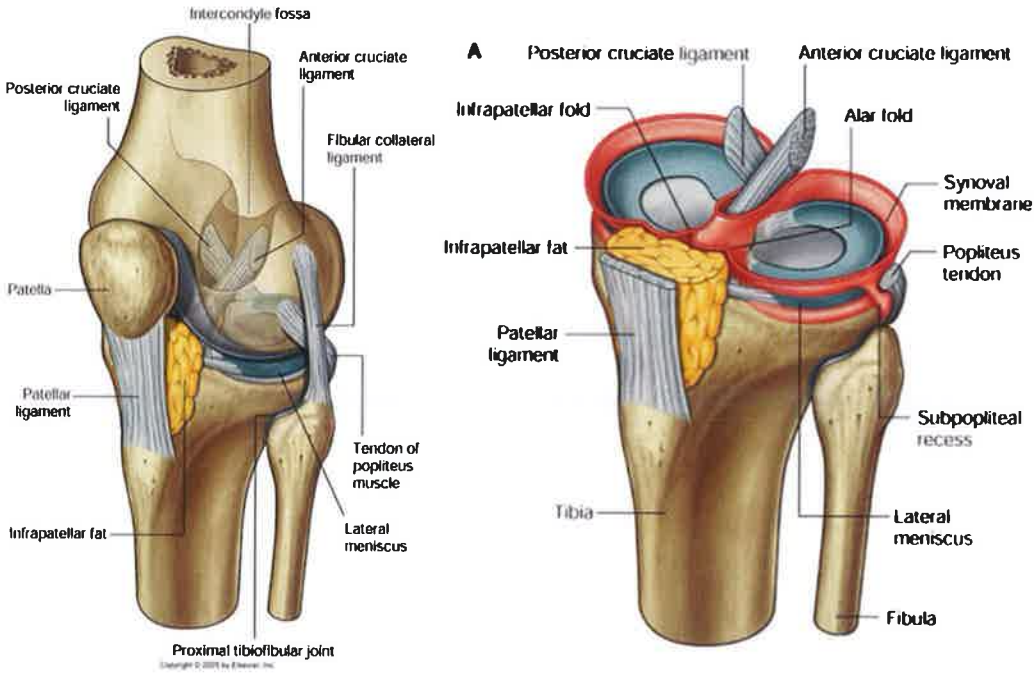

Figure 1.37 The human knee joint (Drake *et al.* 2005)

(ii) Mechanobiology

Within the knee joint, factors such as cartilage contact geometry and functional loading play a role in influencing the health and structure of the component tissues therein (Koo *et al*, 2007). Bullough *et al* (2004) notes that "In general, the opposing articulating surfaces of the joint consist of one convex articular surface and one concave articular surface", and the shape of these articular surfaces is determined by the underlying subchondral bone. The degree to which these articular surfaces lie in contact with each other during static and impact loading may vary, however; this is referred to as *congruency* (Figure 1.38).

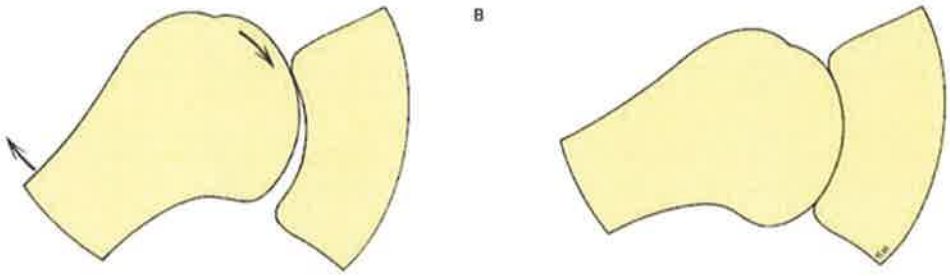

Figure 1.38 Articular congruency

Within the knee, the articular surfaces are relatively incongruent. While in the medial femoro-tibial compartment the convex femoral condyle articulates with a concave tibial facet, within the lateral compartment both the femoral and tibial surfaces are convex in shape (Figure 1.39; Fairbank, 1948; Koo *et al*, 2007).

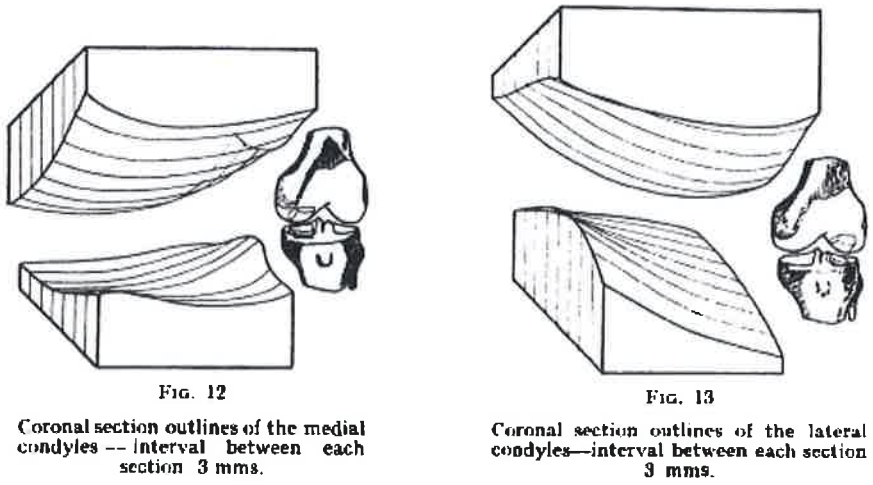
FIG. 12

Coronal section outlines of the medial condyles -- interval between each section 3 mms.

FIG. 13

Coronal section outlines of the lateral condyles—interval between each section 3 mms.

Figure 1.39 Femoro-tibial compartment morphology (Fairbank, 1948)

The menisci play a vital role here; they absorb some of the initial shock on (impact) loading, distribute this stress over a large area of the articular cartilage and also translate the compressive load into a circumferential hoop stress (Krause *et al*, 1976). In an *in-vitro* porcine study (with the knee in varus alignment), Fukada *et al* found that the compressive stress in the medial subchondral bone post-meniscectomy was 4.0 ± 5.2 times higher than that with the meniscus present (Fukada at el, 2000). Fukubayashi also found that removal of the menisci significantly reduced the contact area and increased the contact pressure (Fukubayashi *et al*, 1980; Figure 1.40).

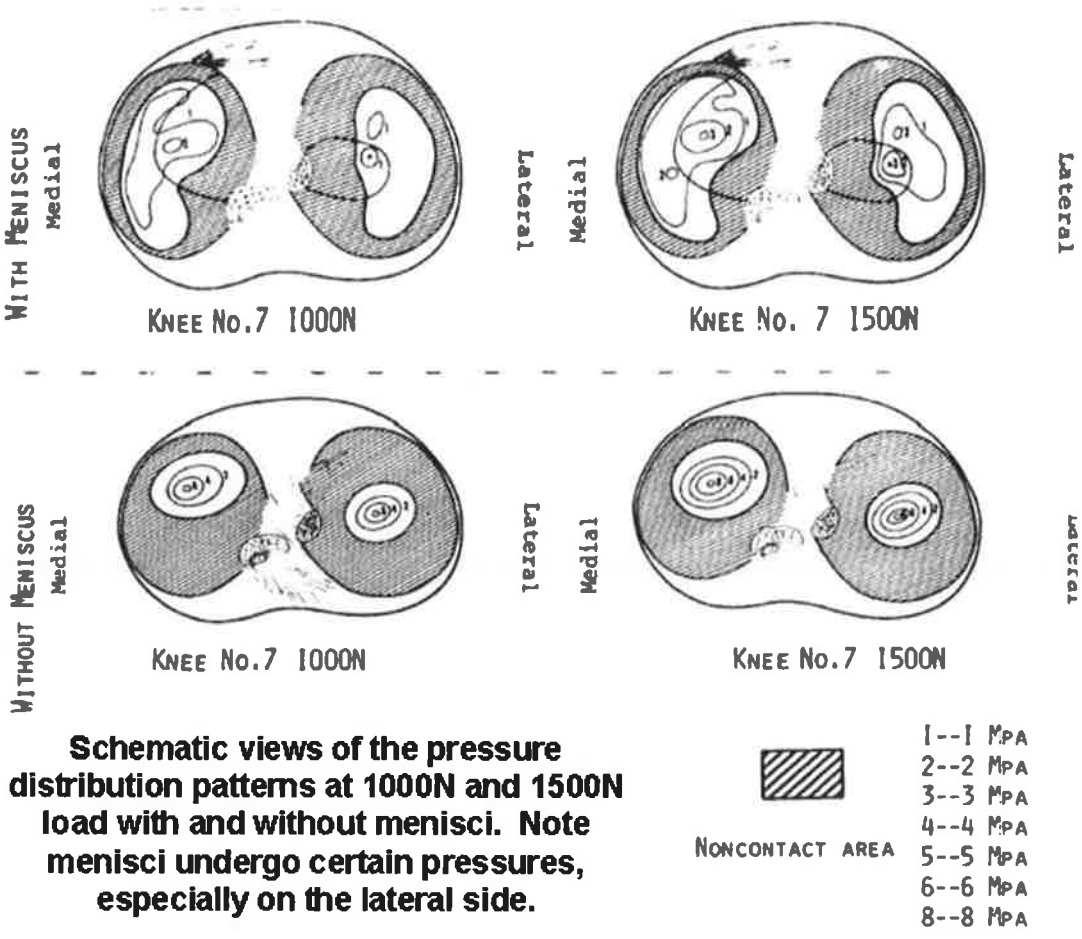

Schematic views of the pressure distribution patterns at 1000N and 1500N load with and without menisci. Note menisci undergo certain pressures, especially on the lateral side.

Edited from *Fukubayashi et al, 1980*

Figure 1.40 Femoro-tibial contact and pressure (Fukubayashi *et al*, 1980)

The pattern of preferential loading from the periphery within the knee joint is not solely due to the presence of the menisci. Bullough also proposes that in a number of joints, including the knee, initial contact between the articular surfaces is made at the periphery (Figure 1.41); as the cartilage deforms in response, the area of contact increases, with an even distribution of load throughout (Bullough *et al*, 2004).

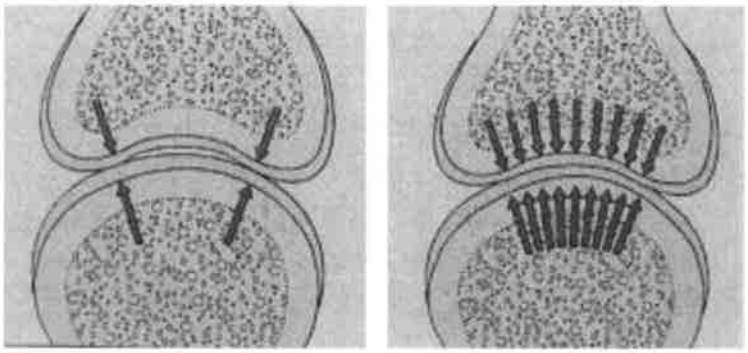

Figure 1.41 Articular load distribution (Bullough, 1997)

Upon further investigation, Bullough *et al* found that the congruency of the articular surfaces is age-dependent (Figure 1.42). He hypothesised that alterations in congruency may result in a redistribution of load, so that pressure was now being placed on areas of the cartilage which had previously been unloaded, thus possibly causing tissue damage of the articular cartilage or remodelling of the underlying bone in compensation (Bullough *et al*, 1983; Bullough, 2004).

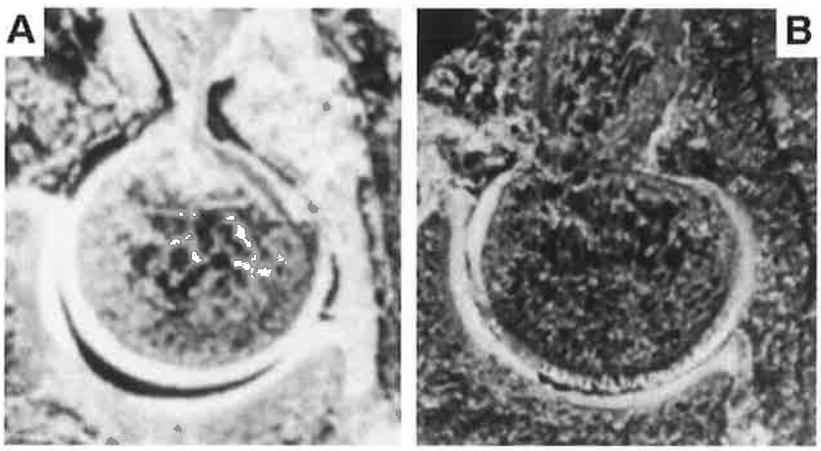

Sagittal plane section through humero-ulnar joint at (A) 18 years and (B) 60 years of age

Figure 1.42 Age-related articular congruency (Bullough *et al*, 1983)

1.5 OSTEOPATHIES

1.5.1 Osteoporosis

Osteoporosis is a metabolic bone disease with significant morbidity, which is characterised by a loss of skeletal mass (Rubin *et al*, 2004; Figure 1.43). It is defined in women as having a bone mineral density of 2·5 standard deviations or more below the average value for premenopausal women (Kanis, 2002; Figure 1.44). This is assessed by means of bone mineral density measurement (BMD) with dual energy X-ray absorptiometry (DEXA), using a standard site such as the proximal femur.

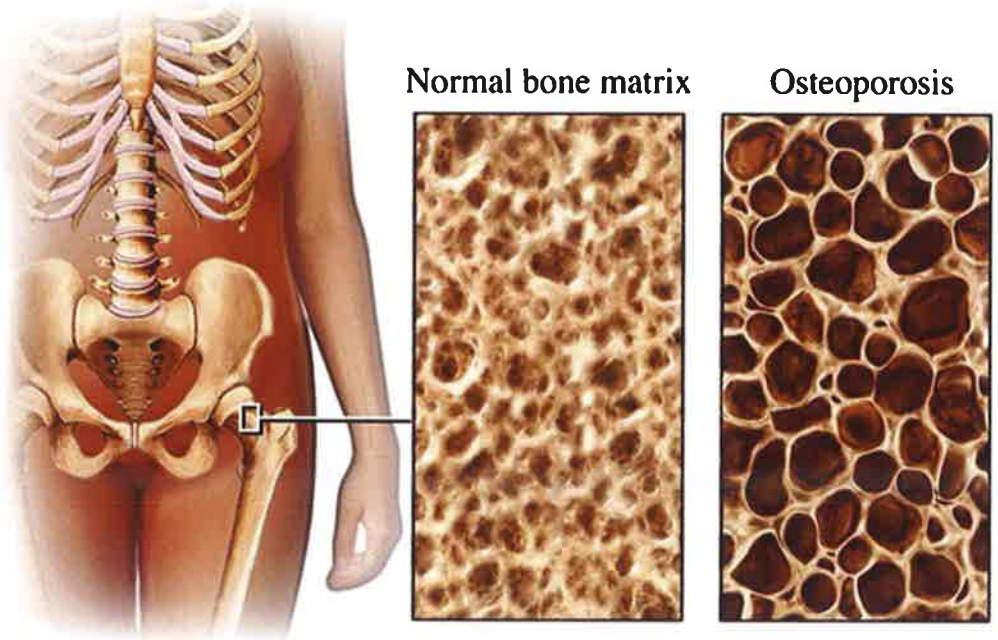

http://familymedicinehelp.com/introduction-to-osteoporosis

Figure 1.43 Osteoporosis

Bone mineral density will typically peak in the fourth decade of life, with age-related bone loss then beginning in both males and females after the age of forty; women then have a further acceleration of bone loss post-menopausally as oestrogen levels reduce (Figure 1.44). This occurs due to an imbalance between the phases of bone resorption and new bone formation during remodelling, and results in a decrease in the amount of bone present (Poole & Compston, 2006).

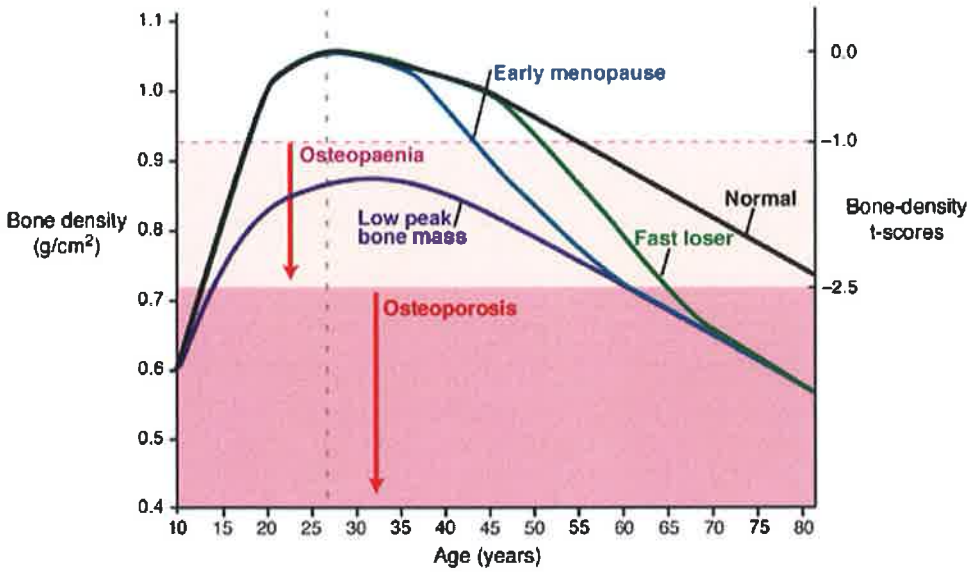

Variation in the bone density of women at different ages

Expert Reviews in Molecular Medicine © 1999 Cambridge University Press

Figure 1.44 Bone mineral density, age-related changes and osteoporosis

The predominant clinical consequence of osteoporosis is the associated rise in fracture risk that occurs with reduced bone mineral density, and the subsequent morbidity and mortality associated with these fractures (Poole & Compston, 2006; Figure 1.45). For example, hip fracture has an associated mortality rate of over 20% within 1 year of fracture, rising to nearly 60% at 5 years (Johnell *et al*, 2004; Figure 1.46).

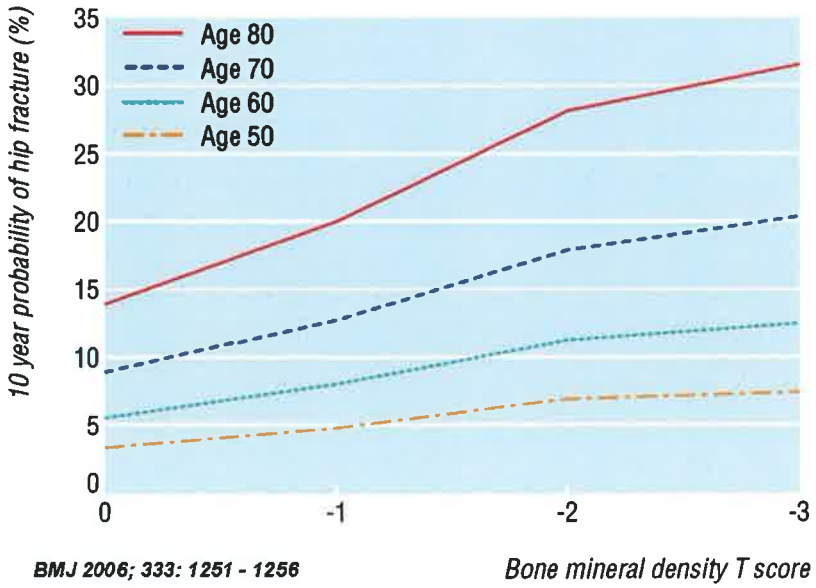

Figure 1.45 Bone mineral density, age and fracture risk

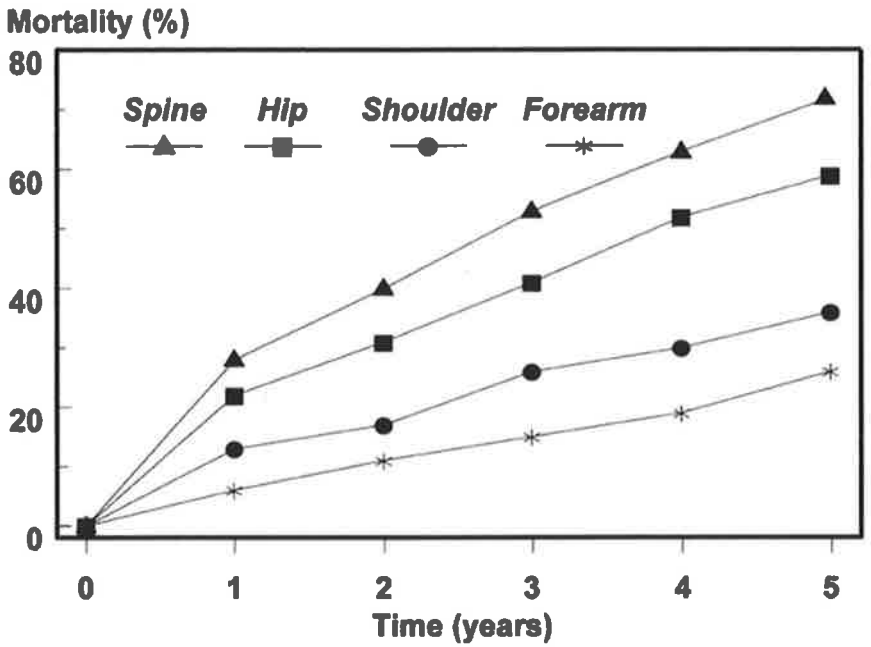

Cumulative mortality following a fracture at the sites shown

Osteoporos Int (2004) 15: 38–42

Figure 1.46 Osteoporotic fractures and mortality

1.5.2 Osteonecrosis & spontaneous osteonecrosis of the knee

True osteonecrosis and spontaneous osteonecrosis of the knee (SPONK) are considered to be two separate entities. True osteonecrosis "*typically occurs in younger patients...effects multiple joints and condyles, and is associated with risk factors such as corticosteroids and alcohol abuse*" (Mears *et al*, 2009). Spontaneous osteonecrosis of the knee typically occurs over the age of 55 and affects a single joint; it is a well-recognised cause of knee pain, with the incidence being higher in women than men (Akamatsu *et al*, 2012; Lotke *et al*, 1977; Mears *et al*, 2009). MRI is useful to detect these lesions within the femoral condyle or tibial plateau (Figure 1.47), but scintigraphy is considered superior (Satku *et al*, 2003).

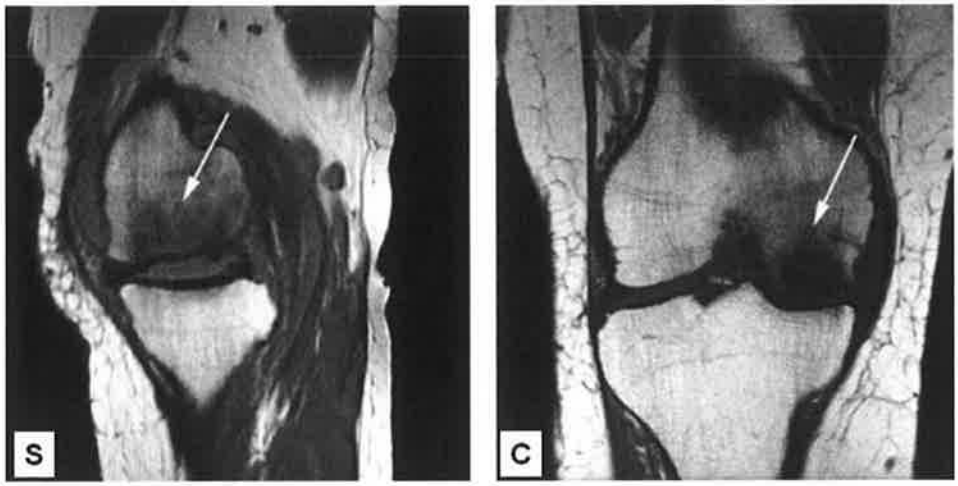

Sagittal & coronal images of the knee joint, showing the lesion in the femoral condyle, which is currently called spontaneous osteonecrosis

Figure 1.47 Spontaneous osteonecrosis of the knee (Robertson *et al*, 2009)

Vascular insufficiency, or trauma of the medial femoral condyle or medial tibial plateau are generally accepted as initiating factors (Akamatsu *et al*, 2012; Narváez *et al*, 2003; Yamamoto & Bullough, 2000). However, the exact pathophysiology of the condition remains uncertain; contrary to what the name suggests, there is usually very little evidence of actual necrosis being present in histological specimens from affected joints (Mears *et al*, 2009). Scintigraphy is considered to be the most reliable diagnostic investigation for SPONK (Al-Rowaih *et al*, 1990; Satku *et al*, 2003); increased bone turnover is associated with an increased incidence of osteoporotic fractures (Hernandez, 2008; Meier *et al*, 2005; Riggs & Melton, 2002). Subchondral insufficiency fractures secondary to osteopenia are also described within the subchondral bone of the femoral head (Breer *et al*, 2012; Takeda 2008); rapid progression to osteoarthritis or joint destruction in both the hip and knee have been reported following diagnosis (Satku *et al*, 2003; Yamamoto & Bullough, 2000b).

1.5.3 Osteoarthritis

Osteoarthritis is a joint disorder and is one of the most prevalent diseases known, particularly in older population groups. The WHO estimate that 190 million people suffer from this condition; some groups have estimated that the majority of adults over the age of 55 have radiographic evidence of osteoarthritis (D'Ambrosia, 2005). It has an enormous economic impact, due to both a reduced work-force because of disability, and the need to provide specialist support and assistance to those most affected. These sums are not inconsiderable when it is taken into account that 80% of those with osteoarthritis will have some restriction of movement and almost a quarter cannot perform the activities of daily living (Buckwalter *et al*, 2004). Treatment to date remains symptomatic; there is as yet no disease-modifying intervention or medication available. The number of total (and revision) joint replacements for osteoarthritis is increasing at a rapid rate; as an example, over 250,000 total knee replacements were performed in the U.S. alone in the year 1999 (Kurtz *et al*, 2005).

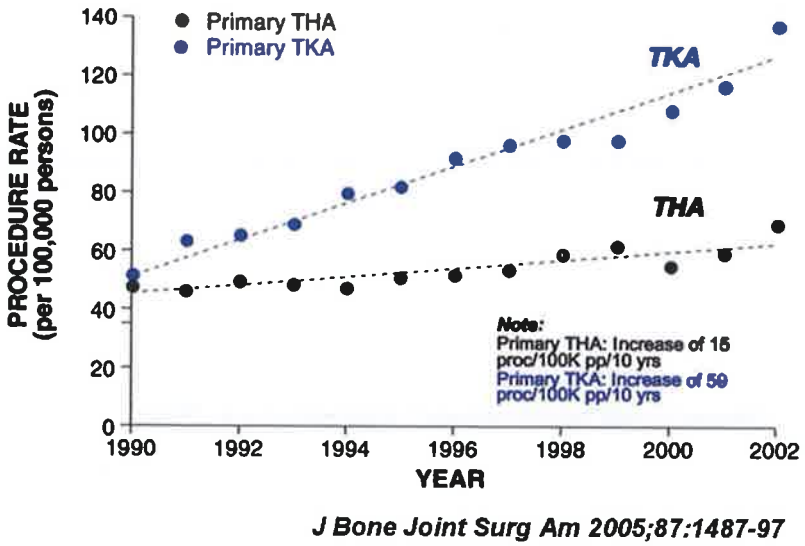

Figure 1.48 Joint replacements for osteoarthritis

Osteoarthritis may occur in any synovial joint, but most commonly develops in the knee, hip, spine and hand (Buckwalter *et al*, 2004). It is characterised by destruction of articular cartilage, leading to fibrillation, fissures, and eventually full-thickness erosion (Figure 1.49). Bone changes will also develop, such as osteophyte formation and alterations to the subchondral bone structure.

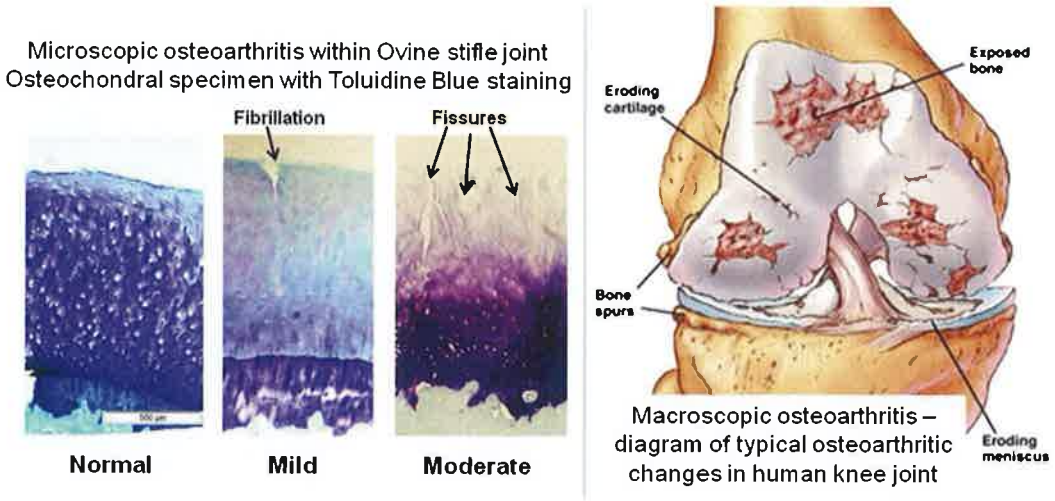

Figure 1.49 Micro- and macroscopic osteoarthritis

The initiating factors of osteoarthritis are still poorly understood; traditionally it was always described as "wear and tear", or degenerative, arthritis. It was assumed to develop as a direct result of some initial biological or mechanical disruption of the joint. This would then change the mechanical stresses acting on the joint, thus causing damage to the articular cartilage layer and alterations in the underlying subchondral bone as it alters / remodels to compensate. Destruction of the joint tissues then progressed until end stage arthritis is reached, with the classical characteristics of cartilaginous damage or denudation, subchondral bone erosion and development of osteophytic lesions (Creamer & Hochberg, 1997; Figure 1.49).

There are now a number of hypotheses which consider the initiating factors or underlying causes of primary osteoarthritis; many agree in principle with the traditional view that the disease process begins within the articular cartilage of the joint. Here, the cartilage matrix may become injured due to abnormal loading pressures; if this is minor, the chondrocytes are able to replace and repair the tissue. In more severe trauma, however, the repair capacity of the chondrocytes is overwhelmed, or the chondrocytes themselves are damaged, and the lesion may progress to cartilage degeneration (Buckwalter & Brown, 2004; Martin & Buckwalter, 2002). In some cases, the trauma applied to the joint need not even be excessive. If the matrix is abnormal, as is the case where the chondrocytes produce abnormal collagen or cytokines, low levels of trauma may be enough to initiate the disease process (Allen, 1998; Goldring, 2002).

Conversely, a number of authors have advocated that that changes in the underlying subchondral bone may actually precede the damage seen within the articular cartilage (Burr, 2004; Radin & Rose, 1986). This hypothesis was advanced by Radin & Rose in 1986, when they proposed that alterations in the mineralisation or structure of the subchondral bone could give rise to "stiffness gradients" in the surface upon which the articular cartilage lies; this discontinuity in stiffness then results in shear stresses within the overlying cartilage when compressed, initiating fibrillation and osteoarthritis (Radin & Rose, 1986; Figure 1.50).

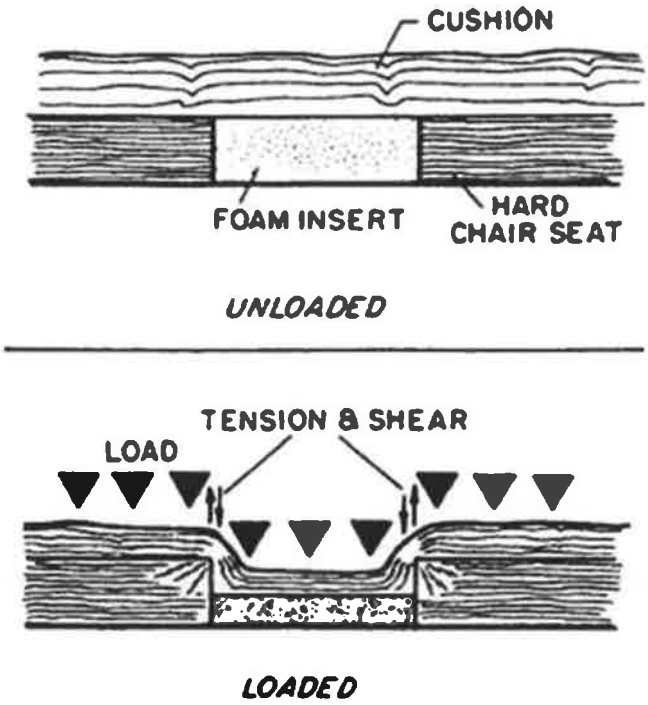

Figure 1.50 Shear stresses during compression in the presence of stiffness gradients (Radin & Rose, 1986)

More recent research has continued to examine the role of the underlying subchondral bone in the pathophysiology of osteoarthritis in a range of animal models, including rats, dogs, guinea-pigs and horses (Anderson-MacKenzie *et al*, 2005; Dedrick *et al*, 1993; Hayami *et al*, 2006; Kawcak *et al*, 2001; Muir *et al*, 2006). The hypothesis that osteoarthritis is systemic musculoskeletal disorder with a metabolic component is also being actively investigated; dysfunction of mesodermal-derived cells, such as myocytes, lipocytes and osteoclasts may be part of the disease process (Aspden, 2008).

1.5 SHEEP

The selection and use of animal models allows investigation of underlying disease mechanisms. Initial considerations regarding species selection include factors such as expense, availability (preferably with genetic homogeneity), docility, and ease of veterinary care and housing of large numbers (Thorndike *et al*, 1998). Sheep fulfil a large number of the above criteria and the ovine model has been used for investigation of a number of conditions to date, including the bone diseases osteoporosis and osteoarthritis (Newton, 2004; Parker *et al*, 2003).

With regard to physiology, the metabolic rate of sheep (Figure 1.51), based on oxygen consumption per gram of body weight, is 0.22 and is closer to that of humans (0.21) than rats (0.87) or dogs (0.33) (Schmidt-Nielsen, 1977).

Figure 6.1. Metabolic rates for mammals and birds, when plotted against body mass on logarithmic coordinates, tend to fall along a single straight line. Adapted from Benedict (1938).

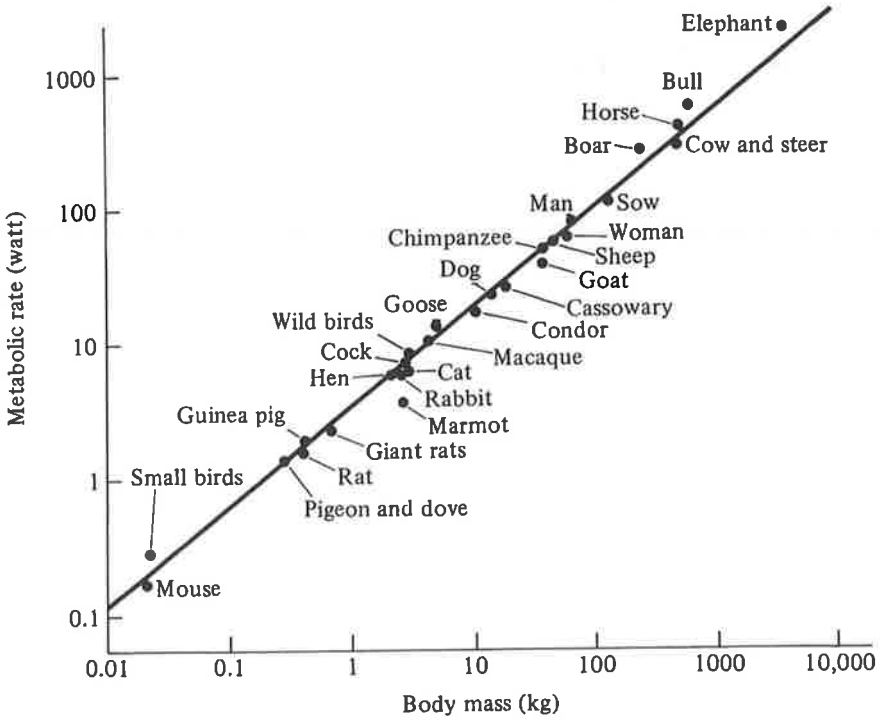

Figure 1.51 Metabolic rates (Schmidt-Nielson, 1984)

The ovine ovary will commence ovulation, and the young ewe enter oestrous for the first time, at approximately 30 weeks of age, with some slight variation according to month of birth (Fitzgerald *et al*, 1982). The length of the oestrous cycle typically ranges from 15 – 18 days, with a plasma hormonal profile as shown in Figure 1.52 (Hansel *et al*, 1983; Zarco *et al*, 1988).

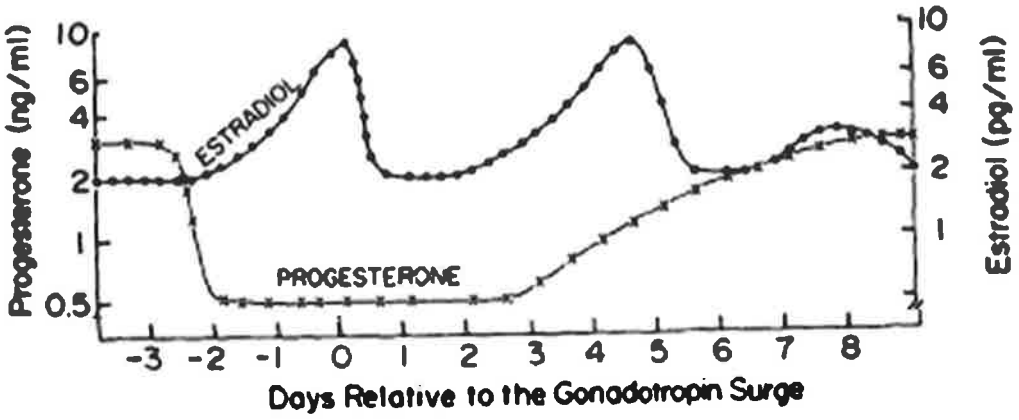

Figure 1.52 Endocrine changes during oestrous (modified from Hansel *et al*, 1983)

During anoestrous, circulating levels of progesterone and oestrogen are at basal levels, with elevations only seen just prior to onset of the next oestrous cycle (Yuthasastrakosol *et al*, 1975). While sheep do not undergo a natural menopause, one may be induced by ovariectomy, which significantly reduces circulating levels of both hormones (Kennedy *et al*, 2009b; Newton *et al*, 2004).

Musculoskeletal similarities exist between the human and ovine skeletons also; the ovine bone remodelling cycle is comparable to that of humans, being of approximately 3 months duration (Lee *et al*., 2002). Ovariectomised (OVX) sheep are now considered to be useful models for a variety of metabolic bone disorders, including bone mineral density loss, osteoporosis and alterations in trabecular bone architecture associated with oestrogen deficiency (Brennan *et al*, 2009; Kennedy *et al*, 2009a; Johnson *et al*., 2002; Newton 2004; Thorndike *et al* 1998; Turner *et al*., 1995). Ovine models for osteoarthritis are also well established in the scientific literature, with the ovine stifle joint (Figure 1.53) being the joint most commonly encountered in these studies (Hwa *et al*, 2001; Little *et al*, 1997; Parker *et al*, 2003; Pritzker, 1994).

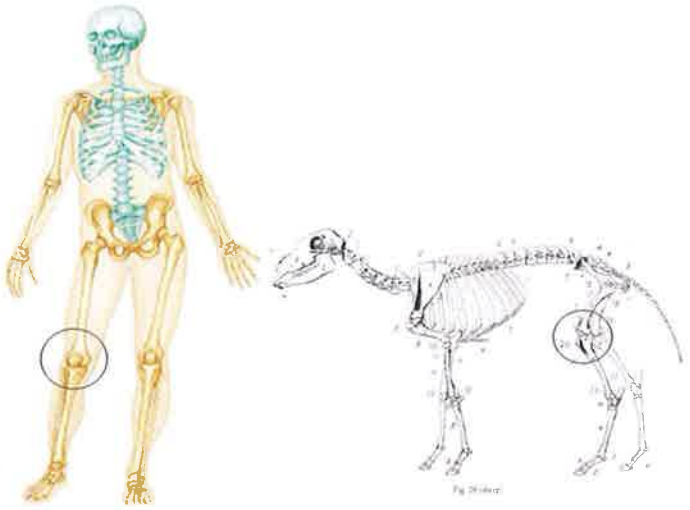

Figure 1.53 Human knee and Ovine stifle joints *in situ*

With regard to many of the structural parameters, the stifle joint may be considered to be a 1:3 scale model of the knee joint (Figure 1.54). However, the distal ovine femur has a smaller trochlear width, a narrower femoral intercondylar notch and slightly different patellofemoral dynamics. The ovine tibia has a greater slope on the plateau and a massive bone stock, with thickened cortex, at its proximal end (when compared to its human counterpart). Soft tissue structures, such as menisci, cruciate ligaments and asymmetrical collateral ligaments are also comparable between human knee and ovine stifle joints (Osterhoff *et al*, 2010).

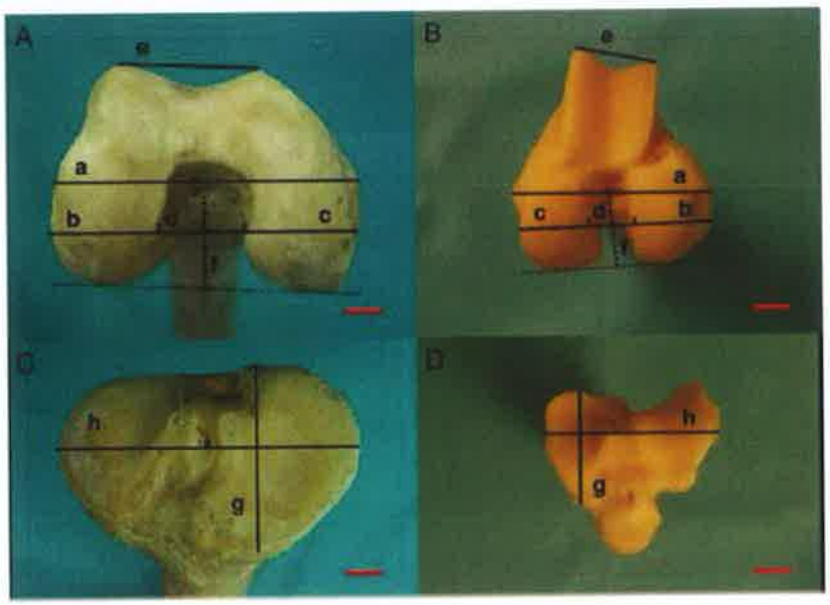

Measurements of the human (A and C) and ovine (B and D) femur (A and B) and tibia (C and D). The red bar represents 1cm.

Figure 1.54 Human knee and Ovine stifle joints (Osterhoff *et al*, 2010)

As previously described, the skeleton is constantly undergoing adaptation in response to mechanical stimuli. It is estimated that approximately 20% of the cancellous bone surface is being remodelled in the typical human skeleton at any given time (Bilezikian *et al*, 2004). This gives rise to a large degree of variability of trabecular, and cortical, structure depending on the species chosen and the bone sampled (Table 1.5).

Authors	Bone	BV/TV (Ratio)	TbN (per mm)	TbTh (mm)	TbSp (mm)
Mitton *et al*, 1998	L4	0.37	1.28	0.29	0.51
Rubin 2002	Femoral Condyles	0.41	2.1	--	0.37
Cornish *et al*, 2006	Mandibular condyle	0.53	2.15	0.24	0.22

Table 1.5 Trabecular architectural parameters in various ovine bones

The skeletal maturity of the animal also makes a statistically significant difference to trabecular architecture in the ovine model. Nafei *et al* found that values of all variables included within their study significantly different in the skeletally mature and immature groups (Table 1.6; Nafei *et al*, 2000). Cornish *et al* found comparable results within the ovine non weight-bearing mandibular condyle (Table 1.7; Cornish *et al*, 2006).

	Skeletally immature	Skeletally mature	p value*
Bone volume fraction (%)	32.7 (1.3)	41.8 (2.4)	0.001
Connectivity density (trabec/mm^3)	8.97 (0.44)	4.00 (0.32)	< 0.001
Mean trabecular volume (mm^3)	0.037 (0.003)	0.125 (0.016)	< 0.001
Bone surface density (mm^2/mm^3)	2.50 (0.04)	2.16 (0.04)	< 0.001
Architectural anisotrophy (volume orientation)	2.52 (0.12)	3..35 (0.21)	< 0.001
**Mann-Whitney U test*			

Table 1.6 Trabecular variations between skeletally immature and mature sheep (Nafei *et al*, 2000)

Mean and standard deviation (in parentheses) of all bone structural index values for lateral, central and medial sections in young and mature sheep.

Section	BV/TV (%)	BS/TV (mm^2/mm^3)	BS/BV (mm^2/mm^3)	Tb.Th (mm)	Tb.Sp (mm)	Tb.N (no./mm)
Lateral young (L)	63.3 (11.76)	**3.82 (0.43)***	6.16 (1.07)	**0.33 (0.05)†**	0.19 (0.08)	**1.91 (0.21)†**
Central young (C)	54.74 (14.69)	3.99 (0.32)	7.77 (2.29)	0.27 (0.08)	0.22 (0.07)	1.99 (0.16)
Medial young (M)	56.86 (13.18)	**4.43 (0.42)***	8.15 (2.09)	0.25 (0.06)	0.19 (0.05)	**2.21 (0.21)†**
Total young	58.3 (13.01)	4.08 (0.45)	7.36 (1.98)	0.28 (0.07)	0.2 (0.06)	2.04 (0.22)
Lateral mature (L)	52.89 (9.60)	4.28 (0.89)	8.29 (1.99)	**0.25 (0.05)†**	0.22 (0.06)	2.14 (0.44)
Central mature (C)	50.05 (10.35)	4.02 (0.53)	8.3 (1.68)	0.24 (0.04)	0.25 (0.08)	2.01 (0.26)
Medial mature (M)	55.01 (10.88)	4.6 (0.82)	8.66 (2.14)	0.24 (0.06)	0.2 (0.05)	2.3 (0.41)
Total mature	52.65 (10.14)	4.3 (0.77)	8.42 (1.88)	0.24 (0.05)	0.22 (0.07)	2.15 (0.38)

Figures in bold indicate a statistical significance at $p < 0.05$ (across like symbols).

Table 1.7 Site-to-site variation in trabecular architecture (Cornish *et al*, 2006) - ovine non weight-bearing mandibular condyle

Even within the same bone, considerable site-to-site differences are frequently observed (Coelho *et al*, 2009), as may also be seen in Table 1.7 (Cornish *et al*, 2006). In a comparison of 3 specimens taken from the cranial, mid-vertebral and caudal regions of the ovine L3 vertebra, Kennedy *et al* found that trabecular number, thickness, spacing, connectivity density, degree of anisotropy and bone mineral density all displayed significant regional variations (Kennedy *et al*, 2009a).

A number of other conditions will affect the trabecular architecture also; one of considerable importance for this thesis is the effect of ovariectomy. Although sheep do not undergo a natural menopause as humans do, an artificial one may be induced for the purposes of research by ovariectomy (Kennedy *et al*, 2009b; Newton *et al*, 2004). The alterations typically observed post-ovariectomy include a reduction in bone volume fraction (BV/TV), a reduction in the number of trabeculae, a reduction in the thickness of the individual trabeculae and an increased distance between them (Jiang *et al*, 2005; Turner *et al*, 1995; Table 1.8). These alterations may be further compounded, for example by treatment with glucocorticoids (Table 1.9). Previous studies using an ovariectomised ovine model to investigate osteoporosis within our own unit have confirmed that bone turnover is significantly elevated at 12 months post-ovariectomy (Kennedy *et al*, 2009b), with a trend towards reduction in bone volume fraction and trabecular thickness at a number of sites (Brennan, 2008; Kennedy *et al*, 2008).

Authors	Bone		BV/TV (Ratio)	TbN (per mm)	TbTh (mm)	TbSp (mm)
Turner *et al*, 1995	Ovine Iliac Crest	CON	0.25	2.0	0.13	0.38
		6 months post-OVX	0.22	1.9	0.12	0.44
		6 months post-OVX	0.24	2.0	0.12	0.40
Jiang *et al*, 2005	Ovine Proximal Femur	CON	0.25	2.0	0.18	0.38
		6 months post-OVX	0.21	1.6	0.17	0.46

Table 1.8 Effects of ovariectomy on trabecular architecture

Authors & animal	Bone	Tx	BV/TV (Ratio)	TbN (per mm)	TbTh (mm)	TbSp (mm)
Schorlemmer *et al*, 2003	Ovine Tibia	1yr OVX	0.27	2.2	0.12	0.34
		1 yr OVX & Glucocorticoid	0.20	2.2	0.09	0.38

Table 1.9 Effects of ovariectomy and Glucocorticoids on trabecular architecture

The effects of interventions such as ovariectomy on cortical bone are less extensively documented. Cortical porosity does increase in the diaphysis of the ovine metatarsal one year post ovariectomy (2.07% vs. 1.04%; Kennedy *et al*, 2009b). Bone quality is also altered; the viscoelastic properties (storage modulus) is significantly lower (5.2%) at the higher frequencies in the ovine radius at 3 years post-ovariectomy (Les *et al*, 2005). Alterations are seen in other species also; in a rat immobilisation model, cortical thickness of the proximal tibial diaphysis is reduced by 18% compared to control animals (276 vs. 335 μm; Laib *et al*, 2000).

With regard to the use of the ovine model to investigate osteoarthritis, a large number of studies typically induce osteoarthritis by means of an experimental injury; monoarticular studies may do this by means of causing an injury to an articular structure in order to destabilise the joint, or by placing the joint under abnormal mechanical loading (Little *et al*, 2008; Pritzker, 1994). A variety of different methods have been used in various animal species, as shown in Table 1.10. However, meniscectomy has proven to be most reliable in the ovine model (Hwa *et al*, 2001; Little *et al*, 1997; Parker *et al*, 2003).

The use of ovariectomy alone as a model of osteoarthritis induction is a more recent addition to the literature. Ovariectomy alone has been shown to have a detrimental effect on the structural, material and biomechanical properties of ovine articular cartilage (Cake *et al* 2005; Turner *et al* 1997); some further studies have also shown that these effects are ameliorated by oestrogen replacement post-operatively, whether by means of a cutaneous patch or by the presence of an oestradiol implant introduced at the initial surgical procedure (Turner *et al*, 1997; Parker *et al*, 2003; Sniekers *et al*, 2008b). This use of the ovariectomy model for osteoarthritis is still controversial; it is possible that the local effects of osteoarthritis induced by ovariectomy and those induced by alteration of the mechanical loading of the joint (i.e. by meniscectomy) may be quite different (Pajamäki *et al*, 2008).

Surgical Induction/Destabilisation		
ACL transection (ACLT)	Rat Guinea pig Rabbit Cat Dog (mongrel, foxhound, beagle)	Speed of onset and severity of disease higher than in humans after same injury
Meniscectomy	Rat Guinea pig Rabbit Dog (mongrel, greyhound) Sheep Monkey (Grivet)	Maybe partial or total, medial or lateral excision, unilateral or bilateral Speed of onset and severity of disease in animals usually higher than in humans after same injury
Meniscal destabilisation	Mouse	Unproven with therapeutic intervention as yet
Combination surgery	Mouse Rat Guinea pig Rabbit	Various combinations of ACL and/or MCL transection with or without meniscectomy or meniscal destabilisation
Impact loading; cartilage scarification	Rabbit Dog	Direct acute trauma to joint
Osteochondral chip and exercise	Horse	Mild post-traumatic cartilage changes
Ovariectomy	Rat Sheep Macaque	Postmenopausal OA: maybe secondary to weight gain and/or bone changes

Table 1.10 Biomechanical models of Osteoarthritis (Little *et al*, 2008)

1.6 AIMS & OBJECTIVES

Ovariectomised (OVX) sheep are now considered to be useful models for a variety of metabolic bone disorders, including bone mineral density loss, osteoporosis and alterations in trabecular bone architecture associated with oestrogen deficiency (Brennan *et al.*, 2009, Kennedy *et al.*, 2009a, Johnson *et al.*, 2002, Newton *et al.*, 2004, Thorndike & Turner, 1998). The primary aims of this thesis are as follows:

1. With regard to the stifle joint, does ovariectomy:
   - instigate a periarticular osteoporosis?
   - influence periarticular bone turnover (modelling and /or remodelling?)
   - induce osteoarthritis?
2. What relationships are there between these processes?

CHAPTER 2: ANIMAL STUDY

2.1 INTRODUCTION

The sheep used within this study were purchased, following initial power analysis and sample size calculations, for use as a model of osteoporosis by Drs Kennedy and Brennan, who have published their findings in a number of journals to date (Brennan 2008; Kennedy *et al*, 2008; Kennedy *et al*, 2009b; Kennedy *et al*, 2009b). The majority of stifle joints and tibiae of the sheep were not used in any of the studies performed by Drs Brennan or Kennedy, and so I was able to obtain these for my own research, examining periarticular osteopathies. Although sheep in the original study were randonised to "Year 1" and "Year 2" groups (referring to time of sacrifice), I only examined joints and tissue from sheep from the year 1 group for my thesis; additionally some tibiae from year 1 sheep were used for other research projects and these animals were therefore not included in my study (Tables 2.1 & 2.4).

At this point I would like to express my thanks to Drs. Oran Kennedy and Orlaith Brennan, who were responsible for shepherding the flock of sheep within this study for approximately $2^1/_2$ years under the supervision of Dr Susan Rackard, Lecturer in Small Animal Surgery (University College Dublin). None of this research would have been possible without their care and attention for the animals involved, and all work and animal husbandry described within Chapter 2 of this thesis is entirely theirs.

2.2 GROUP ASSIGNMENT

Seventy-two skeletally mature, mixed breed female sheep, of approximately 5-9 years of age were purchased at market in August 2003. All animals were housed on Lyons Estate Farm, Newcastle, Co. Dublin where they were maintained at pasture. Animals underwent routine health checks by a veterinarian and received standard routine care during the course of this study, including vaccination, dipping and treatment to prevent infectious foot rot and other diseases. Additionally, all ewes continued to have their hooves trimmed and fleece shorn as necessary during this time period. To facilitate this animal experiment, an animal licence, number B100/2443, was granted by the Department of Health under the Cruelty to Animals Act, 1876 and also approved by the ethics committee in the School of Veterinary Science in University College Dublin.

To enable identification of animals, each sheep was fitted with two ear tags. A sub-dermal microchip was also inserted at the back of the neck, between the shoulders. This was to ensure that in the event of the ear tags becoming damaged or lost over the course of this study, individual sheep would still be identifiable.

Animals were then randomly assigned into one of two groups, control or ovariectomy. Within each of these groups, the animals were sub-divided into year 1 or year 2, giving a total of four groups (See Table 2.2). To permit easy identification of animals in the field, each sheep was branded on the fleece. Control animals were marked with blue ink as C1 and C2, for year 1 and year 2 respectively. Ovariectomised sheep were branded with red ink, T1 (OVX 1) and T2 (OVX 2) indicating year 1 and year 2 respectively.

Year 1 Control (C1)		**Year 1 OVX (T1)**		**Year 2 Control (C2)**		**Year 2 OVX (T2)**	
Number	**Chip**	**Number**	**Chip**	**Number**	**Chip**	**Number**	**Chip**
175/-	8435	**119/- xx**	**7801**	191/-	4054	33/-	4141
4297/457	5631	4294/1563	5012	462/-	4329	282/-	2730
4312/1232	2520	4318/1370	8251	4309/1063	4317	642/-	6717
4315/1282	8721	4329/1436	4649	4316/1023	0149	4308/1325	5679
4317/1329	1822	4337/974	4476	4319/1142	4419	4313/1162	8400
4332/1144	4234	4342/1440	0667	4323/1395	6514	4320/1021	6977
4344/1151	4563	4346/1334	8098	4324/1315	1692	4321/1181	3302
4349/1321	7586	4350/1035	4904	4336/1074	2093	4322/1193	0647
4355/4318	4469	4354/1422	3437	4339/1005	9497	4333/1258	6915
4361/1363	5408	4358/1036	5597	4341/1100	5145	4335/1345	7244
4366/1368	6098	4363/1292	8063	4343/1007	2964	4338/1407	0389
4496/1154	4775	4365/1327	0394	4348/1133	0378	4347/1134	5758
4377/1268	7952	4372/1441	0194	4351/1093	1405	4356/1227	9409
4384/R35	5694	4374/1173	1535	4357/1457	3074	4362/1138	0413
4457/-	3390	4383/J137	0865	4360/1130	8074	4368/1244	8715
4463/156	9595	4479/-	7947	4364/1379	5532	4373/1169	7792
4474/-	1486	4483/J186	1055	4367/1366	9943	4386/H146	0664
4478/181	9270			4371/1053	0989	4477/X131	5112
				4468/ -	3652		
Total n=18		Total n=17		Total n=19		Total n=18	

Table 2.1 Sheep groupings and numbers

2.3 OVARIECTOMY

Between the 17th and 21st of November 2003, the ovariectomy operations were performed in the operating theatre on Lyons Estate Farm. These were performed by Dr Susan Rackard, Lecturer in Small Animal Surgery, UCD, with the assistance of Oran Kennedy and Orlaith Brennan, who kindly provided me with the notes regarding the procedures as detailed in the following sections of this thesis.

2.3.1 Anaesthesia & surgical preparation

The left side of the neck was clipped and an intravenous injection of sodium thiopentone was administered via the left jugular vein. The sheep were then placed in dorsal recumbency on the operating table and intubated using either a size 7 or 8 rubber cuffed endotracheal tube as appropriate. The cuff was inflated, tied to the mandible and anaesthesia maintained on 3-4% halothane (Halothane, Merial Animal Health, Harlow, UK) in oxygen. The hind limbs were secured to the operating table using ropes and the sheep maintained in dorsal recumbency for the duration of the surgical procedure.

An area of the ventral abdomen, extending from just caudal to the mammary glands to the umbilicus, was close-clipped and shaved with a disposable razor; standard aseptic surgical preparation of this field was then performed using chlorhexidine and alcohol. The table was tilted slightly to allow cranial displacement of the rumen and ease identification of the uterus and ovaries.

2.3.2 Surgery & Post-operative care

A sterile disposable paper drape (Baxter) was fenestrated, placed over the prepared surgical site and then secured to the ventral abdomen using 4 Bachaus towel clamps. A ventral midline incision was made commencing just cranial to the umbilicus and extending approximately 10cm cranially. The subcutaneous fat and fascia were bluntly dissected, being careful to protect the milk vein but ligating tributaries thereof when necessary. The linea alba was incised using a scalpel and scissors. The uterus was identified in the caudal abdominal cavity, exteriorised and the ovaries traced. The ovarian vessels were identified and ligated using a simple ligature of 3 metric polydioxannone (PDS, Ethicon, Johnson & Johnson, Brussels, Belgium). The ovary was then resected, with the ligated pedicle carefully checked for haemorrhage before returning it to the abdominal cavity (Figure 2.5). When satisfied that no haemorrhage was evident the pedicle was returned to the abdomen. The contralateral ovary was then resected in identical fashion.

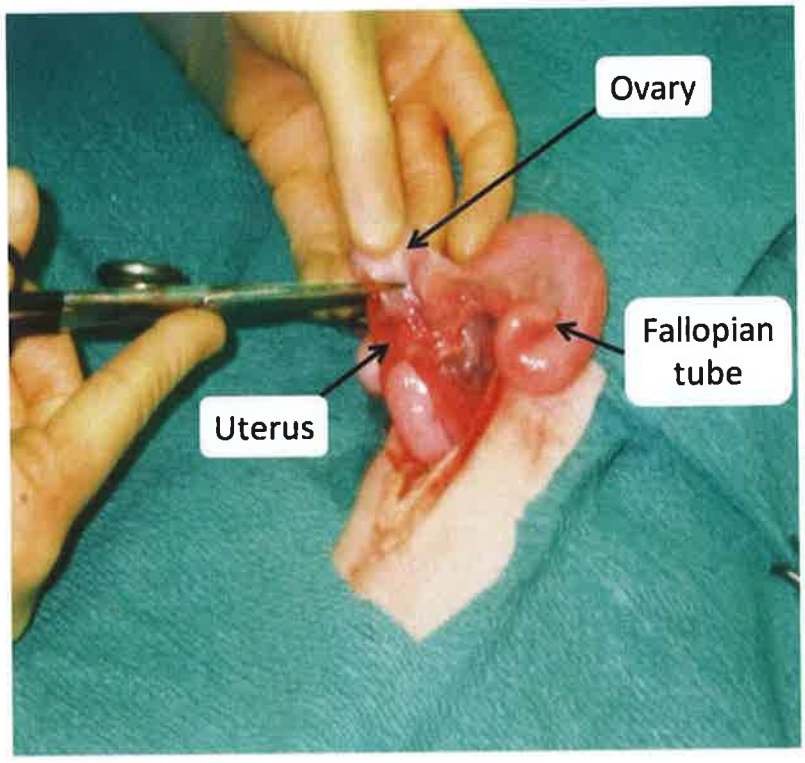

Figure 2.1 Ovariectomy

Prior to abdominal closure benzyl penicillin sodium (10mg/kg, Crystapen, Shering-Plough Animal Health, Ireland) was administered intraperitoneally as an additional prophylactic measure against peritonitis. The linea alba was closed using a simple continuous suture of 5/0 polydioxannone (PDS, Ethicon). The subcutaneous layer was apposed using a simple continuous suture of 3 metric polydioxannone (PDS, Ethicon). Skin closure was achieved with a simple continuous suture of 3/0 polypropylene (Prolene, Ethicon) and the surgical wound sprayed with an aluminium powder based wound spray (Alluspray, Vetoquinol Ireland Ltd, Dublin). A long-acting injection of amoxycillin was administered intramuscularly (15mg/kg, Betamox LA, Norbrook Laboratories Ltd, Ireland). An analgesic, flunixin meglumine, was also administered by intramuscular injection (2.2 mg/kg, Flunixin Inj, Norbrook Laboratories Ltd, Ireland). Oxytetracycline (50mg/kg, Terramycin LA, Norbrook Laboratories Ltd, Ireland) was administered by slow intravenous injection into the jugular vein prior to anaesthetic recovery. The sheep were observed carefully for the return of a swallow reflex and were extubated once this reflex had returned. They remained indoors under observation until completely recovered from anaesthesia and capable of normal ambulation.

The sheep were observed closely over a 48-hour period post-operatively. At 24 hours post-operatively a second injection of flunixin meglumine was administered if deemed necessary based on clinical evaluation. At 48 hours all surgical wounds were re-inspected for signs of swelling, infection or breakdown. Wounds were inspected again at 10 days post-operatively and skin sutures removed at this time. No wound infections were identified in any sheep. One sheep, at 10 days, was found to have a small abdominal incisional hernia (skin intact) which was repaired surgically under anaesthesia. Wound healing occurred uneventfully.

2.3.3 Ovarian function analyses

In the two weeks prior to sacrifice 17β oestradiol and progesterone levels were measured in both the control and ovariectomised sheep. In total, seven blood samples were collected from the jugular vein of each animal on alternate days. These samples were centrifuged; the serum was then removed and frozen at -20°C.

Progesterone levels were quantified using the AutoDELFIA™ Progesterone kit (Unitech Limited, Tallaght, Dublin 24). This assay is a solid phase fluoroimmunassay based on competition between europium-labelled progesterone and sample progesterone for polyclonal anti-progesterone antibodies (derived from rabbit). Oestradiol concentrations were quantified by means of a competitive binding Radioimmunoassay (Adaltis Estradiol Radioimmunoassay; Adaltis Italia S.p.A., Italy).

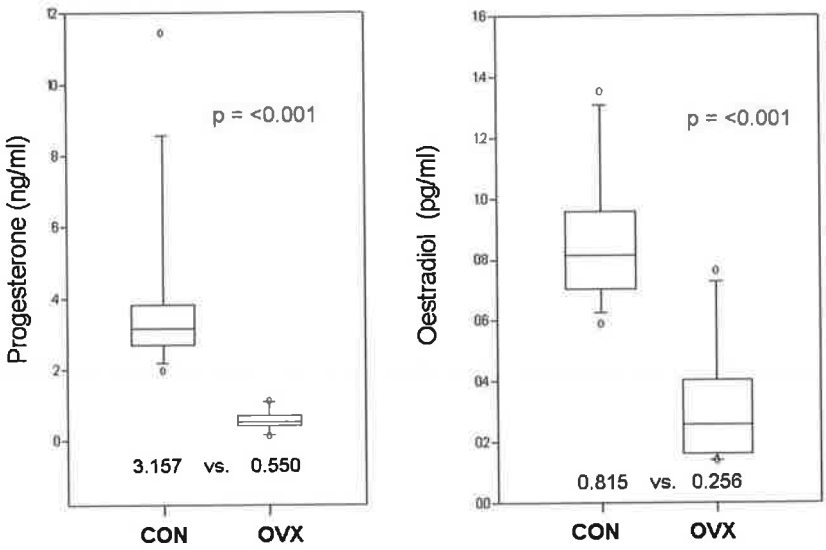

Graph 2.1 Ovarian functional analyses (2 weeks prior to sacrifice)

As would be expected, the ovariectomised sheep had significantly lower progesterone and oestradiol levels at one year post-operatively than the control sheep (Graph 2.1).

2.4.3 Sheep weights

The median weights of both control and OVX groups (year 1) are shown in Graph 2.2. Although the average group weights tended to increase over the 12 months of the study, there was no significant difference noted between the two groups.

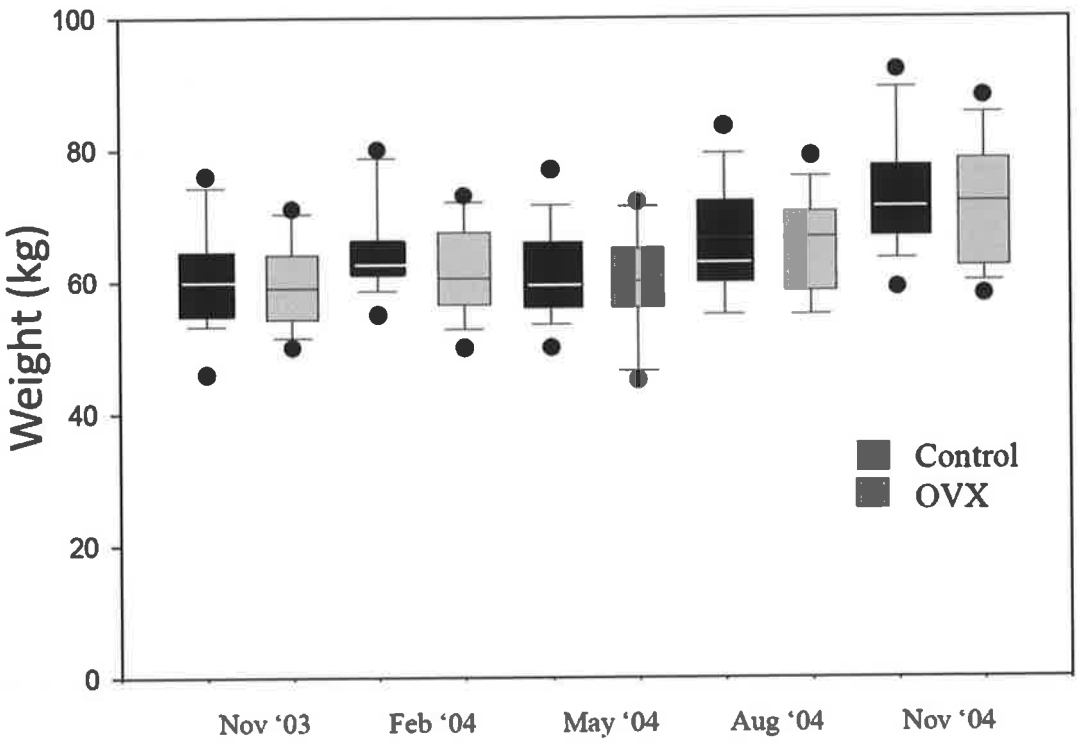

Graph 2.2 Sheep weights

2.4 FLUOROCHROME ADMINISTRATION

Oxytetracycline is available commercially as Terramycin/La Injectable Solution; all other dyes used were purchased as a powder and made into solution (See Table 2.2) with a pH of 7.2 - 7.4. To achieve sterility all solutions were passed through a VacuCap® 90 PF sterile vacuum filtration device (Pall Gelman Laboratory, Co. Meath) using a vacuum pump. An autoclave was used to sterilise all glassware.

Fluorochrome	**Solution Concentration (g/L)**	**Dosage (mg/kg)**
Oxytetracycline[1]	200	50[†]
Alizarin Complexone[2]	30	25[†]
Calcein[3]	5	10[†]*
Xylenol Orange[3]	90	90[†]*
Calcein Blue[3]	30	30[†]*
[†] From Lanyon *et al* (1982), * from Rahn (1977)		
1 Pfizer Animal Health, Dublin 2 Lennox Laboratory Supplies, Dublin 3 Sigma Aldrich, Dublin		

Table 2.2 Fluorochrome concentrations and dosages for in vivo injection

Prior to ovariectomy, all animals were weighed, to allow calculation of the dosage of fluorochrome required. Each OVX animal was injected with oxytetracycline at the time of their surgery; control animals were manually restrained at this time and the oxytetracycline administered without need for sedation. The area covering the left jugular vein was sheared and the left jugular vein identified to allow for administration. Over the rest of the year the sheep were given IV injections of alizarin complexone, calcein, xylenol orange and calcein blue at 12, 24, 36 and 48 weeks post surgery (Table 2.3); the animals were then sacrificed at 52 weeks.

Weeks post surgery	Date	Fluorochrome administered
0	17/11/03	Oxytetracycline
12	3/02/04	Alizarin Complexone
24	29/04/04	Calcein
36	19/7/04	Xylenol Orange
48	18/10/04	Calcein Blue
52	22/11/04	Sacrifice

Table 2.3 Schedule of fluorochrome administration

2.5 ANIMAL SACRIFICE

On the 22nd of November 2004, all the animals were sacrificed. This procedure was carried out in Irish Country Meats in Navan, Co. Meath.

Prior to departing Lyons Estate, all sheep were weighed. To facilitate easy identification of the left and right hocks while in the factory, the left front and hind hocks were sprayed red. The animals were then transported by lorry to Irish Country Meats for slaughter where all animals were processed according to in-house protocol.

Upon entering the facility, the animals were housed in pens. From here, they were lead to the processing line where each was assigned a sequential number, starting at 2346. The sequential number corresponds to the total number of animals processed that day in the factory. This sequential number was noted and cross-referenced with the original identification number as seen on the tag attached to each animal's ear. At this stage it was crucial that the original ID number was correctly matched with the sequence number. Once on the process line, the head and hence the ear tags, are removed from the body of the animal. Therefore, from this point, it is the sequence number that is used to identify the animals. Subsequently, for convenience, the first sequential number, or animal, was re-numbered 1; the second was numbered 2 and so on (Table 2.4).

Number	Original Identification Number	Factory Sequence Number	Group	Sheep weight (kg) (22/11/04)	Carcass weight (kg)
1	4496	2346	CON 1	83	38.9
2	175	2347	CON 1	83	41.2
3	4457	2348	CON 1	64	26.3
4	4329	2349	OVX 1	67	29.4
5	4355	2350	CON 1	85	41.5
6	4377	2351	CON 1	72	32.4
7	4315	2352	CON 1	66.5	34.5
8	4365	2353	OVX 1	75	34.9
9	4337	2354	OVX 1	87	45.1
10	4383	2355	OVX 1	67	29.2
11	4294	2356	OVX 1	64	29.5
12	4463	2357	CON 1	68	33.4
13	4366	2358	CON 1	70	33.1
14	4342	2359	OVX 1	73	37.8
15	4346	2360	OVX 1	71	34.6
16	4317	2361	CON 1	70.5	36.7
17	4474	2362	CON 1	68	29.2
18	4479	2363	OVX 1	83	40
19	4354	2364	OVX 1	63.5	26.4
20	4344	2365	CON 1	68	32.3
21	4374	2366	OVX 1	75	37.6
22	4312	2367	CON 1	78	40.6
23	4318	2368	OVX 1	65	33.1
24	4483	2369	OVX 1	80.5	38.4
25	4372	2370	OVX 1	76	36.2
26	4350	2371	OVX 1	63.5	29.8
27	4384	2372	CON 1	93	45.6
28	4297	2373	CON 1	76	36.5
29	4361	2374	CON 1	66	31.6
30	4478	2375	CON 1	70	34.4
31	4332	2376	CON 1	75	35.6
32	4363	2377	OVX 1	81	40
33	4358	2378	OVX 1	61	24.3
34	4349	2379	CON 1	60	23.7

Table 2.4 Assignment of numbers
(Shaded boxes indicate animals used for other research projects and therefore not included in this study)

As the animals moved along the line, the head was the first section to be removed and these were placed on the ground in the order the animals were sacrificed. This acted as a backup in case of confusion in the cross referencing of sequence number with the original ID number. The hocks were then removed (See section 2.6.1.). The fleece was removed and the animals were eviscerated. All non-bone matter was disposed off as Special Risk Material.

Once at the end of the line, the carcass was weighed and a tag printed showing the date, carcass weight and sequence number. This tag was then attached to the front limbs. The animals were left in cold storage over night to facilitate easy removal of the bones.

2.6 BONE HARVESTING

2.6.1 Pilot study

A pilot study was performed (OB, OK) to draw up the protocol for the harvesting of the bones following sacrifice of the animals. A fully skinned, eviscerated sheep carcass was purchased from Irish Country Meats and brought to the pathology department in the School of Veterinary Science, University College Dublin. Based on the results of this, the following procedure was drawn up:

- *Each animal will be placed in the supine position on a dissecting table with one trained operator (butcher) to dissect soft tissues and one assistant to bag and store each bone.*

- *Both front limbs (including humerus, radius, ulna and scapula) will be disarticulated from the carcass and excess soft tissue removed. Each bone will then be labelled and put in a separate bag.*

- *Both hind limbs (including femur, tibia and fibula) will be disarticulated from the carcass and excess soft tissue removed. Each bone will then be labelled and put in a separate bag.*

- *Using surgical bone cutters/band saw all ribs will be removed ensuring that the cut is made no less than 40mm from the thoracic vertebrae.*

- *The sternum will then be split to allow for compact storage of both sections of the ribcage.*

- *The spinal column will be separated into three parts, the lumbar, thoracic and cervical regions. The lumbar region will be separated through the sacroiliac joint and through the second intervertebral disc above L1, i.e. it will include one set of ribs. The thoracic spine will be separated through the intervertebral disc at T1.*

- *Each part of the spine and the pelvic bone will have excess soft tissues removed and will be labelled and placed in a separate bag.*

- *The labelled bags will be packed into a cardboard box which will then be sealed, numbered and made ready for transportation.*

This pilot study proved very useful; however, on the day slight modifications were made.

2.6.2 Bone harvesting

The day following sacrifice, (23rd November 2004), the bones were harvested from the animals. That morning, while the carcasses were still in the chilling room, a plastic bag was attached to each animal using a plastic tie. Each bag was labelled 1-34. Within each of these bags were 9 other labelled bags. Again each of these bags was labelled with the appropriate 1-34 identification number and the name of the bone(s) which were to be placed in it. These bags were labelled with one of the following:

Left Front Limb (LFL)

Right Front Limb (RFL)

Left Hind Limb (LHL)

Right Hind Limb (RHL)

Pelvis

Ribs

Lumbar Vertebrae (LV)

Thoracic Vertebrae (TV)

Cervical Vertebrae (CV)

From the chilling room the carcasses were led on a pulley system through to the boning hall (clean room).

2.6.3 Boning Hall

Prior to the bones being removed from the animals, a demonstration was given to the butchers working in the factory on how the procedure was to be carried out. The first animal was removed from the pulley and the butchers were shown how each limb was to be disarticulated, the ribs removed and the vertebrae separated.

Within the boning hall, 4 areas were identified and a table was assigned to each of our 4 assistants. Three butchers were then assigned to each table. One of the butchers from each table collected a carcass and collectively they removed all the bones. These bones were handed to the assistant who bagged them. Each bag was then placed into a plastic lined box. Once all the bones were in the box, the box was labelled and moved to be sealed.

2.6.4 Storage

The ovine tibiae obtained from the sheep which were used in this study (Table 2.4) were all stored at -70°C following animal sacrifice, until removed for examination by myself.

CHAPTER 3: THE EFFECT OF OVARIECTOMY ON THE STRUCTURE AND MINERALISATION OF BONE WITHIN THE MEDIAL TIBIAL PLATEAU

3.1 INTRODUCTION

The ovariectomised ewe is a well-accepted model for investigation of osteoporosis, in both trabecular and cortical bone (Jiang *et al*, 2005; Kennedy *et al*, 2009b; Turner *et al*, 1995). Studies examining subchondral or periarticular osteoporosis are rarer, and tend to utilise radiographic methods such as radiographic studies in humans and *in vivo* MicroCT in ovariectomised rats (Karvonen *et al*, 1998; Waarsing *et al*, 2004). Subchondral bone, particularly at the knee or stifle joint, is subjected to repeated loading and mechanical stimulation during the activities of daily living. Within this thesis, I wish to determine whether the subchondral bone, both cortical and trabecular, reflects the changes seen elsewhere in the ovine skeleton post-ovariectomy, or whether the microarchitecture is preserved. The alterations typically observed post-ovariectomy include a reduction in bone volume fraction (BV/TV), a reduction in the number of trabeculae, a reduction in the thickness of the individual trabeculae and an increased distance between them (Jiang *et al*, 2005; Turner *et al*, 1995).

3.2 AIMS OF STUDY

The overall aim of this section of the study was to determine the effects of ovariectomy on the structural and material parameters of the subchondral bone of the ovine tibial plateau as measured by DEXA and MicroCT.

Specific questions:

- Is bone mineral density reduced in the proximal tibia in ovariectomised ewes as compared to control animals?
- Does the subchondral trabecular bone reflect the reduction in trabecular number, width and connectivity seen elsewhere in the post-ovariectomy ovine skeleton?
- Is the subchondral cortical bone altered post-ovariectomy, either in thickness or material density?

3.3 MATERIALS AND METHODS

For the purposes of this thesis as a whole, a number of different investigations were employed. These required different methodologies in the processing of the osteochondral specimens (i.e. decalcified and paraffin embedded, or calcified and embedded in polymerized methylmethacrylate). For this reason, two specimens were obtained from each tibial plateau following DEXA (Dual energy X-ray absorptiometry) scanning. These were all taken from that portion of the plateau which is normally in contact with the femoral condyle during articulation, and not overlain by the menisci (Figures 1.40 & 3.5).

3.3.1 Dual energy X-ray absorptiometry

Initial Dual energy X-ray absorptiometry (DEXA) scanning of the bones for quantification of Bone Mineral Density (BMD) was performed of the tibiae; this examination is the gold standard for detection of osteoporosis in the clinical setting. A fan beam bone densitometer (Hologic QDR-4500TH Elite, Hologic, MA) was used to measure BMD. The estimated area (EA, cm^2) and bone mineral content (BMC) for each of the two tests was recorded. Bone mineral density (g/cm^2) was determined from these by dividing the BMC by the EA.

Figure 3.1 Dual energy X-ray absorptiometry (DEXA)

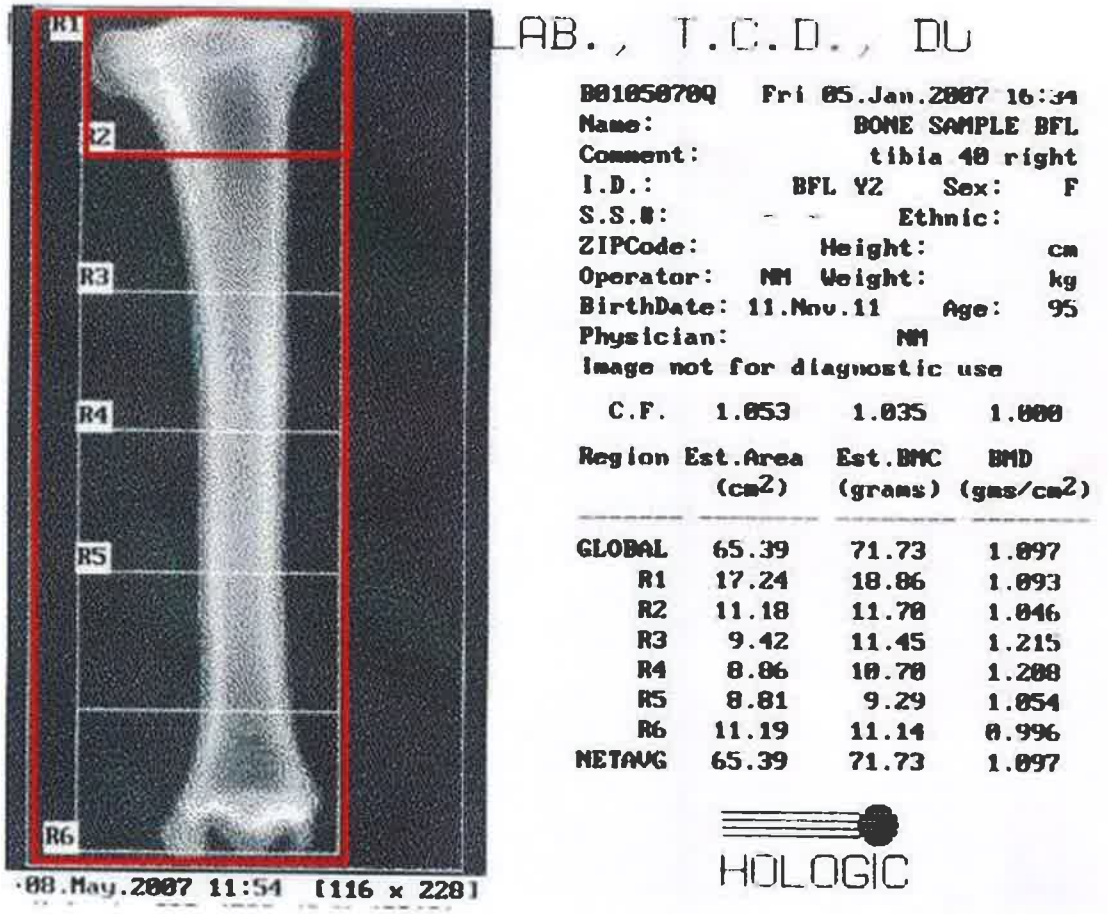

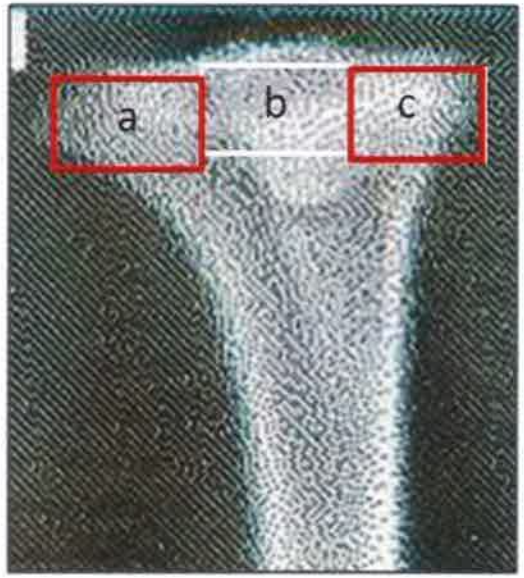

Subregional analysis:
a – Medial plateau
b – Intracondylar area
c – Lateral plateau

Figure 3.2 Subregional analysis of tibial plateau

All DEXA scans were performed in conjunction with Dr Nick Mahony in Trinity College Dublin. Three DEXA readings were examined in this study: initially, the BMD of the whole bone was considered; secondly, the proximal tibia was examined (R1 in Figure 3.2); lastly, subregional analysis was performed of the medal and lateral plateaux (A & C in Figure 3.2).

3.3.2 Removal of tibial plateau from tibia

Removal of the plateau from the intact ovine tibia was performed by use of a Struers Minitom Diamond Saw (Figure 3.3). The intact tibia was placed in the specimen holder of the Diamond Saw, and the proximal 1 – 1.5 cm of the tibial plateau removed. With the majority of specimens, this procedure was accomplished with one cut; however, it was necessary to rotate some specimens within the specimen holder and perform a second cut in order to completely transect the bone and remove the plateau. A digital photograph was obtained of each plateau upon removal from the remainder of the tibia; Figure 3.4 shows a photograph of a typical right plateau.

Figure 3.3 Removal of tibial plateau

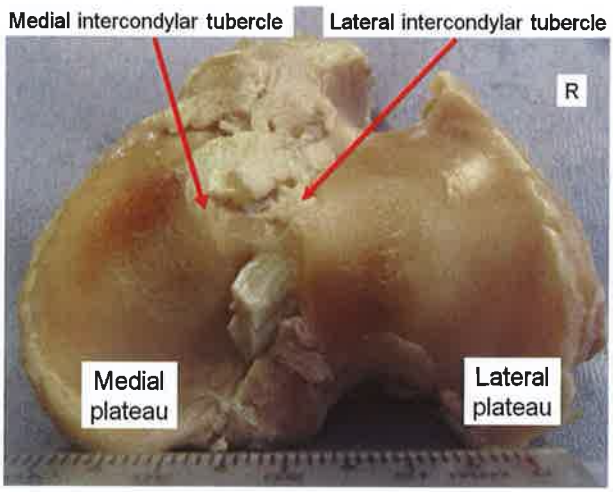

Figure 3.4 Right tibial plateau following removal

3.3.3 Obtaining osteochondral specimens from tibial plateau

Further cuts were then made with the diamond saw, in order to obtain 2 adjacent osteochondral specimens from the medial aspect of the plateau, from the area of maximal femoro-tibial contact and pressure (Figure 1.40; Fukubayashi *et al*, 1980). These specimens are labelled A and B as shown (Figures 3.5 & 3.6).

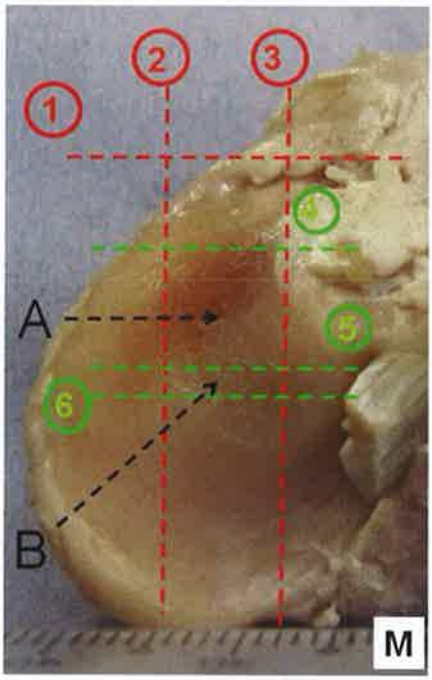

1) The anterior aspect of the plateau is removed, in order to facilitate further cuts
2) A vertical cut is made 11mm medial to the medial intercondylar tubercle
3) A second vertical cut is made 4mm medial to the medial intercondylar tubercle

The resultant segment (between lines [2] & [3]) is now 7mm in width.

4) A cut is made in the coronal plane just anterior to the medial intercondylar tubercle
5) A second coronal cut is made 5mm posterior to (4) above

This is specimen A

6) A third coronal cut is made 1.5mm posterior to (5) above

This is specimen B

Figure 3.5 Right medial tibial plateau – obtaining specimens A and B

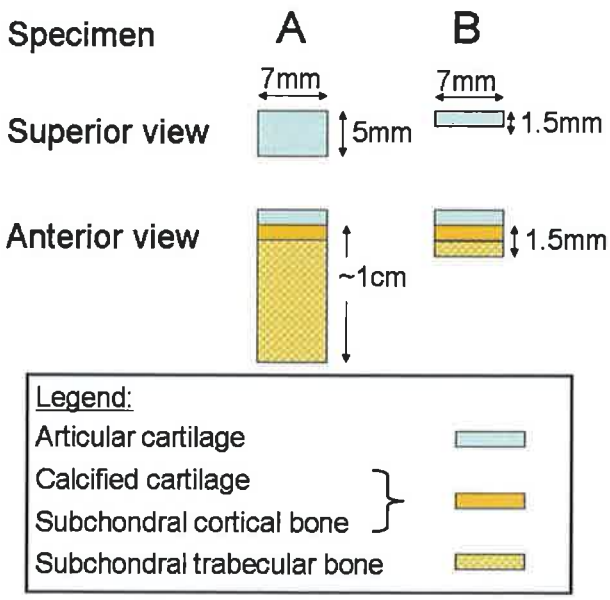

Figure 3.6 Summary of specimens

3.3.4 MicroCT

Three dimensional analyses were performed of specimens (A) from the tibial plateaux using desktop microcomputed tomography, or MicroCT (Figure 3.7; μCT40; Scanco Medical, Basserdorf, Switzerland).

Figure 3.7 Benchtop MicroCT (μCT40)

Specimens were placed in a 20.5mm diameter polyetherimide specimen holder, and secured in position using synthetic foam (Figure 3.8). Care was taken to ensure that all specimens were orientated identically: specimens were placed with the anterior surface facing inferiorly; the subchondral plate of the specimen faced into the MicroCT; rotation of the specimen within the holder was eliminated. The scan was performed at 8μm resolution, with a beam intensity of 70 kVp (I = 114 μA) and a scan integration time of 230 milliseconds. The MicroCT was routinely calibrated with a phantom containing hydroxyapatite (HA) densities of 0, 100, 200, 400 and 800 mg/cm^3, so that HA concentration of the specimens could be ascertained.

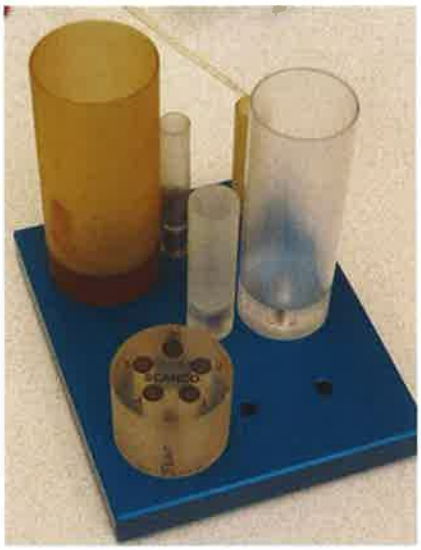

Specimen holders & calibration phantom

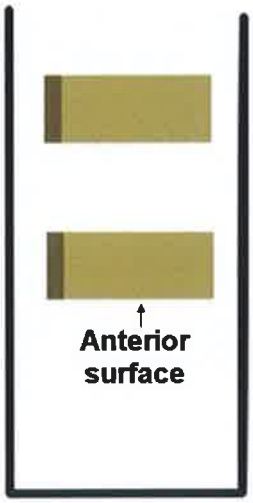

Placement of specimen(s) within holder

Figure 3.8 MicroCT specimens in holder

The MicroCT initially performed a "scout view" of the specimen (Figure 3.9). After ensuring that the specimen was level, with no obvious rotation, reference lines for the volume of the specimen to be definitivly scanned were placed. For this study, the reference lines were placed 4.16mm (416 slices) apart; the resultant scan time for each specimen was approximately 36 minutes.

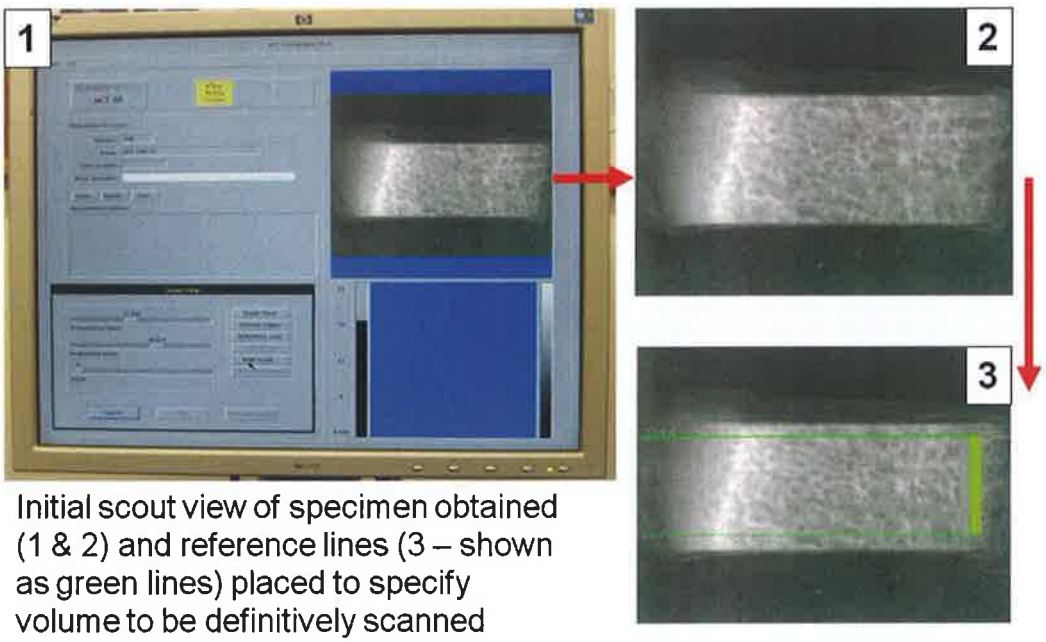

Initial scout view of specimen obtained (1 & 2) and reference lines (3 – shown as green lines) placed to specify volume to be definitively scanned

Figure 3.9 MicroCT scout view

For analysis of the subchondral trabecular bone, a volume of interest (VOI) was defined within the sample. A 7mm x 5mm area (700 x 500 voxels) was taken from each complete 2D slice, beginning 1.5mm below the nadir of the articular surface of each individual slice (Figure 3.10). A global thresholding system was used; a threshold value of 210 was applied, with a sigma of 0.8 and a support value of 1. These were then reconstructed into a 3-dimensional image by the Scanco software, with a results sheet for the specimen generated as shown in Figure 3.11.

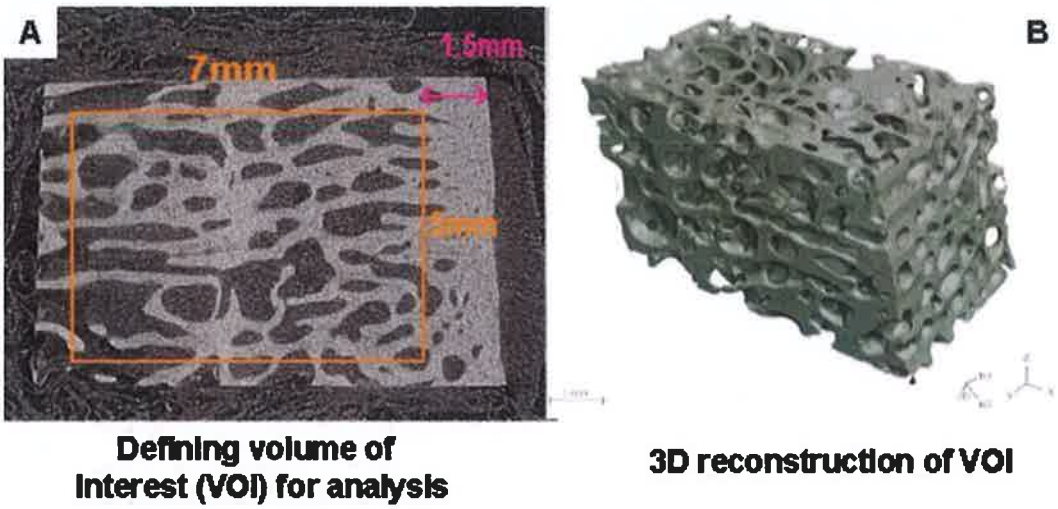

Figure 3.10 MicroCT – VOI for trabecular analysis

jch 31RtM

S-No.: 836 Filename: C0000977
M-No.: 1038 Date: 04-DEC-2007 12:56

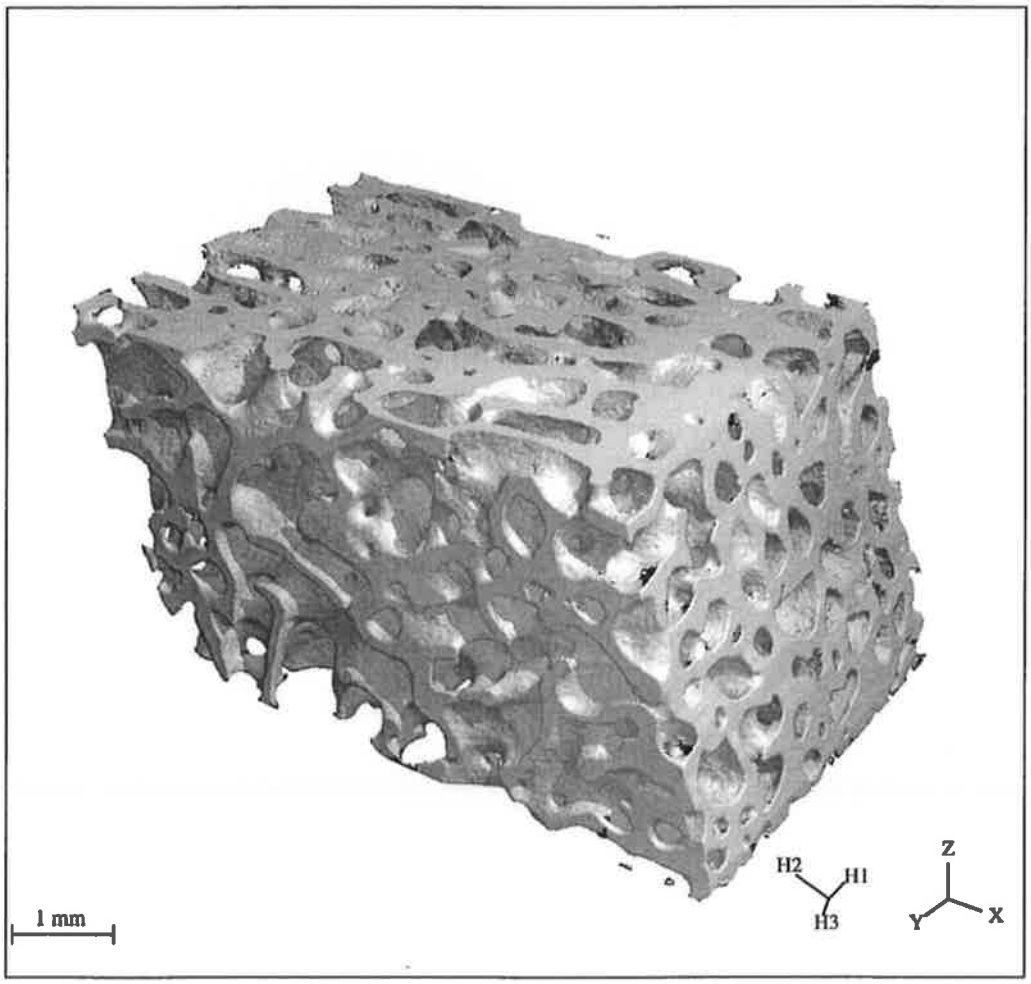

VOI	X	Y	Z	Mean/Density [mg HA/ccm]	
Position [p]	749	856	2	of TV (Apparent)	416.5332
Dimension [p]	820	504	414	of BV (Material)	908.7989
Element Size [mm]	0.0100	0.0100	0.0100		

Direct (No Model)			TRI (Plate Model)			Anisotropy	
TV	[mm³]	144.8935	TV	[mm³]	144.3975	|H1| [mm]	0.3645
BV	[mm³]	55.1415	BV	[mm³]	55.4549	|H2| [mm]	0.5641
BV/TV	[1]	0.3806	BV/TV	[1]	0.3840	|H3| [mm]	0.4196
Conn. D.	[1/mm³]	12.8888	BS	[mm²]	670.4274	DA [1]	1.5476
SMI	[1]	-0.5381	BS/BV	[1/mm]	12.0896		
Tb.N*	[1/mm]	2.6824	Tb.N	[1/mm]	2.3215	Segmentation: 0.8 / 1 / 210	
Tb.Th*	[mm]	0.1915	Tb.Th	[mm]	0.1654	Operator Meas.: Jane Holland	
Tb.Sp*	[mm]	0.4580	Tb.Sp	[mm]	0.2653	Operator Eval.: Oran Kennedy	

µCT 40
SCANCO MEDICAL

Figure 3.11 MicroCT – trabecular analysis

In this thesis, the method employed to determine subchondral plate thickness was configured in order to define the level at which compact bone becomes trabecular – i.e. where the bone volume fraction (BV/TV) changes from being above 0.7 (cortical), to below 0.7 (cancellous). As with the trabecular analysis above, a threshold value of 210 was used throughout, with a sigma of 0.8 and a support value of 1.

Two-dimensional analysis was used to confirm the BV/TV ratio on the first box (Figure 3.12a) was greater than 0.7. The box was then moved inferiorly on the same scan by 1mm and the 2D analysis repeated (Figure 3.12b). If the BV/TV ratio remained above 0.7, the plate thickness was at least 2mm. On subsequent analyses, the box was progressively moved inferiorly by 1mm each time, until the ratio fell below 0.7. If this happens at the 9th box, for example, the depth was determined to be 8 boxes (equivalent to 8mm). This was performed on 10 random 2D sections of each specimen, and the mathematical mean of these measurements was then adjudged to be the subchondral thickness of the specimen.

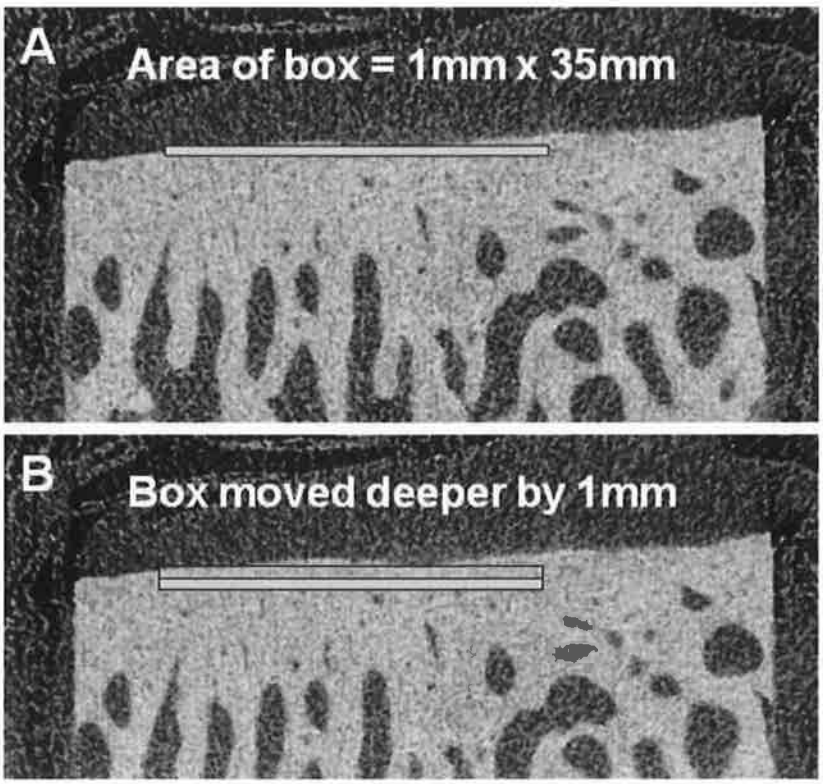

Figure 3.12 MicroCT – analysis of subchondral plate thickness

To ascertain the density of the subchondral plate (including hydroxyapatite concentration) a VOI was set on 350 slices of the specimen; this was 15 x 50mm in size. The box was consistently placed so that the maximum depth of the VOI from the surface was the full 15mm, with the rest of the VOI typically being less (due to the slope of the calcified surface).

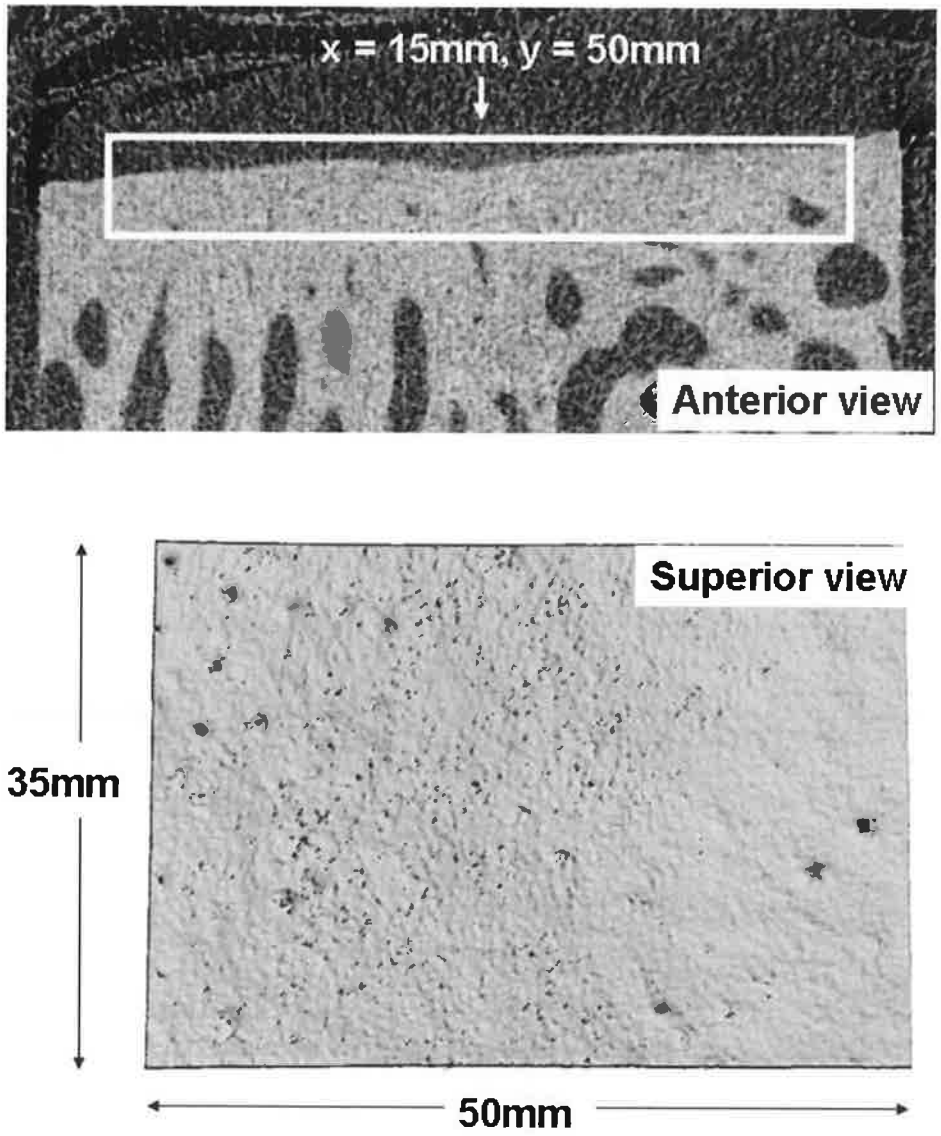

Figure 3.13 MicroCT – VOI for analysis of subchondral plate density

Again, the Scanco software reconstructed the VOI into a 3-dimensional image (Figure 3.13), with generation of a results sheet including parameters such as Bone Volume Fraction and hydroxyapatite concentration.

3.4 RESULTS

3.4.1 Outliers and exclusions

Specimens from 24 sheep were examined in this study; 11 of the sheep underwent ovariectomy (OVX), while the remainder (n = 13) were kept as controls (CON) (Table 2.5).

Initial examination of the data set included a multiple linear regression analysis to identify potential outliers; parameters included in this analysis are shown in Table 3.1 (Osborne & Overbay, 2004). Following this analysis, the results indicated that Sheep 23 (OVX Group) was an outlier (Cook's *D* = 0.828, Leverage = 0.667). Comparison was then made of analyses both including and excluding this sheep from the data set, which confirmed that this specimen had an inordinate effect on statistics.

Dependant variable	Independent variables
Sheep Group	BV / TV Connectivity density Number Thickness Separation Hydroxyapatite concentration

Table 3.1 Outlier Identification

All subsequent analyses within this chapter are performed with the omission of Sheep 23 from the dataset; therefore for the control group n = 13, with the ovariectomy group being slightly smaller, as n = 10. SigmaStat version 3.00 (SPSS Inc.) was used for data analysis throughout this chapter. All data sets were initially analysed for normality and equal variance. A t-test was performed if the appropriate criteria were met ($P > 0.05$ & $P = 0.10$ respectively); if either criterion was failed, a Mann-Whitney-U test was performed instead. Differences were considered significant for values of $p < 0.05$. With regard to power analysis, the majority of analyses reached the desired power of 0.800. The only failure was the analysis of trabecular hydroxyapatite concentration - Power of performed test with alpha = 0.050: 0.050.

3.4.2 Dual energy X-ray absorptiometry

There was no difference in median bone mineral density of the tibia as a whole between the control and ovariectomised sheep (0.98 vs. 0.99 g/cm^2, p = 0.420, Mann-Whitney U test; Graph 3.1).

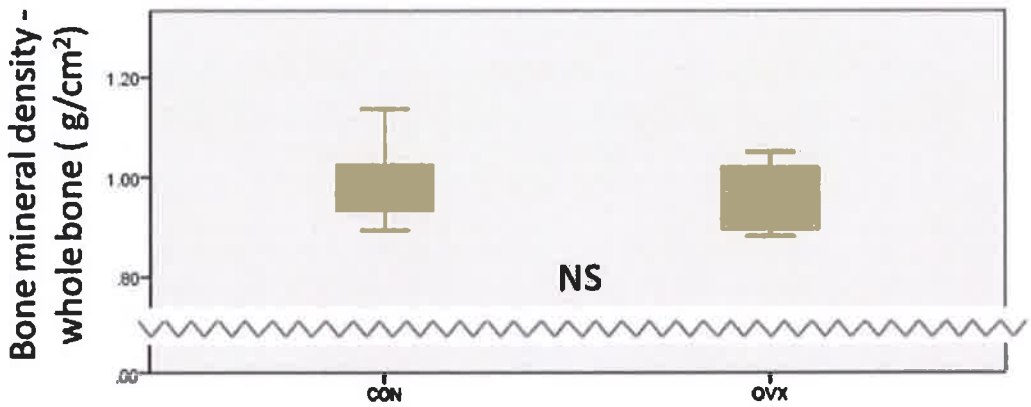

Graph 3.1 Bone mineral density of tibiae (whole bone)

When analysis of bone mineral density was performed of just the proximal tibial segment (R1 as shown in Figure 3.2), there was a significant reduction in bone mineral density in the ovariectomised sheep, as compared to controls (0.92 vs. 0.99 g/cm^2, p = 0.028, Mann-Whitney U test; Graph 3.2).

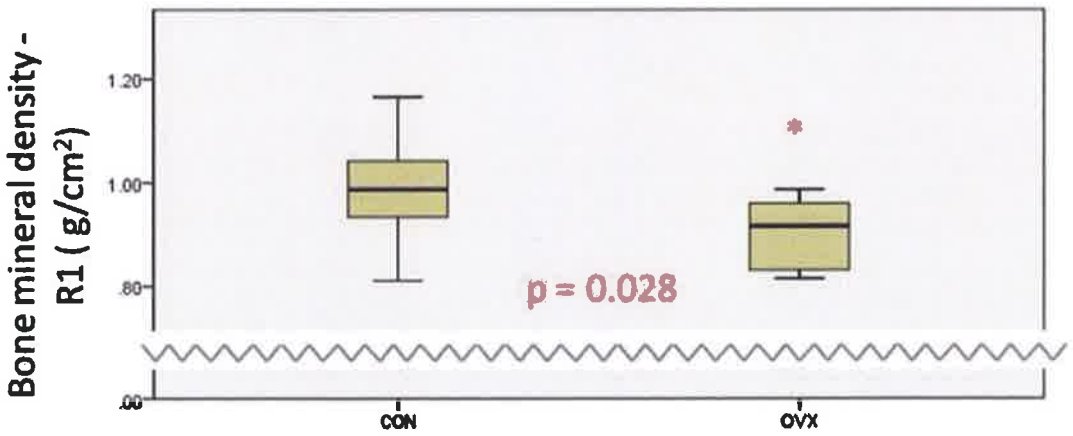

Graph 3.2 Bone mineral density of proximal tibiae (R1)

When further subregional analyses were performed (medial and lateral tibial plateaux as defined in Figure 3.2), it became apparent that the difference in bone mineral density was due to alterations within the medial tibial plateau, not the lateral. The median bone mineral density was significantly reduced in the medial plateau of the OVX sheep as compared to controls (1.02 vs. 1.11 g/cm^2, p = 0.009, Mann-Whitney U test; Graph 3.3); there was a trend towards reduced BMD in the OVX sheep within the lateral , but this was not significant (1.135 vs. 1.214 g/cm^2, p = 0.215, Mann-Whitney U test; Graph 3.4).

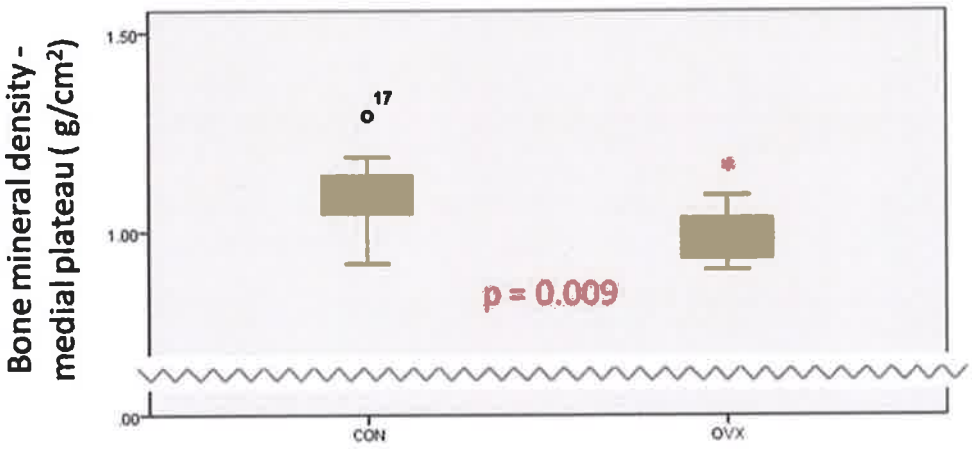

Graph 3.3 Bone mineral density of the medial tibial plateau

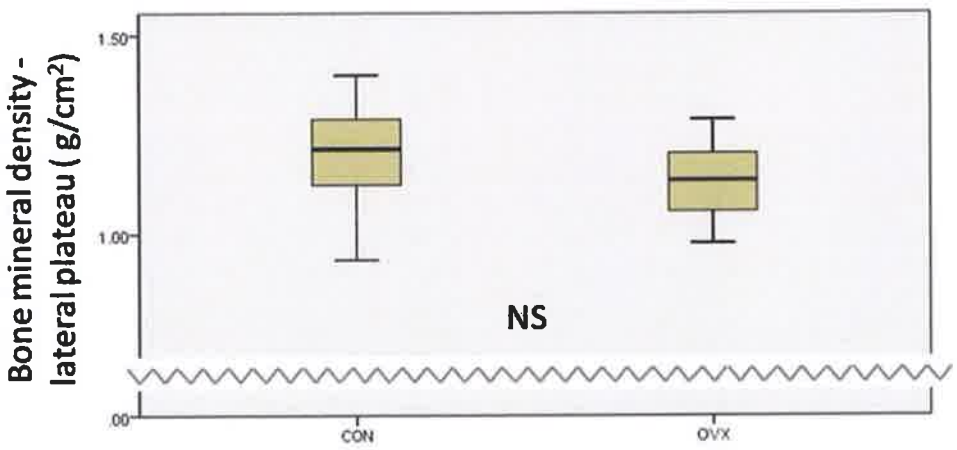

Graph 3.4 Bone mineral density of the lateral tibial plateau

3.4.3 Subchondral Trabecular Bone - MicroCT

On examination of the subchondral trabecular bone microstructure, quantifiable differences were found between the two experimental groups. Bone volume fraction of the subchondral trabecular bone was assessed as the fraction of bone volume per total volume (BV/TV); this was lower in ovariectomised animals than in the control group, and this difference reached statistical significance (0.439 vs. 0.483, p = 0.038, Mann-Whitney U test; Graph 3.5).

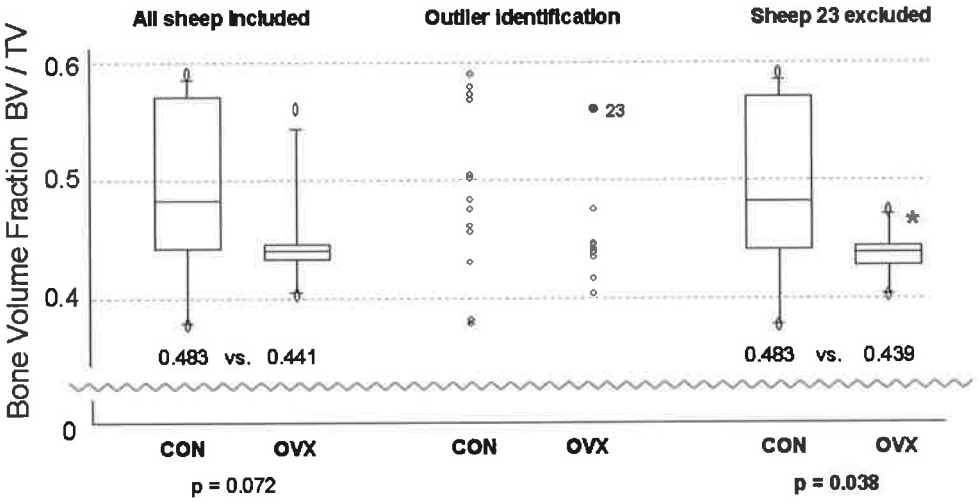

Graph 3.5 Bone Volume Fraction

When the number of individual trabeculae present per mm was examined, there was a trend to a lower number being present in the ovariectomised group, as compared with the control group (2.817 vs. 3.288, p = 0.1, Mann-Whitney U test; Graph 3.6); this failed to reach significance, however.

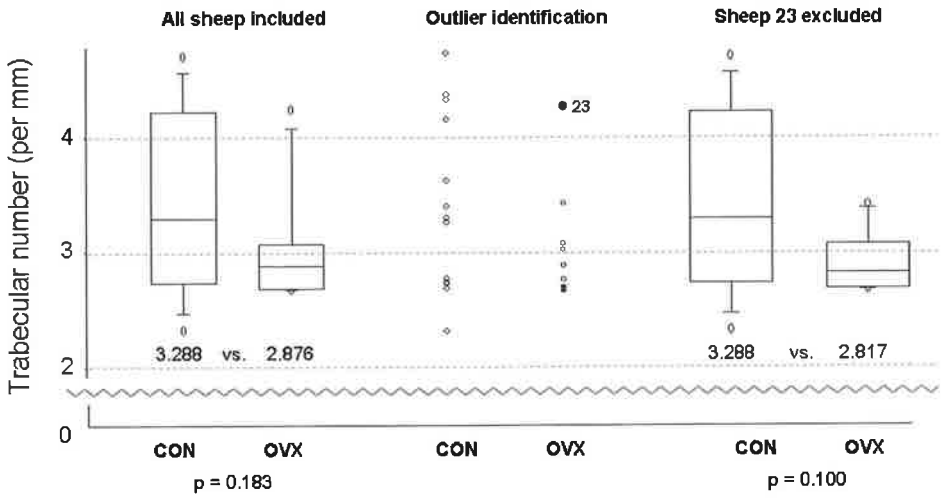

Graph 3.6 Trabecular number

Trabecular thickness was also observed to be reduced in the ovariectomised group, as shown in (0.220 vs. 0.252mm, p = 0.010, Mann-Whitney U test; Graph 3.7); this difference did reach statistical significance. Connectivity density (a measure of the number of connections between trabeculae present per mm^3) was also significantly reduced in the ovariectomised group (7.947 vs. 11.524, p = 0.014, Mann-Whitney U test; Graph 3.8).

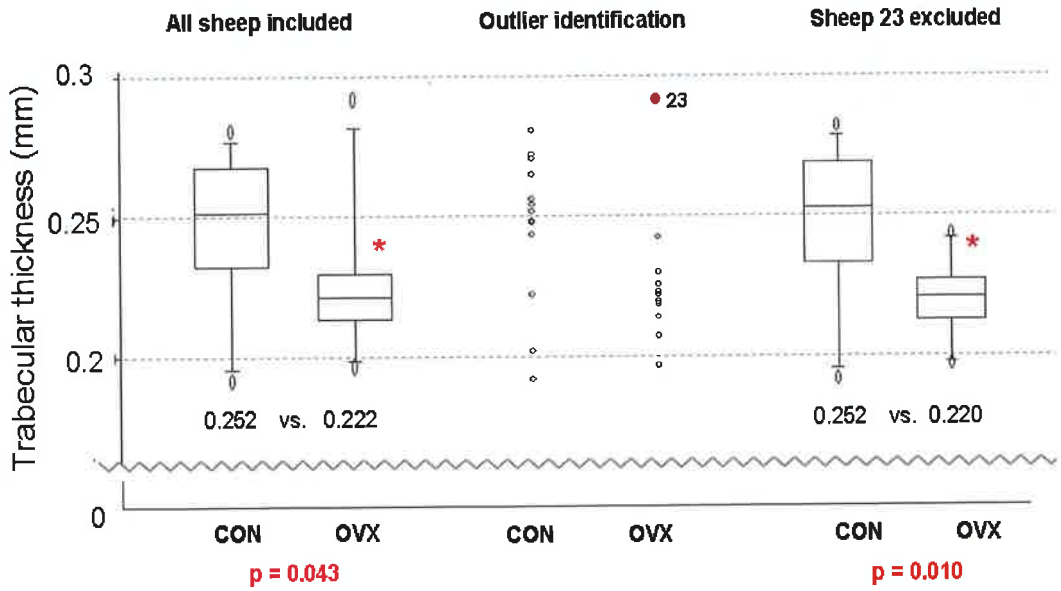

Graph 3.7 Trabecular thickness

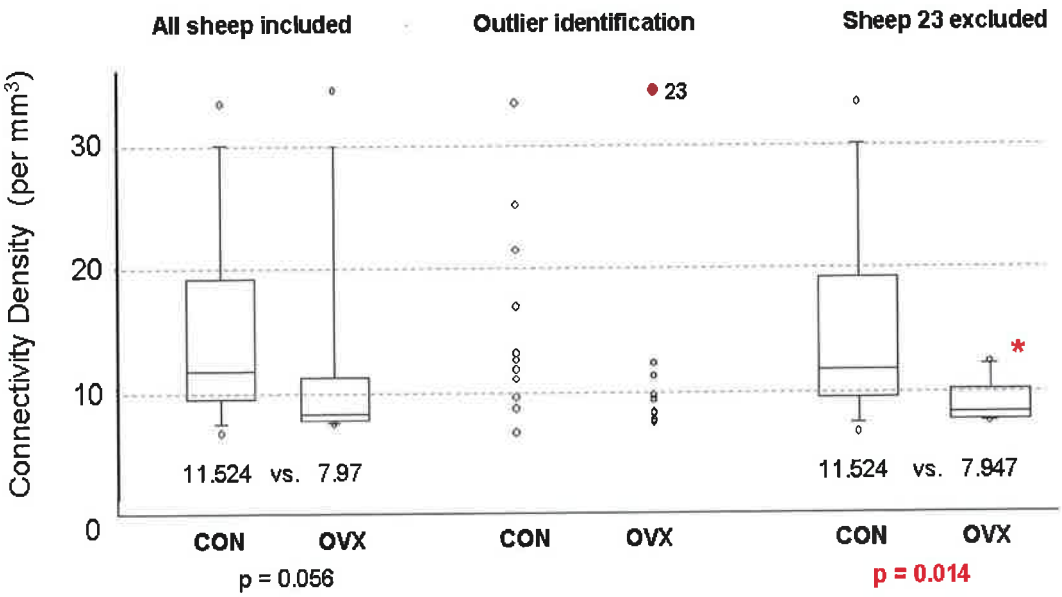

Graph 3.8 Connectivity density

The median distance between the individual trabeculae (trabecular separation or Tb.Sp.), was observed to be greater in the ovariectomised group, although this failed to reach significance (0.426 vs. 0.387mm, p = 0.251, Mann-Whitney U test, Graph 3.9).

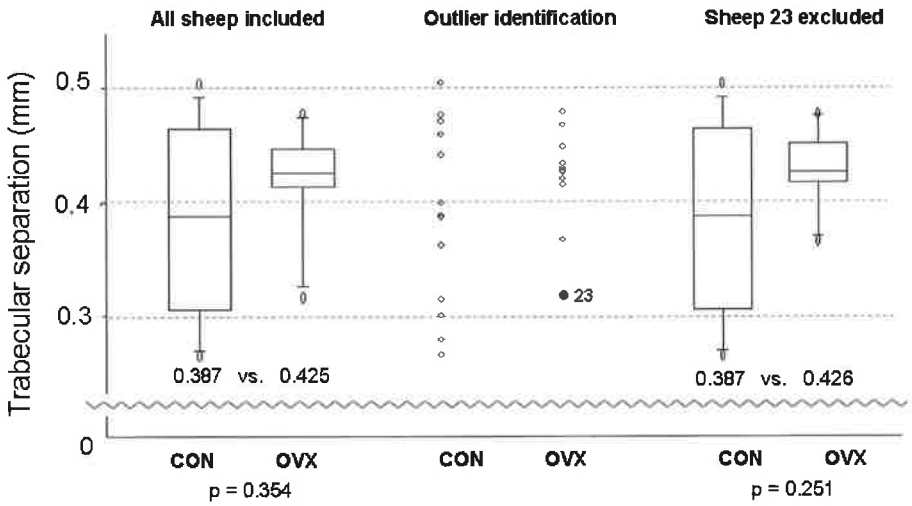

Graph 3.9 Trabecular separation

Given all of the above structural differences between the two study groups, it is perhaps unsurprising that there was also a significant difference in the Structural Model Index (SMI) (-1.159 vs. -0.822, p=0.041, t-test; 95 percent confidence interval for difference of means: 0.0160 to 0.658; Graph 3.10). While SMI is often described as a value from 0 to 3 (an ideal plate and cylinder respectively), a negative SMI may be seen in dense bone, and indicates that there are more concave than convex surfaces present (Issever *et al*, 2003). As such, it is sensitive to relative volume changes; dilatation of an enclosed space will cause SMI to become more negative.

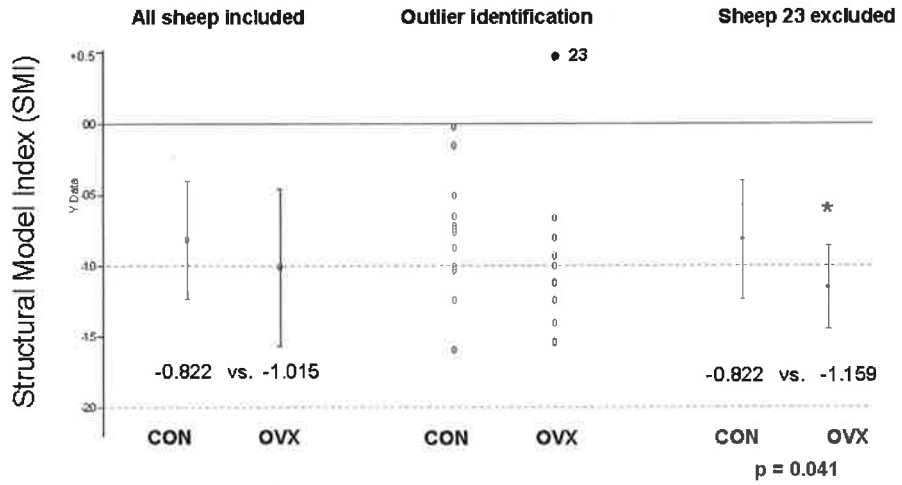

Graph 3.10 Structural Model Index

Finally, when the hydroxyapatite concentration of the trabeculae was ascertained, it was revealed that there was no variation in this parameter between the two groups, despite the aforementioned marked morphological and structural density differences observed (929 vs. 932 mg HA/cm^3, p=0.687, t-test; 95 percent confidence interval for difference of means: -11.315 to 16.846; Graph 3.11).

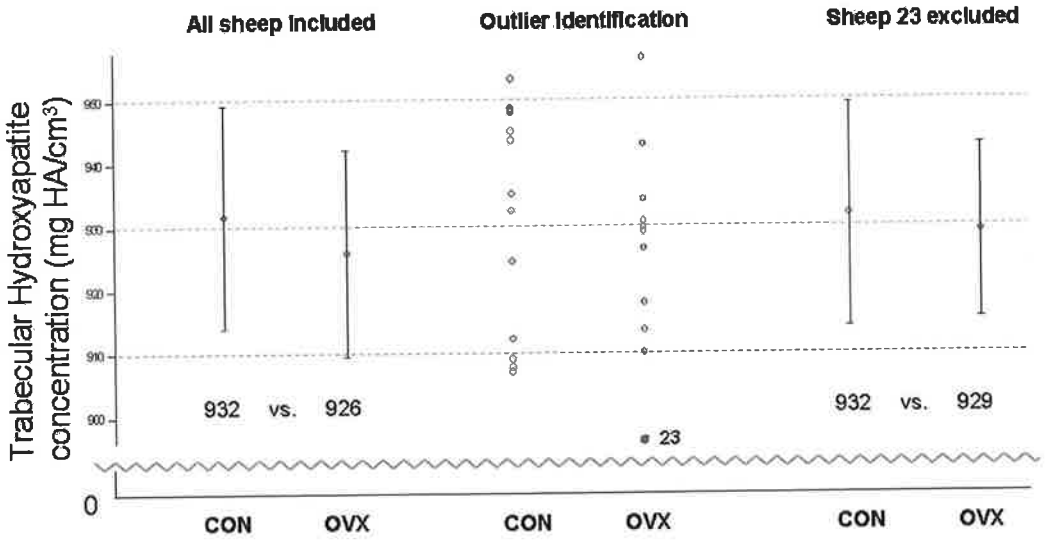

Graph 3.11 Trabecular hydroxyapatite concentration

3.4.4 Subchondral Plate - MicroCT

The mean subchondral plate thickness was observed to be thinner in OVX sheep in comparison to controls, but this result fell just short of significance (1.326 vs. 0.992mm, p= 0.08, t-test; 95 percent confidence interval for difference of means: -0.0432 to 0.712; Graph 3.12). The power of this test was low, however, at 0.300 (desired power with alpha = 0.050 is 0.800).

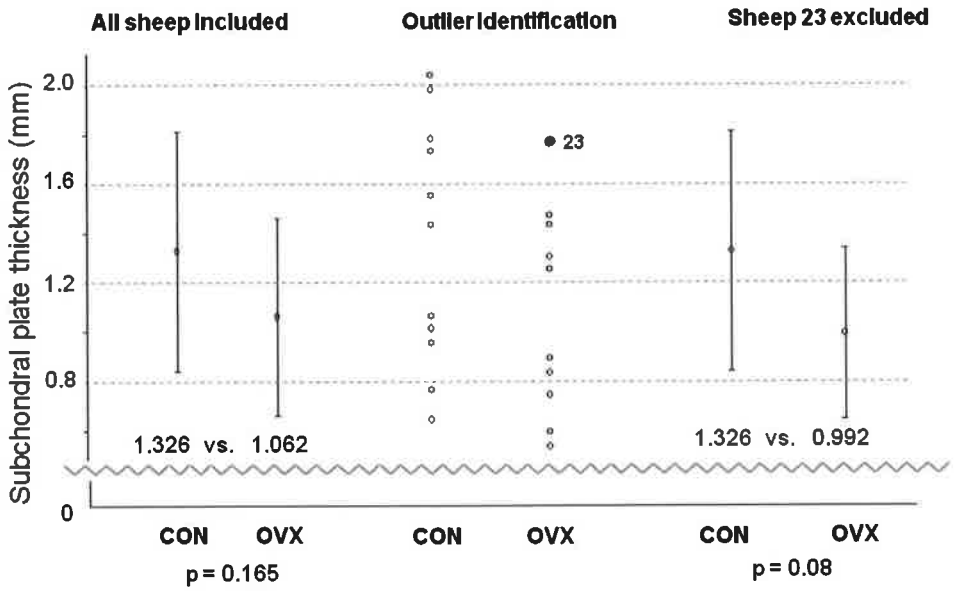

Graph 3.12 Subchondral Plate thickness

The hydroxyapatite concentration of the Subchondral revealed no variation between the two groups (994.8 vs. 996.3 mg HA/cm^3, p=0.868, t-test, Graph 3.13), as had also been the case with the trabecular HA concentration (Graph 3.11).

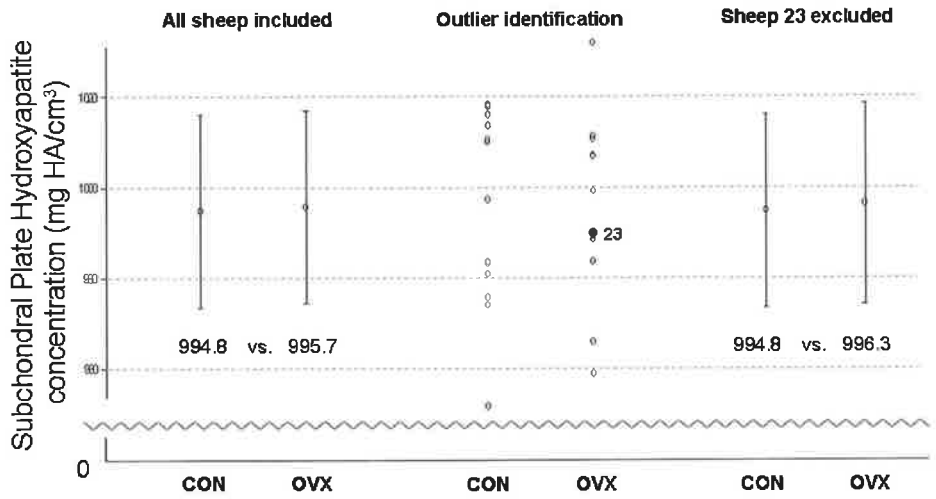

Graph 3.13 Subchondral Plate hydroxyapatite concentration

When hydroxyapatite concentration between the two regions was compared, however, the material density was significantly greater in the subchondral plate than in trabeculae, both within the study population as a whole and when divided into the two main subgroups of CON and OVX (Paired t-test, Graph 3.14).

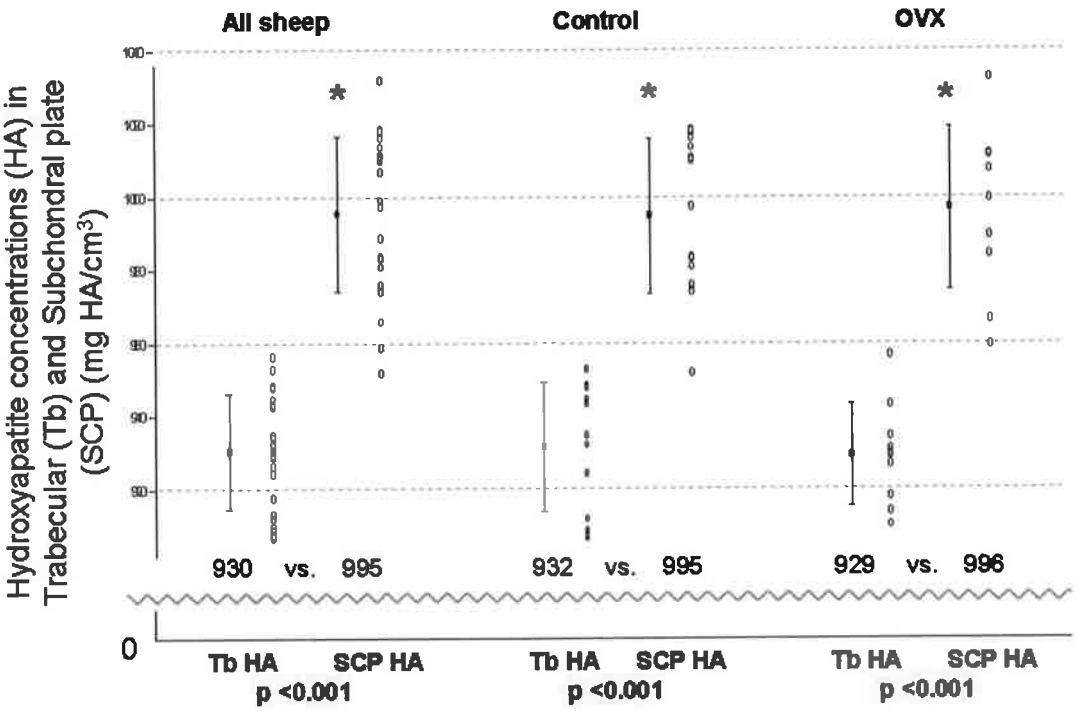

Graph 3.14 Comparison of hydroxyapatite concentration – Tb vs. SCP

3.4.5 Correlating clinical (DEXA) with MicroCT

Correlations (Spearman) were performed between the BMD as measured by DEXA and morphometry as measured by MicroCT. Analyses confirmed that the observed alteration in BMD of the medial tibial plateau was significantly correlated with changes in the subchondral trabecular structure and subchondral plate thickness (Graph 3.15).

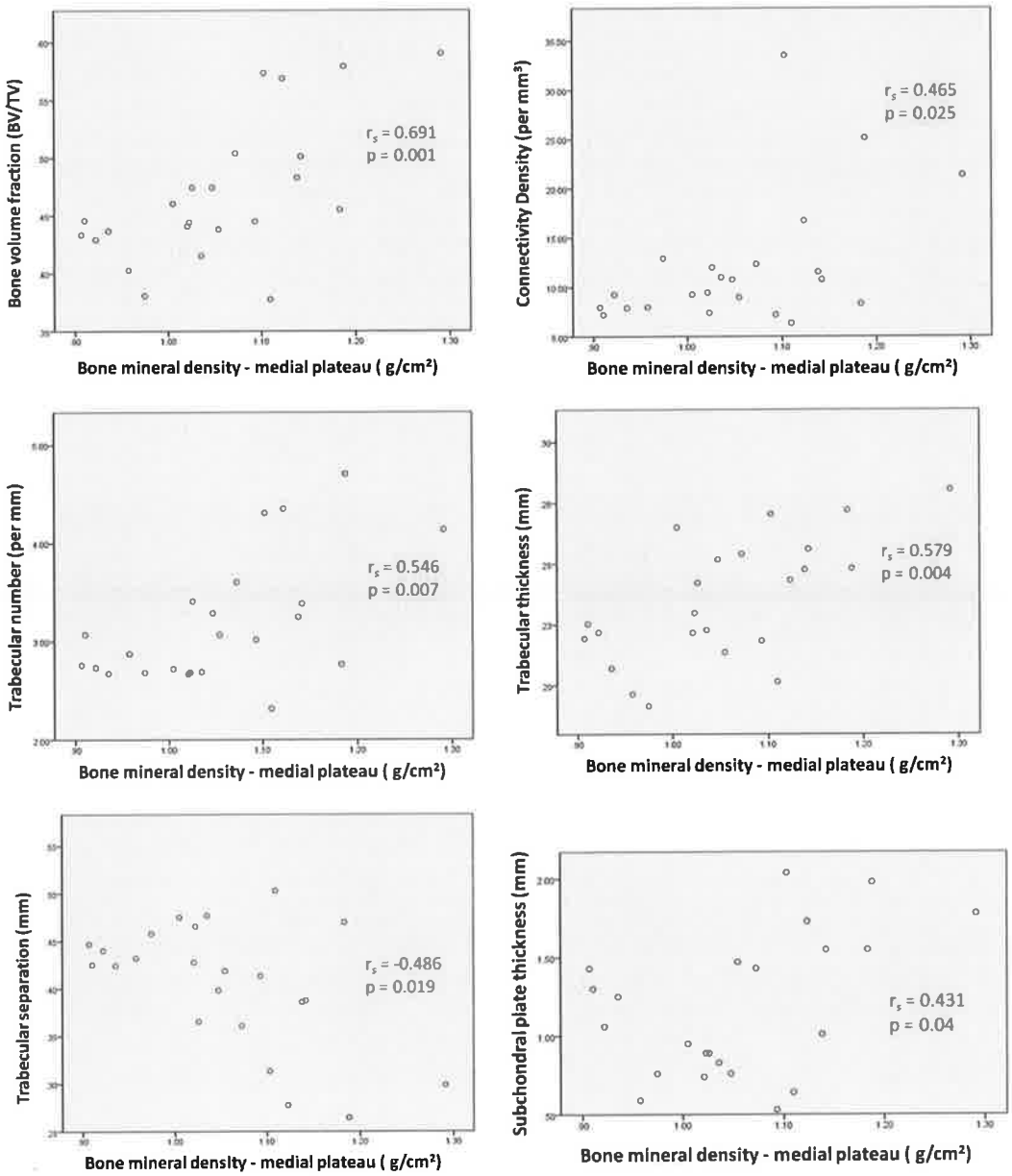

Graph 3.15 Correlating BMD with MicroCT morphometry

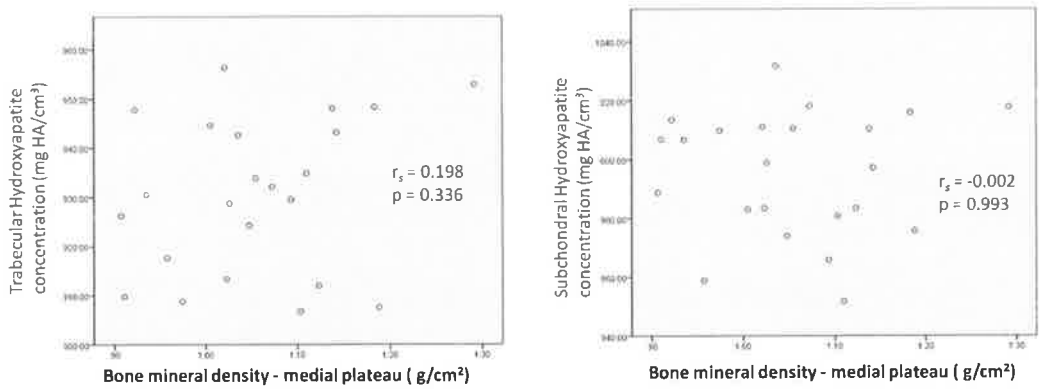

Graph 3.16 Correlating BMD with MicroCT HA concentration

When the mineral densities of the trabecular and subchondral bone, as measured by hydroxyapatite concentration, were then analysed, there was no significant correlation between these concentrations and the BMD (Graph 3.16).

While regression analysis would be of interest to determine which of the morphometric variables shown in Graph 3.15 is of most predictive value for the DEXA BMD, the sample size in this thesis is too small to enable reliable analysis (n=23); the cases-to-Independent Variables (IVs) ratio with regression analysis is ideally 20:1, but should be at least 5:1 (Norman & Streiner, 2008). In my study, with 6 independent variables to consider (Graph 3.15), a minimum sample size of 30 sheep would be necessary.

3.4.6 Summary of Results

Subregional analysis of the tibiae revealed that BMD is reduced in the medial tibial plateau of the ovariectomised sheep. In addition, trabecular thickness, bone volume fraction and connectivity density are all significantly reduced in the OVX group as compared to controls. The number of trabeculae is also reduced and the trabecular separation is increased, although not significantly so. The subchondral plate is also thinner, but the material density is unaffected. Analyses confirmed that the alteration in BMD was significantly correlated with morphometric changes in the trabeculae and subchondral plate, but not with HA concentration.

	Controls	**OVX**	**p**
DEXA			
Whole bone	0.989	0.981 ↓	0.420
Proximal tibia	0.987	0.916 ↓	**0.028 ***
Medial tibial plateau	1.1095	1.022 ↓	**0.009 ***
Lateral tibial plateau	1.214	1.135 ↓	0.215
Trabecular			
Bone volume fraction (BV/TV)	0.483	0.439 ↓	**0.038 ***
Number (/mm)	3.288	2.817 ↓	0.100
Thickness (mm)	0.252	0.220 ↓	**0.010 ***
Connectivity Density (/mm^3)	11.524	7.947 ↓	**0.014 ***
Separation (mm)	0.387	0.426 ↑	0.251
Structural Model Index	-0.822	-1.159 ↓	**0.041 ***
HA/cm^3	932	929	0.687
Subchondral plate			
Thickness (mm)	1.326	0.992 ↓	0.08
HA/cm^3	994.8	996.3	0.868

**statistically significant p-values shown in red*

Arrows indicate whether result in OVX sheep is increased or descreased in comparison to control group

Table 3.2 Summary of results

3.5 DISCUSSION

Tibial subchondral bone structure has been studied in the advanced stages of pathologies such as osteoporosis, osteoarthritis and osteonecrosis in a number of species (Bellido *et al*, 2010; Blain *et al*, 2008; Botter *et al*, 2008; Chappard *et al*, 2006; Day *et al*, 2001; Ding *et al*, 2003; Hwa *et al*, 2001; Karvonen *et al*, 1998; Laib *et al*, 2000; McErlain 2008; Patel *et al*, 2003; Satku *et al*, 2003). However, the effects of ovariectomy in isolation on the subchondral bone structure, independent of any additional pathophysiological changes, have not been extensively documented to date. Ovariectomy in sheep is now being employed as an animal model for investigation of osteoarthritis, in addition to its more established role as a model for conditions such as osteoporosis (Brennan *et al*., 2009, Kennedy *et al*., 2009b, Johnson *et al*., 2002, Little & Smith, 2008; Newton *et al*., 2004, Thorndike & Turner, 1998, Osterhoff *et al*., 2010). Ovariectomy has been shown to have a detrimental effect on the structural, material and biomechanical properties of ovine articular cartilage (Cake *et al* 2005; Turner *et al* 1997), and to lead to the development of osteoarthritis. It is therefore perhaps surprising that the effects of ovariectomy on the subchondral bone itself, independent of the development of further disease states, has received so little attention, particularly as it is possible that the local effects of osteoarthritis induced by ovariectomy and those induced by alteration of the mechanical loading of the joint (i.e. by meniscectomy) may be quite different (Pajamäki *et al*, 2008).

Age-related alterations in the structure and material parameters of subchondral trabecular bone in the human proximal tibia have been investigated within a small number of studies, although for analysis purposes subjects were purely divided into groups based upon age, which included both genders (Ding *et al*, 1997; Ding *et al* 2002). Bone volume fraction and trabecular thickness were found to decrease significantly after the age of 60, with the trabeculae shifting from a plate-like to a rod-like microstructure (Ding *et al* 2002). Koszyca *et al* also found a decrease in BV/TV with age in the knee, and a significant reduction in trabecular thickness (Koszyca *et al*, 1996).

One of the few studies to examine subchondral changes post-ovariectomy was a longitudinal study in rat tibiae, performed using *in-vivo* MicroCT scanning (Waarsing *et al*, 2004). When examining the epiphyseal bone, there was a 25 % reduction in the trabecular bone volume of the ovariectomised rats at 4 weeks; this increased to 30% at 10 weeks. While this was predominantly due to initial thinning of the trabeculae in the first 4 weeks (130 to 116 μm), a gradual increase in the thickness of the few remaining trabeculae from week 4 to week 14 was observed (116 to 122 μm). In contrast, the sham-operated rats showed no changes in bone volume, and the trabeculae showed a mild thickening (116 mm to 121 μm).

My data are consistent with these findings; I also demonstrate a significant reduction in the trabecular bone volume fraction in ovariectomised animals as compared to the control group (0.439 vs. 0.483, $p = 0.038$). It is well established that oestrogen withdrawal by ovariectomy results in substantial increases in basic multicellular unit (BMU) activation, which are responsible for bone remodelling, within 12 months (Kennedy *et al*, 2009b; Newman *et al*, 1995), particularly so in epiphyseal regions where considerable volumes of bone marrow are present. The subchondral bone region is one of relatively high density (reflected in the negative SMI data) (Issever *et al*, 2003) thus this region has considerable trabecular surface area on which newly activated BMUs could act. Therefore, it follows intuitively that increased bone remodelling in a region densely packed with trabeculae would result in reduced bone volume fraction, without necessitating a corresponding reduction in trabecular number.

This hypothesis is further supported by my finding of a significant reduction in trabecular thickness within the ovariectomised sheep as compared to controls, with an increase in the distance between individual trabeculae (TbSp). Despite the marked morphological and structural density differences observed, the material density of the trabecular bone (i.e. hydroxyapatite concentration) was equal at one year in both the control and the ovariectomised animals. Therefore, despite the increased turnover and morphological changes occurring, mineralisation was unaltered, suggesting that while osteoclastic activity was ongoing to reduce the bone volume fraction, very little new young undermineralised tissue was deposited in compensation.

While MicroCT is not feasible within the clinical setting, DEXA is the current gold standard used to ascertain bone density in patient studies. While the BMD value obtained from DEXA is based on a 2-dimensional measurement of area, MicroCT provides results based on three-dimensional analyses; it is to be expected that MicroCT would provide a more accurate assessment of the effects of ovariectomy than DEXA. Values obtained by these two methods displayed significant correlation in this study, confirming the role of DEXA scanning in clinical investigation, despite recent controversy (Bolotin, 2007). Subregional analysis using the DEXA scanning did detect significant differences in BMD of the medial tibial plateau between the two groups. Despite the well-established use of the ovariectomised sheep as a model for osteoporosis, its use as a model for spontaneous osteonecrosis of the knee is undocumented to date. This is despite the fact that the majority of literature examining the aetiology of SPONK agree regarding the role that the underlying subchondral bone plays in the pathogenesis of this condition (Akamatsu *et al*, 2012; Breer *et al*, 2012; Narváez *et al*, 2003; Takeda 2008; Yamamoto & Bullough, 2000). Localised low bone mineral density and osteoporosis are typically present in these patients at presentation; Mears *et al* found significant osteopenia in 64% of specimens studied, while Breer *et al* found that administration of Vitamin D and bisphosphonates, the standard treatment for osteoporosis, led to alleviation of symptoms in a study of 5 consecutive cases of SPONK (Breer *et al*, 2012; Mears *et al*, 2009). The factors which make the OVX ovine model ideal for investigation of osteoporosis also hold true for its potential use as a model for SPONK (Section 2.1); crucially, the ovine stifle joint is also very similar to the human knee in structure, both in the shape of the articular surfaces and the soft tissues that lie therein (Osterhoff *et al*, 2010).

With regard to analysis of the subchondral plate, a number of different methodologies are employed within the literature. Dedrick *et al*, for example, directly measured the thickness of the subchondral plate in 10 sections at three locations and averaged the results for each site to obtain an overall measurement for subchondral plate thickness (Dedrick *et al*, 1993). Some centres have developed specific software to allow identification of the trabecular / cortical interface along the bone diaphysis (Buie *et al*, 2007) and subchondral plates (Sniekers *et al*, 2008a) and so allow automation of cortical and subchondral analysis. Of note, as discrimination between the subchondral bone and the layer of calcified cartilage within the subchondral plate is not possible using MicroCT, the measurements for the subchondral plate included here include both tissues.

This study had a number of limitations. First, the study population was non-uniform; for reasons of availability, mixed breeds of sheep were used in this experiment. Different breeds may have different natural metabolic states and also different metabolic responses to ovariectomy, which could affect the structural parameters investigated. Additionally, while all animals were skeletally mature (with an age range of between 5 to 9 years) the precise age of each sheep was undocumented and unobtainable. Also, while initial power analysis and sample size calculations were performed in advance of purchase, these were determined based on the use of these animals as a model of osteoporosis, not osteoarthritis. However, on statistical analysis, the vast majority of tests reached the desired power of 0.8, the only exception being analysis of trabecular hydroxyapatite concentration as previously described. Unfortunately, the limited study size did exclude the possibility of performing regression analysis, to determine which of the morphometric variables as measured by MicroCT is of most predictive value for the DEXA BMD. Of note, while seasonal variations in ovine bone turnover do occur, due to the longer oestrous cycles present in these animals during the summer months as compared to the rest of the year, all animals were sacrificed on the same (November) day, so any effects from this physiological variable should be minimised (Arens *et al*, 2007; Kennedy *et al*, 2009a).

In conclusion, this chapter shows significant alterations within the subchondral trabecular architecture at one-year post-ovariectomy, with reduced bone volume fraction, thinning of individual trabeculae and an increase in trabecular separation; these findings are consistent with those elsewhere in the ovine skeleton (Cornish *et al.*, 2006; Jiang *et al*, 2005; Mitton *et al.*, 1998; Mittra *et al.*, 2005; Nafei *et al.*, 2000; Newton *et al.*, 2004; Schorlemmer *et al.*, 2003) and with those in human studies of the knee (Koszyca *et al*, 1996).

3.6 CONCLUSIONS

1. DEXA subregional analyses of the proximal tibia and medial tibial condyle show a significant reduction in BMD within the OVX group as compared to controls.

2. Trabecular thickness, bone volume fraction and connectivity density are all significantly reduced in the OVX group as compared to controls.

3. The subchondral plate is significantly thinner in the OVX group as compared to controls.

4. Alterations in BMD were significantly correlated with changes in subchondral microstructure and morphology as measured by MicroCT, but not hydroxyapatite concentrations.

CHAPTER 4: THE EFFECT OF OVARIECTOMY ON SUBCHONDRAL BONE TURNOVER IN THE MEDIAL TIBIAL PLATEAU

4.1 INTRODUCTION

I have demonstrated that the structure of subchondral bone, both the cortical plate and the underlying trabeculae, is altered at one year post-ovariectomy. The skeleton is constantly undergoing adaptation in response to mechanical stimuli. In skeletally mature animals, new bone may be deposited as a result of either modelling or remodelling. Increased bone turnover at other sites in the ovine skeleton has been shown to result in significant changes to the biomechanical behaviour of these bones (Kennedy *et al*, 2008; Kennedy *et al*, 2009b). Osteopenia and subchondral insufficiency fractures are implicated in the aetiology of spontaneous osteonecrosis of the knee (Akamatsu *et al*, 2012; Narváez *et al*, 2003; Yamamoto & Bullough, 2000); increased turnover is implicated by scintigraphy (Satku *et al*, 2003). If elevation of bone turnover is confirmed within the subchondral bone in this model, then utilisation of the ovariectomised ewe should be useful as an animal model for spontaneous osteonecrosis of the knee.

4.2 AIMS OF STUDY

The overall aim of this section of the study was to determine the effects of ovariectomy on new bone formation and mineralisation within the subchondral bone, whether by modelling, remodelling or endochondral ossification. This may be done by measuring the number of fluorochrome labelled osteons / surfaces present. Additionally, an attempt will be made to examine the extent of fluorochrome deposition within the advancing calcified cartilage layer.

Specific questions:

- Is bone turnover within the subchondral trabecular and cortical bone altered post-ovariectomy?

- Are there any significant correlations between alterations in bone turnover and microstructural changes in this region?

4.3 MATERIALS AND METHODS

4.3.1 Staining, embedding and slide preparation

The specimens used for this section of the study were Specimens A, as described in Chapter 3. Following MicroCT, these specimens were cleaned with a water jet and then dehydrated in 70% ethanol for 5 days. The specimens were then dehydrated in graded ethanol within vacuum as shown in Table 4.1.

Dehydration in vacuum	
70% Ethanol	2 hours
80% Ethanol	2 hours
90% Ethanol	2 hours
90% Ethanol	2 hours
100% Ethanol	2 hours
100% Ethanol	2 hours

Table 4.1 Graded dehydration of specimens in ethanol

Following this, specimens were then infiltrated in Methyl Methacrylate solution (MMA), prior to final embedding in Polymerised Methyl Methacrylate (PMMA). This polymer solution consists of Methyl Methacrylate (MMA) with the addition of a softener (di-butyl phthalate), which prevents the finished polymer being too brittle, and a hardener (benzoyl peroxide), which acts as a catalyst and causes the MMA to polymerise (O'Brien *et al*, 2000). The polymer (monomer, softener and hardener) is made up according to the following proportions and can be stored at 4-6°C for long periods: Methyl methacrylate – 200mls; Di-butyl phthalate – 50mls; Benzoyl peroxide - 7g. Specimens were placed in individual glass vials and then infiltrated with MMA solution over a period of 84 hours in vacuum at room temperature, with changes of MMA every 24 hours.

During this time, bases for the final embedding were prepared by placing a small amount (approximately 4mls) of MMA solution into individual glass vials; these were placed in an oven for 24 hours at 65°C to polymerise. Once the bases were "tacky" to touch, they were removed from the oven. They could then be kept at room temperature for long periods until needed for final specimen embedding.

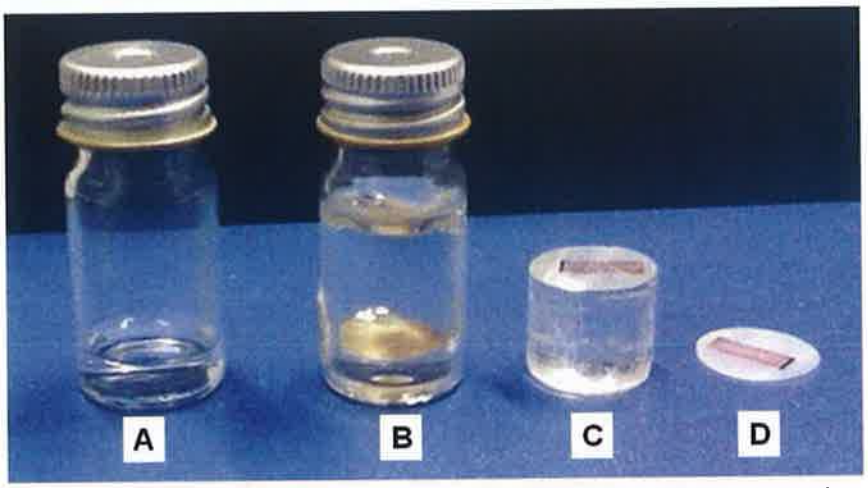

A – PMMA base within vial
B – specimen placed on base & additional MMA added to vial to polymerise
C – PMMA & specimen removed from vial, excess PMMA removed with diamond saw
D – 120μm section obtained

Figure 4.1 PMMA embedding of osteochondral specimens

For final specimen embedding, samples were placed in these pre-prepared vials on top of the PMMA base (Figure 4.1). Additional MMA solution was then added to the vial to ensure that the specimen was completely covered, with additional overlying solution to provide a firm base for clamping during later sectioning. These vials were then placed in the vacuum desiccator (room temperature) for 2 hours to remove any air from the solution. Specimens were then placed in an oven to polymerise the solution over a period of three days, with gradual temperature increases as indicated in Table 4.2.

Temperature	Time
45°C	6 hours
50°C	24 hours
55°C	24 hours
60°C	24 hours

Table 4.2 Polymerisation of PMMA embedded specimens in oven

When removed from the oven, specimens were left to cool for a period of at least 24 hours at room temperature. Removal of the glass surrounding the now embedded specimen was facilitated by gently tapping the glass with a hammer, taking care to avoid scattering glass fragments by placing the vial in a latex or nitrile glove during this procedure. Following removal of all glass, the specimen was washed and then placed into the oven for a further 24 hours at 55°C.

For preparation of slides for microscopy, histological sections with a thickness of approximately 120 – 150 μm were taken from PMMA-embedded osteochondral specimen using a diamond saw (Struers, Accutom 50, Ballerup, Denmark; Figure 4.2). Sections were then reduced to approximately 100 μm, by grinding in aqueous solution, rinsed in distilled water, and finally mounted on glass slides with DPX (using glass cover slips briefly dipped in Xylene).

Figure 4.2 Accutom 50 Diamond Saw

4.3.2 Epifluorescence microscopy

Each slide was examined using bright field microscopy (Nikon Eclipse 90i). Initial basic measurements were performed using a digital image analysis system (NIS Elements BR 3.0, Nikon); these included parameters such as the length of the tidemark (of advancement of the calcified cartilage layer), the area of zone of calcified cartilage and the area of the subchondral bone plate. Each slide was then examined using a combination of ultra-violet (UV) (λ=365nm), blue (λ=470nm) and green (λ=546nm) epifluorescence microscopy at x10 magnification (Table 1.4).

Within the trabecular bone, an area of interest measuring 4 x 7.5mm was analysed from each specimen, lying at a depth of 2.5mm from the bone surface (Figure 4.3). The total area and area of bone was calculated for each area of interest. Each slide was then examined using a combination of ultra-violet (UV) (λ=365nm), blue (λ=470nm) and green (λ=546nm) epifluorescence microscopy at x10 magnification (Table 1.4). Bone turnover was assessed by measuring both the number and length of sites with fluorochrome-labelled bone along the trabecular surfaces per measured bone area (Figures 4.3 & 4.4). These histomorphometric parameters are derived from the American Society for Bone and Mineral Research (ASBMR) nomenclature (Parfitt *et al*, 1987; Schorlemmer *et al*, 2005).

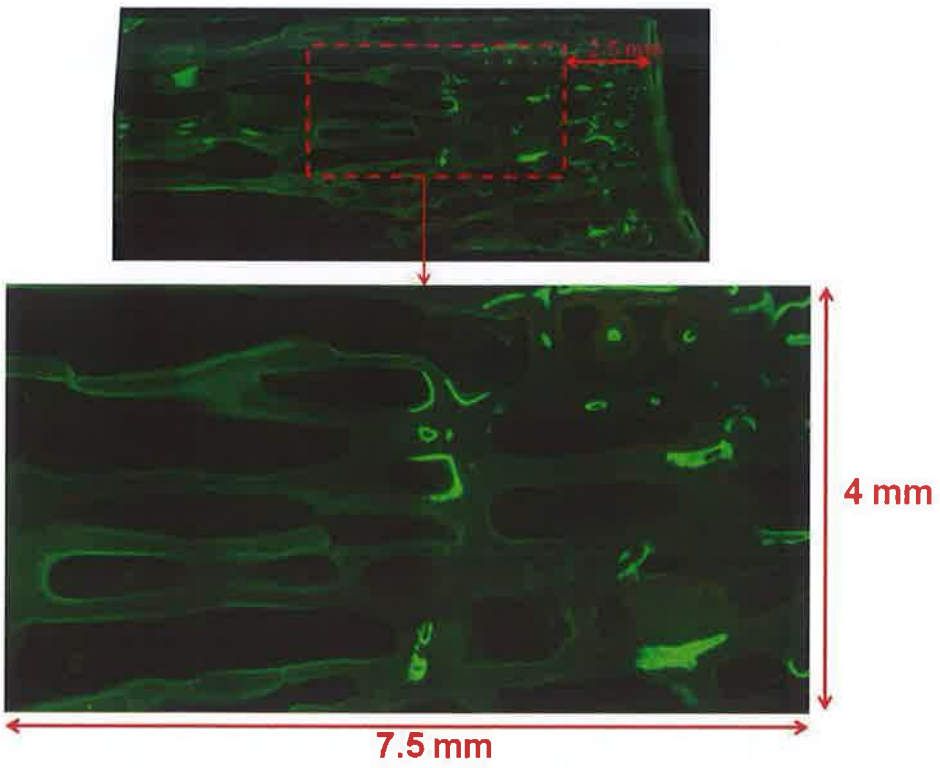

Figure 4.3 Defining the Area of Interest for trabecular microscopy

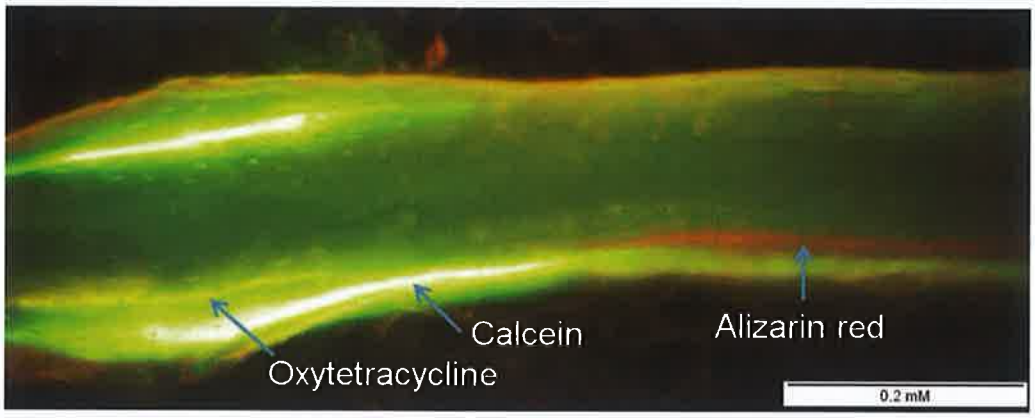

Figure 4.4 Fluorochrome-labelled bone along the trabecular surfaces

The bone turnover within the subchondral bone plate was quantified by calculating the number of labelled secondary osteons present per mm width of the subchondral specimen (#/mm; Figure 4.5). Cartilage calcification or tidemark activity was assessed by measuring the number and length of sites of labelled cartilage along the tidemark per overall length (Figure 4.6).

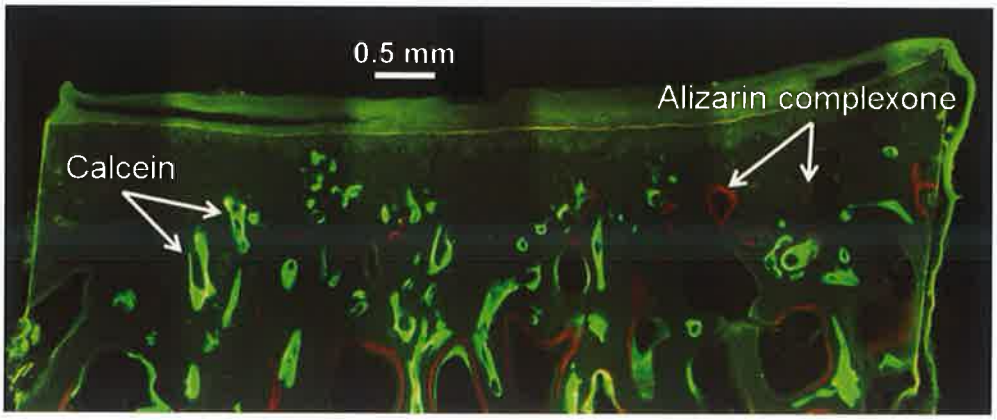

Figure 4.5 Fluorochrome-labelled bone within the subchondral plate

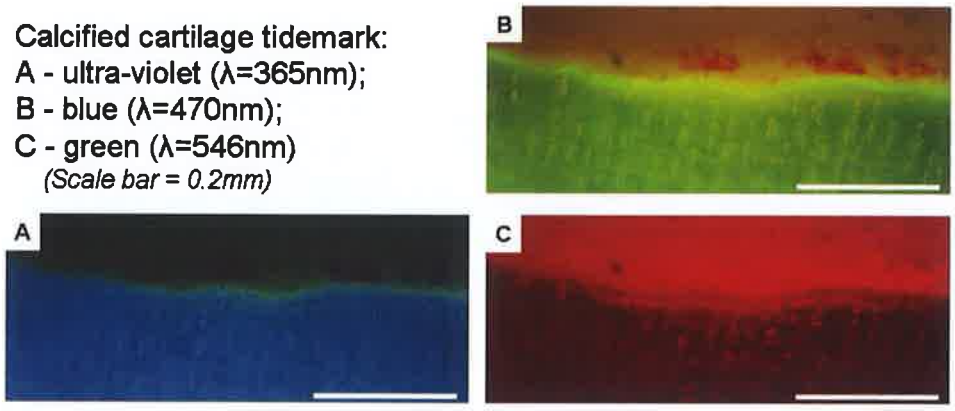

Figure 4.6 Calcein-labelling at the tidemark (cartilage calcification)

4.4 RESULTS

4.4.1 Outliers and exclusions

Specimens from 23 sheep were examined in this chapter following removal of the outlier Sheep 23 as described in Chapter 3. Ten of the sheep underwent ovariectomy (OVX), while the remainder (n = 13) were kept as controls (CON)

For analysis of trabecular bone turnover (Section 4.4.3), two additional sheep were excluded from the study. The specimen from Sheep 7 (CON) was damaged during removal from the glass vial following embedding in PMMA. Sheep 16 (CON) was also excluded, as it also was a marked outlier during analysis of trabecular turnover sites (Graph 4.1). Therefore for analysis of trabecular bone turnover, 21 sheep were examined; 10 of the sheep underwent ovariectomy (OVX), while the remainder (n = 11) were kept as controls (CON).

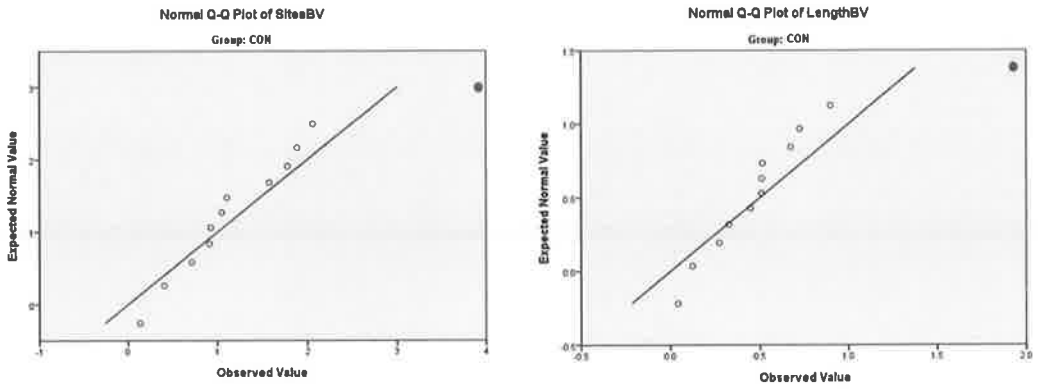

Graph 4.1 Q-Q plot with outlier

PASW Statistics 18 (IBM® SPSS®) was used for data analysis throughout this chapter. Q-Q plots were performed of all data sets to check for normal distribution. A t-test was performed if the appropriate criteria were met; otherwise a Mann-Whitney-U test was performed instead.

4.4.2 Calcein blue

During microscopy of the trabecular bone and the subchondral plate, a large amount of calcein blue was noted in the majority of specimens. This was visible along trabecular surfaces (Figure 4.7) and also within the central lacunae of secondary osteons (Figure 4.8). These did not appear to be areas of bone turnover; along the trabeculae there was no apparent scalloping or cement lines. Some of the secondary osteons had surrounding lamellae of Calcein but no visible intervening lamella of Xylenol between it and the central calcein blue (Figure 4.8). These areas of calcein blue were presumed to be rapid uptake of dye at bone surfaces accessible to the circulation *without* the presence of turnover or active mineralisation being present, as has been previously described (Parfitt, 2003). Due to the difficulty of differentiating these areas from calcein blue-labelling at sites of actual bone turnover, calcein blue labelled areas were excluded from analysis.

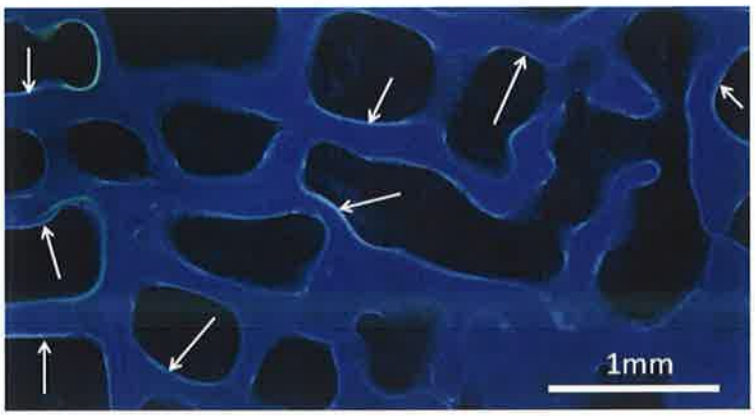

Calcein blue along trabecular surfaces
(Ultraviolet light)

Figure 4.7 Multiple areas of calcein blue along trabecular surfaces

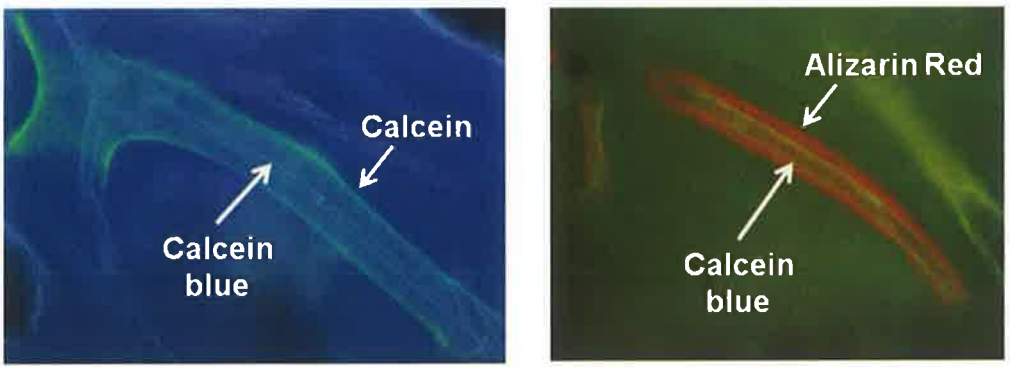

Secondary osteon with Calcein-labelled lamella & calcein blue along central lacuna (Ultraviolet light)

Secondary osteon with Alizarin-labelled lamella & calcein blue along central lacuna (Blue epifluorescence)

Figure 4.8 Calcein blue lining central lacunae of secondary osteons

4.4.3 Subchondral trabecular turnover

(i) Basic morphometry

Some basic parameters were examined during microscopy, prior to quantification of labelled bone present. The bone volume/total volume for each Area of Interest (Figure 4.9) was calculated as defined by the American Society for Bone and Mineral Research (ASBMR) nomenclature (Parfitt *et al*, 1987; Schorlemmer *et al*, 2005). This was then correlated to the bone volume fraction as obtained by MicroCT (Section 3.4.2). As would be expected, there was evidence to suggest a positive correlation between the bone volume fraction obtained via MicroCT and that quantified using microscopy ($r = 0.76$; $p < 0.001$; Graph 4.2).

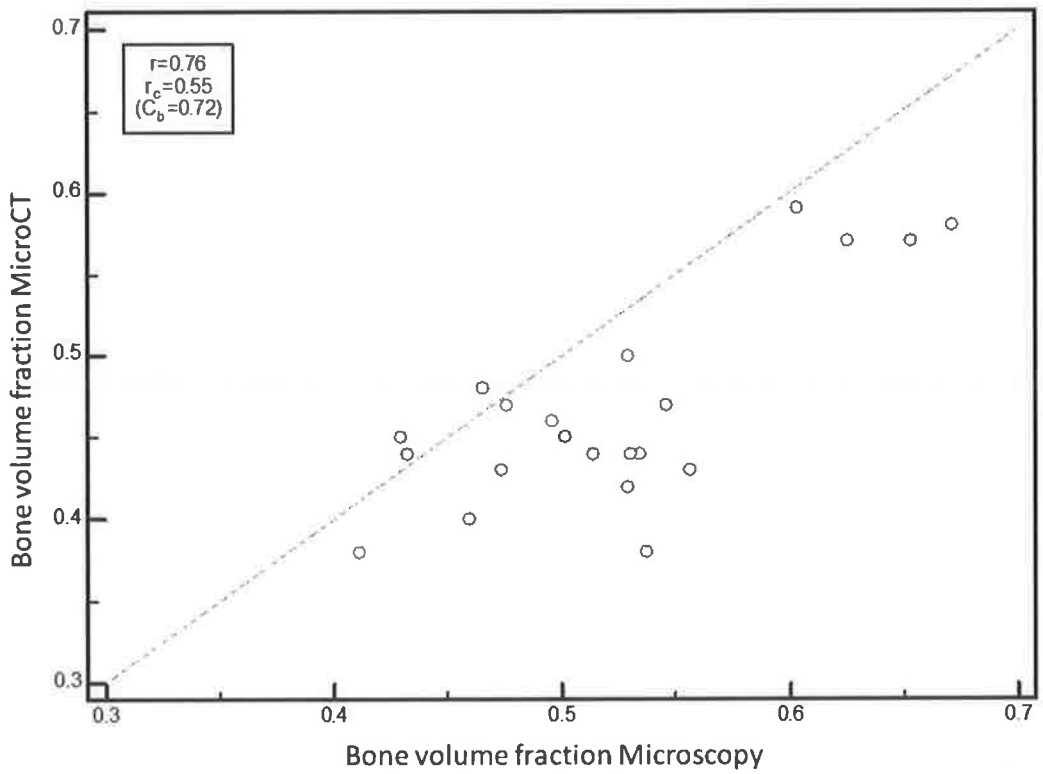

Graph 4.2 Comparison of BV/TV by MicroCT and Microscopy

A high correlation does not always mean that different methods of measurement agree, however, and so the level of concordance (r_c) between the two measures was calculated (Lin, L. I-K. 1989; Lin, L. I-K. 2000). The value of r_c is the product of the correlation coefficient (r) and a correction factor (C_b) and thus r_c cannot exceed r. In this case r_c was 0.55 indicating a bias towards higher values as measured by microscopy. This difference is better visualised using a Bland-Altman plot in Graph 4.3 (Bland & Altman, 1986).

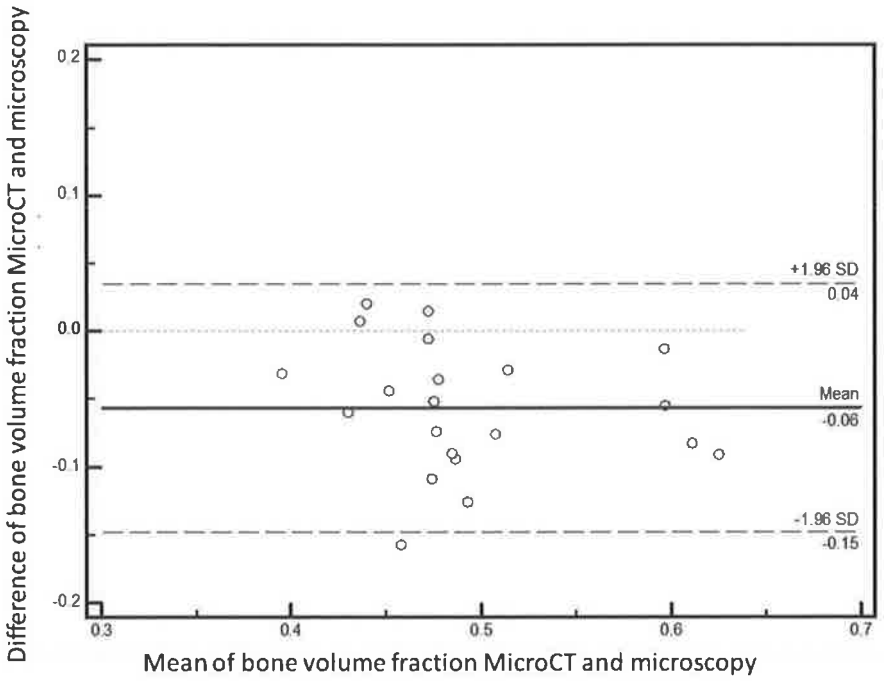

Graph 4.3 Agreement between measures of bone volume fraction

The Bland-Altman plot shows mean difference of 0.06 in favour of measurements by microscopy and the 95%-limits of agreement of -0.15 to 0.04, showing good agreement between the two methods, once this difference, or bias, is taken into consideration. Bone volume fraction (microscopy) was then compared between the two groups; this was slightly lower in ovariectomised animals than in the control group, but not significantly so (0.508 vs. 0.537, p = 0.17, Mann-Whitney U test). Of note, this difference had been significant with Bone volume fraction as measured by MicroCT (0.439 vs. 0.483, p = 0.038, Mann-Whitney U test; Graph 3.5). It should be noted that within previous studies comparing values obtained from 2-D or 3-D methods, a fairly close relationship is typically observed, but some values such as trabecular thickness do tend to be underestimated when using 2-dimensional methods (Ding & Hvid, 2000).

(ii) Hemiosteonal trabecular bone turnover

Bone turnover along the trabecular surfaces was elevated following ovariectomy; the number of sites of labelled bone present per unit area of bone (BV) was significantly higher in OVX sheep as compared to controls (2.024 vs. 1.047 #/mm^2, p = 0.05, Mann-Whitney U test; Graph 4.4).

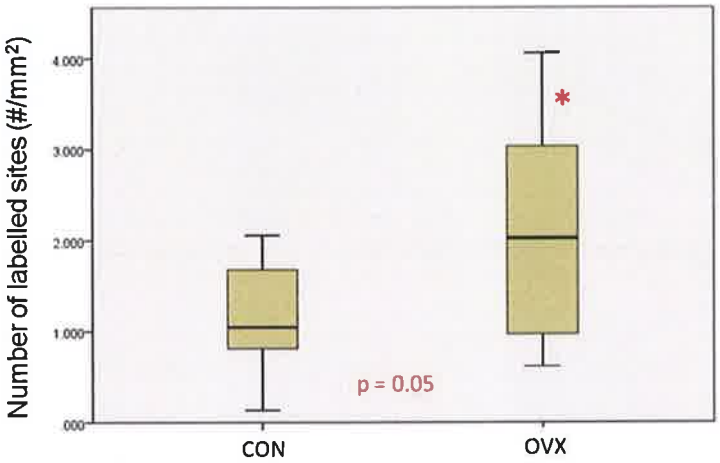

Graph 4.4 Number of sites of labelled trabecular (surface) bone per mm^2

When the total length of the sites of labelled bone per area was calculated, the OVX group again had a longer length of labelled bone present along trabecular surfaces per unit area of bone (mm^2), but this failed to reach significance (0.913 vs. 0.508 mm/mm^2, p = 0.067, Mann-Whitney U test; Graph 4.5).

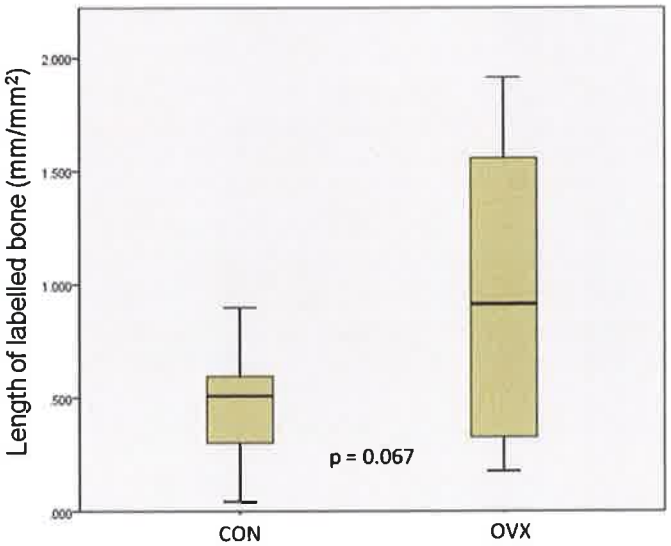

Graph 4.5 Length of labelled trabecular (surface) bone per mm^2

(iii) Intra-trabecular bone turnover sites

In addition to the labelled bone sites visualised along the trabecular surfaces, there were also areas of labelled bone within the trabeculae. Occasionally this seemed to be diffuse and non-specific (Figure 4.9). The majority of these sites however, had the appearance of being cylindrical lamellae of bone, seen in a variety of planes, arranged around a central vessel - characteristic of the secondary osteons formed by osteonal remodelling (Figures 4.10 & 4.11).

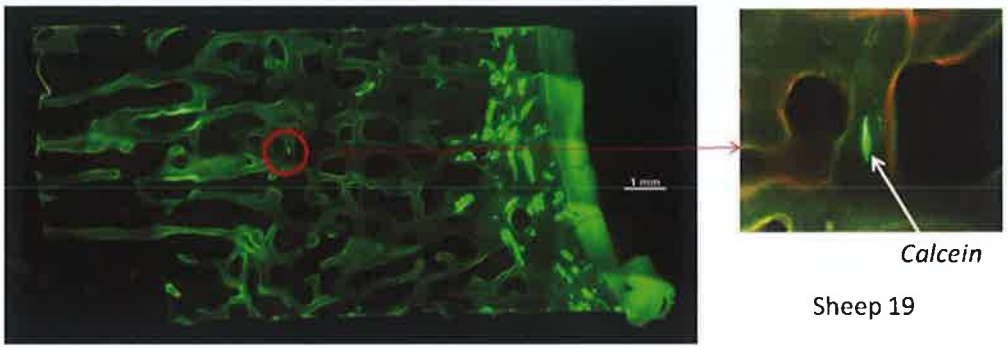

Figure 4.9 Diffusely labelled intra-trabecular bone

When the number of these sites of intra-trabecular labelled lamellar bone was quantified, the number of sites present per unit area was doubled in the OVX Group as compared to controls, but this just failed to reach significance (0.285 vs. 0.13 #/mm^2, p = 0.084, Mann-Whitney U test; Graph 4.6). There were no significant correlations between the number of these structures present and alterations in the subchondral trabecular bone microstructure as measured by MicroCT.

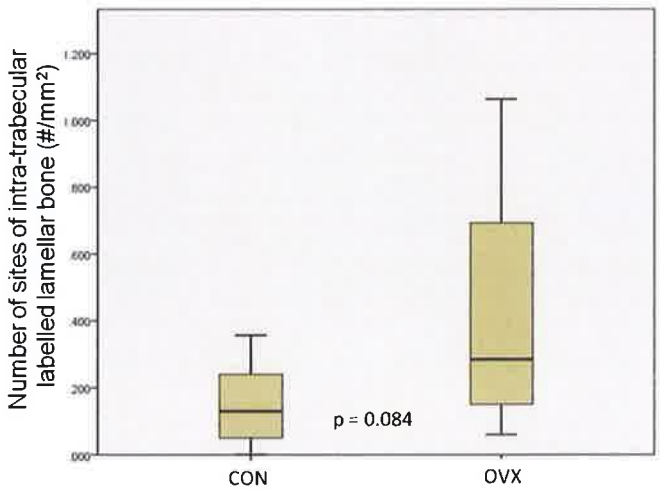

Graph 4.6 Number of sites of intra-trabecular labelled lamellar bone per mm^2

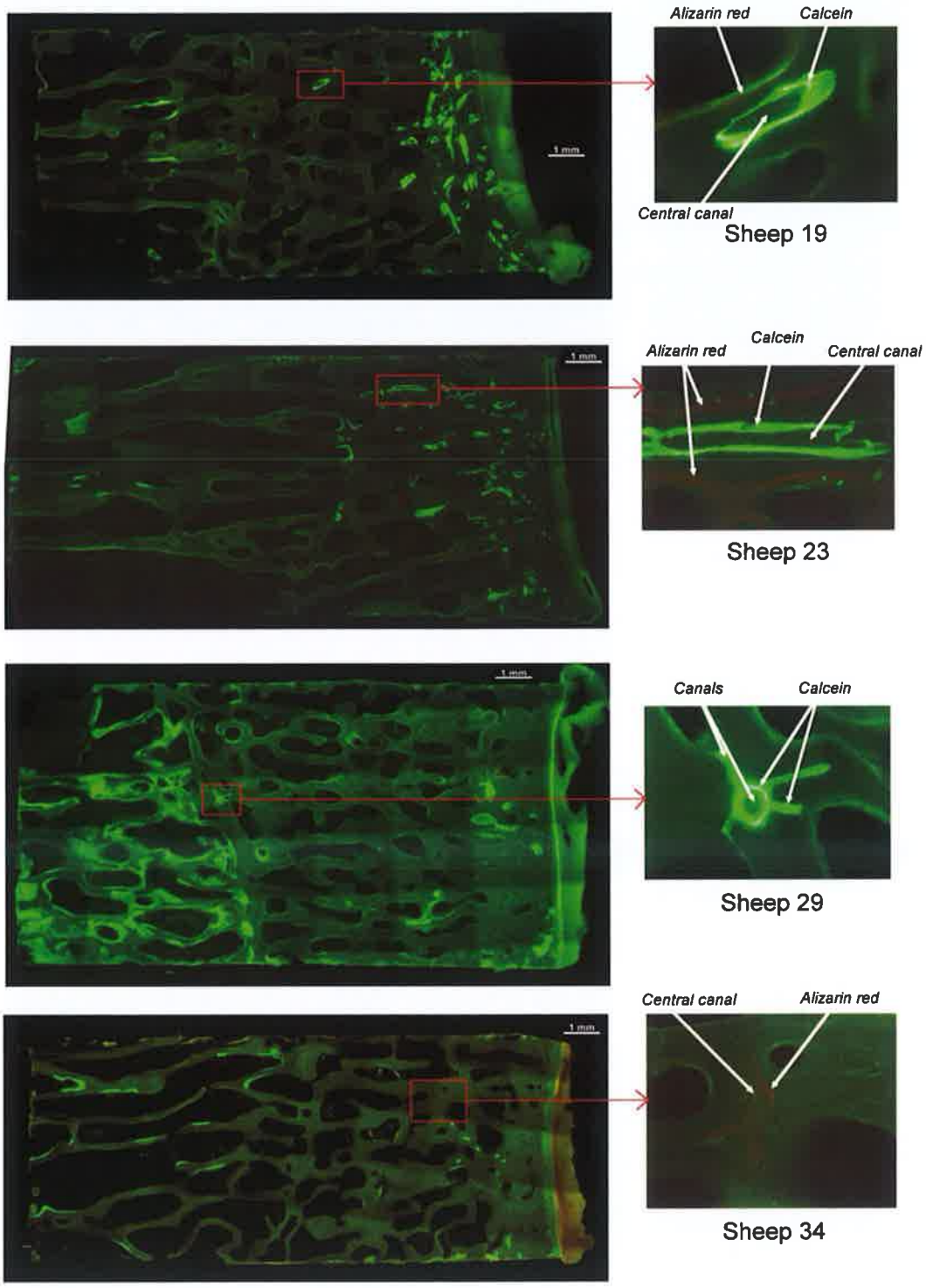

Figure 4.10 Organised (lamellar) labelled intra-trabecular bone

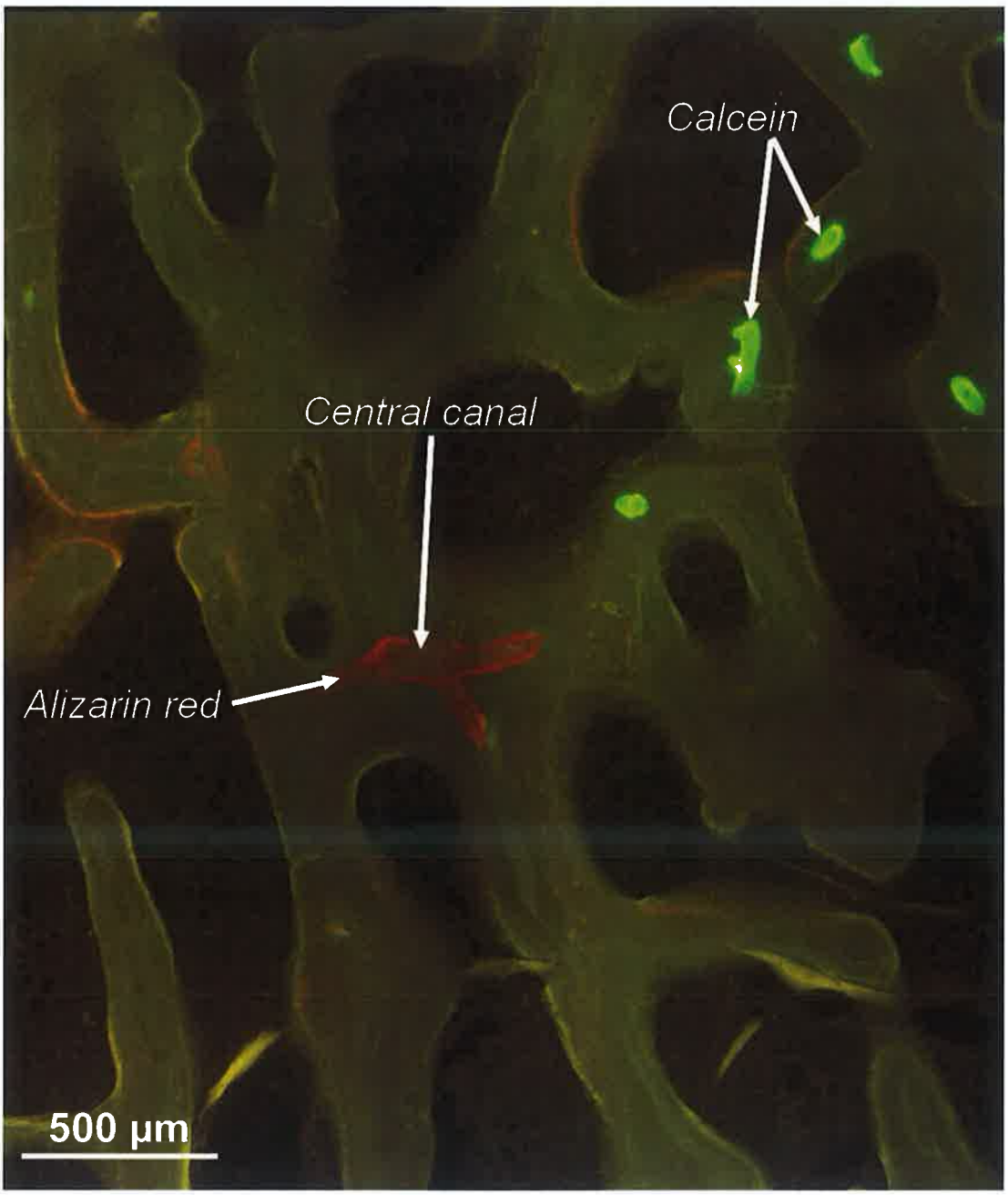

Figure 4.11 Intra-trabecular osteon labelled with Alizarin red

(iv) Turnover & microstructural changes

On examining the relationship between the bone microstructure and bone turnover, as measured by fluorochrome-labelling, there were initially no positive findings, when examining the data as a whole. Once divided into control and OVX groups for subgroup analysis, however, there were marked differences in the correlations seen within the two groups.

Within the control sheep, increase in bone turnover along the trabecular surfaces was significantly correlated with increased bone volume fraction, connectivity density and trabecular number. There was also a significant inverse correlation present with trabecular separation (Table 4.3; Graph 4.7). Within the OVX group, these correlations were non-existent; despite a greater level of bone turnover being present, as seen earlier in this section, the measureable features of bone microstructure appear to reach a plateau and then have no further alterations in response to bone turnover beyond this level.

		Bone Volume Fraction BV/TV	Connectivity density (per mm^3)	Trabecular number (per mm)	Trabecular separation (mm)
CON	r_s	0.673	0.664	0.718	- 0.736
	p	0.023	0.026	0.013	0.01
OVX	r_s	0.224	- 0.030	0.358	0.176
	p	0.553	0.934	0.310	0.627

Table 4.3 Length of sites of labelled bone (mm/mm^2) vs bone microstructure

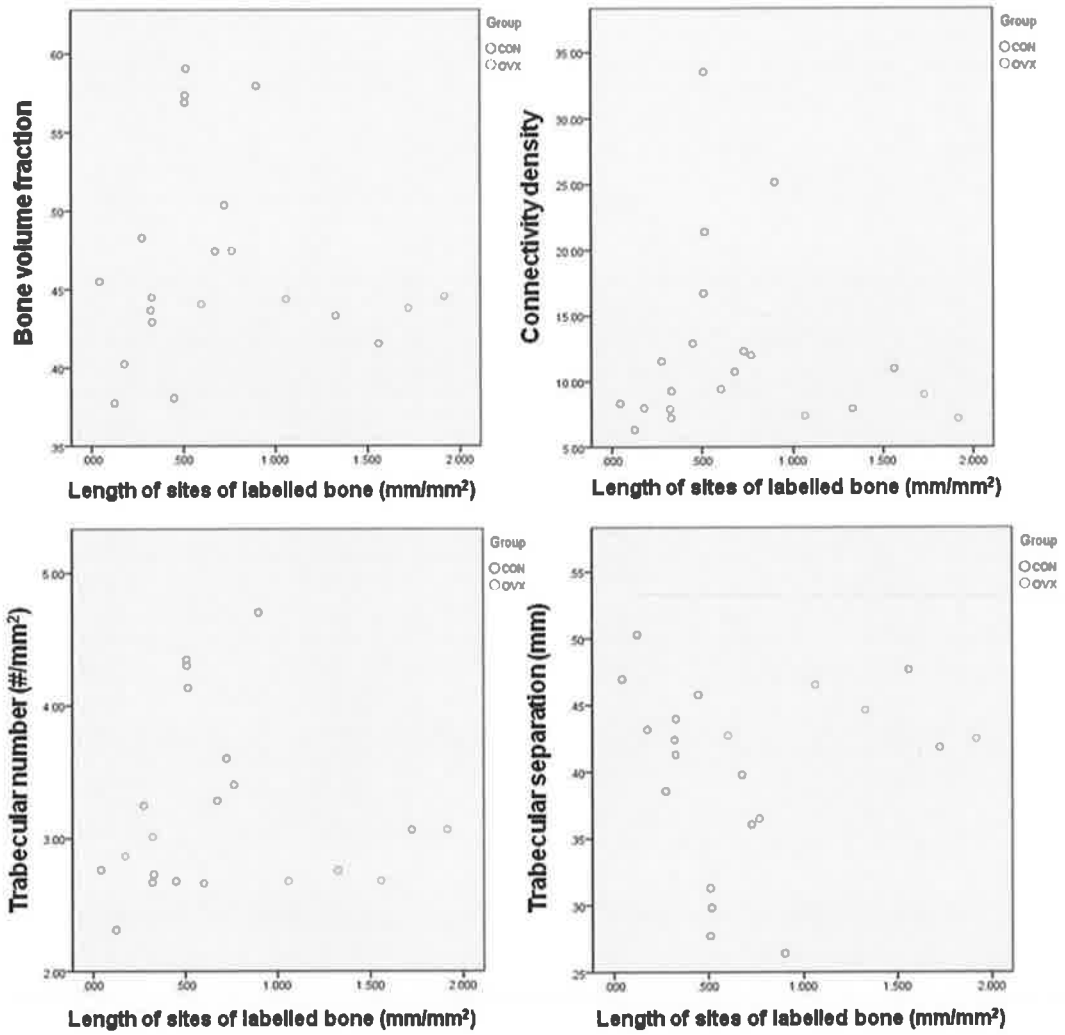

Graph 4.7 Length of sites of labelled bone (mm/mm^2) vs bone microstructure

As previously noted, there were no significant correlations between the number of sites of intra-trabecular labelled lamellar bone present and alterations in the subchondral trabecular bone microstructure as measured by MicroCT, either when examining the data as a whole, or when divided into OVX and Control groups for more detailed analyses.

4.4.4 Subchondral plate turnover

Some basic parameters were examined during microscopy, prior to quantification of labelled bone present. The area of the subchondral plate was quantified for each slide, and divided by the specimen width to estimate an average Subchondral Plate thickness for each specimen via microscopy. As would be expected, there was a highly significant correlation between the subchondral thickness obtained via MicroCT and that quantified using microscopy (r_s = 0.693; p < 0.001; Graph 4.8).

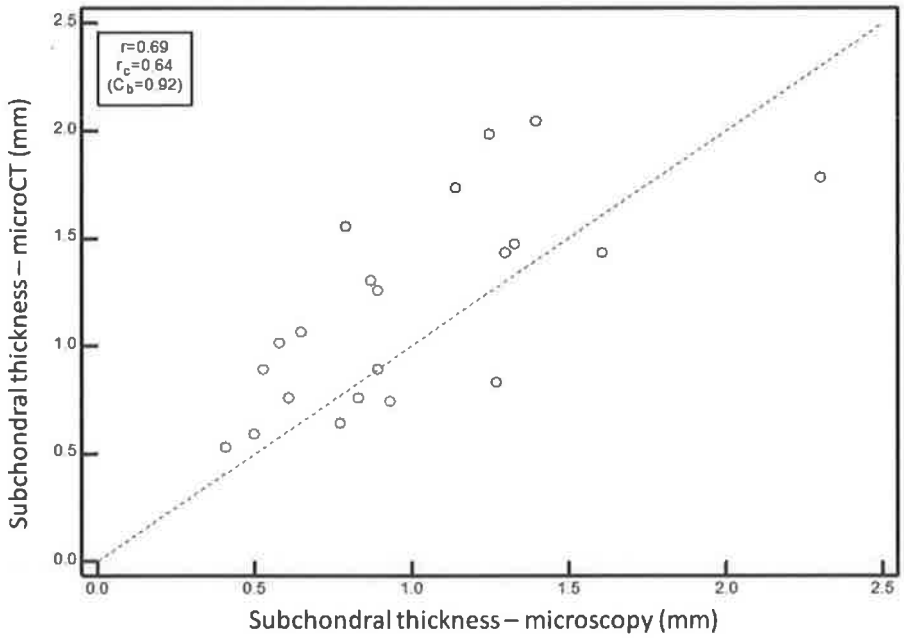

Graph 4.8 Subchondral plate thickness – Microscopy vs. MicroCT

In this case r_c was 0.64 indicating a slight bias towards higher values as measured by MicroCT. This difference is better visualised using a Bland-Altman plot in graph 4.9.

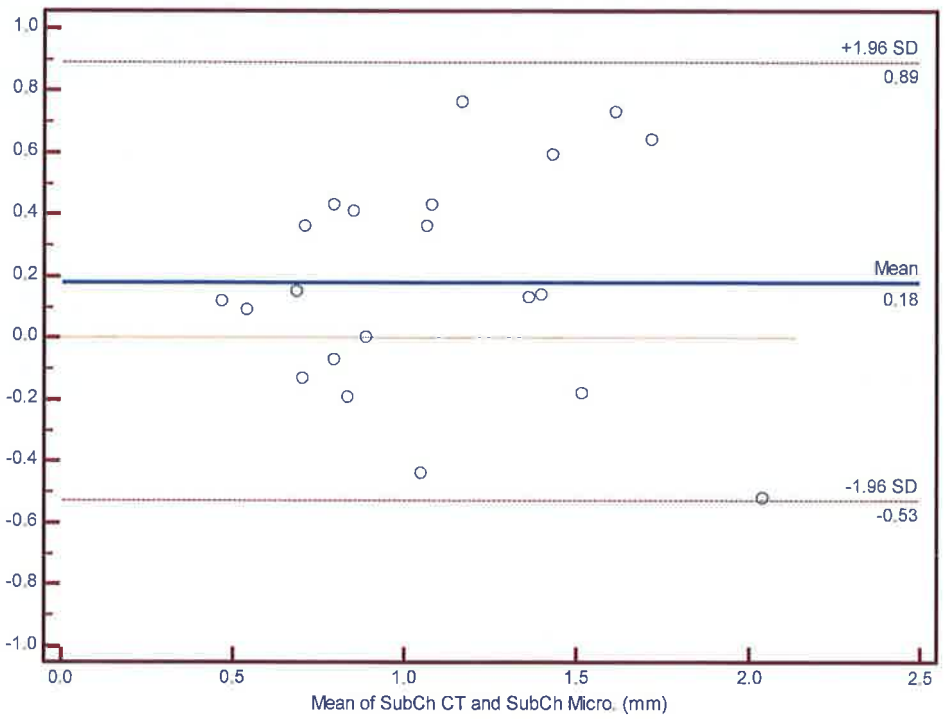

Graph 4.9 Agreement between measures of Subchondral plate thickness

The Bland-Altman plot shows mean difference of 0.18 mm in favour of measurements by MicroCT and the 95%-limits of agreement of -0.527 mm to 0.889 mm. While the observed bias is low, the limits observed are extremely wide. This probably reflects the fact that the microscopic value is more random, being based on a single 120μm section of the subchondral plate, while the value abtained from MicroCT uses multiple measurements across an area 5 x 7mm in size.

One advantage of the microscopic evaluation of the subchondral plate over measurements of plate thickness obtained by MicroCT however, is the ability to differentiate between the bone and calcified cartilage layers within the subchondral plate. With regard to thickness of the calcified cartilage layer, the OVX group were marginally thinner than controls, but this was not significant (1.95 vs. 2.2mm, p = 0.12, Mann-Whitney U test, Graph 4.10).

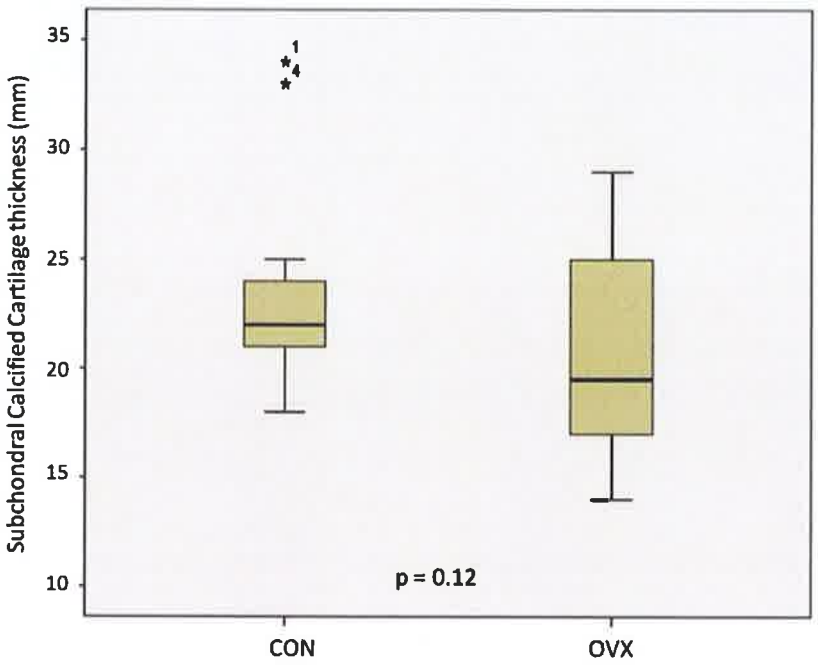

Graph 4.10 Subchondral Calcified Cartilage thickness

The Subchondral Bone was also observed to be thinner in OVX sheep as compared to controls, but not significantly so (6.59 vs. 8.32 mm, p = 0.38, t-test; 95 percent confidence interval for difference of means: -0.231 to 0.578; Graph 4.11).

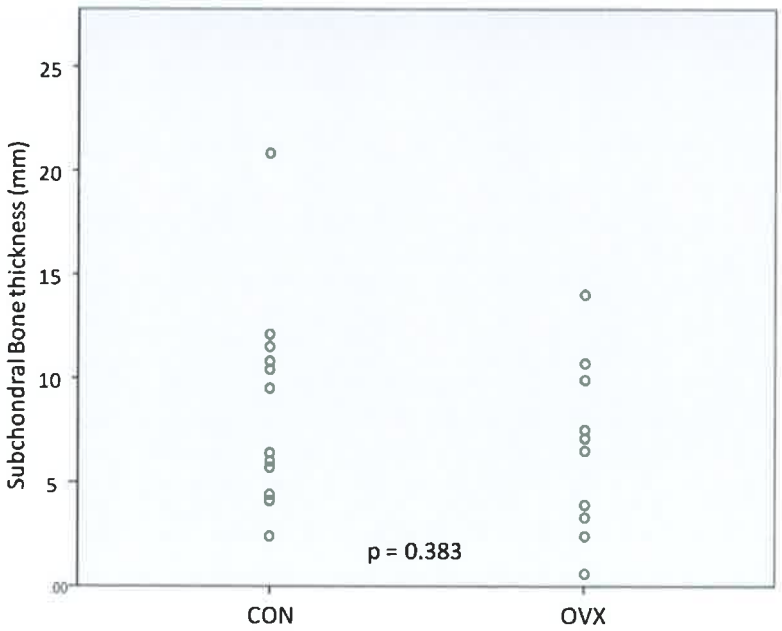

Graph 4.11 Subchondral Bone thickness

Next, bone turnover within the subchondral bone plate was quantified. This was significantly increased in the OVX group as compared to controls, with a higher total number of labelled sites visible in samples from OVX sheep, corrected for specimen width (2.35 vs. 0.85 # / mm; p = 0.003; Mann-Whitney U test, Graph 4.12).

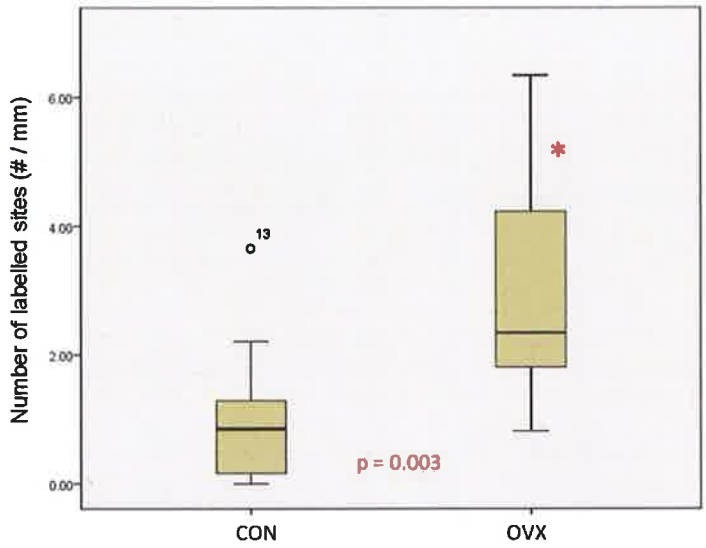

Graph 4.12 Subchondral bone turnover

As noted above, the OVX group had a slightly thinner subchondral bone layer than the control animals. On examining the number of labelled sites per mm^2 of subchondral bone, the difference between the control and OVX groups was even more marked (4.68 vs. 0.69 # / mm^2; p < 0.001; Mann-Whitney U test, Graph 4.13).

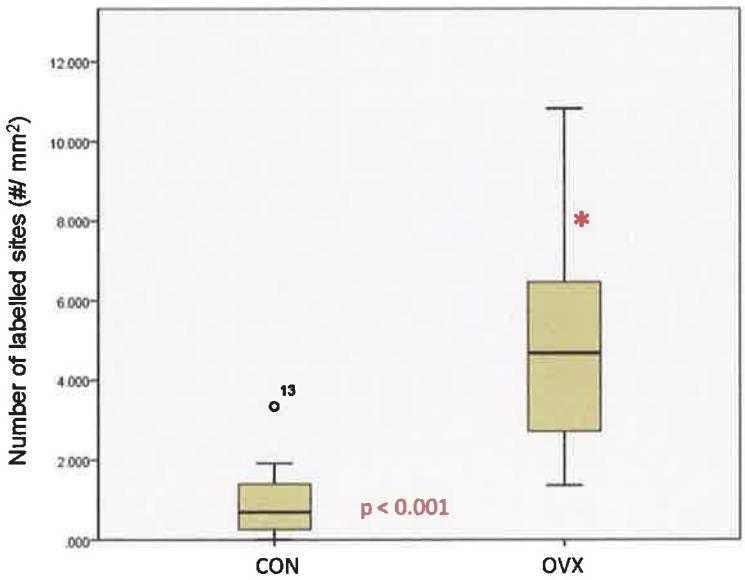

Graph 4.13 Subchondral bone turnover (# / mm^2)

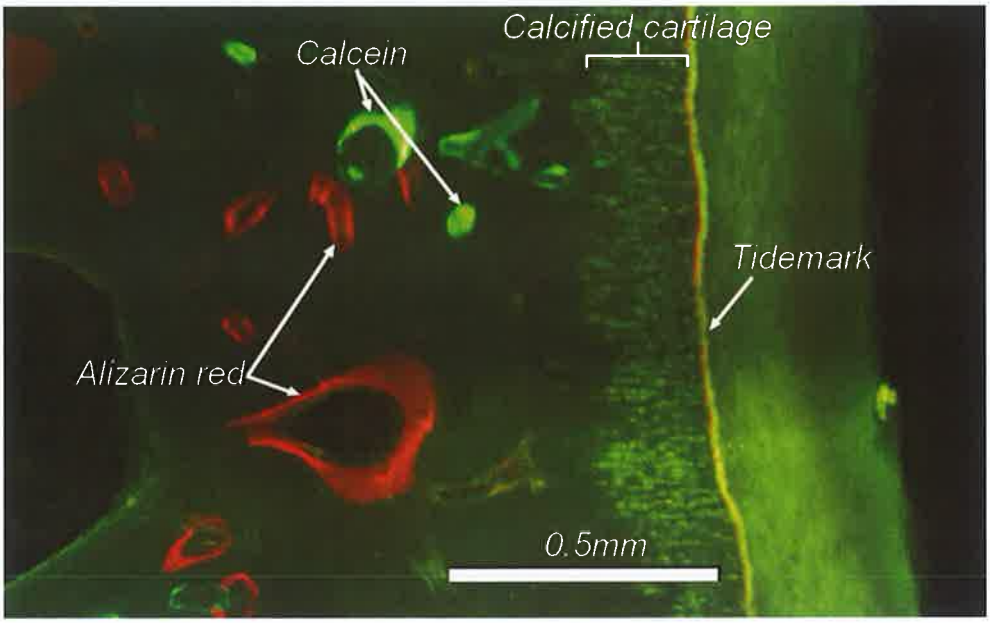

Figure 4.12 Osteonal remodelling within the subchondral plate

As with the trabecular bone turnover (Figure 4.14), an unanticipated feature was found when examining the labelled bone within the subchondral plate; a small number of secondary osteons within the subchondral plate contained two separate lamellae of labelled bone (Figure 4.13), despite these dyes having been administered 3 months apart.

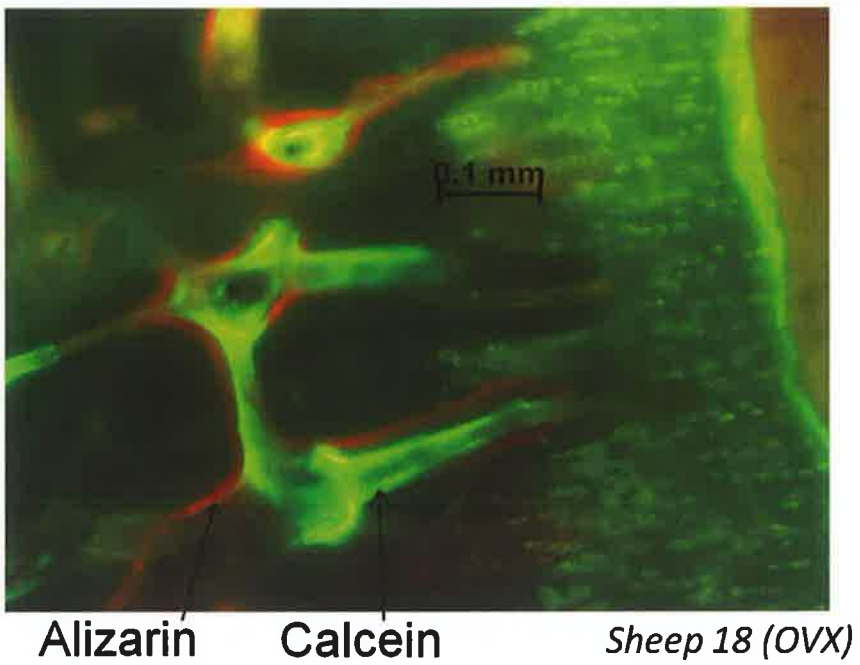

Figure 4.13 Double-labelled secondary osteons within the subchondral bone plate

4.4.5 Cartilage calcification

While both trabecular and subchondral bone showed increased labelling within the OVX specimens (Graphs 4.4, 4.5 & 4.12), the labelling of calcified cartilage at the tidemark revealed the opposite. Here, the length of sites of labelled cartilage along the tidemark (mm/mm) was lower in the OVX group as compared to controls (0.68 vs. 1.02; p = 0.06; Mann-Whitney U test, Graph 4.14).

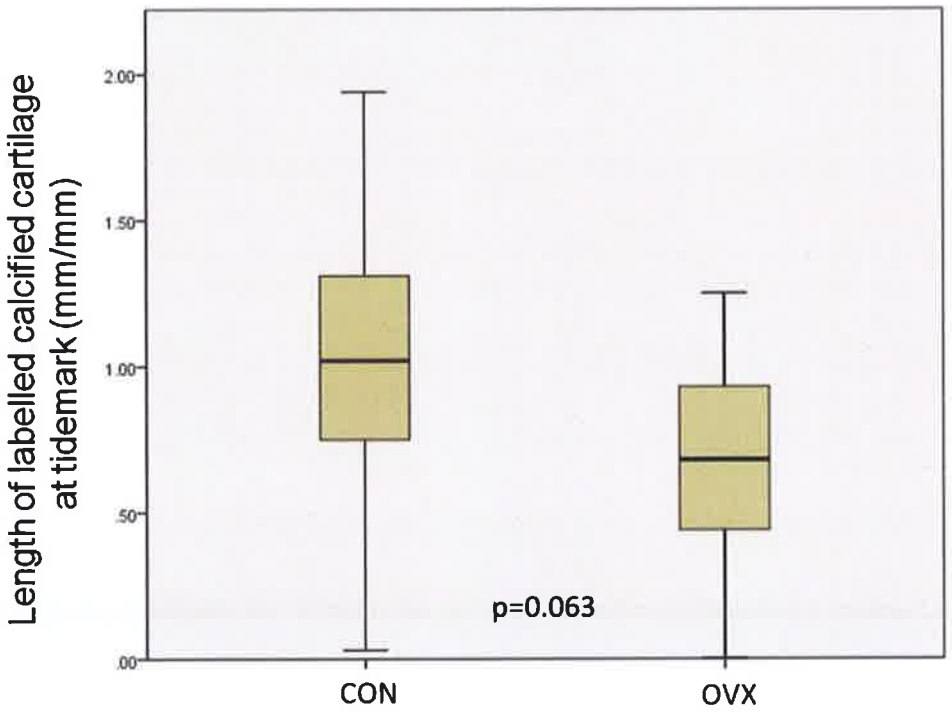

Graph 4.14 Labelled cartilage along the tidemark

4.4.6 Summary of Results

Table 4.4 summarises the findings of this chapter. In brief, trabecular bone volume fraction is slightly reduced within the OVX group as compared to controls. Bone turnover is significantly increased in the OVX group in both trabecular bone and within the subchondral bone plate. Within the calcified cartilage layer however, the OVX group showed less fluorochrome-labelled cartilage than the control group.

	Controls	**OVX**	**p**
Trabecular			
Bone Volume fraction	0.537	0.508 ↓	0.17
Bone Volume fraction (MicroCT)	0.483	0.439 ↓	**0.038 ***
Number of Sites of labelled bone/mm^2	1.047	2.024 ↑	**0.05 ***
Length of labelled bone/mm^2	0.508	0.913 ↑	**0.067**
Number of sites of intra-trabecular labelled lamellar bone	0.13	0.285 ↑	**0.084**
Subchondral plate			
Calcified Cartilage thickness (mm)	2.2	1.95	0.12
Subchondral Bone thickness (mm)	8.32	6.59	0.383
Labelled osteons/mm	0.85	2.35 ↑	**0.003 ***
Labelled osteons/mm^2	0.692	4.68 ↑	**< 0.001 ***
Endochondral ossification			
Length of labelled cartilage at tidemark (mm/mm)	1.02	0.68 ↓	**0.063**
Additional observations			
Calcein blue labelled bone along trabecular surfaces and also within the central lacunae of secondary osteons			
Cylindrical lamellae of labelled bone present within trabeculae, arranged around a central vessel, characteristic of secondary osteons			
Two separate lamellae of labelled bone present within a small number of secondary osteons within the subchondral plate			
**statistically significant p-values shown in red* *Arrows indicate whether result in OVX sheep is increased or descreased in comparison to control group*			

Table 4.4 Summary of results

4.5 DISCUSSION

The majority of studies that investigate osteoporotic bone quality tend to focus on trabecular bone tissue. This is because of the belief that the rate of bone turnover is higher in areas of trabecular bone; thus most of the deterioration in bone quantity and quality, including microarchitecture, will be found in these areas. Neither of these suppositions is necessarily true. Parfitt (2002b) noted that '*it has often been asserted, without qualification, that cancellous bone has higher turnover than cortical bone*.' He went on to comment that there are circumstances in which this is indeed true, but there are also circumstances in which it is not.

Given that the majority of texts refer to cancellous bone remodelling as being hemiosteonal, with turnover only visible along the trabecular surfaces (Parfitt, 1994), the visualisation of intra-trabecular fluorochrome-labelled secondary osteons was an unanticipated finding (Figure 4.10). With direct visual evidence that intra-trabecular osteonal remodelling does indeed occur, a focused search of the literature revealed a small number of publications documenting this phenomenon. In a study examining samples from 41 human iliac biopsies, Sato *et al* found an average of 0.55 (osteonal) channels per mm^2 of bone area (Sato *et al*, 1986). He noted a significant inverse correlation of channels present per unit of tissue area (TV) with increasing age (Figure 4.14), but not per unit of bone area (BV). In his discussion he postulates that "*trabecular osteons are mostly formed during the years of growth and modelling when the skeleton is being built up*". Another reference to trabecular osteons come with reference to removal of microfractures in cancellous bone. Boyde states these microfractures are not removed by immediate resorption, rather that surface bone deposition initially takes place, and that cutting cones subsequently develop within the (now thickened) trabecular plates (Boyde, 2003).

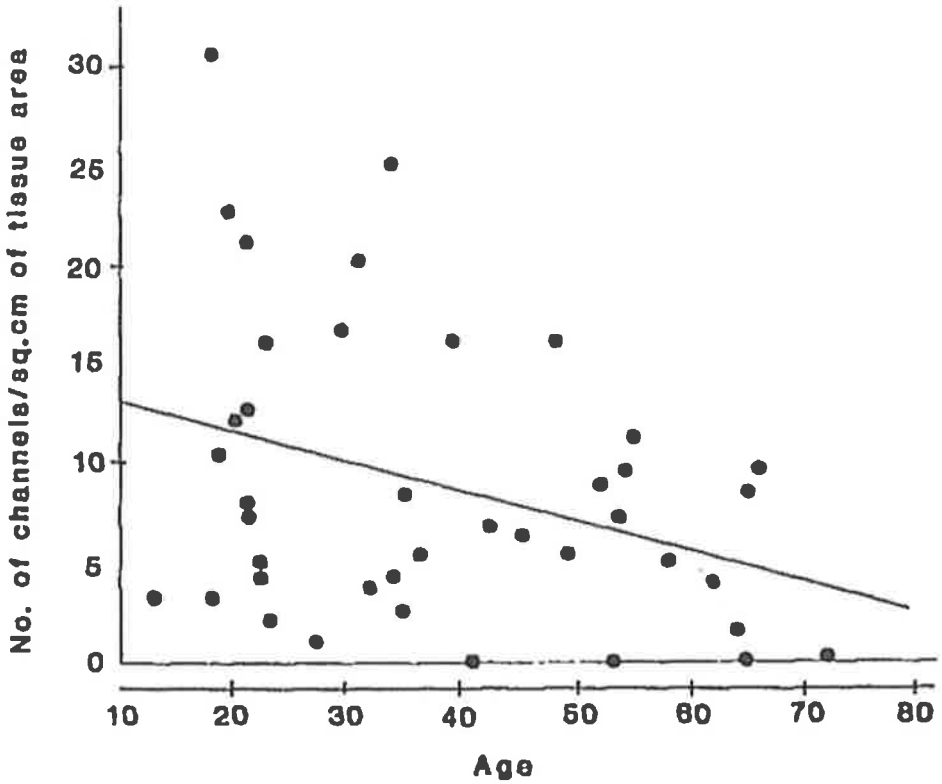

Fig. 7. Scatter diagram of the number of channels per sq. cm of tissue area against age and its regression line.

Figure 4.14 Trabecular channels (per tissue area) vs. age (Sato *et al*, 1986)

My slides show definitive evidence of intra-trabecular osteonal remodelling; while these were more prevalent within the OVX specimens, I found no correlation between the numbers of these osteons present and indices such as tissue or bone area. Sato did note a strong positive correlation between trabecular thickness and the number of channels, both in terms of tissue area and solid bone, but my data did not demonstrate this (r_s = -0.066, p = 0.77; r_s = -0.237, p = 0.300).

The more classically described hemi-osteonal bone turnover along the trabecular surfaces was also elevated following ovariectomy; the number of sites of labelled bone present per unit area of bone was significantly higher in OVX sheep as compared to controls (Graph 4.4). This is to be expected, given that oestrogen withdrawal by ovariectomy has previously been shown to result in substantial increases in basic multicellular unit (BMU) activation, which is responsible for bone remodelling, within 12 months (Kennedy *et al*, 2009b; Newman *et al*, 1995).

When correlations between bone turnover sites and bone morphometry were examined in the two subgroups, although the OVX groups showed no evidence of any positive or inverse relationships between fluorochrome-labelling and bone microstructure, the control group showed strong correlations between increased length of labelled bone along trabecular surfaces and microstructural parameters such as bone volume fraction (BV/TV), connectivity density and trabecular number; an inverse correlation with trabecular separation was also evident. This serves as a reminder that the labelled bone observed in this thesis is not solely due to BMU activation; modelling is also continually occurring along the trabecular surfaces in the healthy skeleton. While the skeleton is undergoing the normal processes of both modelling and remodelling, it is to be expected that the higher rates of newly deposited bone will correlate closely with increased bone volume fraction. In the early post-ovariectomy period, however, modelling is suppressed when the osteopenia is developing (Flieger 1998; Frost 1992) and, as previously stated, there is accelerated bone remodelling following oestrogen withdrawal (Kennedy *et al*, 2009b; Newman *et al*, 1995). While bone formation may increase overall, this rate is inadequate to replace the bone lost by resorption, leading to an elevation in the number and length of labelled sites present, but an overall loss of bone is evident upon examination of the bone microstructure (Riggs & Melton, 1992; Parfitt, 2004). Interestingly, the labelled intra-trabecular osteons, which are presumably present solely due to remodelling, do not show the same pattern as is seen along the surfaces. Here, while the number of labelled osteons is increased within the OVX group as compared to controls, there is no evidence of any correlation with increasing bone volume fraction or connectivity density within either the control or OVX groups; these osteons are merely replacing old bone, not depositing new.

Despite the marked morphological and structural density differences observed, the hydroxyapatite concentration of the trabecular bone was equal in both the control and the ovariectomised animals. Therefore, despite the increased turnover and morphological changes occurring, the mineralisation was unaltered, supporting the above inference that while osteoclastic activity was ongoing to reduce the bone volume fraction, very little new undermineralised tissue was being deposited in compensation.

Bone turnover within the subchondral plate was also significantly increased within the OVX group as compared to controls, whether controlled for specimen width or area (Graphs 4.12 & 4.13); this supports Parfitt's position that trabecular bone remodelling does not always exceed that found within the cortexes (Parfitt, 2002b). The majority of these osteons had a single fluorochrome present, but a small percentage of the subchondral osteons had two, typically alizarin red and calcein (administered at 12 & 24 weeks post-ovariectomy); in all cases the internal labelled lamella surrounded the central canal (Figure 4.12). Osteonal remodelling is performed by basic multicellular units, which typically have a life span of 2 – 8 months; the ovine bone remodelling cycle is generally considered to be comparable to that of humans, being of approximately 3 months duration (Lee *et al.*, 2002; Martin *et al*, 1998; Parfitt, 1994). New bone may take up to 6 months to fully mineralise (Bilzekian, 2004; Burr, 2004); a delay in mineralisation of the innermost lamella is the most likely explanation for the presence of two dyes within a single osteon, despite administration 3 months apart.

Increased bone turnover at other sites in the ovine skeleton does result in significant changes to the biomechanical behaviour of these bones (Kennedy *et al*, 2008; Kennedy *et al*, 2009b). What does this imply regarding the health of the adjacent joint? It has been suggested that in addition to the increased rate of observed osteopenia in specimens from patients diagnosed with spontaneous osteonecrosis of the knee (Mears *et al*, 2009), biochemical markers of bone turnover are also elevated (Berger *et al*, 2005). Spontaneous osteonecrosis of the knee (SPONK) typically occurs over the age of 55 and is a recognised cause of knee pain; women tend to have a higher incidence than men (Akamatsu *et al*, 2012, Lotke *et al*, 1977). Microfractures within osteoporotic subchondral bone are thought to be a possible aetiological mechanism for this condition (Lotke *et al*, 1988; Yamamoto & Bullough, 2000). Subchondral insufficiency fractures secondary to osteopenia have been documented within the subchondral bone of the femoral head (Satku *et al*, 2003; Yamamoto & Bullough, 2000b). Bone turnover has been investigated in the past with regard to its influence on fracture risk (Riggs & Melton, 2002). It has been demonstrated that accelerated bone resorption is associated with an increased incidence of osteoporotic fractures, independent of BMD (Hernandez, 2008; Meier *et al*, 2005). The presence of elevated subchondral bone turnover within the medial tibial plateau lends weight to the hypothesis that individual trabecular fractures may develop in this site, with deleterious consequences for the overlying joint. Interestingly, a recent study suggests that early

treatment with Vitamin D and bisphosphonates, a standard treatment regimen for osteoporosis which reduces bone turnover, is beneficial in SPONK, with remission of symptoms and pathological findings on Magnetic Resonance Imaging (Breer *et al.* 2012).

While turnover was increased within the trabeculae and subchondral bone of the OVX specimens, the labelling of calcified cartilage at the tidemark revealed the opposite. Here, the length of sites of labelled cartilage along the tidemark (mm/mm) was lower in the OVX group as compared to controls. The calcified cartilage layer was thinner in ovariectomised sheep, but not significantly so. Lane *et al* also found that the calcified cartilage layer reduced in thickness with age, but noted an increase in the number of visible tidemarks (Lane *et al*, 1980). It has been previously noted, however, that as the zone of calcified cartilage is labelled from the synovial fluid, intravenous fluorochrome administration may lead to patchy labelling; intra-articular injections are more reliable for this purpose (Oegema *et al* 1997).

In conclusion, this study shows significant alterations in bone turnover in both trabecular bone and within the subchondral bone plate at one-year post-ovariectomy. This is due to suppression of modelling and accelerated bone remodelling following oestrogen withdrawal. Remodelling of trabecular bone was due to both classically described hemi-osteonal and intra-trabecular osteonal remodelling. Osteons within the subchondral plate may have relatively late mineralisation of lamellae; the effect that this may have on the structural properties of the subchondral plate, or the health of the overlying cartilage, remains uncertain. However, the presence of both localised osteopenia and accelerated bone remodelling within the medial tibial plateau provide a possible mechanism for subchondral microfractures in the aetiology of SPONK. Further utilisation of the ovariectomised ewe should be useful for further study in this field.

4.6 CONCLUSIONS

1. Bone remodelling was significantly increased in the OVX sheep as compared to controls, in both trabeculae and the subchondral plate.

2. Bone modelling is suppressed within the OVX group as compared to controls.

3. In addition to the typical hemi-osteonal turnover observed along the surfaces of trabecular, cylindrical lamellae of labelled bone were also present within trabeculae, arranged around a central vessel, characteristic of secondary osteons.

4. Within the subchondral plate, there were often two dyes visible within a single osteon, despite being administered 3 months apart. New bone may take up to 6 months to fully mineralise; a delay in full mineralisation of the innermost lamella is the most likely explanation.

5. The presence of both localised osteopenia and accelerated bone remodelling within the medial tibial plateau provide a possible mechanism for subchondral microfractures in the aetiology of spontaneous osteonecrosis of the knee.

CHAPTER 5: THE EFFECT OF OVARIECTOMY ON THE ARTICULAR CARTILAGE OF THE MEDIAL TIBIAL PLATEAU

5.1 INTRODUCTION

The use of ovariectomy alone as a model of osteoarthritis induction is a recent addition to the literature (Cake *et al* 2005; Turner *et al* 1997) and reviews as to its reliability as a model are inconclusive (Sniekers *et al*, 2008b). In addition, osteoarthritis and osteoporosis have traditionally been viewed as being mutually exclusive (Dequeker, 1997; Stewart & Black, 2000). While some studies show that increased subchondral bone mineral density is associated with reduced joint space narrowing and osteoarthritis progression (Bruyere *et al*, 2003), other research suggests that periarticular osteoporosis commonly occurs with osteoarthritis (Karvonen *et al*, 1998; Patel *et al*, 2003). It has long been hypothesised that alterations observed in the subchondral bone, the thinning of the plate and underlying trabeculae, will change the pattern of mechanical loading on the overlying cartilage (Radin & Rose, 1986). Alterations within the subchondral bone are certainly evident in mid and late-stage osteoarthritis; whether these changes occur simultaneously with, precede or even perhaps initiate, the deterioration of the articular cartilage seen in osteoarthritis is still undetermined.

The ovariectomised ewe is a useful model for elevated bone turnover and this is increased in established osteoarthritis, as measured by scintigraphy, but few studies have performed direct evaluation of the remodelling rate by histological examination (Benske *et al*, 1988; Hayami *et al*, 2004; Sharif *et al*, 1995). Measurement of bone resorption markers suggests that these are elevated early in the disease process (Kwan Tat *et al*, 2010). In addition, while endochondral ossification at the interface between bone and cartilage is usually present at a physiological rate, this process is described as being accelerated in osteoarthritis, with tidemark advancement (Burr, 2004; Oegema *et al*, 1997). Whether these changes precede or follow degradation in the overlying cartilage is unknown; the hypothesis that alterations in the mineralisation or structure of the subchondral bone may be the initiating factor in the development of disease in the overlying cartilage is not new (Radin & Rose, 1986). Certainly once osteoarthritis is established, whatever the initiating cause, there is absolute consensus that alterations in the subchondral bone do occur, which will then have a considerable effect on the stresses within the overlying cartilage (Burr, 2004).

5.2 AIMS OF STUDY

The primary aim of this section of the study was to determine whether ovariectomy had any impact on development of osteoarthritis within the ovine stifle joint at 1 year post-operatively. The secondary aim was to determine whether there were any significant correlations present between articular cartilage degeneration and alterations in microstructural parameters or turnover rates in the underlying bone.

Specific questions:

- Does ovariectomy induce osteoarthritis?
  - Is osteoarthritis increased at the medial tibial plateau in ovariectomised ewes as compared to control animals?
- What relationships are there between these processes?
  - Is osteoarthritis associated with osteopenia of the subchondral trabecular bone, or is there an inverse relationship present?
  - Is osteoarthritis associated with a thickening or thinning of the subchondral bone plate?
  - Do alterations in bone turnover have any significant effect on the degree of osteoarthritis visible in the overlying articular cartilage?
  - Is the rate of endochondral ossification increased in osteoarthritis?

5.3 MATERIALS AND METHODS

5.3.1 Macroscopic staging of osteoarthritis

The macroscopic stage of osteoarthritis present was assessed immediately following removal of the plateau from the tibia. A digital photograph was obtained of each plateau, to allow subsequent image analysis and calculation of the surface area affected by osteoarthritis, as required by the Osteoarthritis Research Society International (OARSI) scoring system. (Pritzker *et al*, 2006; Figure 5.1).

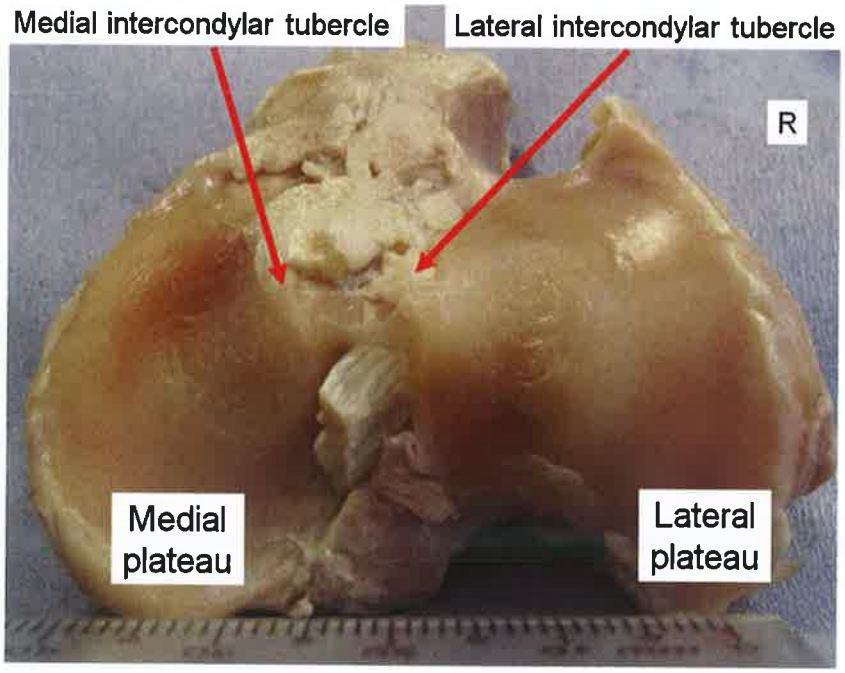

Figure 5.1 Right tibial plateau following removal

5.3.2 Specimen decalcification and paraffin embedding

Specimen B (obtained as described in Chapter 3) was fixed in neutral buffered formalin for 24 hours and then decalcified in 10% formic acid for 7 days. During decalcification, specimens were suspended within solution in a cotton mesh bag and gently agitated throughout, with the solution changed every 24 hours (Figure 5.2).

Figure 5.2 Suspension and agitation of specimens during decalcification

Specimens then underwent standard tissue processing in a Leica ASP 300 (Table 5.1; Figure 5.3) and were then paraffin embedded in standard blocks. During embedding, specimens were orientated within the block in such a way that, when subsequently microtomed, full osteochondral sections were obtained (Figure 5.4).

Reagent	Time (hr)
Formalin	2.00
70% Ethanol	1.00
95% Ethanol	1.00
100% Ethanol	3.00
Xylene	3.00
Wax (60 °C)	3.00

Table 5.1 Tissue Processing protocol

Figure 5.3 Tissue processor, paraffin embedder and cold-plate

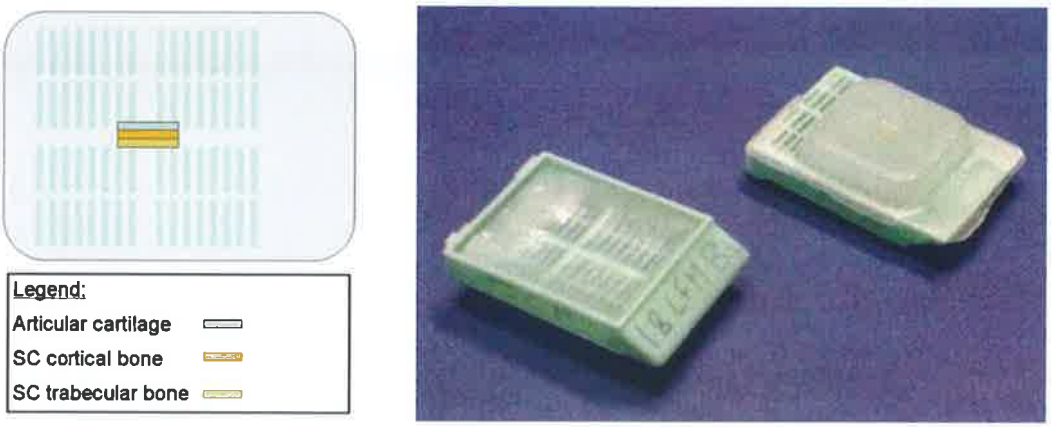

Figure 5.4 Paraffin-embedded specimens

Blocks were then placed on a rotary Leica microtome (Leica RM2255, Leica Microsystems, Germany); serial sections were cut at 10μm, floated in a water bath and then mounted on Polysine adhesion glass slides (Fisher).

5.3.3 Toluidine Blue staining

In order to allow quantification of the degree of osteoarthritis present, slides were then stained with toluidine blue / fast green (Getzy *et al*, 1982, Little *et al* 1997). Slides were initially placed in an oven at 55°C for 30 minutes, then a xylene bath for 10 minutes, followed by graded ethanol baths and rinsed in distilled de-ionized water. They were subsequently placed in 0.04% Toluidine Blue / 0.1 M sodium acetate buffer pH 4.0 for 10 minutes, rinsed in distilled de-ionized water and counterstained in 0.1% aqueous fast green solution for 2 minutes. Slides were then rinsed in distilled de-ionized water, dehydrated in 100% ethanol, cleared in xylene, air-dried at room temperature and finally mounted with DPX (Figure 5.5).

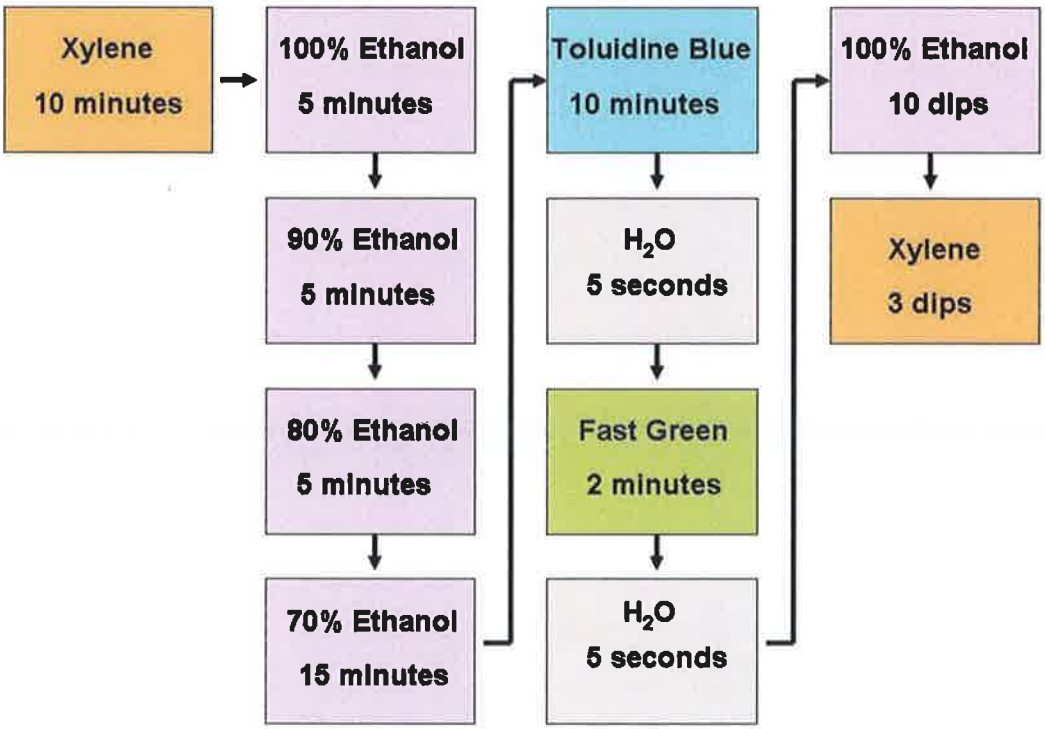

Figure 5.5 Flow diagram of method used for staining osteochondral sections

5.3.4 Histological grading of osteoarthritis

In this study, two histological methods were utilized for the quantification of the degree of osteoarthritis present in the articular cartilage. The first of these is a modification of the Histological / Histochemical grading system first described by Mankin *et al* (Little *et al*, 1997; Mankin *et al*, 1971). The second method employed was introduced more recently by the Osteoarthritis Research Society International (OARSI), as it was felt that Mankin's system had a number of disadvantages: it was originally described for specimens with advanced osteoarthritis, and so is not ideal for the description of early or mild osteoarthritis; it merely gives a grade but no indication of stage or extent of disease on the articular surface. Additionally, inter- and intra-observer variability have been described with Mankin's (Custers *et al*, 2007; Pritzker *et al*, 2006).

(i) Mankin's Scoring System

The original method described by Mankin *et al* assigned sub-scores to articular cartilage specimens for categories including matrix structure, cell distribution and density, the integrity of the tidemark and the degree of Safranin O staining (a metachromic dye which binds to glycosaminoglycans). The sub-scores for each category are totalled to give a final overall score (Mankin *et al*, 1971).

HISTOLOGICAL-HISTOCHEMICAL GRADING *

	Grade		Grade
I. Structure		III. Safranin-O staining	
a. Normal	0	a. Normal	0
b. Surface irregularities	1	b. Slight reduction	1
c. Pannus and surface irregularities	2	c. Moderate reduction	2
d. Clefts to transitional zone	3	d. Severe reduction	3
e. Clefts to radial zone	4	e. No dye noted	4
f. Clefts to calcified zone	5		
g. Complete disorganization	6		
II. Cells			
a. Normal	0		
b. Diffuse hypercellularity	1	IV. Tidemark integrity	
c. Cloning	2	a. Intact	0
d. Hypocellularity	3	b. Crossed by blood vessels	1

* Serial histological sections, cut at five micrometers and stained with hematoxylin and eosin and safranin-O-fast green-iron hematoxylin, were analyzed for abnormalities in structure, cell population, safranin-O stain distribution, and tidemark integrity and scores assigned as the histologic-histochemical grade.

Table 5.2 Mankin's original scoring system (Mankin *et al*, 1971)

Toluidine Blue (particularly when counterstained with Fast Green) is now more frequently used for the depiction of glycosaminoglycans within articular cartilage as it has some advantages with regard to improved reliability with metachromatic staining (Getzy *et al*, 1982). In view of this, a modification of Mankin's score, which subdivides specimen staining into territorial and interterritorial sub-categories, has been devised (Figure 5.6); this is the method employed in this thesis, which allows for a Mankin score ranging from 0 to 29 (Table 5.3; Little *et al*, 1997).

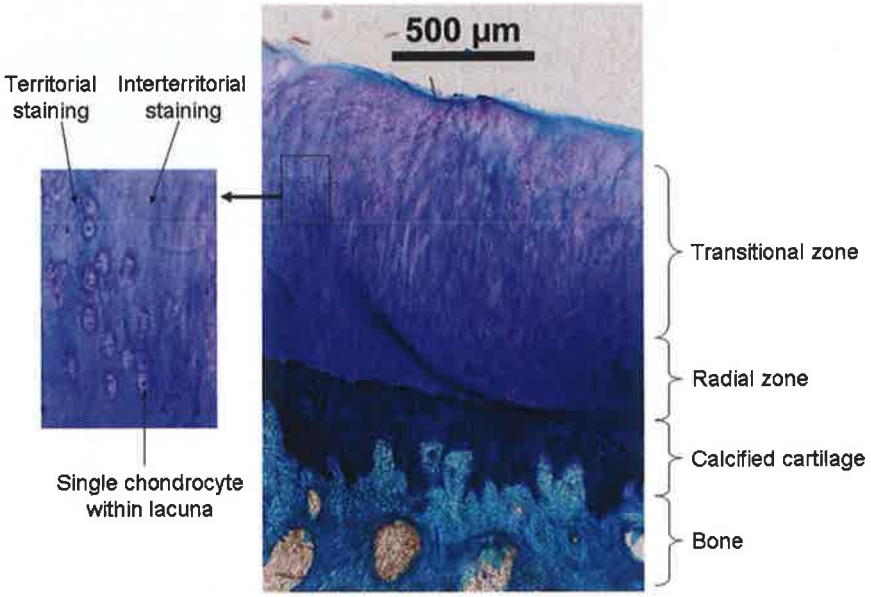

Figure 5.6 Osteochondral specimen with Toluidine Blue staining

Table 1. Histological and histochemical grading of articular cartilage lesions.

I. Structure	
Normal	0
Slight surface irregularities	1
Moderate surface irregularities	2
Severe surface irregularities	3
Clefts into transitional zone (1/3 depth)	4
Clefts into radial zone (2/3 depth)	5
Clefts into calcified zone (full depth)	6
Fibrillation and/or loss to transitional zone (1/3 depth)	7
Fibrillation and/or loss to radial zone (2/3 depth)	8
Fibrillation and/or loss to calcified zone (full depth)	9
Fibrillation and/or loss to subchondral bone	10
II. Cellularity	
Normal	0
Increase or slight decrease	1
Moderate decrease	2
Severe decrease	3
No cells	4
III. Cell cloning	
Normal	0
Several doublets	1
Many doublets	2
Doublets and triplets	3
Multiple cell nests	4
IV. Territorial toluidine blue	
Normal	0
Increase or slight decrease in staining	1
Moderate decrease	2
Severe decrease	3
No staining	4
V. Interterritorial toluidine blue	
Normal	0
Loss of staining in tangential zone (1/3 depth)	1
Loss of staining in transitional zone (2/3 depth)	2
Loss of staining in radial zone (full depth)	3
No staining	4
VI. Tidemark/calcified cartilage/subchondral bone	
Intact subchondral bone plate + single tidemark	0
Intact subchondral bone plate + multilayered tidemark	1
Blood vessels through subchondral bone to calcified cartilage	2
Tidemark crossed by blood vessels	3

Table 5.3 Modified Mankin's scoring system (Little *et al*, 1997)

(ii) Osteoarthritis Research Society International (OARSI) score

The Osteoarthritis Research Society International (OARSI) scoring system gives an overall score that is dependent upon both the grade of osteoarthritis (OA) present, similar to Mankin's score above, and the OA ***stage***, which quantifies the extent of joint involvement (Pritzker *et al*, 2006).

The OARSI stage is a measure of the extent of involvement of the articular cartilage in the disease process; in this study it was quantified by means of image analysis of photographs of the tibial plateau using Scion Image (Scion Corporation, Maryland, 2005). The total and osteoarthritic areas of the tibial plateau were measured, and then the percentage of articular surface involvement was calculated: stage sub-scores were then assigned as per the protocol in Table 5.4.

OA cartilage histopathology—stage assessment

Stage	% Involvement (surface, area, volume)
Stage 0	No OA activity seen
Stage 1	<10%
Stage 2	10–25%
Stage 3	25–50%
Stage 4	>50%

Stage = extent of joint involvement.

Table 5.4 OARSI Stage (Pritzker *et al*, 2006)

The OARSI grade is a measure of the degree of severity of the tissue damage seen on histological / microscopic examination, as determined using the criteria shown in Table 5.5, and typical specimens are depicted in Figure 5.7.

Grade (key feature)	Subgrade (optional)	Associated criteria (tissue reaction)
Grade 0: surface intact, cartilage intact	No subgrade	Intact, uninvolved cartilage
Grade 1: surface intact	1.0 Cells intact 1.5 Cell death	Matrix: superficial zone intact, edema and/or fibrillation Cells: proliferation (clusters), hypertrophy Reaction must be more than superficial fibrillation only
Grade 2: surface discontinuity	2.0 Fibrillation through superficial zone 2.5 Surface abrasion with matrix loss within superficial zone	As above +Discontinuity at superficial zone ±Cationic stain matrix depletion (Safranin O or Toluidine Blue) upper 1/3 of cartilage (mid zone) ±Disorientation of chondron columns
Grade 3: vertical fissures	3.0 Simple fissures 3.5 Branched/complex fissures	As above ±Cationic stain depletion (Safranin O or Toluidine Blue) into lower 2/3 of cartilage (deep zone) ±New collagen formation (polarized light microscopy, Picro Sirius Red stain)
Grade 4: erosion	4.0 Superficial zone delamination 4.5 Mid zone excavation	Cartilage matrix loss, cyst formation within cartilage matrix
Grade 5: denudation	5.0 Bone surface intact 5.5 Reparative tissue surface present	Surface is sclerotic bone or reparative tissue including fibrocartilage
Grade 6: deformation	6.0 Joint margin osteophytes 6.5 Joint margin and central osteophytes	Bone remodelling. Deformation of articular surface contour (more than osteophyte formation only) Includes: microfracture and repair

I. Grade = depth progression into cartilage.

Table 5.5 OARSI Grade (Pritzker *et al*, 2006)

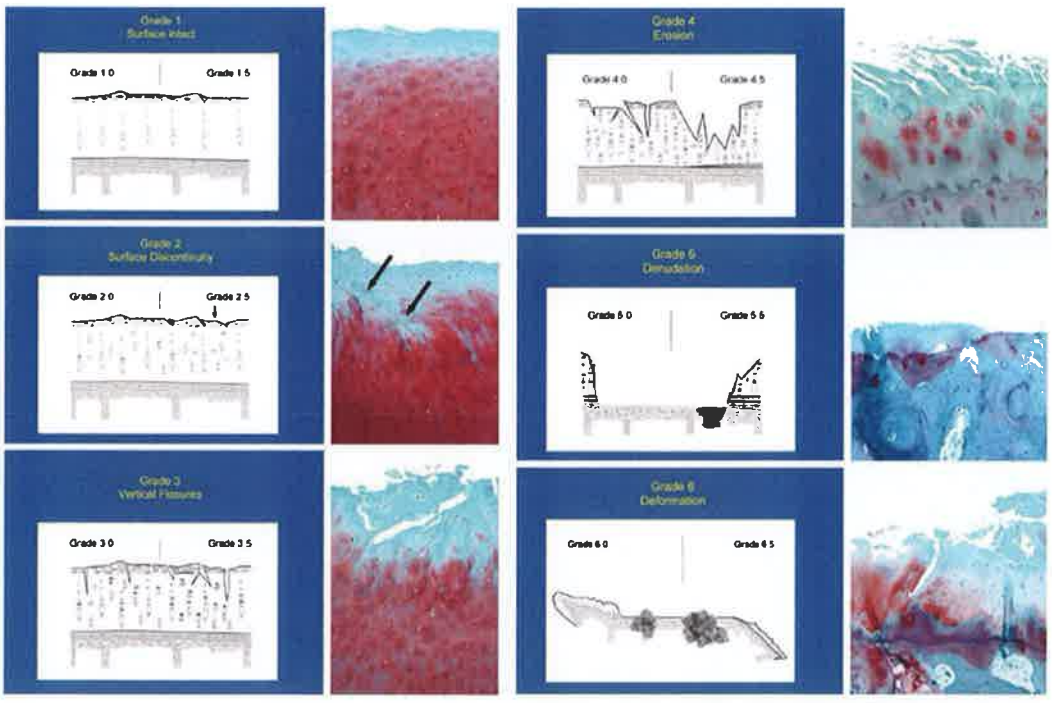

Pritzker et al. Osteoarth Cart 2006;14 (1):13 - 29

Figure 5.7 OARSI Grade (Pritzker *et al*, 2006)

The OARSI score is then obtained by multiplication of the grade (0 - 4) and stage (0 – 6) sub-scores, to give an overall score ranging from 0 to 24.

5.4 RESULTS

As described in Chapter 3, one of the ovariectomised sheep (no. 23) again proved to be an outlier, skewing the statistical analyses (Graph 5.1). This sheep was again removed from all analyses within this chapter. Two additional sheep (7 & 16) were excluded from analysis of bone turnover as described in Chapter 4.

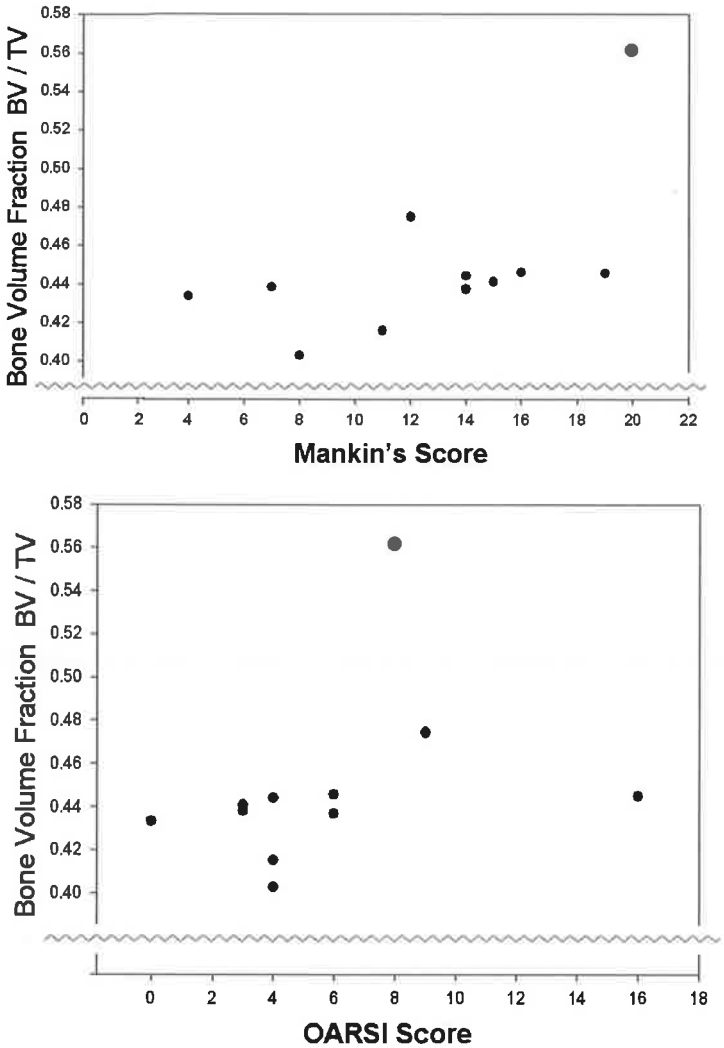

Graph 5.1 Outlier Identification (Histological OA vs. Bone Volume fraction)

SigmaStat version 3.00 (SPSS Inc.) was used throughout. All data sets were initially analysed for normality and equal variance. A t-test was performed if the appropriate criteria were met ($P > 0.05$ & $P = 0.10$ respectively); if either criterion was failed, a Mann-Whitney-U test was performed instead.

5.4.1 Ovariectomy and osteoarthritis

Osteoarthritic changes were quantified using two methods; Mankin's histopathological scoring system and the OARSI score. As these two measures use two different scales it was more appropriate to look at how each measure ranked the changes rather than using the raw scales. As would be expected, there was evidence of a positive correlation between the ranks of these two scoring systems was highly significant (r = 0.61, p = 0.003; Graph 5.2).

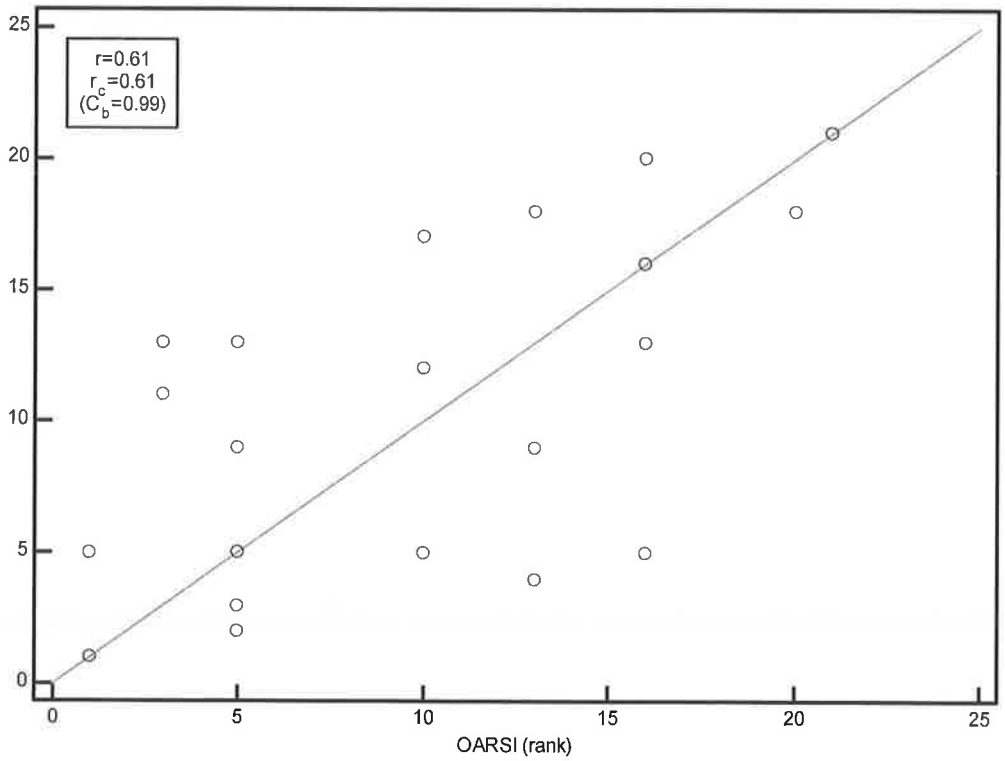

Graph 5.2 Correlation between (ranked) OARSI and Mankin's scores

In this case the value for r_c was 0.61 which was approximately the same value for the correlation coefficient (the correction factor C_b was 0.99) indicating no bias towards either scale. This difference is better visualised using a Bland-Altman plot in Graph 5.3.

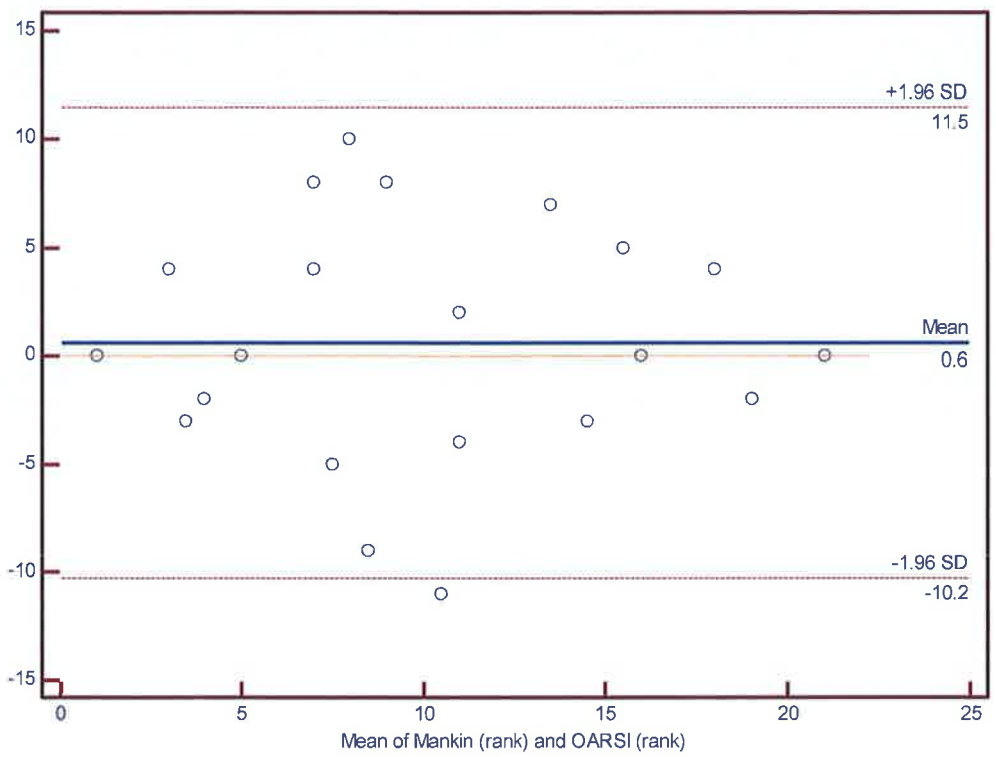

Graph 5.3 Rank agreement between OARSI and Mankin's scores

The Bland-Altman plot shows slight mean rank difference of 0.6 in favour of measurements by the Mankin scale and the 95%-limits of agreement of -10.2 to 11.5 rank positions. While the observed bias is quite low, the limits observed are extremely wide. Again, this probably reflects the fact that the Mankin's score is based solely on the maximal grade of osteoarthritis observed at a single point, while the OARSI also accounts for what proportion of the articular surface is involved.

Most specimens showed some evidence of osteoarthritis. However, there was no difference in the degree of osteoarthritis observed between the OVX and Control groups using either scoring method; Mankin's score (12.7 vs. 11.3, p=0.443, t-test; 95 percent confidence interval for difference of means: -5.189 to 2.349; Graph 5.4), OARSI score (4 vs. 6, p = 0.706).

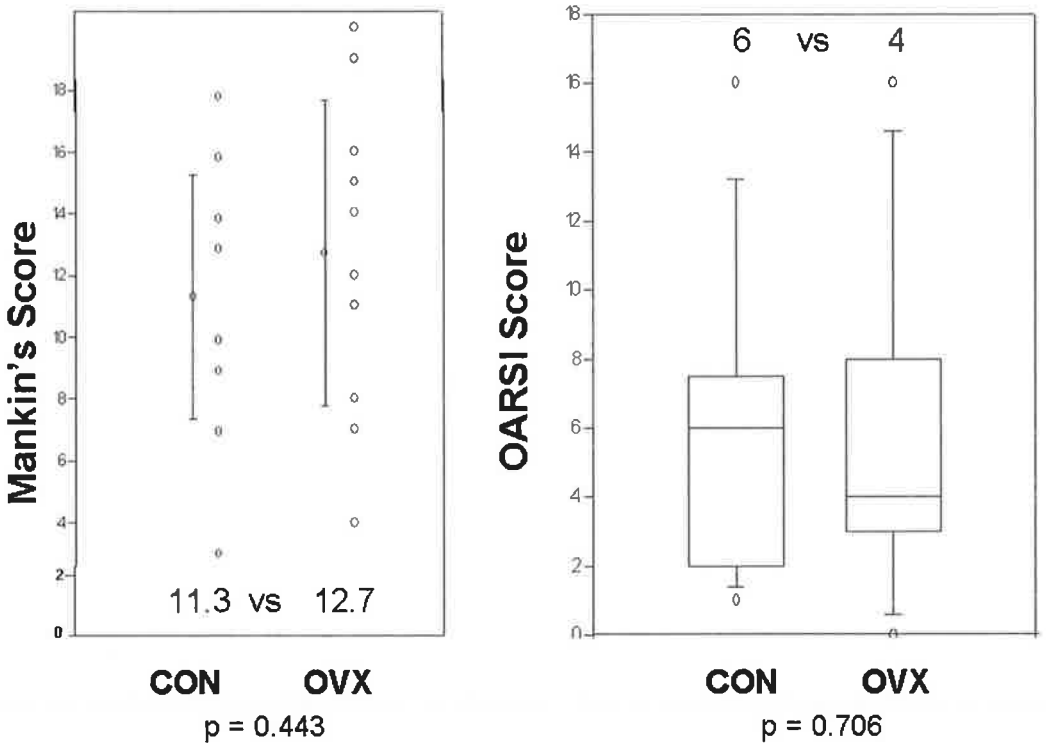

Graph 5.4 Ovariectomy & Osteoarthritis

5.4.2 Osteoarthritis and bone mineral density

Next, correlations were performed between the histological scores and bone mineral density as described in Chapter 3. As most of these data were non-parametrically distributed, Spearman's rank order correlation was employed for this purpose. Increasing osteoarthritis score was not associated with any detectable alteration in bone mineral density, including subregional analyses (Table 5.6).

n = 23		Bone mineral density (g/cm^2)			
		Whole tibia	Proximal tibia (R1)	Medial plateau	Lateral plateau
OARSI	r_s	-0.054	-0.105	-0.131	-0.205
	p	0.816	.0650	0.572	0.372
Mankin's	r_s	-0.104	-0.070	-0.056	-0.106
	p	0.654	0.765	0.809	0.646

Table 5.6 Histological OA vs. Bone mineral density

5.4.3 Osteoarthritis and subchondral trabecular bone

(i) Basic morphometry

Correlations were then performed between the histological scores and trabecular microstructural parameters (as described in Chapter 3). There was an inverse relationship observed between connectivity density and the OARSI score, but this did not reach significance (r_s = -0.364, p = 0.086; Table 5.7; Graph 5.5).

n = 23		Trabecular						
		BV/TV	Tb.N	TbTh	Conn Dens	TbSp	SMI	HA
OARSI	r_s	-0.0942	-0.115	-0.114	-0.364	0.0942	-0.265	0.100
	p	0.666	0.595	0.598	0.0868	0.666	0.219	0.646
Mankin's	r_s	0.0557	-0.150	-0.048	-0.211	-0.002	-0.466	-0.019
	p	0.799	0.489	0.823	0.328	0.991	0.0252	0.926

Table 5.7 Histological OA vs. trabecular microstructure

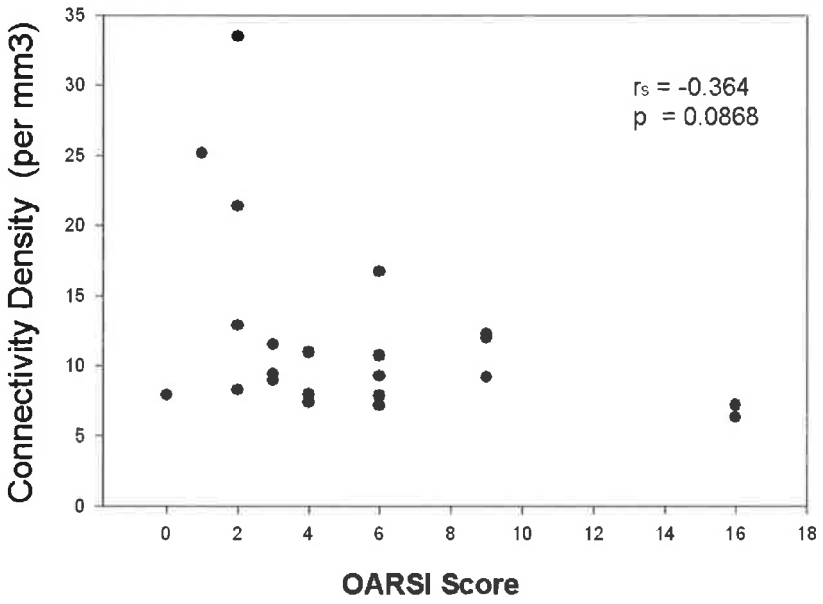

Graph 5.5 Osteoarthritis vs. Connectivity Density

(ii) Fluorochrome-labelled bone

While there was a trend towards reduced trabecular hemi-osteonal (or surface) turnover in sheep with increasing osteoarthritis, the number of intra-trabecular osteons (as measured in Chapter 4) showed a mild elevation. These trends were far from statistically significant, however (Table 5.8).

n = 21 CON = 11 OVX = 10		**Number of Sites of labelled bone (#/mm^2)**	**Length of sites of labelled bone (mm/mm^2)**	**Number of sites of intra-trabecular labelled lamellar bone (#/mm^2)**
OARSI	r_s	-0.073	-0.149	0.249
	p	0.754	0.518	0.277
Mankin's	r_s	-0.170	-0.114	0.160
	p	0.460	0.662	0.489

Table 5.8 Histological OA vs. Trabecular bone turnover

5.4.4 Osteoarthritis and the subchondral bone plate

(i) Basic morphometry

Next, correlations were performed between histological osteoarthritis and subchondral plate thickness and hydroxyapatite concentrations (again as described in Chapter 3.4). When looking at the sheep overall, there was a significant inverse relationship observed between osteoarthritis and subchondral plate thickness (r_s = -0.443, p = 0.034; Table 5.8, Graph 5.6).

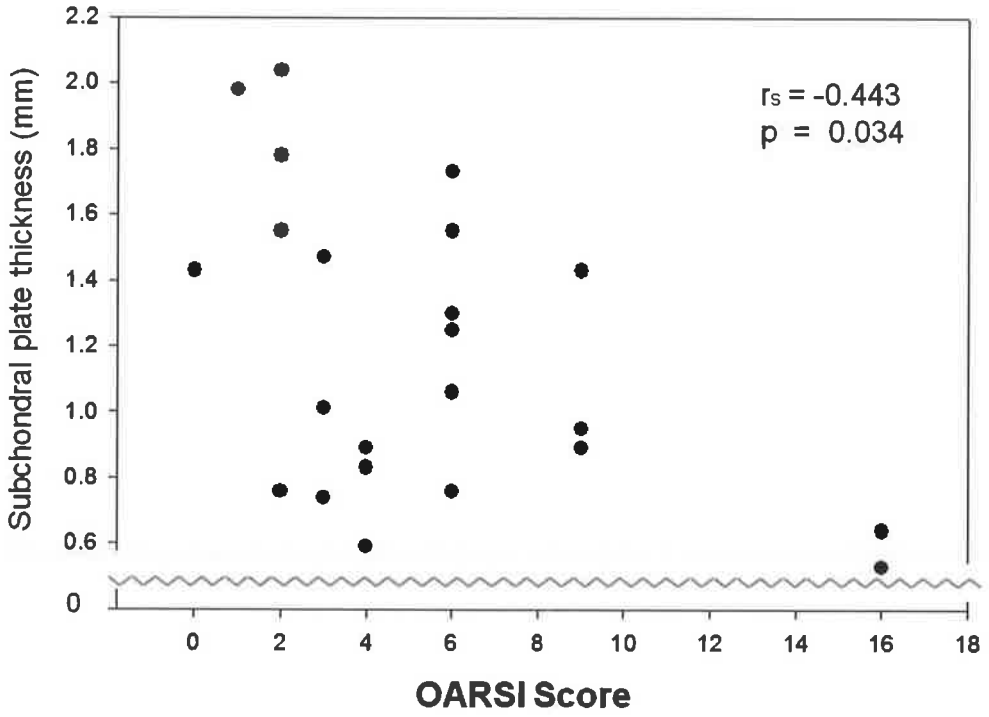

Graph 5.6 Histological OA vs. Subchondral plate thickness (MicroCT)

As stated in Chapter 4, one advantage of the microscopic measurement over MicroCT is the ability to differentiate between the bone and the calcified cartilage within the subchondral plate. On microscopic assessment, the thinning was observed to be primarily within the bone of the subchondral plate, not the calcified cartilage layer (r_s = -0.424, p = 0.044; Table 5.9, Graph 5.7).

n = 23 CON – n = 13 OVX – n = 10		Subchondral Plate				
		Thickness				HA
		Overall (MicroCT)	**Overall (Hist)**	**Bone (Hist)**	**Cartilage (Hist)**	**Overall (MicroCT)**
OARSI	r_s	-0.443	-0.384	- 0.424	- 0.082	-0.252
	p	0.0342	0.071	0.044	0.709	0.242
Mankin's	r_s	-0.263	-0.308	- 0.284	- 0.255	-0.235
	p	0.222	0.153	0.19	0.24	0.276

Table 5.9 Histological OA vs. SCP microstructure

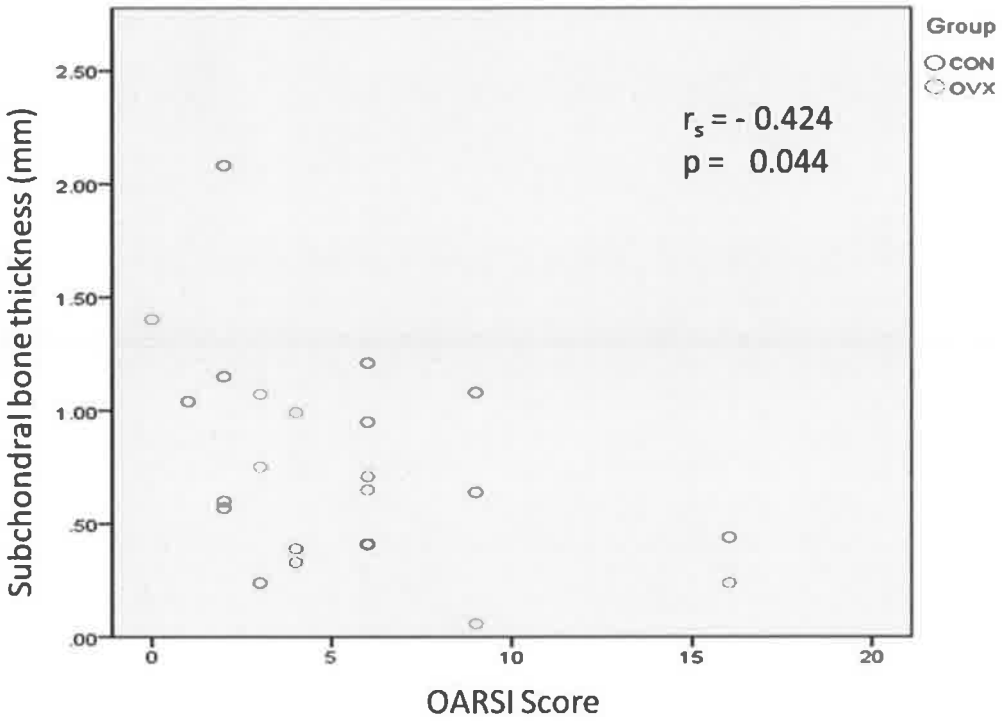

Graph 5.7 Histological OA vs. Subchondral bone thickness (microscopy)

(ii) Fluorochrome-labelled bone

Correlations were then performed between osteoarthritis and the number of labelled osteons visible in the subchondral plate (as described in Chapter 4); none of these analyses were statistically significant (Table 5.10).

n = 23 CON – n = 13 OVX – n = 10		**Subchondral Plate**		
		Labelled osteons (total)	**Labelled osteons /mm**	**Labelled osteons /mm^2**
OARSI	r_s	- 0.066	- 0.05	0.208
	p	0.766	0.819	0.341
Mankin's	r_s	0.003	0.048	0.256
	p	0.989	0.827	0.238

Table 5.10 Histological OA vs. SCP turnover

(ii) Cartilage calcification

There was a slight trend towards increased labelling at the tidemark of cartilage calcification with increasing osteoarthritis, but this was far from significant (Table 5.11).

n = 23 CON – n = 13 OVX – n = 10		**Subchondral Plate**
		Labelled cartilage /cm
OARSI	r_s	0.188
	p	0.391
Mankin's	r_s	0.116
	p	0.597

Table 5.11 Histological OA vs. Labelled calcified cartilage

5.4.4 Summary of results

Most specimens showed some evidence of osteoarthritis. There was no difference in the level of osteoarthritis observed between the OVX and Control groups using either histological scoring method. There were no significant correlations between osteoarthritis and alterations in bone mineral density, subchondral trabecular histomorphometry, or bone turnover. However, osteoarthritis was associated with a thinning of the subchondral plate, specifically the subchondral cortical bone (Table 5.12).

	r_s	p
Bone mineral density		
Whole bone & sub-regional analyses	-	NS
Trabecular		
Morphometry	-	NS
Bone turnover	-	NS
Subchondral plate		
Morphometry		
Subchondral Plate thickness (MicroCT)	- 0.443	**0.034***
Subchondral Plate thickness (histology)	-0.384	0.071
Subchondral Bone thickness (histology)	- 0.424	**0.044***
Calcified Cartilage thickness (histology)	- 0.082	0.709
Bone turnover	-	NS
Endochondral ossification		
Length of labelled cartilage at tidemark (mm/mm)	-	NS
**statistically significant p-values shown in red*		

Table 5.12 Summary of results

5.5 DISCUSSION

Traditionally, osteoarthritis has been described as "wear and tear" arthritis, due primarily to mechanical factors (Kawcak *et al*, 2001). The hypothesis is that loss of articular cartilage occurs, changing the mechanical stresses acting on the joint, thus causing an alteration in the underlying subchondral bone as it remodels to compensate. There is now considerable debate, however, as to whether the changes in the underlying subchondral bone may actually precede the damage seen within the articular cartilage (Burr, 2004; Kawcak *et al*, 2001; Lajeunesse, 2004; Li & Aspden, 1997; Radin *et al*, 1986). Most studies examining osteoarthritis have been performed in mid or late-stage disease; the natural history of the degenerative process in its early stages is still not well understood. Certainly once osteoarthritis is established, whatever the initiating cause, there is absolute consensus that subchondral alterations do occur, which will then have a considerable effect on the stresses within the overlying cartilage (Bobinac *et al*, 2003; Burr 2004). Ovariectomy is being investigated in the literature as a possible model for osteoarthritis; some studies have shown ovariectomy to alter the structural, material and biomechanical properties of articular cartilage (Cake *et al*, 2005; Parker *et al*, 2003; Turner *et al* 1997). Others, upon reviewing all available literature, have concluded that the results are inconclusive (Sniekers *et al*, 2008b). Within my study of 23 ewes, I was unable to detect any measurable difference in osteoarthritis between the two study groups, using either of the two most prevalent histological scoring methods.

Reviews of the literature also seem conflicting when examining the relationship between osteoarthritis, regardless of the method used to induce disease, and osteoporosis. Traditionally, the two diseases have often been seen as mutually exclusive (Dequeker, 1997; Stewart & Black, 2000; Zhang *et al*, 2010). While some studies show that increased subchondral bone mineral density is associated with reduced joint space narrowing and osteoarthritis progression (Bruyere *et al*, 2003), other research suggests that periarticular osteoporosis commonly occurs with osteoarthritis (Karvonen *et al*, 1998; Patel *et al*, 2003).

I found no correlation between osteoarthritis and bone mineral density or alterations in subchondral trabecular histomorphometry in my study. The intra-articular collagenase injection osteoarthritis model in high-bone mass (C3H/HeJ) mice has shown thinning of subchondral trabeculae and increased trabecular spacing after 4 weeks (Botter *et al*, 2008); a canine anterior cruciate ligament transection model (ACLT) had similar findings, with trabeculae being significantly thinner in the operated, osteoarthritic knee (as compared to contralateral) for up to 54 months post ACLT (Dedrick *et al*, 1993). The literature shows that bone morphometry then alters in the mid to late stages of osteoarthritis. One guinea pig model recorded initial thinning of the trabeculae, which was then followed by subsequent trabecular thickening; it should be noted, however, that these animals were not skeletally mature (Layton *et al*, 1998). Bobinac *et al* also found increased bone volume fraction in subchondral trabecular bone of tibial plateaux removed for total knee replacement surgery; individual trabeculae were thickened and more widely spaced (Bobinac *et al*, 2003). Similar findings have been reported with femoral head specimens following total hip replacement (Chappard *et al*, 2006; Zhang *et al*, 2010).

Again, there are few studies examining the subchondral plate in early osteoarthritis (Botter *et al*, 2011; Kuroki *et al*, 2011). My data did show that osteoarthritis was associated with a thinning of the subchondral bone plate. In the intra-articular collagenase injection model in both high-bone mass (C3H/HeJ) and low-bone (C57Bl/6) mass mice, the subchondral bone plate of the collagenase injected joints in both strains of mice became thinner at 4 weeks, independent of the site of cartilage damage (Botter *et al*, 2008). One longitudinal canine study used an anterior cruciate transection model, and found that while the medial tibial subchondral plate was actually marginally thinner in the OA knee at 3 months, it then became thicker than the control group at 18 and 54 months (Dedrick *et al*, 1993). This agrees with the majority of clinical studies, which show that symptomatic osteoarthritis typically has a thickened or sclerotic subchondral plate (Buckland-Wright, 2004; Grynpas *et al*, 1991; Li *et al*, 1999).

With regard to bone turnover, this is thought to be increased in symptomatic osteoarthritis, as measured by scintigraphy, but few studies have performed direct evaluation of the remodelling rate by histological examination (Sharif *et al*, 1995; Benske *et al*, 1998; Hayami *et al*, 2004). Measurement of bone resorption markers suggests that these are elevated early in the disease process (Kwan Tat *et al*, 2010). In a murine model, Benske found "*an increased, regionally limited proliferation of the subchondral bone in arthrosis; and the proliferation of the subchondral bone depended on the extent of cartilage degeneration*" (Benske *et al*, 1988). I found no correlation between bone turnover rates of either the subchondral trabecular bone or bone plate with osteoarthritis.

While endochondral ossification at the interface between bone and cartilage is usually present at a physiological rate, this process is described as being accelerated in osteoarthritis, with tidemark advancement (Burr, 2004; Oegema *et al*, 1997). In my study, I did find a trend towards increased fluorochrome labelling at the tidemark of cartilage calcification with increasing osteoarthritis, but this was not significant. One caveat with this result is that articular cartilage is nourished via synovial fluid; intravenous fluorochromes may not penetrate well to the calcification front within the cartilage. Previous studies investigating tidemark advancement have used intra-articular fluorochrome injections for labelling, rather than intravenous administration (Oegema *et al*, 1997).

It is possible, however, that the osteoarthritis grade may have been underestimated in this model. In order to perform standardised analysis of the subchondral bone morphometry and turnover, Specimen A was taken from the same point of maximal femoro-tibial contact and pressure in all sheep (Figure 1.40 & 3.5). Specimen B was taken just posterior to this; however, this may not always have been the site of maximal osteoarthritis, as would be the usual procedure when taking a specimen for grading, and so the grade of osteoarthritis may be underestimated in some sheep. For this reason, I feel that the OARSI score is probably more reliable than the Mankin's, given that the former system also stages the macroscopic area of affected cartilage, rather than relying on a disease grade from one isolated piece of cartilage; this is a view supported by other studies (Custer *et al*, 2007).

As noted previously, osteoarthritis and osteoporosis have traditionally been viewed as being mutually exclusive (Dequeker, 1997; Stewart & Black, 2000). However, diseases do not always occur in isolation. Osteoarthritis is predominantly prevalent in the same epidemiological group as osteoporosis, i.e. postmenopausal women; what effect will there be if osteoarthritis does occur with pre-existing osteoporosis? Calvo *et al* investigated this question in a rabbit model. Six rabbits had osteopenia induced by ovariectomy, followed by medial meniscectomy and anterior cruciate transection (ACLT) to induce osteoarthritis; six control rabbits had medial meniscectomy and ACLT alone (Calvo *et al*, 2007). Calvo concluded that "*OP increases the severity of cartilage damage in experimental OA*".

Bellido *et al* performed a similar study, again in rabbits; one group (OPOA) had osteopenia induced by ovariectomy, followed 7 weeks later by medial meniscectomy and anterior cruciate transaction (ACLT) to induce osteoarthritis; control animals (OA) had medial meniscectomy and ACLT alone (Bellido *et al* 2010). He also found that "*the severity of cartilage damage was increased in OPOA knees vs. controls ($P < 0.05$)*" (Bellido *et al*, 2010). Furthermore, he concluded that "*microstructure impairment at subchondral bone associated with an increased remodelling aggravated cartilage damage in OA rabbits with previous OP. Our results suggest that an increased subchondral bone resorption may account for the exacerbation of cartilage damage when early OA and OP coexist simultaneously in same individuals.*" It is possible that this explains why reviews of the literature have been inconclusive. While ovariectomy may not increase the risk of osteoarthritis per se, it will cause osteopenia; if osteoarthritis then occurs, the synergy between these two disease processes will mean that the osteoarthritis in the ovariectomised group will be more severe. The role of bisphosphonates is also being queried in osteoarthritis, with at least one animal study suggesting a chondroprotective effect (Hayami *et al*, 2004). Again, perhaps this is due to the fact that treatment of an underlying osteopenia will then result in a less florid form of any accompanying or subsequent osteoarthritis.

In conclusion, I found no evidence that osteoarthritis is increased in ewes at one year post-ovariectomy. While previous studies have suggested a link between trabecular thinning and osteoarthritis, I was unable to confirm this; osteoarthritis was associated with a thinning of the subchondral bone plate. However, while ovariectomy may not increase the risk of osteoarthritis *per se*, it will cause osteopenia; if osteoarthritis then occurs, the synergy between these two disease processes may mean that the osteoarthritis in the ovariectomised group will be more severe.

5.6 CONCLUSIONS

1. The correlation between the OARSI and Mankin's histopathologic scoring systems was highly significant, and the two were also in close agreement.
    - I believe that OARSI is more reliable, given the limitations of this study, as discussed (p172).

2. There was no difference in the osteoarthritis of the medial tibial plateau in ovariectomised ewes as compared to control animals. It is not a reliable model for osteoarthritis; mechanical models are to be recommended instead.

3. There was no evidence of any significant correlations between increasing osteoarthritis and bone mineral density or subchondral trabecular histomorphometry.

4. There was a significant correlation observed between increasing osteoarthritis and reduced subchondral plate thickness.
    - This thinning was observed to be most significant within the cortical bone of the subchondral plate.

5. While ovariectomy may not increase the risk of osteoarthritis *per se*, it will cause osteopenia; if osteoarthritis then occurs, the synergy between these two disease processes may cause the osteoarthritis in the ovariectomised group to be more severe.

CHAPTER 6: DISCUSSION

6.1 INTRODUCTION

Sheep are a practical model for postmenopausal conditions and have been used for investigation of a number of conditions to date, including the bone diseases osteoporosis and osteoarthritis (Newton, 2004; Parker *et al*, 2003; Thorndike *et al*, 1998). The metabolic rate of sheep is close to that of humans (Schmidt-Nielsen, 1977), as is the ovine bone remodelling cycle, being of approximately 3 months duration (Lee *et al*., 2002). While sheep do not undergo a natural menopause, one may be induced by ovariectomy, which significantly reduces circulating levels of progesterone and oestradiol (Kennedy *et al*, 2009b; Newton *et al*, 2004). With regard to many of the structural parameters, the ovine stifle joint may be considered to be a 1:3 scale model of the knee joint; soft tissue structures, such as menisci, cruciate ligaments and asymmetrical collateral ligaments are also comparable between human knee and ovine stifle joints (Osterhoff *et al*, 2010).

I used 24 sheep in this study; following identification of Sheep 23 as a marked outlier (Section 3.4.1), 23 sheep were used for analysis. 10 of these sheep underwent ovariectomy (OVX), while the remainder (n=13) were kept as controls (CON). Five fluorochrome dyes were administered intravenously at 12 week intervals via the jugular vein to both groups, to label sites of bone turnover. These animals were then sacrificed at 12 months post-operatively. The intravenous administration of dye for labelling of newly-mineralised bone proved to be very successful. Ovarian functional analyses showed that the ovariectomised sheep had significantly lower progesterone and oestradiol levels at one year post-operatively than the control sheep (Graph 2.1).

I will now consider the findings of the preceding experimental chapters in the context of the three osteopathies; osteoporosis, osteoarthritis and osteonecrosis.

6.2 OSTEOPOROSIS

The alterations typically observed in the ovine skeleton post-ovariectomy include a reduction in bone volume fraction (BV/TV), a reduction in the number of trabeculae, a reduction in the thickness of the individual trabeculae and an increased distance between them (Jiang *et al*, 2005; Turner *et al*, 1995). Age-related alterations in the structure and material properties of the subchondral trabecular bone in the human proximal tibia have been investigated within a small number of studies, although for analysis purposes subjects were purely divided into groups based upon age, which included both genders (Ding *et al.*, 1997, Ding *et al.*, 2002). Bone volume fraction (apparent density) and trabecular thickness were found to decrease significantly after the age of 60, with the trabeculae shifting from a plate-like to a rod-like microstructure (Ding *et al.*, 2002).

This study shows significant alterations within the subchondral trabecular architecture at one-year post-ovariectomy, with reduced bone volume fraction, thinning of individual trabeculae and an increase in trabecular separation; these findings are consistent with those elsewhere in the ovine skeleton (Cornish *et al.*, 2006; Jiang *et al*, 2005; Mitton *et al.*, 1998; Mittra *et al.*, 2005; Nafei *et al.*, 2000; Newton *et al.*, 2004; Schorlemmer *et al.*, 2003).

While there was no difference in bone mineral density of the tibia as a whole between the two groups, subregional analysis revealed that bone mineral density (BMD) is reduced in the medial tibial plateau of the ovariectomised sheep. This was reflected in the alterations seen using MicroCT; bone volume fraction of the subchondral trabecular bone was reduced in the ovariectomised sheep as compared to control animals, with trabecular thinning and reduced connectivity density. Analyses confirmed that the observed alteration in BMD was significantly correlated with changes in the subchondral trabecular structure and subchondral plate thickness (Graph 3.15). The subchondral bone plate was observed to be slightly thinner in the ovariectomised sheep, but not significantly so.

Despite the marked morphological and structural density differences observed, the material density of the trabecular bone (i.e. hydroxyapatite concentration) was equal at one year in both the control and the ovariectomised animals. Therefore, despite the increased turnover and morphological changes occurring, the mineralisation was unaltered, suggesting that while osteoclastic activity was ongoing to reduce the bone volume fraction, very little new undermineralised tissue was being deposited in compensation.

- Is bone mineral density reduced in the proximal tibia in ovariectomised ewes as compared to control animals?
    - Yes, using subregional analysis of the proximal tibia and medial plateau

- Does the subchondral trabecular bone reflect the reduction in trabecular number, width and connectivity seen elsewhere in the post-ovariectomy ovine skeleton?
    - Yes - bone volume fraction was reduced, and trabecular thinning and reduced connectivity density were also evident

- Is the subchondral bone plate altered post-ovariectomy, either in thickness or material density?
    - The subchondral bone plate is thinner post ovariectomy, but the mineral density is unaffected.

6.3 OSTEONECROSIS (SPONK)

The labelled bone observed in this thesis is not solely due to BMU activation; modelling is also continually occurring along the trabecular surfaces in the healthy skeleton. Bone turnover along the trabecular surfaces was elevated following ovariectomy; the number of sites of labelled bone present per unit area of bone was significantly higher in OVX sheep as compared to controls (Graph 4.4). In addition, I found evidence of intra-trabecular remodelling - cylindrical lamellae of bone, seen in a variety of planes, arranged around a central vessel - characteristic of the secondary osteons formed by osteonal remodelling (Figures 4.14 & 4.16). The number of sites present per unit area (mm^2) was doubled in the OVX Group as compared to controls, but failed to reach statistical significance.

Although the OVX groups showed no evidence of any positive or inverse relationships between fluorochrome-labelling and bone microstructure, the control group showed strong correlations between increased length of labelled bone along trabecular surfaces and microstructural parameters such as bone volume fraction (BV/TV), connectivity density and trabecular number; an inverse correlation with trabecular separation was also evident.

In the early post-ovariectomy period, bone modelling is suppressed (Flieger 1998; Frost 1992) and, as previously stated, oestrogen withdrawal has been shown to result in substantial increases in basic multicellular unit (BMU) activation, which is responsible for bone remodelling (Kennedy *et al*, 2009b; Newman *et al*, 1995). While bone formation may increase overall, this rate is inadequate to replace the bone lost by resorption, leading to an elevation in the number and length of labelled sites present, but an overall loss of bone is evident upon examination of the bone microstructure (Riggs & Melton, 1992; Parfitt, 2004). Interestingly, the labelled intra-trabecular osteons, which are presumably present solely due to remodelling, do not show the same pattern as is seen along the surfaces. Here, while the number of labelled osteons is increased within the OVX group as compared to controls, there is no evidence of any correlation with increasing bone volume fraction or connectivity density within either the control or OVX groups; these osteons are merely replacing old bone, not depositing new.

Bone turnover has been investigated in the past with regard to its influence on fracture risk (Riggs & Melton, 2002). It has been demonstrated that accelerated bone resorption is associated with an increased incidence of osteoporotic fractures, independent of BMD (Hernandez, 2008; Meier *et al*, 2005). The presence of osteopenia and elevated subchondral bone turnover within the medial tibial plateau provides a possible mechanism for subchondral microfractures in the aetiology of SPONK. Further utilisation of the ovariectomised ewe should be useful for further study in this field. Interestingly, a recent study suggests that early treatment with Vitamin D and bisphosphonates, a standard treatment regimen for osteoporosis which reduces bone turnover, is beneficial in SPONK, with remission of symptoms and pathological findings on Magnetic Resonance Imaging (Breer *et al*. 2012).

- Is bone turnover within the subchondral trabecular and cortical bone altered post-ovariectomy?
    - Yes - bone turnover is significantly higher in both trabecular and subchondral bone at one-year post-ovariectomy

- Are there any significant correlations between alterations in bone turnover and microstructural changes in this region?
    - There were initially no positive findings, when examining the data as a whole
    - Within the control sheep, increase in bone turnover along the trabecular surfaces was significantly correlated with increased bone volume fraction, connectivity density and trabecular number. There was also a significant inverse correlation present with trabecular separation (Table 4.4; Graph 4.7).
    - Within the OVX group, these correlations were non-existent

6.4 OSTEOARTHRITIS

While previous studies have suggested a link between trabecular thinning and osteoarthritis, I was unable to confirm this; osteoarthritis was associated with a thinning of the subchondral plate, specifically the subchondral cortical bone. This agrees with Dedrick, who found that while the medial tibial subchondral plate is thinner in mechanically-induced OA at 3 months, it then becomes thickened as compared to controls at 18 and 54 months (Dedrick *et al*, 1993). This is consistent with the majority of clinical studies, which show that symptomatic osteoarthritis typically has a thickened or sclerotic subchondral plate (Buckland-Wright, 2004; Grynpas *et al*, 1991; Li *et al*, 1999). The physiology and biomechanics of the subchondral bone is greatly altered depending on whether the disease is in its early or late stage.

With regard to bone turnover, this is thought to be increased in symptomatic osteoarthritis, as measured by scintigraphy, but few studies have performed direct evaluation of the remodelling rate by histological examination (Sharif *et al*, 1995; Benske *et al*, 1998; Hayami *et al*, 2004). Measurement of bone resorption markers show that these are elevated early in the disease process (Kwan Tat *et al*, 2010). In a murine model, Benske found "an increased, regionally limited proliferation of the subchondral bone in arthrosis; and the proliferation of the subchondral bone depended on the extent of cartilage degeneration" (Benske *et al*, 1988). I found no correlation between bone turnover rates of either the subchondral trabecular bone or bone plate with osteoarthritis. I did find a slight trend towards increased fluorochrome labelling at the tidemark of cartilage calcification with increasing osteoarthritis in this study, but this was not significant.

The majority of ovine studies in the past have typically induced osteoarthritis by means of an experimental injury; monoarticular studies may do this by means of causing an injury to an articular structure in order to destabilise the joint, or by placing the joint under abnormal mechanical loading (Little *et al*, 2008; Pritzker, 1994). A variety of different methods have been used in various animal species, as shown in Table 5.1. Kuroki suggests that subchondral changes are quite different at 12 weeks depending on the exact type of insult used to induce OA (Kuroki *et al*, 2011). However, meniscectomy has proven to be most reliable in the ovine model (Hwa *et al*, 2001; Little *et al*, 1997; Parker *et al*, 2003).

Ovariectomy is being employed in current literature as a model for osteoarthritis; however, the local effects of osteoarthritis induced by ovariectomy and those induced by alteration of the mechanical loading of the joint (i.e. by meniscectomy) may be quite different (Pajamäki *et al*, 2008). Some studies have shown ovariectomy to alter the structural, material and biomechanical properties of articular cartilage (Cake *et al*, 2005; Parker *et al*, 2003; Turner *et al* 1997). Others, upon reviewing all available literature, have concluded that the results are inconclusive (Sniekers *et al*, 2008b). Within my study of 23 ewes, I was unable to detect any measurable difference in osteoarthritis between the two study groups, using either of the two most prevalent histological scoring methods. It is not a reliable model for osteoarthritis; mechanical models are to be recommended instead. While ovariectomy may not increase the risk of osteoarthritis *per se*, it will cause osteopenia; if osteoarthritis then occurs, the synergy between these two disease processes will mean that the osteoarthritis in the ovariectomised group will be more severe (Bellido *et al*, 2010; Calvo *et al*, 2007).

- Is osteoarthritis increased at the medial tibial plateau in ovariectomised ewes as compared to control animals?
    - No

- Is osteoarthritis associated with osteopenia of the subchondral trabecular bone, or is there an inverse relationship present?
    - Previous studies have suggested a link between trabecular thinning and osteoarthritis, but I was unable to confirm this

- Is osteoarthritis associated with a thickening or thinning of the subchondral bone plate?
    - Osteoarthritis was associated with a thinning of the subchondral plate, specifically the subchondral cortical bone

- Do alterations in bone turnover have any significant effect on the degree of osteoarthritis visible in the overlying articular cartilage?
    - I found no correlation between bone turnover rates of either the subchondral trabecular bone or bone plate with osteoarthritis

- Is the rate of endochondral ossification increased in osteoarthritis?
    - I did find a slight trend towards increased fluorochrome labelling at the tidemark with increasing osteoarthritis, but this was not significant

6.5 FUTURE WORK

The presence of osteopenia and elevated subchondral bone turnover within the medial tibial plateau provides a possible mechanism for subchondral microfractures in the aetiology of SPONK. Further utilisation of the ovariectomised ewe should be useful for further study in this field; if so, an animal trial examining the use of bisphosphonates in the early management of SPONK could allow for histological investigation of treated joints as compared to controls.

This study has failed to detect any measurable difference in osteoarthritis between the two study groups, despite the use of the ovariectomised ewe as a model for osteoarthritis in the literature. Currently, I believe that it is not a reliable model for osteoarthritis and that mechanical models are to be recommended instead. However, a further study extending the time-period post-operatively to over 2 years may allow a more definitive statement to be made.

Examination of specimens at this time-period may also allow confirmation that the subchondral plate reverses the thinning seen at one year post-ovariectomy with increasing osteoarthritis, and instead becomes thickened in more advanced disease, as is described in the literature Buckland-Wright, 2004; Dedrick *et al*, 1993; Grynpas *et al*, 1991; Li *et al*, 1999).

6.6 CONCLUSIONS

1. The ovariectomised ewe is a useful model for osteoporosis, and should also prove useful for spontaneous osteonecrosis of the knee. It is not a reliable model for osteoarthritis; mechanical models are to be recommended instead.

2. DEXA subregional analyses of the proximal tibia and medial tibial condyle show a significant reduction in BMD within the OVX group as compared to controls.

3. Trabecular thickness, bone volume fraction and connectivity density are all significantly reduced in the OVX group as compared to controls.

4. The subchondral plate is significantly thinner in the OVX group as compared to controls.

5. I found evidence of intra-trabecular remodelling - cylindrical lamellae of bone, seen in a variety of planes, arranged around a central vessel - characteristic of secondary osteons formed by osteonal remodelling.

6. Bone remodelling was significantly increased in the OVX sheep as compared to controls, in both trabeculae and the subchondral plate.

7. Bone modelling is suppressed within the OVX group as compared to controls.

8. There was no difference in the osteoarthritis score observed between the ovariectomy and control groups.

9. There was no evidence of any significant correlations between increasing osteoarthritis and bone mineral density or subchondral trabecular histomorphometry.

10. There was a significant correlation observed between increasing osteoarthritis and reduced subchondral plate thickness. This thinning was found to be most significant within the cortical bone of the subchondral plate.

BIBLIOGRAPHY

Akamatsu Y, Mitsugi N, Hayashi T, Kobayashi H, Saito T. Low bone mineral density is associated with the onset of spontaneous osteonecrosis of the knee. Acta Orthop 2012; Epub 2012/04/28: ISSN 1745-3682

Allen DA. Structure and Physiology of Joints and Their Relationship to Repetitive Strain Injuries. Clin Orth Rel Res 1998; 351: 32 - 38

Ai-Rowaih A, Wingstrand H, Lindstrand A, Björkengren A, Thomgren KG, Gustafson T. Three-phase scintimetry in osteonecrosis of the knee. Acta Orthopaedica 1990; 61: 120-127.

Anderson-MacKenzie JM, Quasnichka HL, Starr RL, Lewis EJ, Billingham ME, Bailey AJ. Fundamental subchondral bone changes in spontaneous knee osteoarthritis. Int J Biochem Cell Biol 2005 Jan; 37(1): 224-36

Arens D, Sigrist I, Alini M, Schawalder P, Schneider E, Egermann M. Seasonal changes in bone metabolism in sheep. The Veterinary Journal 2007; 174 (3): 585-591.

Armstrong SJ, Read RA, Price R. Topographical variation within the articular cartilage and subchondral bone of the normal ovine knee joint: a histological approach. Osteoarth Cart 1995; 5: 25 - 38

Aspden RM, osteoarthritis: a problem of growth not decay? Rheumatology 2008; 47: 1452 – 1460.

Athanasou NA, Cellular Biology of Bone-Resorbing Cells. J Bone Joint Surg 1996; 78-A: p1096 – 1112.

Aubin JE. Bone stem cells. J Cell Biochem (Suppl) 1998; S 30/31: 73 - 82

Belchier J. An Account of the Bones of Animals Being Changed to a Red Colour by Aliment Only. By John Belchier, Surgeon, F. R. S. Philosophical Transactions (1683-1775); Vol. 39, 1735 - 1736 (1735 - 1736): p 287-288

Belchier J. A Further Account of the Bones of Animals Being Made Red by Aliment Only. By John Belchier, F. R. S. Philosophical Transactions (1683-1775); Vol. 39, 1735 - 1736 (1735 – 1736): p 299-300

Bellido M, Lugo L, Roman-Blas JA, Castañeda1 S, Caeiro JR, Dapia S, Calvo E, Largo R, Herrero-Beaumont G. Subchondral bone microstructural damage by increased remodelling aggravates experimental osteoarthritis preceded by osteoporosis. Arthritis Research and Therapy 2010; 12 : R152. http://arthritis-research.com/content/12/4/R152

Benske J, Schunke M, Tillmann B. Subchondral bone formation in arthrosis. Polychrome labeling studies in mice. Acta Orthop Scand 1988 Oct; 59(5): 536-541

Berger CE, Kröner A, Kristen KH, Minai-Pour M, Leitha T, Engel A. Spontaneous osteonecrosis of the knee: biochemical markers of bone turnover and pathohistology. Osteoarthritis Cartilage. 2005; 13(8): 716-721.

Bilezikian JP, Raisz LG, Rodan GA *et al*, eds. 2004 (2nd edn). Principles of Bone Biology; Volume 1. Academic Press, Harcourt Inc., San Diego.

Blain H, Chavassieux P, Portero-Muzy N. Bonnel F, Canovas F, Chammas M, Maury P, Delmas PD. Cortical and trabecular bone distribution in the femoral neck in osteoporosis and osteoarthritis. Bone 2008; 43: 862–868

Bland JM, Altman DG. Statistical methods for assessing agreement between two methods of clinical measurement. Lancet 1986; i, 307-310.

Bobinac D, Spanjol J, Zoricic S, Maric I. Changes in articular cartilage and subchondral bone histomorphometry in osteoarthritic knee joints in humans. Bone 2003; 32: 284-290.

Bock HC, Michaeli P, Bode C, Schultz W, Kresse H, Herken R, Miosge N. The small proteoglycans decorin and biglycan in human articular cartilage of late-stage osteoarthritis. Osteoarth Cart 2001; 9 (7): 654 – 663

Bolotin HH. DXA in vivo BMD methodology: An erroneous and misleading research and clinical gauge of bone mineral status, bone fragility, and bone remodelling. Bone 2007; 41: 138-154.

Botter SM, van Osch GJVM, Waarsing JH, van der Linden JC, Verhaar JAN, Pols H AP, van Leeuwen JPTM , Weinans H. Cartilage damage pattern in relation to subchondral plate thickness in a collagenase-induced model of osteoarthritis. Osteoarthritis and Cartilage 2008; 16: 506-514

Botter SM, van Osch GJVM, Clockaerts S, Waarsing JH, Weinans H, van Leeuwen JPTM. Osteoarthritis induction leads to early and temporal subchondral plate porosity in the tibial plateau of mice: An in vivo microfocal computed tomography study. Arth & Rheum 2011; 63: 2690-2699

Bowman SM, Guo XE, Cheng DW, Gibson LJ, Hayes WC, McMahon TA. Creep damage contributes to the fatigue behaviour of bovine trabecular bone. Journal of Biomechanics 1998; 120 (5): 647-654

Boyde A. The real response of bone to exercise. J Anat 2003: 203; 173-189.

Breer S, Oheim R, Krause M, Marshall R, Amling M, Barvencik F. Spontaneous osteonecrosis of the knee (SONK). Knee Surgery, Sports Traumatology, Arthroscopy; Epub 26/4/2012: DOI: 10.1007/s00167-012-2017-3

Brennan, O. Bone quality and its relationship with bone fragility and osteoporosis. Department of Anatomy. Dublin, Royal College of Surgeons in Ireland. (2008)

Buckwalter JA. Bone Structure and Function. In: Griffin PP, editor. Instructional Course Lectures. Chicago, Illinois: American Academy of Orthopaedic Surgeons; 1987. p. 27-48

Buckwalter JA, Brown T. Joint Injury, Repair, and Remodeling - Roles in Post-Traumatic Osteoarthritis. Clin Orthop Relat Res 2004; 423: 7 – 16

Buckwalter JA, Saltzman C, Brown T. The impact of osteoarthritis: implications for research. Clin Orthop Relat Res 2004 (427 Suppl): S6-15.

Buckland-Wright C. Subchondral bone changes in hand and knee osteoarthritis detected by radiography. Osteoarthritis Cartilage 2004; 12 Suppl A: S10-19

Buie HR, Campbell GM, Klinck J, MacNeil JA, Boyd SK. Automatic segmentation of cortical and trabecular compartments based on a dual threshold technique for in vivo micro-CT bone analysis. Bone 2007; 41: 505–515

Bullough PG, Jagannath A. The morphology of the calcification front in articular cartilage. J Bone Joint Surg 1983; 65-B (1): 72 - 78

Bullough PG. 1997. Orthopaedic Pathology, 3rd edition. London: Mosby-Wolfe.

Bullough PG. The role of joint architecture in the etiology of arthritis. Osteoarth Cart 2004; 12: S2 – S9

Burr DB. Targeted and non-targeted remodeling. Bone 2002; 30 (1): 2 – 4

Burr BD, Robling AG, Turner CH. Effects of Biomechanical Stress on Bones in Animals. Bone 2002; 30 (5): 781 – 786

Burr BD. Anatomy and physiology of the mineralized tissues: Role in the pathogenesis of osteoarthrosis. OsteoArthritis and Cartilage 2004; 12: S20–S30

Calvo E, Castañeda S. Osteoporosis increases the severity of cartilage damage in an experimental model of osteoarthritis in rabbits. OsteoArthritis and Cartilage 2007; 15: 69-77

Carter DR, Beaupré GS. 2001. Skeletal function and form. Cambridge University Press.

Chappard C, Peyrin F, Bonnassie A, Lemineur G, Brunet-Imbault B, Lespessailles E, Benhamou CL. Subchondral bone micro-architectural alterations in osteoarthritis: a synchrotron micro-computed tomography study. OsteoArthritis and Cartilage 2006; 14: 215 - 223

Cornish RJ, Wilson DF, Logan RM, Wiebkin OW. Trabecular structure of the condyle of the jaw joint in young and mature sheep: a comparative histomorphometric reference. Arch Oral Biol 2006;51(1):29-36.

Coelho PG, Fernandes PR, Rodrigues HC, Cardoso JB, Guedes JM. Numerical modeling of bone tissue adaptation—A hierarchical approach for bone apparent density and trabecular structure. J Biomech 2009; 42: 830–837.

Creamer P, Hochberg MC. Osteoarthritis. The Lancet 1997; 350 (9076): 503-509

Culav EM, Clark CH, Merrilees MJ. Connective tissues: matrix composition and its relevance to physical therapy. Phys Ther. 1999; 79: 308 –319.

Custers RJH, Creemers LB, Verbout AJ, van Rijen MHP, Dhert WJA, Saris DBF. Reliability, reproducibility and variability of the traditional Histologic / Histochemical Grading System vs the new OARSI Osteoarthritis Cartilage Histopathology Assessment System. OsteoArthritis and Cartilage 2007; 15: 1241 - 1248

D'Ambrosia RD. Epidemiology of osteoarthritis. Orthopedics 2005; 28 (2 Suppl): s 201-205.

Day JS, Ding M, van der Linden JC, Hvid I, Sumner DR, Weinans H. A decreased subchondral trabecular bone tissue elastic modulus is associated with pre-arthritic cartilage damage. Journal of Orthopaedic Research 2001; 19: 914 – 918.

Dedrick DK, Goldstein SA, Brandt KD, O'Connor BL, Goulet RW, Albrecht M. A longitudinal study of subchondral plate and trabecular bone in cruciate-deficient dogs with osteoarthritis followed up for 54 months. Arth and Rheum 1993; 36 (10): 1460 - `1467.

Dequeker J. Inverse relationship of interface between osteoporosis and osteoarthritis. J Rheumatol 1997; 24: 795-798.

Ding M, Dalstra M, Danielson CC, Kabel J, Hvid I, Linde F. Age variations in the properties of human tibial trabecular bone. J Bone Joint Surg [Br] 1997;79-B:995-1002.

Ding M, Hvid I. Quantification of age-related changes in the structure model type and trabecular thickness of human tibial cancellous bone." Bone 2000; 26(3): 291-295

Ding M, Odgaard A, Linde F, Hvid I. Age-related variations in the microstructure of human tibial cancellous bone. J Orthop Res 2002; 20: 615-621

Ding M, Odgaard A, Hvid I. Changes in the three-dimensional microstructure of human tibial cancellous bone in early osteoarthritis. J Bone Joint Surg [Br] 2003; 85-B: 906 - 912.

Drake RL, Vogl W, Mitchell AWM. Grays Anatomy for Students, 2005. Elsevier, Churchill Livingstone. Philadelphia, USA.

Dun H, Jundt J, Riddle JM, Pitchford W, Christopherson T. The Tibial Subchondral Plate. J Bone Joint Surg 1987; 69-A (6); 1212 - 1220

Fairbank TJ. Knee joint changes after meniscectomy. J Bone Joint Surg 1948; 30-B (4): 664 – 670)

Fallahi A, Kroll B, Warner LR, Oxford RJ, Irwin KM, L Mercer LM, Shadle SE, Oxford JT. Structural model of the amino propeptide of collagen XI α1 chain with similarity to the LNS domains. Protein Science 2005; 14: p1526 - 1537

Ferguson VL, Bushby AJ, Boyde A. Nanomechanical properties and mineral concentration in articular calcified cartilage and subchondral bone. J Anat 2003 Aug; 203(2): 191-202

Fitzgerald J, Butler WR. Seasonal effects and hormonal patterns related to puberty in ewe lambs. Biol Reprod 1982; 27: 853 - 863

Flieger J, Karachalios Th, Khaldi L, Raptou P, Lyritis G. Mechanical Stimulation in the Form of Vibration Prevents Postmenopausal Bone Loss in Ovariectomised Rats. Calcified Tissue International 1998; 63: 510-514

Frost HM. Skeletal Structural Adaptations to Mechanical Usage (SATMU): 2. Redefining Wolff's Law: The remodeling Problem. The Anat Record 1990; 226: 414 – 422

Frost HM, Jee WSS On the rat model of human osteopenias and osteoporoses. Bone Miner 1992; 18: 227–236

Frost HM. A 2003 Update of Bone Physiology and Wolff's Law for Clinicians. Angle Orthod 2004; 74: 3–15

Fukada Y, Takai S, Yoshino N, Murase K, Tsutsumi S, Ikeuchi K, Hirasawa Y. Impact load transmission of the knee joint-influence of leg alignment and the role of meniscus and articular cartilage. Clin Biomech 2000; 15: 516 - 521

Fukubayashi T, Kurosawa H. The contact area and pressure distribution pattern of the knee. Acta Orthop Scand 1980; 51: 871 - 879

Gelse K., Pöschl E., and Aigner T. Collagens-structure, function and biosynthesis. Advanced Drug Delivery Reviews, 55:1531–1546, 2003.

Genetics Home Reference, U.S. National Library of Medicine. http://ghr.nlm.nih.gov/search?query=collagenandshow=genes. Last accessed 19/07/10.

Getzy LL, Malemud CJ, Goldberg VM, Moskowitz RW. Factors influencing metachromic staining in paraffin-embedded sections of rabbit and human articular cartilage: a comparison of the Safronin O and Toluidine Blue O techniques. J Hist 1982; 5 (3): 111 – 116.

Gilbert SF. Developmental Biology, 6th Edn. Sinauer Assoc. Inc., Mass, USA. http://www.ncbi.nlm.nih.gov/books/bv.fcgi?db=Booksandrid=dbio.section.3479. Last accessed 28/04/11.

Goldring MB. The role of the chondrocyte in osteoarthritis. Arth and Rheum 2000; 43 (9): 1916–1926

Grynpas MD, Alpert B, katz I, Lieberman I, Pritzker KPH. Subchondral bone in osteoarthritis. Cacif Tissue Int 1991; 49: 20-26

Hall BK. Historical overview of studies on bone growth and repair. In: Hall BK, editor. Bone. Vol. 6. Boca Raton: CRC Press; 1992.

Hansel W, Convey EM. Physiology of the Estrous Cycle. J Anim Sci 1983; 57:404-424.

Hayami T ,Pickarski M, Wesolowski GA, McLane J, Bone A, Destefano J, Rodan GA, Duong le T. The role of subchondral bone remodeling in osteoarthritis: reduction of cartilage degeneration and prevention of osteophyte formation by alendronate in the rat anterior cruciate ligament transection model. Arthritis Rheum 2004 Apr; 50(4): 1193-206

Hayami T, Pickarski M, Zhuo Y, Wesolowski GA, Rodan GA, Duong le T. Characterization of articular cartilage and subchondral bone changes in the rat anterior cruciate ligament transection and meniscectomized models of osteoarthritis. Bone 2006 Feb;38(2):234-43

Hernandez, CJ. How can bone turnover modify bone strength independent of bone mass? Bone 2008; 42(6): 1014-1020.

Hwa SY, Burkhardt D, Little C, Ghosh P. The Effects of Orally Administered Diacerein on Cartilage and Subchondral Bone in an Ovine Model of Osteoarthritis. J Rheumatol 2001; 28: 825–34

Issever AS, Burghart A, Patel V, Laib A, Lu Y, Ries M, Majumdar S. A micro-computed tomography study of the trabecular bone structure in the femoral head. J Musculoskelet Neuronal Interact 2003; 3: 176-184.

Jee WSS (1983) The skeletal tissues. In: Weiss L (Ed) Histology, Cell and Tissue Biology. Elsevier Biomedical, New York, USA.

Jiang Y, Zhao J, Geusens P, Liao EY, Adriaensens P, Gelan J, Azria M, Boonen S, Caulin F, Lynch JA, Ouyang X and. Genant HK. Femoral neck trabecular microstructure in ovariectomised ewes treated with calcitonin: MRI microscopic evaluation. Journal of Bone and Mineral Research 2005; 20(1): 125-30.

Johnell O, Kanis JA, Odén A, Sernbo I, Redlund-Johnell I, Petterson C, De Laet C, Jönsson B. Mortality after osteoporotic fractures. Osteoporos Int (2004) 15: 38–42

Johnson, R. B., Gilbert, J. A., Cooper, R. C., Parsell, D. E., Stewart, B. A., Dai, X., Nick, T. G., Streckfus, C. F., Butler, R. A. and Boring, J. G. (2002) Effect of estrogen deficiency on skeletal and alveolar bone density in sheep. J Periodontol 73(4): 383-91

Kanis JA. Diagnosis of osteoporosis and assessment of fracture risk. Lancet 2002; 359: 1929–36

Kawcak CE, McIlwraith CW, Norrdin RW, Park RD, James SP. The role of subchondral bone in joint disease: a review. Equine Vet J 2001; 33 (2): 120-126.

Kawcak CE, McIlwraith CW, Park RD. The role of subchondral bone in joint disease. AAEP Proceedings 2001; 47: p 157 – 163

Kelly TAN, Wang CCB, Mauck RL, Ateshian GA, Hung CT. Role of cell-associated matrix in the development of free-swelling and dynamically loaded chondrocyte-seeded agarose gels. Biorheology 2004; 41: 223–237

Kennedy OD, Brennan O, Rackard SM, O'Brien FJ, Taylor D, Lee TC. Variation of trabecular microarchitectural parameters in cranial, caudal and mid-vertebral regions of the ovine L3 vertebra. J Anat 2009a; 214: 729–735

Kennedy OD, Brennan O, Rackard SM, Staines A, O'Brien FJ, Taylor D, Lee TC. Effects of Ovariectomy on Bone Turnover, Porosity, and Biomechanical Properties in Ovine Compact Bone 12 Months Postsurgery. J Orthop Res 2009b; 27: 303–309

Koo S, Andriacchi TP. A comparison of the influence of global functional loads vs. local contact anatomy on articular cartilage thickness at the knee. J Biomech 2007) 40: 2961–2966

Koszyca B, Fazzalari NL, Vernon-Roberts B. Calcified cartilage, subchondral and cancellous bone morphometry within the knee of normal subjects. The Knee 1996; 3: 15 – 22.

Krause WR, Clemson MS, Pope MH, Johnson RJ, Wilder DG, Burlington BMSE. Mechanical Changes in the Knee after Meniscectomy. J Bone Joint Surg 1976; 58-A (5): 599 – 604

Kuettner KE, Aydelotte MB, Thonar EJMA. Articular cartilage matrix and structure: a minireview. J Rheumatol 1991; 18 (Suppl 27): 46 – 48

Kumar P, Clark M. Clinical Medicine, 3rd edn. Baillière Tindall, London

Kuroki K, Cook CR, Cook JL. Subchondral bone changes in three different canine models of osteoarthritis. Osteoart & Cart; 19; 1142-1149

Kurtz S, Mowat F, Ong K, Chan N, Lau E, Halpern M. Prevalence of primary and revision total hip and knee arthroplasty in the United States from 1990 through 2002. J Bone Joint Surg Am 2005; 87 (7): 1487-1497.

Kwan Tat S, Lajeunesse D, Pelletier JP, Martel-Pelletier J. Targeting subchondral bone for treating osteoarthritis: what is the evidence? Best Pract Res Clin Rheumatol 2010; 24 (1): 51-70.

Laib A, Barou O, Vico L, Lafage-Proust MH, Alexandre C, Rügsegger P, 3D micro-computed tomography of trabecular and cortical bone architecture with application to a rat model of immobilisation osteoporosis. Med. Biol. Eng. Comput., 2000, 38, 326-332

Lajeunesse D. The role of bone in the treatment of osteoarthritis. Osteoarthritis and Cartilage 2004; 12: S34-S38

Lammi PE, Lammi MJ, Hyttinen MM, Panula H, Kiviranta I, Helminen HJ. Site-specific Immunostaining for Type X Collagen in Noncalcified Articular Cartilage of Canine Stifle Knee Joint. Bone 2002; 31 (6): 690- 696

Landis W.J. The strength of a calcified tissue depends in part on the molecular structure and organisation of its constituent mineral crystals in their organic matrix. Bone, 16(5):533–544, 1995.

Lane Smith R, Thomas KD, Schurman DJ, Carter DR, Wong M, van der Meulen M. Rabbit knee immobilization: Bone remodeling precedes cartilage degradation. J Orthop Res 1992; 10 (1): 88 - 95

Lane LB, Bullough PG. Age-related changes in the thickness of the calcified zone and the number of tidemarks in adult human articular cartilage. J Bone Joint Surg 1980; 62-B (3): 372 - 375

Layton MW, Goldstein SA, Goulet RW, Feldkamp LA, Kubinski DJ, Bole GG. Examination of subchondral bone architecture in experimental osteoarthritis by microscopic computed axial tomography. Arthritis Rheum 1988; 31 (11): 1400-1405.

Lee TC, Taylor D. Bone remodelling: should we cry Wolff? Ir J Med Sci. 1999; 168 (2): 102 - 5

Lee TC, Staines A, Taylor D. Bone adaptation to load: microdamage as a stimulus for bone remodelling. J. Anat. 2002; 201: pp437–446

Lee TC, Mohsin S, Taylor D, Parkesh R, Gunnlaugsson T, O'Brien FJ, Giehl M, Gowin W. Detecting microdamage in bone. Journal of Anatomy 2003; 203: 161–172.

Les CM, Vance JL, Christopherson GT, Turner AS, Divine GW, Fyhrie DP. Long-term ovariectomy decreases ovine compact bone viscoelasticity. J Orthop Res 2005; 23: 869-876

Li B, Aspden RM. Composition and mechanical properties of cancellous bone from the femoral head of patients with osteoporosis or osteoarthritis. J Bone Miner Res 1997; 12(4): 641-51

Li B, Marshall D, Roe M, Aspden RM. The electron microscope appearance of the subchondral bone plate in the human femoral head in osteoarthritis and osteoporosis. J Anat 1999; 195: 101-110.

Lin, L. I-K. 1989. A concordance correlation coefficient to evaluate reproducibility. Biometrics 45: 255-268.

Lin, L. I-K. . 2000. A note on the concordance correlation coefficient. Biometrics 56: 324-325.

Little C, Smith S, Ghosh P, Bellenger C. Histomorphological and immunohistochemical evaluation of joint changes in a model of osteoarthritis induced by lateral meniscectomy in sheep. J Rheumatol 1997; 24: 2199 – 2209.

Little C, Smith MM. Animal Models of Osteoarthritis. Curr Rheum Rev 2008; 4 (3): 175-182.

Lotke PA, Ecker ML, Alavi A. Painful knees in older patients: radionuclide diagnosis of possible osteonecrosis with spontaneous resolution. J Bone Joint Surg Am 1977; 57 (5): 617-621.

Lotke PA, Ecker ML. Osteonecrosis of the knee. J Bone Joint Surg Am. 1988; 70(3): 470-473.

Mankin HJ, Dorfman H, Lippiello L, Zarins A. Biochemical and Metabolic Abnormalities in Articular Cartilage from Osteo-Arthritic Human Hips. II. Correlation of morphology with biochemical and metabolic data. J Bone Joint Surg Am. 1971;53:523-537.

Martin JA, Buckwalter JA. Aging, articular cartilage chondrocyte senescence and osteoarthritis. Biogerontology 3: 257–264, 2002

Martin RB, Burr DB, Sharkey NA. 1998. Skeletal Tissue Mechanics. Springer-Verlag New York, Inc.

Martin RB, Burr DB. 1989. Structure, function and adaptation of compact bone. Raven Press, New York.

Mathews CK, van Holde KE. 1990. Biochemistry. The Benjamin/Cummings Publishing Company Inc., Redwood City, California.

Matsui H, Shimizu M, Tsuji H. Cartilage and Subchondral Bone Interaction in Osteoarthrosis of Human Knee Joint: A Histological and Histomorphometric Study. Micros Res Tech 1997; 37: 333 - 342

McCormick D, van der Rest M, Goodship J, Lozano G, Ninomiya N, Olsen BR. Structure of the Glycosaminoglycan Domain in the Type IX Collagen-Proteoglycan. PNAS 1987; vol. 84 (12): 4044-4048

McErlain DD, Appleton CTG, Litchfield RB, Pitelka V, Henry JL, Bernier SM, Beier F, Holdsworth DW. Study of subchondral bone adaptations in a rodent surgical model of OA using in vivo micro-computed tomography. Osteoarthritis and Cartilage 2008; 16: 458 – 469.

Mears SC, McCarthy EF, Jones LC, Hungerford DS, Mont MA. Characterization and pathological characteristics of spontaneous osteonecrosis of the knee. Iowa Orthop J 2009; 29: 38 – 42.

Meier C, Nguyen TV, Center JR, Seibel MJ, Eisman JA. Bone Resorption and Osteoporotic Fractures in Elderly Men: The Dubbo Osteoporosis Epidemiology Study. JBMR 2005; 20(4): 579-587.

MicroscopyU. Spring KR, Davidson MW, Nikon Instruments, Inc. http://www.microscopyu.com/articles/fluorescence/fluorescenceintro.html. Last accessed 6/10/2010.

Milch RA, Rall DP, Tobie JE. Fluorescence of tetracycline antibiotics in bone, J Bone Joint Surg 1958; 40A: 897- 910.

Mittra E, Rubin C, Qin YX. Interrelationship of trabecular mechanical and microstructural properties in sheep trabecular bone. J Biomech 2005;38(6):1229-37.

Mitton D, Cendre E, Roux JP, Arlot ME, Peix G, Rumelhart C, *et al.* Mechanical properties of ewe vertebral cancellous bone compared with histomorphometry and high-resolution computed tomography parameters. Bone 1998;22(6):651-8.

Molecular expressions™. Optical microscopy primer. Michael W. Davidson, Mortimer Abramowitz, Olympus America Inc., and The Florida State University. 20th June 2006. http://micro.magnet.fsu.edu/primer/index.html. Last accessed 05/10/10

Mollenhauer J, Mok MT, King KB, Gupta M, Chubinskaya S, Koepp H, Cole AA. Expression of Anchorin CII (Cartilage Annexin V) in Human Young, Normal Adult, and Osteoarthritic Cartilage. J Histo Cytochem 1999; 47 (2): 209 – 220

Muir P, McCarthy J, Radtke CL, Markel MD, Santschi EM, Scollay MC, Kalscheur VL. Role of endochondral ossification of articular cartilage and functional adaptation of the subchondral plate in the development of fatigue microcracking of joints. Bone 2006 Mar; 38(3): 342-349

Nafei A, Kabel J, Odgaard A, Linde F, Hvid I. Properties of growing trabecular ovine bone. PART II: ARCHITECTURAL AND MECHANICAL PROPERTIES. J Bone Joint Surg [Br] 2000; 82-B: 921-927.

Narváez JA, Narváez J, De Lama E, Sánchez A. Spontaneous osteonecrosis of the knee associated with tibial plateau and femoral condyle insufficiency stress fracture. Eur Radiol. 2003; 13: 1843-1848. Epub 2002 Dec 19.

Newman, E., A.S. Turner and J.D. Wark: The potential of sheep for the study of osteopenia: current status and comparison with other animal models. Bone 16(4), 277S-84S (1995)

Newton BI, Cooper RC, Gilbert JA, Johnson RB, Zardiackas LD. The Ovariectomised Sheep as a Model for Human Bone Loss. J. Comp. Path. 2004, Vol. 130, 323–326

Noble J, Alexander K. Studies of Tibial Subchondral Bone Density and Its Significance. J Bone Joint Surg 1985; 67-A: 295 - 302

Norman GR, Streiner DL. Biostatistics: The Bare Essentials 3rd Edn. PMPH, Shelton, Connecticut (2008)

Oatis C (ed). Kinesiology: The Mechanics and Pathomechanics of Human Movement. Lippincott Williams and Wilkins, London.

O'Brien FJ, Taylor D, Dickson GR, Lee TC. Visualisation of three-dimensional microcracks in compact bone. J. Anat. 2000; 197: 413 - 420

Oegema TR, Carpenter RJ, Hofmeister F, Thompson RC. The Interaction of the Zone of Calcified Cartilage and Subchondral Bone in Osteoarthritis. Microsc Res Tech 1997; 37: 324–332

Osborne JW, Overbay A. The power of outliers (and why researchers should always check for them). Practical Assessment, Research and Evaluation, 9(6). Retrieved May 25, 2010 from http://PAREonline.net/getvn.asp?v=9andn=6 .

Osterhoff G, Löffler S, Steinke H, Feja C, Josten C, Hepp P. Comparative anatomical measurements of osseous structures in the ovine and human knee. The Knee 2010; doi:10.1016/j.knee.2010.02.001

Pajamäki I, Sievänen H, Kannus P, Jokihaara J, Vuohelainen T, Järvinen TLN. Skeletal effects of estrogen and mechanical loading are structurally distinct. Bone 2008: 43; 748–757.

Parfitt AM, Drezner MK, Glorieux FH, Kanis JA, Malluche H, Meunier PJ, Ott SM, Recker RR. Bone Histomorphometry: Standardization of Nomenclature, Symbols and Units. J Bone Min Res 1987; 2 (6): 595 – 610.

Parfitt AM. Bone Histomorphometry: Standardization of Nomenclature, Symbols and Units (Summary of Proposed System). Bone 1988; 9: 67 – 69.

Parfitt AM. Targeted and Nontargeted Bone Remodeling: Relationship to Basic Multicellular Unit Origination and Progression. Bone 2002; 30 (1): 5 - 7

Parfitt AM. Misconceptions (2): Turnover is always higher in cancellous than in cortical bone. Bone 2002: 30; 807 - 809

Parfitt AM. Misconceptions (3): calcium leaves bone only by resporption and enters only by formation. Bone 2003: 33; 259 - 263

Parker D, Hwa SY, Sambrook P, Ghosh P. Estrogen replacement therapy mitigates the loss of joint cartilage proteoglycans and bone mineral density induced by ovariectomy and osteoarthritis. APLAR J Rheum 2003; 6: 116 - 127

Patel V, Issever AS, Burghard A, Laib A, Ries M, Majumdar S. MicroCT evaluation of normal and osteoarthritic bone structure in human knee specimens. J Orthop Res 2003; 21: 6-13.

Poole KES, Compston JE. Osteoporosis and its management. BMJ 2006; 333: 1251 – 1256

Pritzker KPH. Animal models for osteoarthritis: processes, problems and prospects. Ann Rheum Dis 1994; 53: 406 – 420

Pritzker KPH, Gay S, Jimenez SA, Ostergaard K, Pelletier JP, Revell PA, Salter D, van der Berg WB. Osteoarthritis cartilage histopathology: grading and staging. Osteoarth Cart 2006; 14; 13 – 29.

Radin EL, Rose RM. Role of subchondral bone in the initiation and progression of cartilage damage. Clin Orthop Relat Res 1986; 213: 34-40.

Rahn BA, Perren SM. Xylenol orange, a fluorochrome useful in polychrome sequential labeling of calcifying tissues. Stain Technol 1971; 46: 125-129.

Rahn BA. Fluorochrome labelling of bone dynamics. European Cells and Materials 2003; 5 (Suppl. 2); p 41

Riggs BL, Melton LJ. The Prevention and Treatment of Osteoporosis. NEJM 1992; 327 (9): 620-627

Riggs BL, Melton LJ. Bone turnover matters: the raloxifene treatment paradox of dramatic decreases in vertebral fractures without commensurate increases in bone density. JBMR 2002; 17: 11-14

Robertson DD, Armfield DR, Towers JD, Irrgang JJ, Maloney WJ, Harner CD. Meniscal root injury and spontaneous osteonecrosis of the knee: an observation. J Bone Joint Surg Br 2009; 91-B:190-195.

Rodan GA. Introduction to Bone Biology. Bone 1992; 13: S3 – S6

Ross MH, Reith EJ, Romrell LJ, eds. 1989 (2nd edn.). Histology: A text and atlas. Williams and Wilkins, Baltimore.

Roughley PJ, Lee ER. Cartilage Proteoglycans: Structure and Potential Functions. Microsc Res Tech 1994; 28: 385 - 397

Royal Society Website, http://www.royalsoc.ac.uk/page.asp?id=1744. Last accessed 09/07/09

Rubin C, Turner S, Mu R, Mittra E, McLeod K, Line W, Qin YX. Quantity and Quality of Trabecular Bone in the Femur Are Enhanced by a Strongly Anabolic, Noninvasive Mechanical Intervention. J Bone Min Res 2002; 17 (2): 349 – 357.

Rubin E, Gorstein F, Rubin R, Schwarting R, Strayer D *et al*, eds. 2004 (4th edn.). Rubin's Pathology. Lippincott Williams and Wilkins, London.

Sadler TW. 2004 (9th edn.). Langman's Medical Embryology. Lippincott Williams and Wilkins, London.

Satku K, Kumar VP, Chong SM, Thambyah A. The natural history of spontaneous osteonecrosis of the medial tibial plateau. J Bone Joint Surg Br 2003; 85; 983 – 988.

Sato K, Wakamatsu E, Sato T, Honma T, Kotake H, Byers PD. Histomorphometric study of trabecular channels in normal iliac bone. Calcified Tissue International 1986: 39(1); 2-7.

Schorlemmer S, Gohl C, Iwabu S, Ignatius A, Claes L, Augat P. Glucocorticoid treatment of ovariectomised sheep affects mineral density, structure, and mechanical properties of cancellous bone. J Bone Miner Res 2003; 18(11):2010-2015.

Schmidt-Nielson K. 1977. Animal Physiology: Adaptation and Environment, Cambridge University Press, London.

Schmidt-Nielson K. 1984. Scaling: Why is animal size so important? Cambridge University Press, London.

Sharif M, George E, Dieppe PA. Correlation between synovial fluid markers of cartilage and bone turnover and scintigraphic scan abnormalities in osteoarthritis of the knee. Arthritis Rheum 1995; 38(1): 78-81

Schorlemmer S, Ignatius A, Claes L, Augat P. Inhibition of cortical and cancellous bone formation in glucocorticoid-treated OVX sheep. Bone 2005; 37: 491–496

Sissons HA. Experimental determination of rats of longitudinal bone growth. J Anat 1953; 87:228–236.

van der Sluijs JA, Geesink RGT, van der Linden AJ, Bulstra SK, Kuyer R, Drukker J. *The reliability of the mankin score for osteoarthritis.* J Orthop Res 1992; 10 (1): 58 – 61.

Sniekers YH, , Intema F, Lafeber FPJG, van Osch1 GJVM, van Leeuwen JPTM, Weinans H, Mastbergen SC. A role for subchondral bone changes in the process of osteoarthritis; a micro-CT study of two canine models. BMC Musculoskeletal Disorders 2008, 9:20.

Sniekers YH, Weinans H, Bierma-Zeinstra SM, van Leeuwen JPTM van Osch GJVM. Animal models for osteoarthritis: the effect of ovariectomy and estrogen treatment – a systematic approach. Osteoarth Cart 2008; 16: 533 - 541

Standring S, Ellis H, Healy JC, Johnson D, Williams A *et al*, eds. 2005. Gray's Anatomy. Churchill Livingstone, London

Stewart A, Black AJ. Bone mineral density in osteoarthritis. Curr Opin Rheumatol 2000; 13: 464-467.

Takeda M, Higuchi H, Kimura M, Kobayashi Y, Terauchi M, Takagishi K. Spontaneous osteonecrosis of the knee. J Bone Joint Surg Br 2008; 90-B (3): 324-329.

Taylor D, Hazenberg J, Lee TC. The cellular transducer in bone: What is it? Technology and Health Care 2006; 14: 367–377

Thorndike EA, Turner AS. In search of an animal model for postmenopausal diseases. Front Biosci 1998; 3: 17-26.

Turner CH, Burr DB. Basic Biomechanical Measurements of Bone: A Tutorial. Bone 1993; 14: 595 – 606

Turner AS, Villanueva AR, Alvis MR, Aberman HM. Unusual histomorphometric changes in the iliac crest in ovariectomised and sham-operated ewes. Veterinary Comparative Orthopaedics and Traumatology 1995; 8: 184-190.

Turner AS, Athanasiou KA, Zhu CF, Alvis MR. Biochemical effects of estrogen on articular cartilage in ovariectomised sheep. Osteoarth Cart 1997; 5: 63 – 69

Turner CH. Three Rules for Bone Adaptation to Mechanical Stimuli. Bone 1998; 23 (5): 399 – 407

Waarsing J H; Day J S; van der Linden J C; Ederveen A G; Spanjers C; De Clerck N; Sasov A; Verhaar J A N; Weinans H. Detecting and tracking local changes in the tibiae of individual rats: a novel method to analyse longitudinal in vivo micro-CT data. Bone 2004; 34 (1): 163-9.

Whitby LG, Smith AF, Beckett GJ, Walker SW. Lecture Notes on Clinical Biochemistry. 5th ed. Oxford: Blackwell Scientific Publications; 1994.

Woods and Ellis, eds. Laboratory Histopathology: A Complete Reference, 1994. Churchill Livingstone, New York.

Wolff J. Uber die innere Architectur der Knochen und ihre Bedeutung fur die Frange vomKnochenwachsthum, Virchow's Arch 50 (1870), 389–450.

Yamamoto T, Bullough PG. Spontaneous osteonecrosis of the knee: the result of subchondral insufficiency fracture. J Bone Joint Surg Am. 2000; 82(6): 858-866.

Yamamoto T, Bullough PG. The role of subchondral insufficiency fracture in rapid destruction of the hip joint: A preliminary report. Arth and Rheum 200b; 43; 2423-2427.

Yuthasastrakosol P, Palmer WM, Howland BE. Luteinizing hormone, oestrogen and progesterone levels in peripheral serum of anoestrous and cyclic ewes as determined by radioimmunoassay. J Reprod Fert 1975; 43: 57 - 65

Zarco L, Stabenfeldt GH, Quirke JF, Kindahl H, Bradford GE. Release of prostaglandin and the timing of events associated with luteolysis in ewes with oestrous cycles of different lengths. J Reprod Fert 1988; 83: 517 - 526

Zhang ZM, Li ZC, Jiang LS, Jiang SD, Dai LY. Micro-CT and mechanical evaluation of subchondral trabecular bone structure between postmenopausal women with osteoarthritis and osteoporosis. OSTEOPOROS Osteoporos Int 2010; 21: 1383-1390.